Hybrid nanocellulose/nanoclay composites for food packaging applications

Trifol Guzman, Jon

Publication date:
2016

Document Version
Publisher's PDF, also known as Version of record

Hybrid nanocellulose/nanoclay composites for food packaging applications

TRIFOL GUZMAN, Jon

17/05/2016

Preface

The work presented herein is the result of my PhD study, which was carried out mainly at the Danish Polymer Centre (DPC), at the Department of Chemical and Biochemical Engineering at the Technical University of Denmark (DTU), but also at LGP2, Grenoble INP-Pagora, University of Bologna, University of Sheffield Hallam and at Kungliga Tekniska Högskolan, where I had external stays. This study was carried out as a part of a larger project, NewGenPak (New Generation of Functional Cellulose Based Packaging Materials for Sustainability).

I would like to dedicate this thesis in memory of Professor Iñaki Mondragón, who was my mentor during my Master's project and will always be in my thoughts. I would also like to acknowledge the NewGenPak consortium, especially Dr. Julien Bras, Dr. Marco Giacinti, Dr. Matteo Minelli, Prof. Chris Breen, Dr. Francis Clegg, Dr. Richard T. Olsson and Dr. Richard Andersson, who guided me admirably during my external stays. I would also like to thank Dr. David Plackett, who guided me from Canada, and my supervisor board, namely Prof. Ole Hassager, Dr. Peter Szabo and Dr. Anders Egede Daugaard, for steering me through my PhD. I would like also to acknowledge Ms. Kim Chi Szabo, Mr. Lars Schulte and Dr. Ramona Valentina Mateiu for their support on some analysis. I would also like to highlight the contribution of the COST program with the Actions FP1003, FP1105, FP1205 and FP1405 for their support on my formation. A special acknowledgement is extended to all of my DPC colleagues, purely for being my colleagues. But especially I would like to acknowledge my parents for supporting me throughout my life.

Jon Trifol Guzman
17/05/2016

Abstract

In this research, cellulose nanofibres (CNFs) were extracted and dispersed through a combination of alkali-acetylation treatments followed by soft mechanical treatments. Thereafter, PLA-based nanocomposites with CNF, nanocrystalline cellulose (CNC) and/or commercially available nanoclay (Cloisite™ 30B) were prepared and evaluated for use in food packaging. It was determined that composites with CNF or CNC and clay led to a great reduction in the oxygen transmission rate (OTR) and the water vapour transmission rate (WVTR) (up to a 90% reduction in the OTR and 76% in the WVTR for PLA/CNF 5%/C30B 5%). A significant increase in thermomechanical resistance was obtained (the storage modulus of PLA/CNF 5%/C30B 5% at 85°C, was 3.7 times higher than for neat PLA) and increased crystallisation kinetics (the PLA/CNF 1%/C30B 1% showed an 81% reduction in half-crystallisation time compared with neat PLA) without a significant reduction in optical properties at moderate nanoparticle loading.

Furthermore, it was found that solvent casting at a low temperature induced sub-micron-sized spherulites, which had little influence on water diffusion and transparency decline. On the other hand, high temperature processing led to larger spherulite sizes, which had a more significant impact on water diffusion and transparency reduction but also showed an increased water sorption. Finally, it was found that cellulose nanofibers reduced water diffusion to an extent similar to C30B (21% vs. 27%), while hybrid composites showed 49% decrease, albeit CNF based composites showed increased water sorption (7% for PLA/CNF 1% composite and 9% for PLA/CNF 1%/C30B 1% when compared with neat PLA).

The reduced diffusivity of the hybrid nanocomposites suggested that the material was promising for active packaging, since low diffusivity leads to the slower release of active compounds such as essential oils. On top of that the CNF was surface modified with hydrocinnamic acid (gCNF), with the aim of reducing even more the release rate of carvacrol and to enhance the CNF dispersion with the PLA matrix. Consequently, carvacrol-loaded PLA/CNF, PLA/gCNF and hybrid PLA/CNF/C30B composites were prepared and evaluated on controlled release applications. It was established that the surface modification of CNF greatly enhanced the dispersion of the gCNF and that carvacrol loaded hybrid composites showed a decreased release rate, high ductility and a reduced WVTR which made those composites promising material for food packaging films.

Resumé

I dette forskningsprojekt blev cellulosebaserede nanofibre (CNF) udvundet fra Sisal ved hjælp af en kombination af alkalibehandling og skånsom mekanisk forarbejdning. Efterfølgende blev de udvundne fibre benyttet til at fremstille PLA-baserede nanokompositter med CNF, nanokrystallinsk cellulose (CNC) og kommercielt tilgængeligt nanoler (Cloisite 30B). Kompositterne blev undersøgt med henblik på anvendelse som fødevareemballage. Hybridkompositter bestående af CNF eller CNC kombineret med ler viste sig, sammenlignet med ren PLA, at muliggøre en stor reduktion i permeabilitet for ilt (OTR) og vanddamp (WVTR). Der blev målt op til 90% reduktion i OTR og 76% i WVTR for PLA/CNF 5%/C30B 5% samt forbedrede termomekaniske egenskaber. Elasticitetsmodulet for PLA/CNF 5%/C30B 5% var 3,7 gange større end for ren PLA. Krystallisationskinetikken blev ligeledes forbedret idet f.eks. PLA/CNF 1%/C30B 1% viste en 81% reduktion i halveringstiden sammenlignet med ren PLA. Begge nævnte forbedringer kunne opnås uden åbenbar forringelse af de optiske egenskaber.

De undersøgte nanokompositter blev fremstillet ved solventstøbning. Ved krystallisation ved lave temperaturer blev det observeret, at sfærulit-dannelsen bestod af ganske små domæner (mindre end 1 µm) med lille påvirkning af vand-diffusion og transparens. På den anden side viste forsøgene, at solventstøbning ved højere temperaturer gav anledning til dannelse af større domæner med tydelig påvirkning af vand-diffusion og transparens. Endelig blev det demonstreret, at cellulose nanofibre (CNF) reducerer vanddiffusionen på lignende måde som ler (C30B) (21% henholdsvis 27% reduktion). De fremstillede hybride kompositter udviste 49% reduktion dog udviste disse kompositter et forøget vandoptag (7% forøgelse i PLA/CNF 1% komposit og 9% forøgelse i PLA/CNF 1%/C30B 1% sammenlignet med ren PLA). Den reducerede diffusivitet i de hybride nanokompositter antyder, at materialerne kunne være lovende til anvendelser med såkaldt ”active packaging”. Den lavere diffusivitet betyder, at aktive substanser vil afgives langsommere såsom essentielle olier, som er rapporteret til at give blødgørende egenskaber til PLA. Endvidere blev cellulosefibrene (CNF) overflademodificeret med hydrokanelsyre (gCNF), hvilket er rapporteret at reducere afgivelseshastigheden for carvacrol samt forbedre dispergeringen af CNF i PLA-matricen. Carvacrol-prepparerede prøver af PLA/CNF, PLA/gCNF og PLA/CNF/C30B blev fremstillet med henblik på ”controlled release” anvendelser. Det blev demonstreret, at de overflademodificerede cellulosefibre gCNF havde forbedrede dispergeringsegenskaber. Desuden blev det vist, at de carvacrol-prepparerede hybride kompositter havde nedsat afgivelseshastighed, høj duktilitet samt en reduceret WVTR, hvilket peger på disse kompositter som lovende filmmateriale til fødevareemballage.

Index

Abbreviations and symbols

AM	Amorphous
C30B	Cloisite C30B
CNC	Nanocrystalline cellulose
CNF	Cellulose nanofibres
Cp	Heat Capacity
CR	Carvacrol
DCM	Dichlorometane
DMA	Dynamic mechanical analysis
DMAc	Dimethylacetamide
DMF	Dimethylformamide
DC	Degree of crystallinity
DPC	Danish Polymer Centre
DSC	Differential scanning calorimetry
DTU	Technical University of Denmark
FC	Fully crystallised
FT-IR	Fourier transformed infrared spectroscopy
gCNF	Grafted cellulose nanofibres
HA	Hydrocinnamic acid
HDPE	High-density polyethylene
KT	Department of Chemical and Biochemical Engineering on DTU
KTH	Kungliga Tekniska Högskolan
LDPE	Low-density polyethylene
LLDPE	Linear low-density polyethylene
MAF	Mobile amorphous fraction
MDSC	Modulated DSC
MeOH	Methanol
NMP	N-Methyl-2-pyrrolidone
OM	Optical microscopy
OTR	Oxygen transmission rate
PLA	Poly(lactic acid)
POM	Polarised optical microscopy
QSM	Quartz spring microbalance
RAF	Rigid amorphous fraction
RH	Relative humidity
SC	Solvent casting
SEM	Scanning electron microscopy
TEM	Transmission electron microscopy
TEMPO	(2,2,6,6-Tetramethylpiperidin-1-yl)oxyl
T_g	Glass-transition temperature
THF	Tetrahydrofuran
T_m	Melting temperature
TOCN	Tempo oxidized cellulose nanofibers
UNIBO	University of Bologna

UV	Ultraviolet
UV-vis	Ultraviolet-visible
WVTR	Water vapour transmission rate
XRD	X-Ray diffraction

Introduction

In this thesis the effect of reinforcing a commercially available, bio-based and biodegradable polymer (PLA) with cellulose nanofibres and clay on food packaging-related properties will be studied. One of the key factors in ensuring a reliable food supply involves protecting the food throughout the supply chain, which is done by packaging it correctly. The present work sits within the context of next-generation packaging, sustainable packaging, understood as bio-based and biodegradable packaging. However, in general, the properties of biopolymers have to be enhanced in order to meet food packaging industry requirements.

Objectives

The development of bio-based and biodegradable packaging has caught the attention of the scientific community and has been the subject of numerous scientific publications. This study was carried out as a part of a larger project, NewGenPak (New Generation of Functional Cellulose Fibre-Based Packaging Materials for Sustainability), involving ten PhD students and three post-docs from several institutions (Sheffield Hallam University, Karlstad University, Technical University of Denmark, University of Bologna, Chesapeak, Imerys, INP-Pagora, Azienda Speciale Innovhub – Stazioni Sperimentale per l'industria, ITENE, Zachodniopomorski Uniwersytet Technologiczny w Szczecinie, Papiertechnische Stiftung and Bumaga BV). The project pursued several objectives: (I) to conduct top-level research and devise innovative solutions for sustainable packaging, (II) to advance the state of the art in sustainable packaging in three specific areas, namely next-generation packaging composites, cellulose fibre-based active packaging and the environmental, economic and societal aspects of packaging production, (III) to educate the next generation of researchers within a broad European research training network, (IV) to improve researchers career prospects through complementary training and (V) to strengthen further the long-term sustainable packaging research and training base in the EU by bringing together universities, research institutes and industrial players.

The aim of this PhD thesis is to study the effect of combining nanocellulose and nanoclay on a bio-based and biodegradable polymer matrix in relation to its performance as a film for food packaging. Nanoclay might not be considered as a biodegradable material; however, in the present work the clay concentration used is minimal and hence leads to a material that is mainly biodegradable. It would be an interesting undertaking to analyse the maximum amount of non-biodegradable material admissible in a product in order to be considered as biodegradable, but this is definitely not the aim of the present study. In addition it is most certainly not the aim of this work to discuss the

best solution (e.g. reliable polymer recycling chain, energy conversion, use of bio-based and/or biodegradable products, politics to minimise the consumption of polymers) to achieve a sustainable packaging. In this work the use of bio-based and biodegradable products as food packaging material is going to be studied.

Outline

The thesis is divided into nine chapters. The first chapter provides an overview of the state of the art of the topic. In Chapter 2, a procedure to produce acetylated cellulose nanofibres (CNF) is presented and discussed; furthermore, CNF films and CNF plus the by-product of nanocellulose extraction films, are prepared and tested to prove the high performance of the nanoparticle. Chapters 3 and 4 deal with the preparation of PLA-based nanocomposites – in Chapter 3, composites with a single nanoparticle will be prepared, while in Chapter 4 hybrid composites with nanocellulose and clay will be compared. Chapters 5 and 6 deal with crystalline morphology – in Chapter 5, a deep evaluation of the isothermal crystallisation behaviour of PLA, PLA/CNF 1%, PLA/C30B 1% and PLA/CNF 1%/C30B1% is undertaken, and in Chapter 6, the effect of nanoparticles and different crystalline morphologies on optical transparency and mass transport is studied. In Chapter 7, the potential of nanoparticles, surface modifications of nanocellulose and different crystalline morphologies of PLA-based nanocomposites on the controlled release of carvacrol are the subjects of study. Conclusions and outlooks can be found in Chapter 8, and finally, in Chapter 9, the experimental procedures used herein are outlined accordingly.

Appendix 1:

Optimisation of nanocomposite preparation, processing and testing.

Appendix 2:

Trifol, J., Sillard, C., Plackett, D., Bras, J., Szabo, P., Daugaard, A. E., Chemically extracted nanocellulose from sisal fibres by employing a simple and industrially relevant process. *Cellulose* (under review).

Appendix 3:

Trifol J., Plackett D., Sillard C., Hassager O., Daugaard A.E., Bras J., Szabo P. A comparison of partially acetylated nanocellulose, nanocrystalline cellulose and nanoclay as fillers for high-performance polylactide nanocomposites. *J Appl Polym Sci* 2016; **133**:1–13. doi:10.1002/app.43257.

Appendix 4:

Trifol, J., Plackett, D., Sillard, C., Szabo, P., Bras, J., Daugaard, A.E., Hybrid poly (lactic acid)/nanocellulose/nanoclay composites with synergistically enhanced barrier properties and improved thermomechanical resistance. *Polymer International 2016.* doi:10.1002/pi.5154

Other publications (not included in the thesis):

Meriçer, Ç. Minelli, M., De Angelis, M., Giacinti, M., Laurita, R., Gherardi, M., Colombo, V., **Trifol, J.**, Szabo, P., Lindström, T. Atmospheric plasma assisted PLA/Microfibrillated cellulose (MFC) multilayer biocomposite for sustainable barrier application. *Industrial crops and products* 2016; **17**: 1321-1329. doi:10.1016/j.indcrop.2016.03.020.

Mohanty S, Alm M, Hemmingsen M, Dolatshahi-Pirouz A, **Trifol J**, Thomsen P et al. 3D printed silicone-hydrogel scaffold with enhanced physicochemical properties. *Biomacromolecules* 2016. doi: acs.biomac.5b01722.

Mohanty S, Sanger K, Heiskanen A, **Trifol J**, Szabo P, Dufva M et al. Fabrication of scalable tissue engineering scaffolds with dual-pore microarchitecture by combining 3D printing and particle leaching. *Materials Science and Engineering C* 2016; **61**: 180–189. doi:10.1016/j.msec.2015.12.032.

Mohanty S, Muhammad HB, **Trifol J**, Szabo P, Burri HVR, Canali C et al. Fabrication of scalable and structured tissue engineering scaffolds using water dissolvable sacrificial 3D printed moulds. *Materials Science and Engineering C* 2015; **55**: 569–578. doi: 10.1016/j.msec.2015.06.002.

Nanostructured composite materials reinforced with nature-based nanocellulose. G. Vargas, **J. Trifol,** I. Algar, A. Arbelaiz, G. Mondragon, S.C.M. Fernandes, F. Mujika, A. Eceiza (2015). Natural Filler and Fibre Composites: Development and Characterisation. WIT Transactions on State-of-the-art in Science and Engineering – Wessex Institute of Technology. ISBN: 978-1-78466-147-2.

1. Background

This chapter provides comprehensive background information on the specific requirements that a material has to fulfil in order to be used in food packaging, and the challenges involved in currently used bio-based and biodegradable materials to achieve these requirements.

1.1 Food packaging requirements

The packaging has the role of protecting the food during the supply chain. The shape and material of it will change for each specific application, but, in general, it is made of wood, plastic and metals among others.

Packaging, in general, and polymer-based food packaging in particular, has a number of specific requirements that have to be fulfilled by candidate materials (Sorrentino et al. 2007; Siracusa et al. 2008). Among them, the more relevant are the following: mechanical properties, barrier properties, thermomechanical properties, transparency and cost.

The requirement for suitable mechanical properties came about because the main objective of food packaging is to protect food, and so it has to be able to resist any impacts that might occur throughout the supply chain (Siracusa et al. 2008). In addition, a brittle material might be challenging to work with in some processing steps. Furthermore, packaging has to protect food, not only from physical damage, but also from other external agents. Essentially, food packaging materials require good barrier properties for two main reasons. First, the presence of oxygen and/or water in food can heighten the food degradation process (Dennison and Kirk 1978), and second, effective aroma barrier properties are required to maintain organoleptic quality (Colomines et al. 2010). Moreover, optical transparency is interesting (Lee et al. 2008a) because usually the customer wants to see food

before buying it, and so high transparency and clarity are required. Likewise, the selective blocking of UV light, which contributes to food degradation, is also an relevant feature (Sanchez-Garcia and Lagaron 2010a).

On top of that there are a number of other general requirements such as thermoestability, which is required not only for some food packaging applications, such as microwave-heated food, but also whilst thermoforming (Siracusa et al. 2008), and the cost of the material, which is a really important parameter; traditionally, the food industry has considered packaging as a cost instead of as an investment, meaning that all packaging solutions have to be economically efficient.

Finally, there are other requirements that are not studied in the present work. For example, printability is also welcome in polymers for food packaging, since labelling packages is useful for tracking them throughout the supply chain or for providing useful information such as an expiry date. Although there are other solutions available, such as the use of tags, direct printing is in general the cheapest option.

While packaging has been considered traditionally as *passive*, meaning that its only role is to contain food, nowadays so-called *active* and *intelligent* packaging solutions are finding an increased number of applications. Active packaging is defined as "packaging in which subsidiary constituents have been deliberately included in or on either packaging material or the package headspace to enhance the performance of the package system" (Robertson 2006). Some examples thereof are oxygen scavengers – usually iron oxides – that have the ability to absorb oxygen, thus enhancing the shelf life of food, or packaging which releases anti-microbiological compounds and hence affect microbiological growth within the food. On the other hand, *intelligent* packaging uses the communication function of the package to facilitate decision-making and to achieve the benefits of enhanced food quality and safety, for instance using biosensors to track conditions within the supply chain or to determine when it is safe to consume the product.

Finally, packaging should be environmentally friendly, not only due to the intensive use of resources in packaging production, but also because this supposes a large output of material that has to be managed in the right way (i.e. by using bio-based and biodegradable polymers).

1.2 Bio-based and biodegradable polymers

To provide a definition of both terms, it can be said that bio-based materials include "industrial products, not food or feed, made from renewable agricultural and forestry feed stocks, including wood, wood wastes and residues, grasses, crops, and crops by-products" (Mohanty et al. 2002),

while biodegradable polymers are “those that undergo microbially induced chain scission, leading to mineralization, photodegradation, oxidation, and hydrolysis, which can alter the polymer during the degradation process” (Mohanty et al. 2002). It is worth highlighting that although many bio-based materials are biodegradable, not all bio-based materials are biodegradable, and neither are all biodegradable products bio-based (i.e. green polyethylene is not biodegradable but it is bio-based, and polycaprolactone originates from petroleum but is biodegradable).

Today´s society is polymer-based; in 2010, for example, nearly 300 million tons of polymers were produced (Halden 2010). Polymers are everywhere: biscuit packaging, water bottles, laptop components and other commodities such as pens, phones, cars, etc., amounting to roughly the amount of polymer that would be required to coat Denmark (excluding Greenland and Faroe islands) in a layer 8 mm thick. This large-scale production creates two problems. First, petroleum is a non-renewable resource; hence, the intensive use of this resource might lead to future shortages. The second problem is the disposal of all of this material. Apart from being an environmental issue, this might also be a human and animal health hazard (Halden 2010; Rochman et al. 2013; Bouwmeester et al. 2015), and so for that reason, during the last few decades, society´s concerns for environmental issues have increased and solutions have been demanded.

The main issue with bio-based and biodegradable polymers is that they still have many technical deficiencies compared to petroleum-based products, and in general they cannot fulfil the technical requirements of food packaging (Sorrentino et al. 2007). The focus of this PhD thesis is on evaluating the potential of reinforcing biopolymers with nanocellulose and nanoclay, in order to challenge petroleum-based polymers used in food packaging applications.

There are already a number of bio-based and biodegradable polymers (hemicellulose, starch, poly(hydroxy alkanoate), poly(lactic acid) and so on), but for the present work poly(lactic acid) has been chosen as a matrix, due to the fact that it is already commercially available and because it is a promising bio-based material.

Using both bio-based and biodegradable polymers, like PLA, is a promising way to solve the environmental issue. On the one hand, there will always be the possibility of growing raw materials that can be converted to lactide, the monomer of PLA, thus granting the ready availability of the product, and their biodegradable behaviour will solve the issue of disposal and close down the CO_2 cycle. Accordingly, nowadays, the use of both bio-based and biodegradable polymers such as PLA is generally finding an increasing number of applications. In fact, the world production of lactic acid in

2015 was estimated at 329,000 tons, and this figure is expected to grow up to 367,000 tons by 2017 (Subramanian et al. 2015).

However, PLA has been deemed to be an inferior material compared to classical polymers. In particular, poor thermomechanical properties, slow crystallisation and medium barrier properties have been some of the major obstacles in expanding its use (Nampoothiri et al. 2010).

1.3 Bionanocomposites

As a result of the weaknesses inherent in PLA, several different strategies have been introduced in order to improve its properties. These include modifying it (Rasal et al. 2010), blending it with other polymers such as PEG (Sheth et al. 1997) or essential oils (Del Nobile et al. 2009), reinforcing it with agents such as natural fibres (Bogoeva-Gaceva et al. 2007), chitosan (Chinh et al. 2014), xylans (Fundador and Iwata 2013), calcium carbonate (Kasuga et al. 2003) and, especially, bionanocomposites, reinforcing it with particles with at least one dimension below 100 nm, such as silver nanoparticles (Suyatma et al. 2004), nanoclays (Sengupta et al. 2007), nanocellulose (Khalil et al. 2012), carbon nanotubes (Chen et al. 2005) and so on.

Nanocellulose

Cellulosic nanoparticles, such as cellulose nanofibres (CNF) or cellulose nanocrystals (CNC), can be obtained from any cellulose source, such as lignocellulosic materials, but they can also be derived from alternative sources such as bacteria or animals (tunicate). They have caught the attention of numerous researchers, not only for their biodegradability, bio-based origins and availability, but also due to their good reinforcing properties, such as a specific Young's modulus 3.4 times that of steel (Eichhorn and Dufresne 2010), which makes them promising potential reinforcing agents for PLA.

Any industrially-relevant procedure that involves nanocellulose will require, first, supply on an industrial scale. As long as cellulose is the most abundant bio-derived polymer in the world, with a yearly production of about 10^{11} tons (Azizi Samir et al. 2005), the supply of raw material will not be a challenge, though the production of cellulose nanofibers or cellulose nanocrystals might still be an issue, especially due to the low prices required for certain applications such as food packaging. For that reason, there is a large research body examining the production of nanocellulose from cheaper raw materials such as sludge (Jonoobi et al. 2012b), waste sugarcane bagasse (Mandal and Chakrabarty 2011) and pineapple leaf (Cherian et al. 2010) among others.

Usually, the procedure for obtaining CNF involves submitting cellulose pulp to high shear rates, i.e. grinding, micro fluidisation, homogenisation or other similar techniques. These methods usually require large quantities of energy, so extensive research has been targeted at finding methods for pre-treatment, to reduce the required energy hence reducing the costs. These methods usually involve using enzymatic treatments (Henriksson et al. 2007) or (2,2,6,6-Tetramethylpiperidin-1-yl)oxy(TEMPO) (Isogai et al. 2011) to decrease the required amount of energy required to break down the hydrogen bonds (Qing et al. 2013; Abdul Khalil et al. 2014). However, the output of the CNF production system is usually a high-viscosity product with high water content, which may ultimately increase transportation and handling costs. In a similar way, the CNC are usually extracted by acid hydrolysis, usually sulfuric acid hydrolysis, of cellulose fibers (Habibi et al. 2010). This procedure, apart from the challenges coming from the purification of the CNC also will lead to a high-viscosity product with high water content. For that reason the production of both CNC and CNF still requires from some cost optimization.

In this context other alternative ways to produce cellulose nanofibres, such as by combining oxalic acid and steam explosion (Deepa et al. 2011) and cellulose nanocrystals (i.e. sub-critical water (Novo et al. 2015) or ionic liquids (Abushammala et al. 2015)) have been developed. In addition, acetylation with nitric and acetic acid, along with mild alkali treatments, has been used already to extract cellulose from sisal fibres (Morán et al. 2007), and this cellulose was thereafter hydrolysed with sulphuric acid to extract cellulose nanocrystals.

Nanocellulose-based composites

There are several reports on the reinforcing effect of nanocellulose (CNF or CNC) on PLA (Siqueira et al. 2009; Eichhorn and Dufresne 2010; Kowalczyk et al. 2011; Fortunati et al. 2012b), with several different results reported in the literature. The reason for these discrepancies might be the large amount of parameters involved in the reinforcing effect, such as the quality of the reinforcement agent (i.e. aspect ratio), the dispersion of the nanoparticle in the matrix and the presence of aggregates, among others. Some reports, for instance, claim great reductions in tensile strength and the Young's modulus (Sanchez-Garcia and Lagaron 2010a), while others show small increases at low concentrations (Pei et al. 2010). Generally, though, the reinforcement of CNF is more pronounced at high temperatures (Jonoobi et al. 2010; Espino-Pérez et al. 2013), when the mechanical resistance of the polymer decreases dramatically.

The PLA has moderate barrier properties, it shows an OTR ranging from 11000 – 36000 mL µm m^{-2} day^{-1} at 23°C and different RH (relative humidities) (Chang et al. 2003; Yuniarto et al. 2014) and a

WVTR of 5250 g µm m^{-2} day^{-1} at 23°C and 90% RH (Tsuji et al. 2006) while the reference polymer for barrier properties, PET has an OTR of approximately 3000 – 4200 mL µm m^{-2} day^{-1} at 25°C (Johansson and Leufvén 1994) and WVTR values of around 420 g µm m^{2} day^{-1} at 23°C and 85% RH (Hoffmann 1998). In order for PLA to become an industrial alternative to PET, a significant reduction (approximately 85% reduction in OTR and 92% in WVTR) on permeability is therefore required.

The use of both types of nanocellulose (CNF and CNC) to enhance the barrier properties of PLA has also been reported previously, again with very different results. In the case of oxygen barrier properties, the best result is a decrease of 90% in oxygen permeability, which was achieved by using 1 wt% of CNC and PLA in dichloromethane via a freeze-drying technique (Sanchez-Garcia and Lagaron 2010a). There are also reports of moderate improvements in the oxygen barrier properties of PLA films (9%-43%) (Fortunati et al. 2012b), and finally there are some reports of PLA nanocomposites reinforced with CNC showing worse oxygen barrier properties than neat PLA (Espino-Pérez et al. 2013).

The water vapour barrier properties of PLA/nanocellulose composites reported in the literature also vary somewhat. For CNC, as an example, it was found a reduction of 82% in WVTR which was achieved by using 3 wt% of CNC and PLA in dichloromethane via a freeze-drying technique (Sanchez-Garcia and Lagaron 2010b), but in contrast a negligible reduction in WVTR for PLA after adding either 1% w/w or 5% w/w CNC was found (Fortunati et al. 2012b). In another example, a large increase (almost a three-fold increase when adding 15% CNC to PLA) for non-modified CNC on the WVTR was found (Espino-Pérez et al. 2013). In the case of cellulose nanofibres, CNF, it was found that the incorporation of non-modified CNF with PLA led to large increase on water sorption, however, the water sorption increase was reduced when the CNF was acetylated (Tingaut et al. 2010). Furthermore, it has been also reported that the reinforcement of PLA with acetylated CNF led to small variations in WVTR (Abdulkhani et al. 2014).

In addition, nanocellulose (CNF and CNC) has been reported to have nucleating agent behaviour and to enhance the crystallisation kinetics (Pei et al. 2010; Kose and Kondo 2013) of PLA. Finally, as long as the size of CNF is below the visible wavelength, if it is properly dispersed within the matrix the transparency of the films should not be affected. Actually, CNF-based nanopapers are reported to be transparent (Siró et al. 2011).

In any case, a key point for obtaining enhanced PLA/CNF nanocomposite properties involves achieving the excellent dispersion of nanoparticles in the polymer matrix. As long as the polymers are hydrophobic while the nanocellulose is hydrophilic, some strategies such as the use of

surfactants (Fortunati et al. 2012a) or grafting hydrophobic chains (Siqueira et al. 2010a) onto the nanocellulose are required, in order to achieve good dispersion. In this work a method to produce high-yield, acetylated CNF, by means of chemical methods, is developed. Due to the high yield and the acetylated nature of these nanoparticles, these approaches are very promising for enhancing the performance of PLA for food packaging applications, from both a technical and a financial point of view. In fact, the use of acetylated CNF to prepare PLA based composites has been already studied in the literature and although the both a acetylated and non-acetylated CNF showed similar mechanical properties (Jonoobi et al. 2012a) it was found that the acetylation of CNF was reducing the water sorption of composites (Tingaut et al. 2010) although no improvement on the WVTR was also observed (Abdulkhani et al. 2014).

Nanoclay-based composites

The use of nanoclay, which originates from different sources, such as montmorionite (Leszczyńska et al. 2007) and kaolin (Zaharia et al. 2015), in polymer nanocomposites has already been the subject of many studies (Rhim et al. 2009; Zaidi et al. 2009; Corrêa et al. 2011). Overall, the clay is surface-modified to increase its compatibility with the polymer matrix as well as to facilitate its dispersion (Fornes et al. 2004).

In this work commercially available clay, Cloisite C30B^{TM}, is used because it has been employed in several works to enhance the properties of PLA – with good results. The addition of this clay to PLA has led to an increase in the tensile modulus and impact strength of 13% and 27% respectively at 3% loading (Mohapatra et al. 2012), 63% the tensile modulus at 5% loading (Zaidi et al. 2009) and has decreased water vapour permeability by 40% at 5% loading (Duan et al. 2013).

Nanocellulose/nanoclay-reinforced composites

Such a combination of nanoclay and nanocellulose fibres was investigated in preparation of thin nanoclay/nanocellulose films. In one case, addition of 20 wt% of vermiculite to a CNF matrix led to a decrease in OTR of 86% at 50% RH and to a decrease of 94% at 80% RH(Aulin et al. 2012), while incorporation of 50 wt% of MNT to a CNF matrix resulted in a five-fold reduction in OTR at 95% RH(Liu et al. 2011). However, the combination of nanoclay and nanocellulose has also been investigated in composites, where poly(vinyl alcohol)/CNF-based composites showed increased thermomechanical properties, reduced strain at breaking and a decreased oxygen transmission rate above 30% RH (although they also showed increased water absorption) in line with increased clay content (Spoljaric et al. 2013). Furthermore, the replacement of 1 wt% of nanoclay with 1 wt% of CNC in a PLA/montmorillonite composite containing 5 wt% nanoclay led to an eight-fold increase in

strain at break for the composites (from 10.6% to 78.8%) (Arjmandi et al. 2015b). In a similar fashion the addition of CNC to the composite led to enhanced water absorption and different water diffusion, depending on the amount of CNC added (Arjmandi et al. 2015a). Finally, the combination of CNC and nanoclay has also been shown to lead to increased thermomechanical properties for PLA-grafted maleic acid composites (Hong and Kim 2013).

Crystallinity

As happens in other semi-crystalline polymers, PLA benefits from a high degree of crystallinity (Garlotta 2001). As such, it improves its barrier properties (Picard et al. 2011; Gorrasi et al. 2013) and mechanical properties (Perego et al. 1996; Suryanegara et al. 2009; Guinault et al. 2010) in line with increasing crystallinity, which consequently makes its slow crystallisation a challenge for promoting the material's industrial relevance. For this reason is not surprising that the crystallisation behaviour of PLA-based nanocomposites, such as PLA/CNF (Suryanegara et al. 2009) (which concluded that increased crystallinity lead to slightly increase on mechanical stability) and PLA/clay (Picard et al. 2011) (which concluded that increased crystallinity lead to decreased permeability), or even PLA-based composites with clay and banana fibres (Jandas et al. 2013) have already been the subject of some studies. Additionally, the impact of crystallinity on neat PLA's barrier properties (Siparsky et al. 1997; Cairncross et al. 2006; Cocca et al. 2011) and clay-based composites (Picard et al. 2011) has also been the subject of study. Nevertheless, the crystallinity of polymers is an exceptionally broad topic that usually has been reduced to the degree of crystallinity, whereas less attention has been paid to the influence of other parameters such as the so-called 'rigid amorphous fraction' (RAF), spherulite size, spherulite distribution or the difference between the two thermally-induced crystalline phases, namely the ordered α and the disordered α'. Traditionally, semicrystalline polymers were described as being constituted by two phases, one crystalline and one amorphous. However, there is intermediate nanophase present at the interface between the crystals and the surrounding melt (Wunderlich 2003), i.e. the aforementioned RAF, in contrast with the unconstrained phase, in which the mobile amorphous fraction (MAF) is found. Furthermore, traditionally it has been considered that crystalline PLA exhibits three polymorphic phases, α, β, γ and D/L stereocomplex (Lin et al. 2010). In general, the α form is the one that can be expected from solution casting or from melt compounding; however, it has been found that this α form exists in two different polymorphs (ordered "α" and disordered "α'") with different chain packaging (Zhang et al. 2008).

Due to the complexity of describing the crystalline morphology of PLA, it is not surprising that there are different reports regarding how crystallinity affects water sorption. A decrease in water sorption

with increased crystallinity (50% crystalline PLA showed approximately a 26% decrease in water sorption when compared with amorphous PLA) (Cairncross et al. 2006), the different behaviour of crystallinity on water sorption, depending on testing conditions (Siparsky et al. 1997), as well as increased water sorption in line with increased crystallinity (a 63% increase in water sorption when comparing samples crystallised at 170°C, 70% of crystallinity, when compared with samples crystallised at 70°C ,33% of crystallinity) (Koo et al. 2012) have already been reported. Regarding the effect of crystallinity on diffusion, there has also been reported a decrease of between 44% and 22% from amorphous to crystallised samples (Gorrasi et al. 2013), from different behaviour (ranging from negligible influence to a 92% increase in water diffusion), depending on the testing conditions (Siparsky et al. 1997). Finally, in relation to overall water barrier properties, a 52% decrease in the water vapour transmission rate (WVTR) of PLLA after 12.5 minutes of crystallisation at 140°C (Tsuji et al. 2006) has also been noted.

Although these results are related to water vapour transport, there are also different findings on the effect of crystallinity on oxygen transport through PLA films. While some reports claim a largely decreased (up to 85%) oxygen diffusion with approximately 60 minutes of crystallisation at 125°C (Drieskens et al. 2009) the opposite behaviour is also reported in other works (Courgneau et al. 2012) where a large increase in oxygen diffusion (approximately 50%) was observed when amorphous PLA was crystallized at 120°C. In addition, for poly(ethylene terephthalate) the RAF has been reported to have an increased oxygen solubility (0.203 – 0.119 cc(STP) cm^{-3} atm^{-1}) when compared with the MAF (0.095 cc(STP) cm^{-3} atm^{-1}).

The effect of crystallinity on the barrier properties of PLA is therefore still an open question, which becomes even more complex when nanocomposites are considered. Nanoparticles indeed might affect permeability in different ways, i) by directly increasing the tortuous path inside the polymer (Alexandre et al. 2009), ii) by means of crystallinity changes induced by their presence (Pei et al. 2010) and iii) through variations in the polymer chain's mobility which control penetrant diffusion in the matrix (Moore et al. 2004). Nonetheless, understanding such processes is of great interest, as it would greatly help in designing new and optimised composite materials based on this biodegradable polymer.

2. CNF extraction protocol

As the main objective of this PhD thesis is to prepare CNF-based composites, a procedure to obtain CNF is required initially. At the beginning of the present work (September 2012), to the best knowledge of the author, there was no reliable external supply of CNF, and so a procedure to produce it had to be developed. In the present chapter a protocol to obtain acetylated CNF via a combination of strong alkali and acetylation treatments, followed by soft mechanical treatments (magnetic stirring), is discussed.

In addition, the resulting pulp was hydrolysed with sulphuric acid to achieve cellulose nanocrystals (CNC). Furthermore, in order to prove extraction efficiency, apart from microscopies, where no aggregates were found and rheological characterisation, the extracted CNF was used to prepare highly transparent and clear films, which proved the efficiency of the procedure. Finally, the residues of the alkali treatments required to extract the CNF were reincorporated in the CNF films.

This work is based on the manuscript *Chemically Extracted Nanocellulose from Sisal Fibres by Employing a Simple and Industrially Relevant Process*, which can be found in Appendix 2.

2.1 Effect of chemical pre-treatments on sisal fibres

The protocol (Figure 2.1) consists of a sequence of chemical treatments: Strong multistep alkali treatments, which are responsible of swelling the fibers, a bleaching to remove the remaining lignin and an acetylation where acetate groups are grafted onto cellulose surface. Initially, the fibres were cleaned with NaOH 2 wt%, to remove oil residues and impurities. Thereafter, a strong alkali treatment of sisal (S) was performed (SM, B in Figure 2.1). The alkali treatment swells the fibres,

breaking the strong association, due to hydrogen bonds, between the cellulose chains and then opens up the structure to additional chemical treatments (Mwaikambo and Ansell 1999). After this treatment the fibres were light-brown in colour, which is attributed to the deposition of extracted lignin on their surface. The deposited lignin was removed in a bleaching step (SMB, C in Figure 2.1), and finally the influence of hydrogen bonds between the fibres was reduced through acetylation (SMBA, D in Figure 2.1). Thereafter, in the swollen state, OH groups from the cellulose nanofibres are grafted with acetate groups, thereby permanently reducing the energy required to break the strong association between the cellulose nanofibres in subsequent processing steps. The result of this sequence of chemical treatments was a pulp consisting mainly of modified micro-sized fibres which could easily be reduced to a low water content by filtration or decantation, and therefore would be easy to transport or store as a precursor for the later preparation of CNF dispersions. An aqueous dispersion of CNF with high nanofibre purity could be obtained directly from this intermediate by magnetic stirring (CNF, E in Figure 2.1).

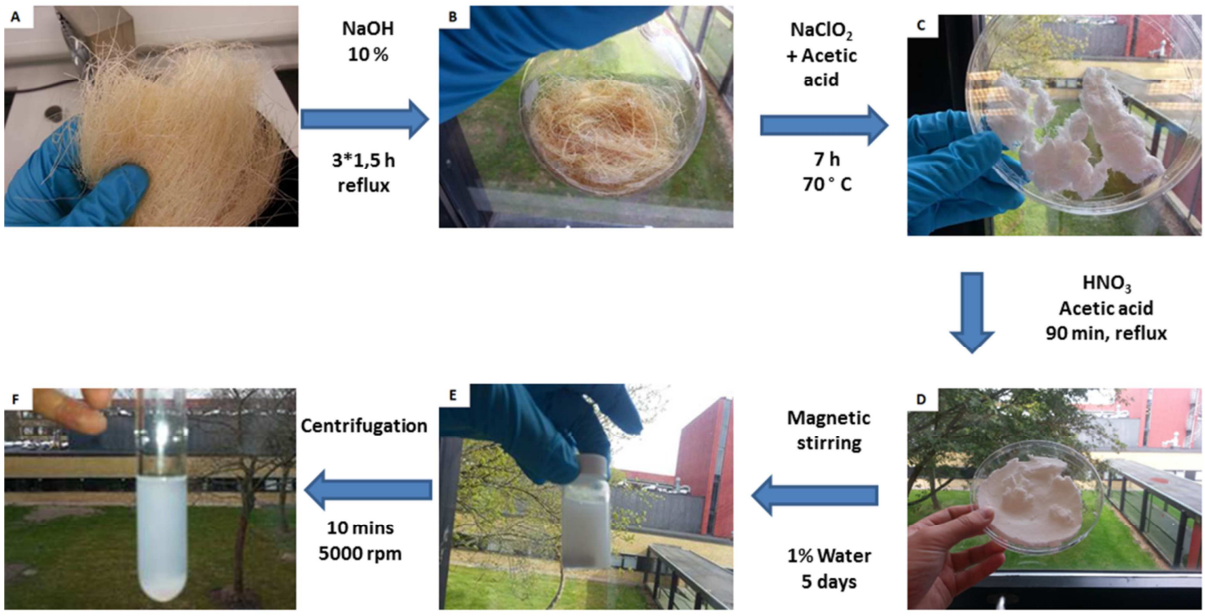

Figure 2.1 Overview of the CNF extraction protocol. A) Sisal fibres (S); B) Sisal fibres after alkali treatment (SM); C) Sisal fibres after mercerisation and bleaching (SMB); D) Sisal fibres after mercerisation, bleaching and acetylation (SMBA); E) SMBA after dispersion in water (CNF) and F) Stable CNF dispersion after centrifugation.

The yield of cellulosic material after each step of the extraction protocol is shown in Figure 2.2.

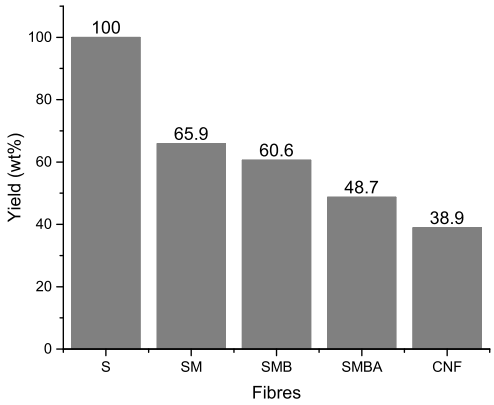

Figure 2.2 Mass yield of the treated fibres after drying a sample of the respective suspensions (dry basis).

Sisal fibres are generally reported to consist of about 60-70 wt% cellulose, 10-15 wt% hemicellulose and 8-12 wt% lignin (Bismarck et al. 2001; Mondragon et al. 2014). After all of the chemical treatments and purification steps, 39 wt% of the original sisal fibres were converted into a CNF dispersion, which corresponds to an extraction of approximately 60 wt% of the total amount of cellulose from the sisal fibres and sits in the higher range of recovery rates when compared with other reports in the literature (Wang and Cheng 2009; de Morais Teixeira et al. 2010; Tejado et al. 2012).

The isolated material was characterised by SEM after each step, in order to illustrate the effects of each of the treatments, as shown in Figure 2.3.

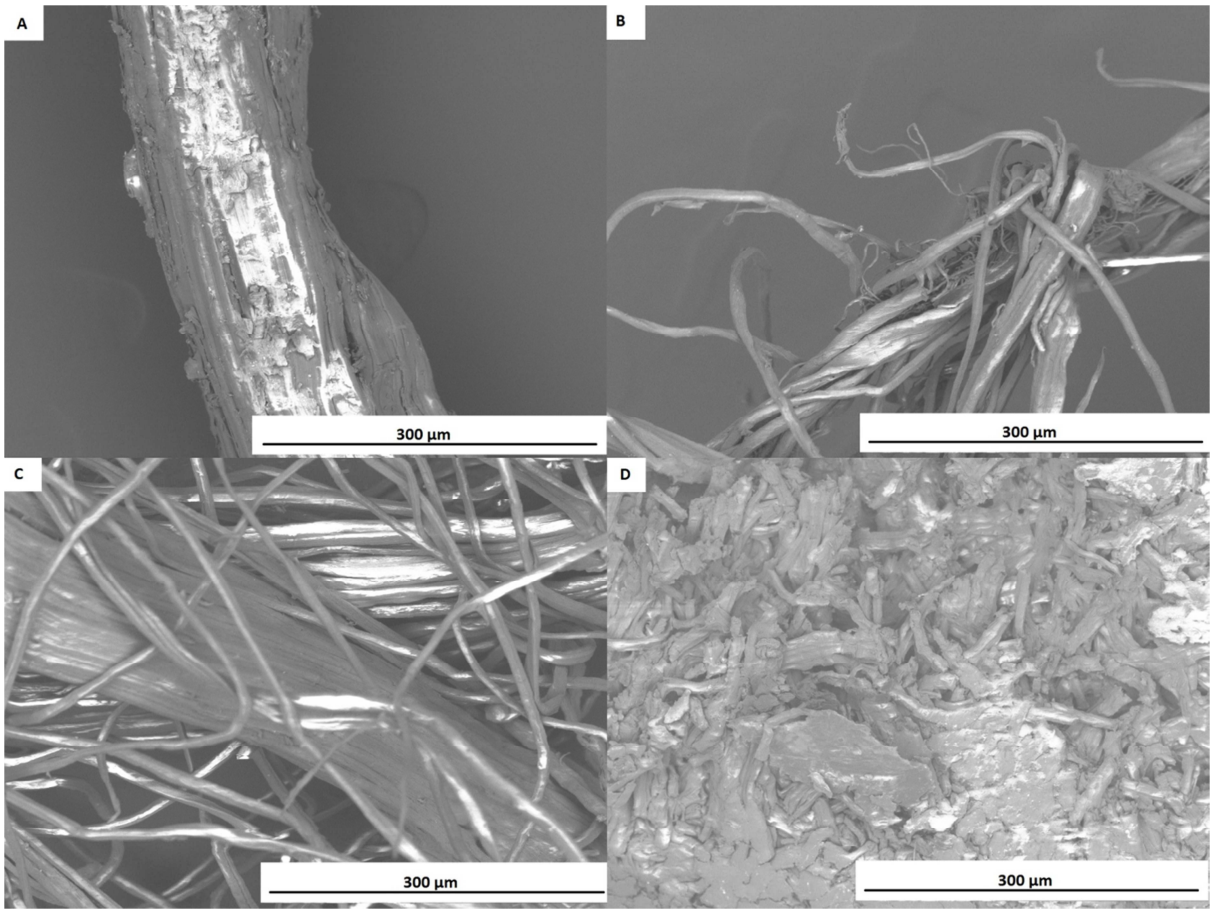

Figure 2.3 SEM pictures of the fibres at the various stages of the process, showing the transgression from large fibre bundles to the fully treated acetylated fibres in the final pulp. A) Sisal Fibers S, B) Alkali treated SM, C) Bleached fibers SMB, D) Acetylated pulp (SMBA).

The micrographs in Figure 2.3 show how each step in the process affects the fibres. The strong alkali treatment swells the fibres and results in the disruption of the large fibre bundles (SM). In the bleaching step even more individual fibres are produced (SMB), due to the removal of the remaining lignin, which reduces cohesion between the fibrils. Finally, it is notable how the acetylation step destroys the structure of the macroscopic fibres (SMBA), thereby resulting in the formation of a more uniform mass consisting of much smaller fibres.

The results of the extraction protocol in terms of chemical and thermal properties are shown by FTIR and TGA in Figure 2.4.

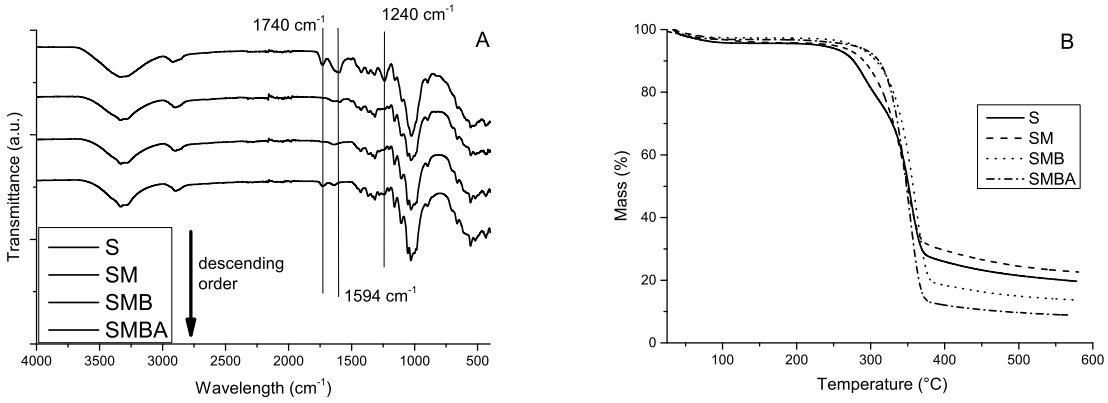

Figure 2.4. Analysis of the extracted CNF at each step in the process by FT-IR (A) and by TGA (B).

In Figure 2.4A, chemical changes to the fibres are observed by changes in the IR spectra. There is a significant removal of hemicellulose during the first alkali treatment from S to SM confirmed through the disappearance of the carbonyl stretching at 1740 cm^{-1} (acetyl and ester groups, characteristic of hemicellulose) and at 1240 cm^{-1} (C-O stretching vibration of the hemicellulose). In addition, the disappearance of the peak at 1594 cm^{-1} (related to the in-plane C-C in the plane symmetrical stretching of aromatic rings, characteristic of lignin) from SM to SMB shows that the majority of the lignin has been removed from the fibre. This is confirmed by the fact that the fibres are completely white after bleaching. The removal of a significant part of the hemicelluloses is corroborated by TGA in Figure 2.4B, where an increase in the onset of thermal degradation can be observed after both the alkali treatment and the bleaching step. The degradation of hemicellulose is usually seen in the range 200-400°C, where the mass loss of the sisal fibres is higher than for the other fibrous intermediates.

Finally, the acetylation of the pulp in the last step of the process is confirmed by the reappearance of the peak at 1740 cm^{-1}, attributed to new acetate groups. It was found that the alkali treatments removed not only lignin and hemicellulose, but also significant amounts of cellulose. The surface charge of the extracted CNF was investigated by conductimetry, which showed that the isolated CNF had no significant surface charge.

2.2 Effect of soft mechanical treatments on the acetylated pulp

The chemical treatments are not enough to extract the CNF from the fibers, soft mechanical treatments, such as magnetic stirring, are required to fully disperse the CNF in water. For this reason, the viscosity of a 4 wt% of acetylated pulp in water mixture was measured after 2 hours and

20 hours of magnetic stirring. Furthermore, the viscosity of both solutions was compared to that of commercially available CNF, as shown in Figure 2.5.

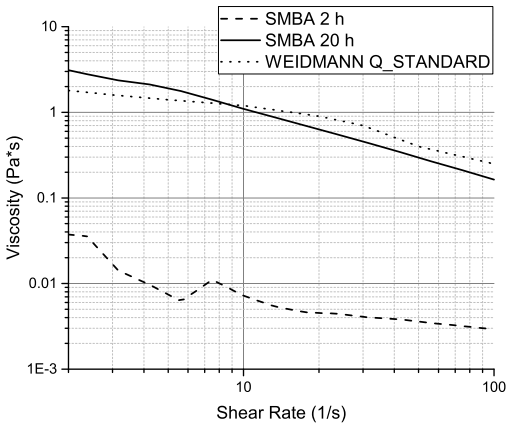

Figure 2.5 Viscosity of 4 wt% SMBA in water after magnetic stirring for 2 hours and 20 hours compared to a commercial CNF (Weidmann Q standard).

Viscosity increases dramatically between 2 and 20 hours of magnetic stirring, due to the nanofibrillation of the pulp, proving that it successfully disperses the CNF. Furthermore, it was observed that after 20 hours viscosity became so high that magnetic stirring was no longer powerful enough to stir the suspension efficiently. The viscosity of the resulting dispersion after 20 hours was similar to a commercially available CNF produced by Weidmann (Q standard).

As shown in Figure 2.5 the magnetic stirring successfully extract the CNF from the fibers, however, at 4 wt% the viscosity is too high for the magnetic stirring. For this reason, in further extraction procedures the concentration of pulp was decreased to 1 wt%. An aqueous solution of SMBA (1 wt%) was simply stirred for five days on a magnetic stirrer. Samples of this solution were analysed by optical microscopy after different stirring times, as shown in Figure 2.6.

Here, it can be seen how a very simple process like magnetic stirring breaks up the aggregates and ultimately results in the preparation of a stable aqueous dispersion of the nanofibres after 48 hours. After two days of magnetic stirring, it is no longer possible to see large fibres in the optical microscope, thus suggesting that the majority of them are on the nanoscale.

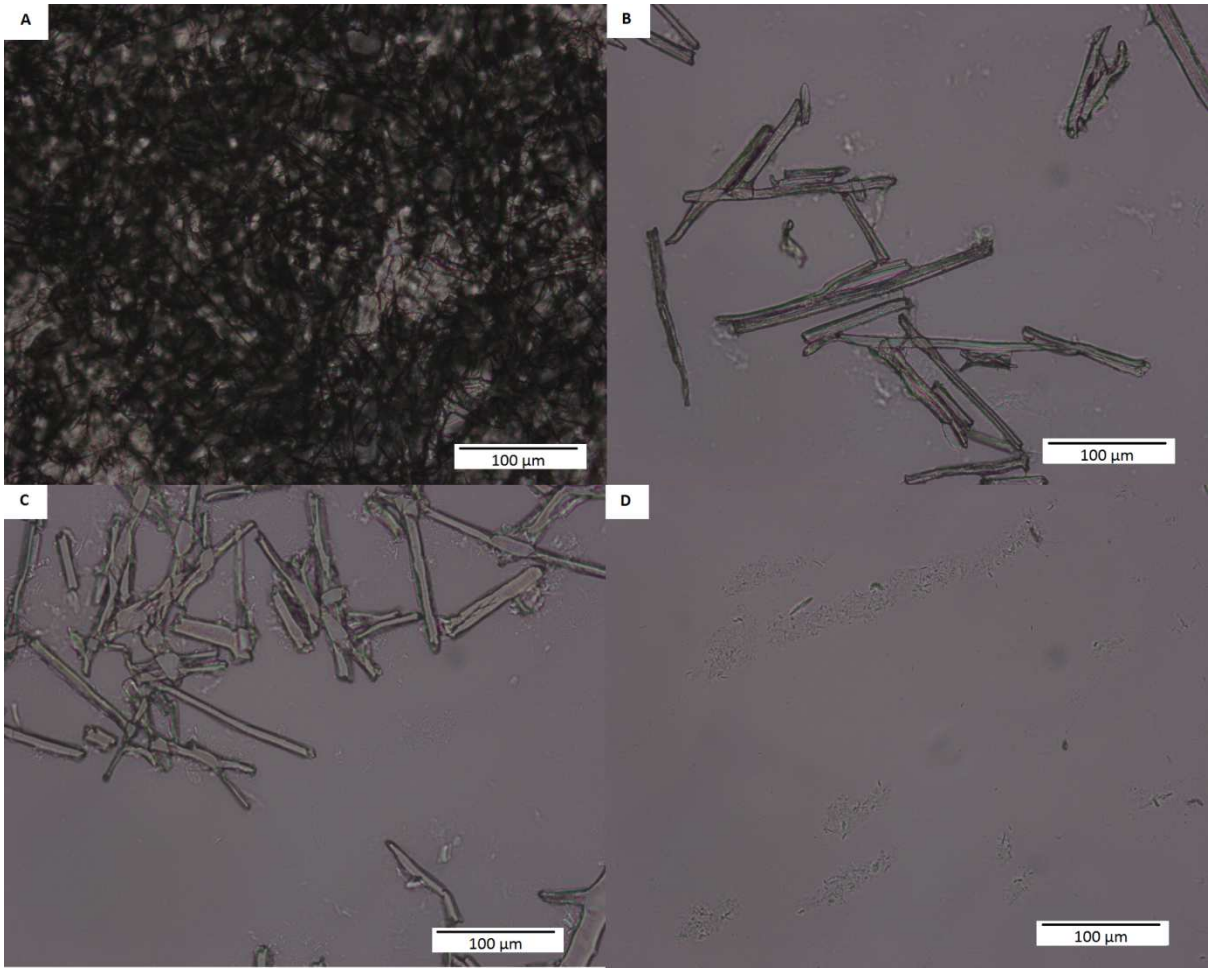

Figure 2.6 Optical micrographs of a 1wt% mixture of the acetylated pulp (SMBA) after magnetic stirring in water for 0 min (A), 15 min (B), 1 hour (C) and 48 hours (D).

Furthermore, the sizes of the cellulose nanofibres were additionally investigated using scanning electron microscopy (SEM) and transmission electron microscopy (TEM), as shown in Figure 2.7 and Figure 2.8.

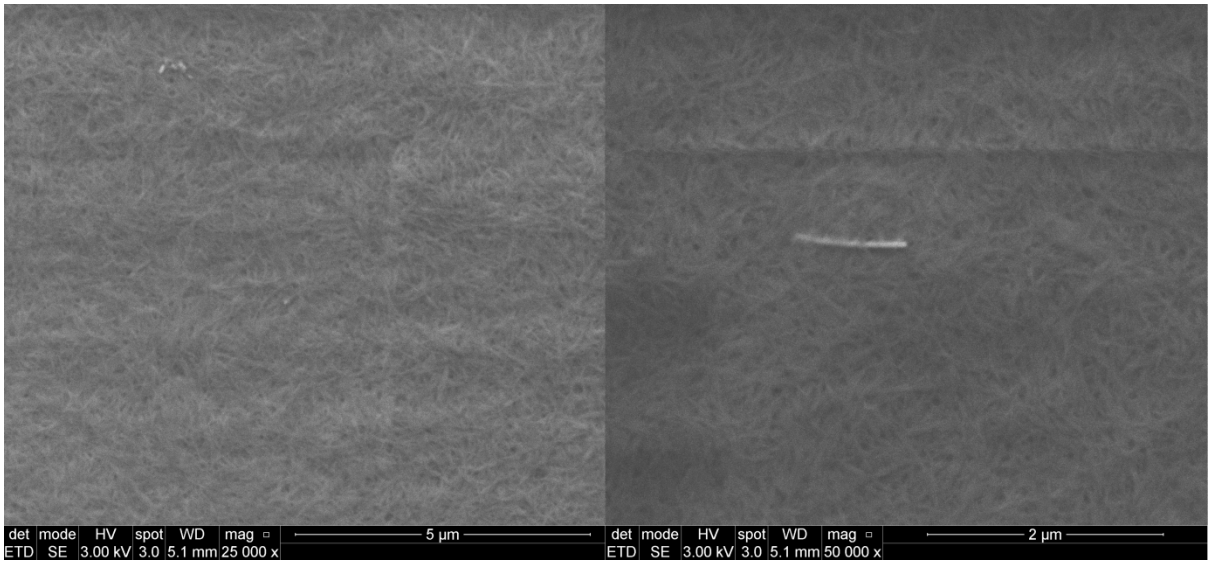

Figure 2.7 SEM micrographs of a cast drop of 0.6 wt% CNF dispersion on an aluminium film, resulting in the formation of a thin film with a thickness of around 100 nm.

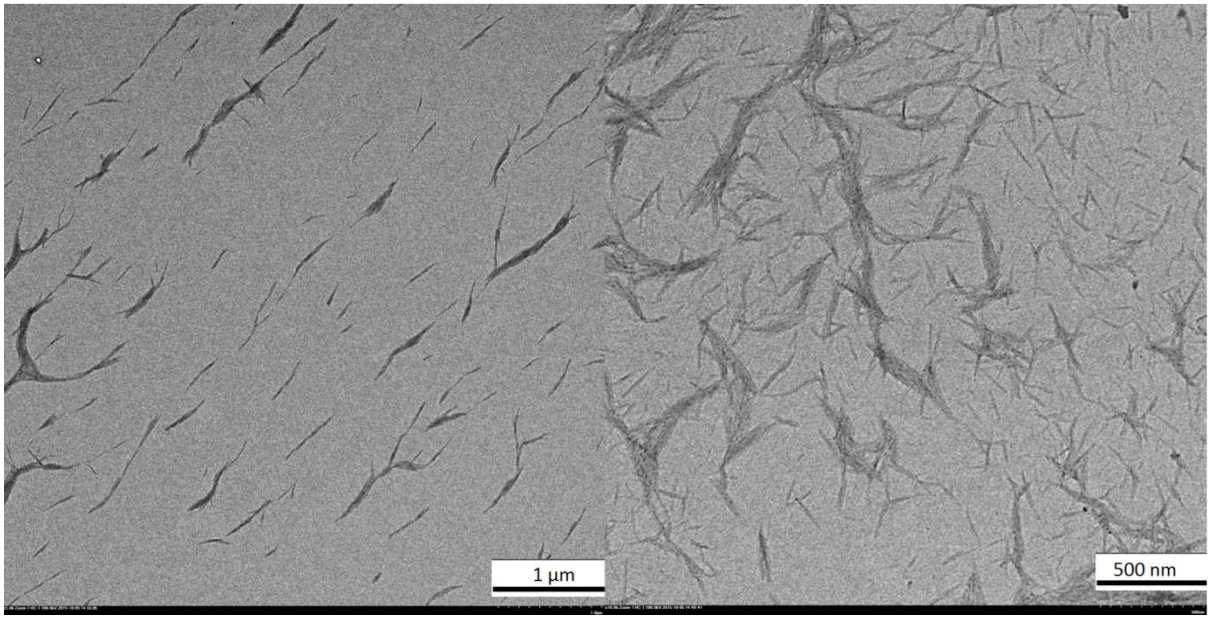

Figure 2.8 Analysis of the structure of the isolated CNF by TEM at different magnifications.

From both SEM and TEM it is clear that no large fibres are present in the film cast from the dispersion. The fibres are estimated to have a diameter of 27 +/- 13 nm and a length of 658 +/- 290 nm.

Cellulose nanofibre crystallinity was investigated by X-ray diffraction (XRD), as shown in Figure 2.9.

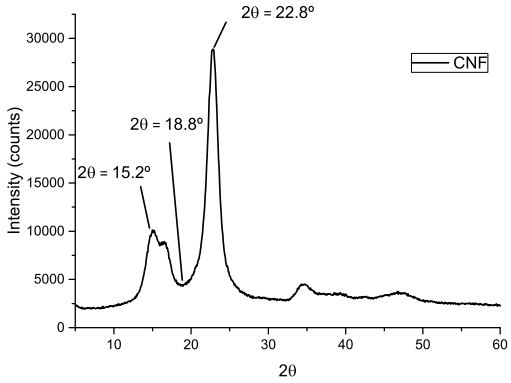

Figure 2.9 XRD pattern of the neat CNF.

The XRD spectra shows the expected peaks from a cellulose material with peaks at $2\theta=15.2^{o}$ and $2\theta=22.8^{o}$. The crystallinity index of the extracted fibres was calculated using the Buschle-Diller and Zeronian equation (Eq 2.1).

$$I_C = 1 - \frac{I_1}{I_2} \text{ (Eq 2.1)}$$

Where I_1 is the peak at $2\theta=18.8^{o}$ (amorphous peak) and I_2 is the peak at $2\theta=22.8^{o}$ (crystalline peak), I_c, the crystalline index, was determined to be 84%. This value is in the upper range of the crystallinity reported in the literature where similar crystallinities were observed for sisal-based CNF (93%)(Siqueira et al. 2010a), Luffa cylindrical fibres (90%)(Siqueira et al. 2010b) and for Tempo-oxidized CNF (TOCN) (59%-92%) (Saito and Isogai 2004).

The method used to determine the crystallinity of cellulose is based on the intensity of a crystalline and amorphous peak. The reason of choosing this method is because it is widely used and therefore allows an easy comparison of results even though it is known of overestimate the crystallinity index (Park et al. 2010)

2.3 Characterisation of neat CNF and CNF/residue films

To illustrate the purity of the CNF dispersion, it was used to prepare larger CNF-based films by solution casting either the pure CNF dispersion or a combination of the CNF dispersion and the extracted residues from the alkali treatments (65%CNF/35%Residue). The prepared films had high levels of clarity and good transparency, as shown in Figure 2.10.

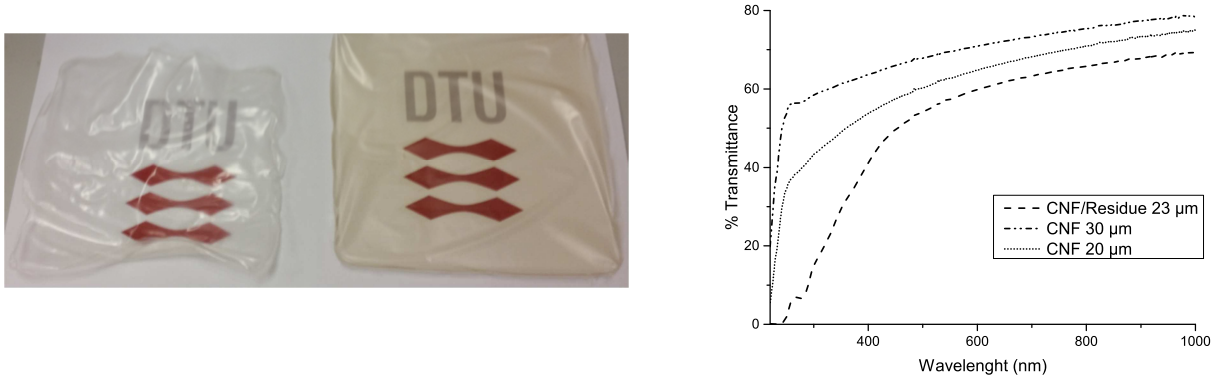

Figure 2.10 Left: Optical image of the prepared film (pure CNF on the left and CNF with the residue solution on the right); Right: Transmittance of the CNF films determined by UV-Vis spectroscopy.

Table 2.1: Optical properties of the films, determined by using a hazemeter.

	CNF	CNF/Residue
Transparency (%)	91.6 +/- 0.2	88.2 +/- 0.2
Haze (%)	26.7 +/- 0.4	36.2 +/- 1.3
Clarity (%)	69.8 +/- 1.2	44.6 +/- 1.8

The film prepared from the pure CNF was fully transparent, whereas the film with the added residues (extracted cellulose, lignin and hemicellulose from the mercerisation step) resulted in a light-brown but more uniform film. Adding the residue to the CNF film resulted in slightly reduced transparency and clarity at visible wavelengths, as well as in the increased haze of the thin films. While high haze makes the films useful for solar cell applications, a film with high clarity is interesting for other applications. Furthermore, CNF/residue film additionally has a decreased UV transmittance, due to the presence of lignin which acts as a UV absorber and as an antioxidant. Ultimately, these materials are intended for use as packaging materials, and for this application reduced UV transmittance as well as the antioxidative properties of the lignin look extremely promising with respect to the preservation of packaged food.

A cross-sectional view of the films by SEM can be seen in Figure 2.11.

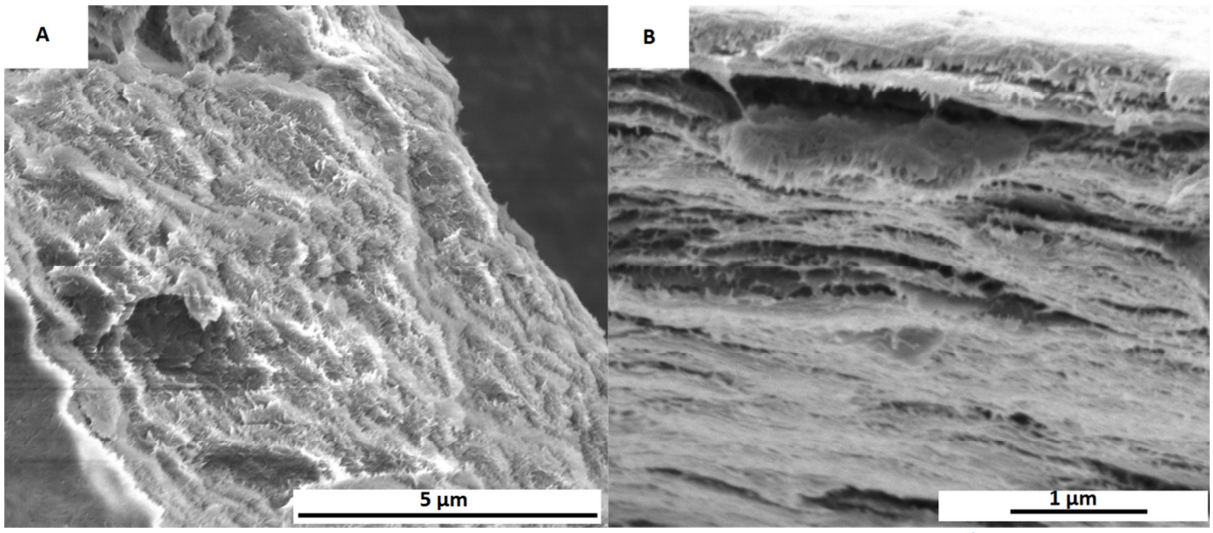

Figure 2.11. SEM analysis of the fractured cross-section of a) Neat CNF film and B) CNF/Residue film.

The SEM micrographs show that there are no large agglomerates on the fractured interphase from the films, thereby illustrating the high purity of the CNF dispersions. The micrographs also show clear differences in the layered structures of the two films, where the CNF/residue film is clearly much more compact compared to the pristine CNF film, which appears to have a more open structure. This feature of the CNF/Residue film is attributed to lignin in the residue, which is expected to result in the reduced swelling of the CNF during the drying stage, since the hydrophobicity of lignin films, apart from their brittleness, has been reported to have good properties at low relative humidity, though their barrier properties (Aulin et al. 2010; Minelli et al. 2010) dramatically decrease with increasing relative humidity.

For this reason, any process that might decrease water sorption would be very useful for new CNF film applications. The CNF nanomaterials prepared herein are acetylated, which could potentially affect water sorption, and the hydrophobicity of the lignin could enhance this behaviour. In an effort to investigate this notion, the advancing water contact angles of the prepared films were determined. Both films had comparable water contact angles of 49° +/- 3 for the CNF film and 52° +/- 1 for the CNF/Residue film, which is similar to other non-functionalised nanocellulose (41° (Rodionova et al. 2010), 50-60° (Siqueira et al. 2010a), 50° (Wu et al. 2014)). Apparently, acetylation does not significantly increase the hydrophobicity of thin films. The observed water sorption (Figure 2.12), approximately 2.6% at 23^{o}C and 50% RH (relative humidity) for both types of films, was reduced compared to other nanocellulose films, where CNF and nanocrystalline cellulose have been shown to have water sorption rates of 6.5% at 25°C and 50% RH (Belbekhouche et al. 2011), or 4% at 35°C and 50% RH for enzymatically pre-treated CNF (Minelli et al. 2010).

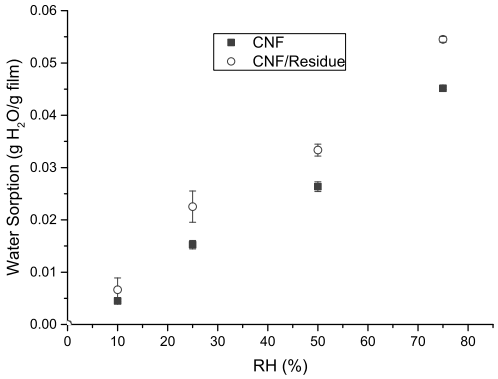

Figure 2.12 Water sorption of neat CNF and CNF/Residue film measured at 23°C.

Finally, the mechanical properties of the film were characterised (Table 2.2), and the CNF film showed inferior mechanical properties, probably due to its unevenness as well as to the presence of functional groups which could prevent the formation of effective hydrogen bonding between nanofibres. However, the CNF/residue film showed much greater mechanical behaviour, proving that the residue was effectively plasticising the film.

Table 2.2: Mechanical properties of the CNF Films.

	Stress (MPa)	Elongation (%)	E (GPa)
CNF	24.7 +/- 6.2	1.2 +/- 0.0	2.4 +/- 0.1
CNF/Residue	42.6 +/- 4.5	2.6 +/- 0.3	1.8 +/- 0.0

2.4 Extraction of CNC

Apart from the CNF, CNC was also extracted from sisal fibres with the aim of comparing both nanoparticles as reinforcing agent for PLA. In the present case, CNC was extracted by sulphuric acid hydrolysis (32 wt%, 45°C, 2 h) followed by dialysis, from SMBA. CNC samples were evaluated by SEM, FT-IR and XRD.

In Figure 2.13 the SEM micrograph of a CNC film is shown where it can be seen how the CNC are not as debundled as they CNF were. In addition it was found that the CNC formed non-transparent, white films.

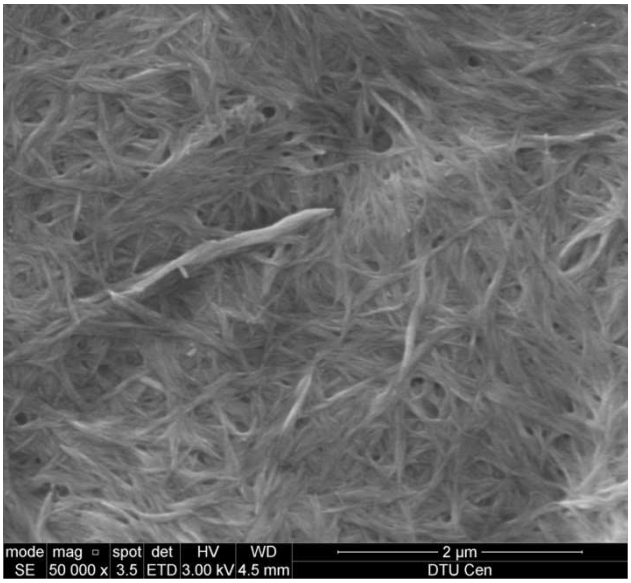

Figure 2.13 CNC characterisation by scanning electron microscopy.

In Figure 2.14A the FTIR spectra of CNC can be observed while in Figure 2.14B the XRD pattern of the CNC is shown.

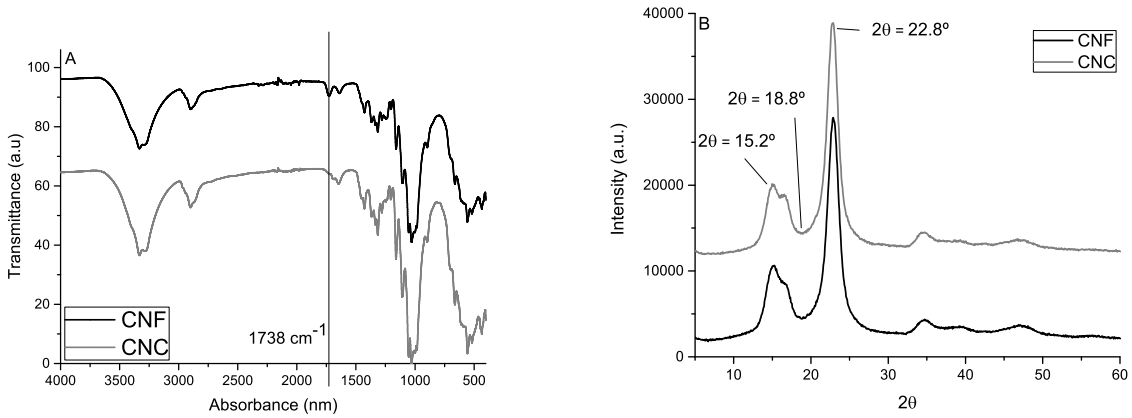

Figure 2.14 Analysis of the CNC (CNF as reference): A) FTIR spectroscopy. B) XRD pattern.

From Figure 2.14A it can be seen how while CNF shows a peak at 1740 cm^{-1} this peak is absent on CNC, meaning that the acetyl groups of the CNF were removed by the acid hydrolysis. In addition, from the XRD pattern a similar crystallinity index was calculated for both CNF (84%) and CNC (85%). This is attributed to the fact that CNF had been already submitted to harsh treatment, which in turn affected the amorphous cellulose.

2.5 Cellulose nanofibres or cellulose nanocrystals?

The cellulose nanofibres showed a high crystallinity index (84%) and a small aspect ratio (length = 658.3 +/- 290.6, diameter = 27.1 +/- 13.5, L/D = 24.28); this relatively low aspect ratio is more likely to correspond to nanocrystalline cellulose. However, in the present work this nanomaterial has been considered as cellulose nanofibres, because a certain amount of mechanical treatment was still required to extract and individualise the cellulose nanofibres. Furthermore, the high crystallinity index can be explained due to the fact that the used method, the peak intensity method was used – and this method is known for overestimation (Park et al. 2010).

2.6 Advantages of the procedure

In this study an efficient protocol to extract and individualise a high yield of CNF, with several advantages compared to others, is presented. First, the result from chemical processing is a pulp which can be easily filtrated or decanted and allows for easy cleaning or liquid exchange. Second, this pulp after acetylation does not form hydrogels, so its water content can be easily reduced, thus resulting in a reduction in transportation costs. Third, the chemicals used in the process are very common and not especially expensive. Moreover, these chemicals could be reclaimed in the process, and lignin and hemicellulose could be recuperated as by-products. Fourth, magnetic stirring is likely to be a low-energy consumption technique and it is likely that it could be easily substituted by an industrially-relevant procedure. Fifth, the yield of acetylated pulp is 39%, while sisal fibres usually contain 60-70% of cellulose, and so a large amount of cellulose is recovered as CNF. Sixth, the CNFs are acetylated, which means that they are potentially easier to disperse in a polymer matrix; furthermore, they showed reduced water sorption. Seventh, this method leads to a high yield of nanocellulose fibres, with no large aggregates present, as illustrated in the high-transparency films.

Consequently, it can be concluded that this procedure is potentially industrially relevant. However, significant optimisation of reaction times and mechanical treatments should be done before stepping any closer to the industrial production of these CNFs.

3. Performance of CNF as a reinforcement for PLA: A comparison with neat PLA, C30B and CNC

In this chapter, the acetylated CNF as well as the CNC obtained in Chapter 2 will be used to reinforce PLA. Due to its high crystalinity index, high purity (understood as low amount of aggregates) and acetylated nature, CNF extracted from alkali-acetylation treatment showed great potential for reinforcing PLA. Therefore, in this chapter, PLA/CNF composites are presented, and their performance as food packaging films will be evaluated. This evaluation will focus on areas which, to my understanding, are more critical for PLA, namely barrier and thermomechanical properties as well as optical transparency, and the comparison will be focused on low concentration composites. Furthermore, apart from using neat PLA as a reference material, the performance of CNF will be compared with C30B and CNC, which are considered potential alternatives for this application.

This work is based on the journal article *A Comparison of Partially Acetylated Nanocellulose, Nanocrystalline Cellulose and Nanoclay as Fillers for High-Performance Polylactide Nanocomposites*, published in *Journal of Applied Polymer Science* in December 2015, which can be found in Appendix 3. Relevant information about composite preparation, processing and optimisation can be found in Appendix 1.

3.1 Nanocomposite characterization

PLA composites with 1%, 3% or 5% of CNF, CNC or C30B were prepared by using an optimised protocol for each nanomaterial (illustrated in Appendix I). To assess the suitability of each nanoparticle as a reinforcing agent, the performance of nanocomposites on four of the most

important food packaging properties (barrier, mechanical and thermomechanical properties as well as transparency) was evaluated. In order to make a fair comparison of all of the particles, firstly a dispersion study was performed. The goal was to compare well-dispersed clay with well-dispersed nanocellulose.

In the Figure 3.1, SEM images of PLA/CNF and PLA/CNC nanocomposites are shown, and it is notable that no large aggregates within the matrix can be observed for any of the nanocellulose entities. Furthermore, some individualised CNF and CNC can be observed, proving that the CNF was successfully dispersed within the matrix.

In general, relatively minor differences could be observed between CNF and CNC, although the CNF is acetylated. This effect is attributed to the fact that DMF is a very good solvent for the nanocellulose (both nanoparticles formed stable dispersion at 1 wt% concentration on DMF), and therefore the compatibilising effect of the acetate groups is reduced.

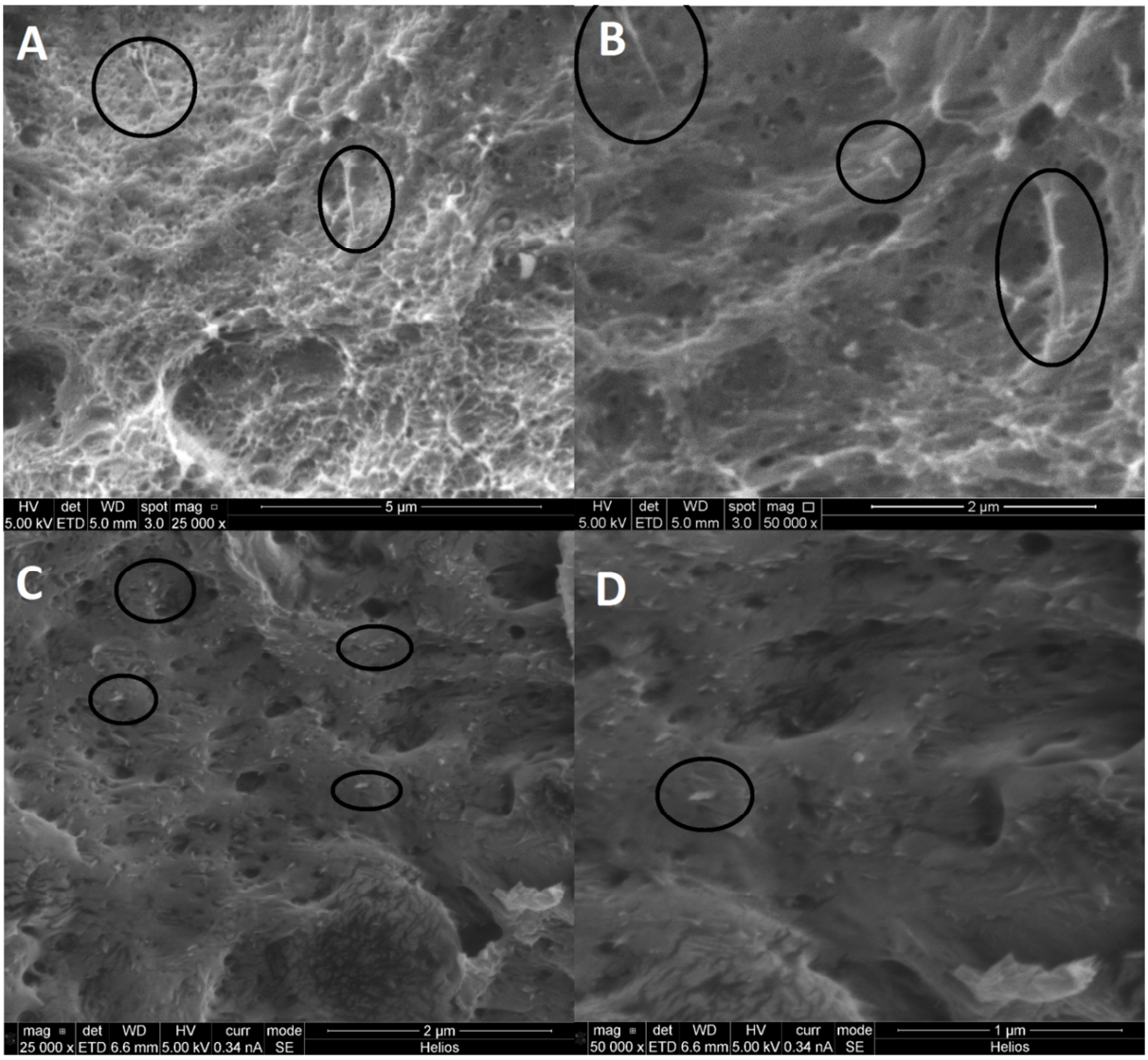

Figure 3.1 Cross-section of PLA/CNF nanocomposites (up) and PLA/CNC nanocomposites (down).

The C30B dispersion was further investigated by XRD and TEM. From the XRD pattern (Figure 3.2) it can be observed how the peak at $2\theta = 4.75°$, which corresponds to the d-spacing of the clay and is present in neat C30B, almost disappears in the case of nanocomposites. The absence of a peak means there is not a constant distance between the clay platelets, which suggests that there are no large aggregates of clay, therefore suggesting that there is a good distribution of clay within the matrix. Moreover, from the TEM images (some representative images can be found in Figure 3.3) no evidence of large aggregates was found, thus suggesting that the clay is well dispersed.

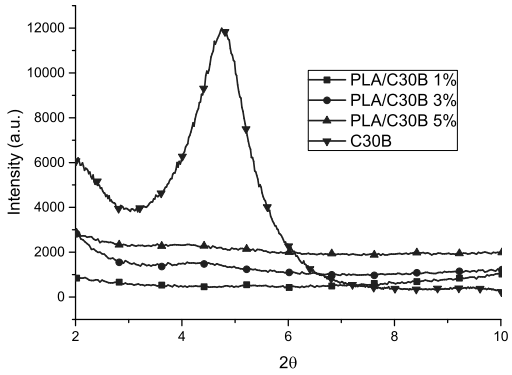

Figure 3.2 XRD pattern of neat C30B and C30B-based nanocomposites.

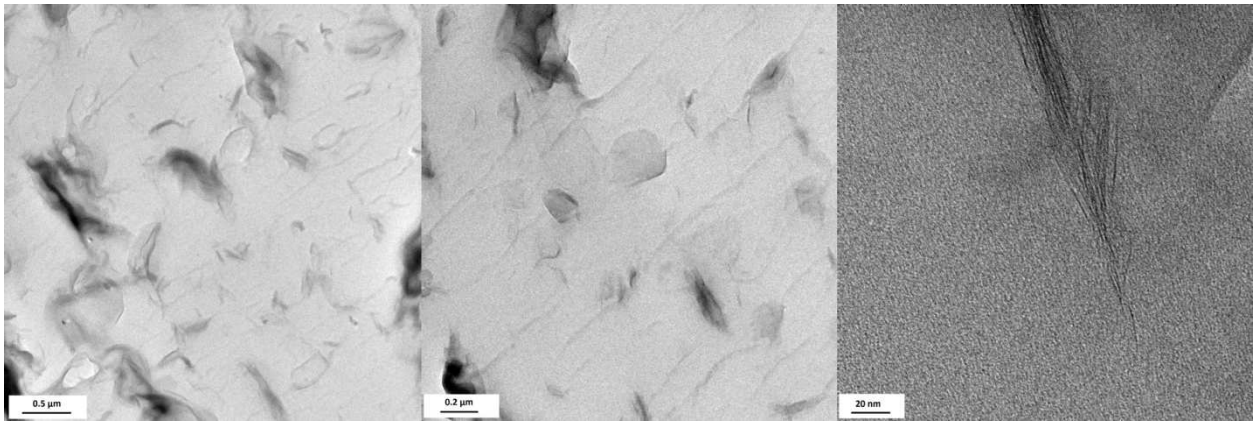

Figure 3.3 TEM of PLA/C30B 5% nanocomposite.

Accordingly, no large aggregates were found in any of the dispersion studies, and so it can be concluded that all of the composites showed reasonable dispersion, which allows for a direct comparison to be made between them.

Apart from nanoparticle dispersion, polymer crystallinity is also reported to play an important role in determining mechanical and barrier properties (Suryanegara et al. 2009; Picard et al. 2011). Thus, describing the crystallinity of the nanocomposites is critical in terms of drawing conclusions about their properties. Nevertheless, crystallinity is a very complex phenomenon, and an accurate description in this regard might exceed the scope of this work. For this reason, in this chapter only, a basic study of crystallinity will be presented, i.e. the degree of crystallinity, which, in general, is the only crystallinity characterisation procedure used in nanocomposite studies.

In general, all of the nanocomposites showed a higher degree of crystallinity than neat PLA, but they also showed similar degrees of crystallinity, thereby suggesting that nanocomposites are suitable for comparison. In addition, no significant changes were observed in T_g or T_m.

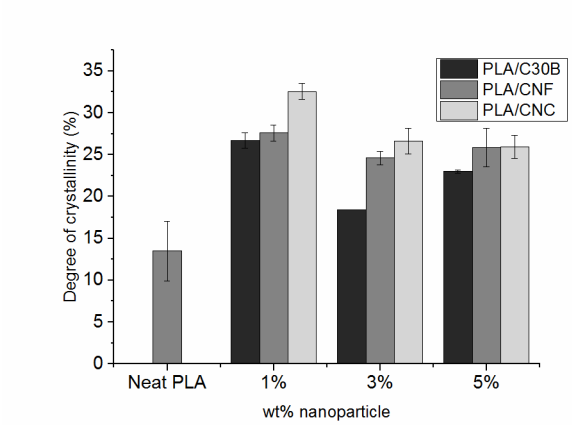

Figure 3.4 Degree of crystallinity of the nanocomposites (from the 1st heating cycle). A melting enthalpy of 93 J g^{-1} was considered for 100% crystalline PLA.

3.2 Evaluation of the performance of the composites as food packaging materials

The transparency of the nanocomposites has not been studied as widely as other properties, such as mechanical or thermomechanical, although they are indeed relevant for certain food packaging applications such as films. In many of these cases, the industry requires transparent and colourless films – an opaque film will not allow the customer to see the food, making it less likely that the consumer will buy it.

In Figure 3.5, the UV-Vis spectra of the nanocomposites are shown.

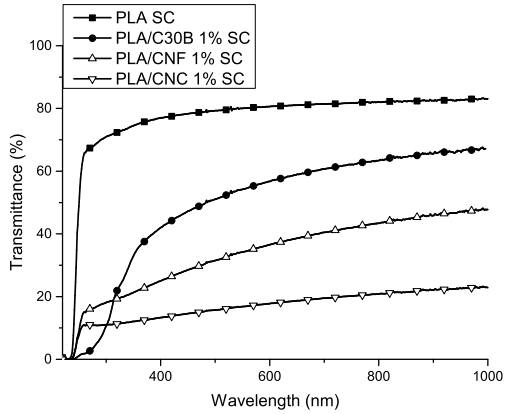

Figure 3.5 Optical transmittance of the nanocomposites (%wt).

The addition of nanoparticles slightly decreases the transparency of the films; however, part of this decrease could be ascribed to the increased degree of crystallinity of the composites compared with neat PLA. Indeed, the crystalline domains show a different refraction index, which causes opacity. When evaluating the performance of the nanoparticles it can be seen how clay led to more transparent films; moreover, it shows a significant reduction in the transmittance of UV radiation,

which is an interesting feature since the UV light can enhance the degradation of food. Finally, CNF showed increased transparency when compared with CNC.

In Figure 3.6, the OTR at 23°C and 50% RH (relative humidity), as well as the WVTR at 23°C and 50% RH of the neat PLA and its nanocomposites, can be found. Generally the permeability results for PLA and PLA/C30B-based nanocomposites were comparable to those found in the literature, either for WVTR (Żenkiewicz and Richert 2008) or for OTR (Sanchez-Garcia and Lagaron 2010a; Najafi et al. 2012).

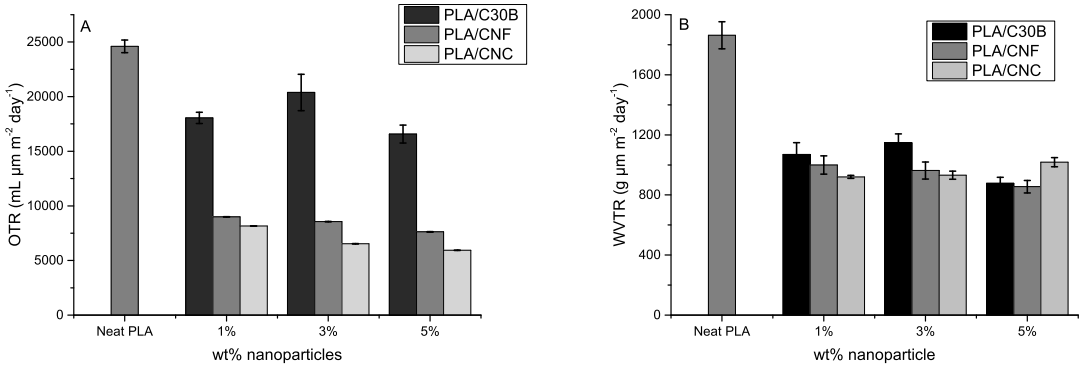

Figure 3.6 OTR and WVTR of PLA and nanocomposites at 23°C and 50% RH.

As can be observed in Figure 3.6A, all of the nanocomposites showed better barrier properties than the neat PLA, which could be partially attributed to the fact that the composites exhibited a higher degree of crystallinity than the neat PLA. Surprisingly, nanocellulose-based composites showed lower oxygen transmission rates than nanoclay-based composites, even though they had a similar degree of crystallinity. Furthermore, in Figure 3.6B, it can also be seen how the composites show a clear reduction in the WVTR when compared with neat PLA. In this case it is evident that all three nanoparticles show similar behaviour. This is likely to be ascribed to nanoparticle hydrophilicity; as long as C30B is highly hydrophobic, it is likely to be more effective in reducing the water vapour transmission rate than oxygen transmission rate, while the hydrophilicity of both CNF and CNC makes them less effective reducing the WVTR.

Mechanical properties are critical for food packaging applications, since the packaging has to protect food from damage throughout the entire supply chain. Mechanical tests were performed for PLA and its nanocomposites to check the effect of each of the nanoparticles on mechanical properties as shown in Table 3.1, and the values for PLA were in the range of other reports (Courgneau et al. 2011; Kowalczyk et al. 2011).

Table 3.1 Mechanical properties of PLA and nanocomposites (%wt)[a]

			PLA/C30B		
		0	1%	3%	5%
E	(GPa)	2.4 +/- 0.3	2.1 +/- 0.2	2.3 +/- 0.1	2.5 +/- 0.1
σ	(MPa)	55 +/- 2	51 +/- 0.7	51 +/- 2.8	54 +/- 2
ε	%	3.9 +/- 0.2	3.8 +/- 0.4	3.6 +/- 0.2	3.4 +/- 0.1
			PLA/CNF		
		0	1%	3%	5%
E	(GPa)	2.4 +/- 0.3	2.3 +/- 0.1	2.9 +/- 0.1	2.8 +/- 0.1
σ	(MPa)	55 +/- 2	60 +/- 1.0	60 +/- 3.2	64 +/- 3.2
ε	%	3.9 +/- 0.2	4.2 +/- 0.1	3.5 +/- 0.2	3.7 +/- 0.2
			PLA/CNC		
		0	1%	3%	5%
E	(GPa)	2.4 +/- 0.3	2.3 +/- 0.2	2.5 +/- 0.1	2.6 +/- 0.1
σ	(MPa)	55 +/- 2	59 +/- 2.9	57 +/- 2.2	51 +/- 1.6
ε	%	3.9 +/- 0.2	4.1 +/- 0.3	3.5 +/- 0.1	3.1 +/- 0.2

a) E is the Young's modulus in GPa, ε strain at breaking (%) and σ tensile stress MPa.

In this work it was found that, as a general rule, the addition of nanoparticles did not affect dramatically the mechanical properties of the nanocomposites; nonetheless, PLA/CNF composites showed slightly better performance than the other nanocomposites. The PLA/CNF 1% nanocomposite showed a 10% improvement in terms of elongation and tensile stress and a 5% loss on the Young's modulus.

Thermomechanical resistance was investigated by DMA, as shown in Figure 3.7.

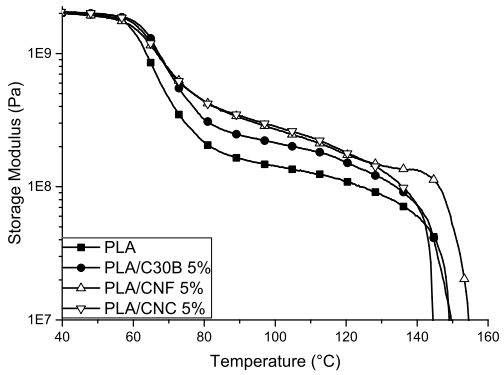

Figure 3.7 DMA of PLA, PLA/C30B 5%, PLA/CNF 5% and PLA/CNC 5% composites (%wt).

Low thermomechanical stability means that the thermoforming of PLA remains a challenge for the industry. Moreover, there are a number of food applications that require higher PLA thermal stability, such as disposable glasses for hot drinks.

As evidenced in Figure 3.7, there is a clear improvement in the thermomechanical properties of PLA and the nanocomposites when surpassing the T_g of PLA. After this point, the mechanical properties of the neat PLA decreases very rapidly, whereas the nanoparticles offer greater resistance, with this being more pronounced for CNF than for C30B. This can be attributed to the fact that nanocellulose can make stronger percolated networks, while the reinforcement of clay – due to the stress transfer mechanism – is not as effective. There is little difference between the effect of CNF and CNC, though, probably because CNF is expected to be better dispersed; CNC can form stronger percolated networks due to stronger hydrogen-bonding interactions between rods.

3.3 Summary

The performance of CNF as a reinforcing agent for PLA in films for food packaging applications was evaluated by comparing the performance of PLA/CNF composites with neat PLA, PLA/C30B and PLA/CNC.

It was found that the addition of even moderate amounts, such as 1% of CNF to PLA, significantly enhanced oxygen and water vapour barrier properties as well as thermomechanical properties, and it slightly increased mechanical properties compared to PLA, without affecting transparency to any great extent. When comparing CNF with CNC, it was observed that both nanocellulose-based materials exhibited similar performance, except for the fact that the PLA/CNC composites showed inferior transparency. On the other hand, when compared with PLA/C30B composites, apart from their bio-based and biodegradable behaviour the PLA/CNF composites showed superior oxygen and thermomechanical properties. Therefore, it can be concluded that the PLA/CNF nanocomposite is a promising bio-based and biodegradable material for food packaging applications.

4. Synergetic behaviour when combining nanocellulose and nanoclay in a polymer matrix

In the previous chapter, it was established that the addition of CNF to PLA, even in quantities as low as 1%, led to a significant improvement in barrier and thermomechanical properties; however, the further addition of CNF did not lead to any additional improvement in properties. This finding is relevant, since regardless of the improvement in terms of barrier properties, a larger increase is still required, in order to challenge PET, as mentioned in the introduction, approximately a 85% reduction on the OTR and a 92% reduction on the WVTR will still be needed.

In the present chapter, both nanocellulose and nanoclay were used as reinforcing agents for PLA, and the effect of combining both nanoparticles were studied. In the present work, C30B was added to PLA/CNF-based composites, to evaluate if the addition of different nanoparticles would show synergetic behaviour, because if this were the case, the resulting hybrid composite would be much closer to the technical requirements of food packaging.

This work is based on the journal article *Hybrid poly (lactic acid)/nanocellulose/nanoclay composites with synergistically enhanced barrier properties and improved thermomechanical resistance*, accepted for publication in *Polymer International* on May 2016. The manuscript can be found in Appendix 4. Relevant information about composite preparation, processing and measure optimisation can be found in Appendix 1.

4.1 Nanocomposite characterization

The dispersion of nanocellulose and nanoclay in the composites was evaluated by SEM of the cross-sectional views of the fractured films, as shown in Figure 4.1. Composites with the highest CNF content and the lowest C30B content (5wt%-1wt%) were chosen to evaluate the dispersion of CNF, while composites with the lowest CNF content and highest C30B content (1wt%-5wt%) were chosen to evaluate clay dispersion.

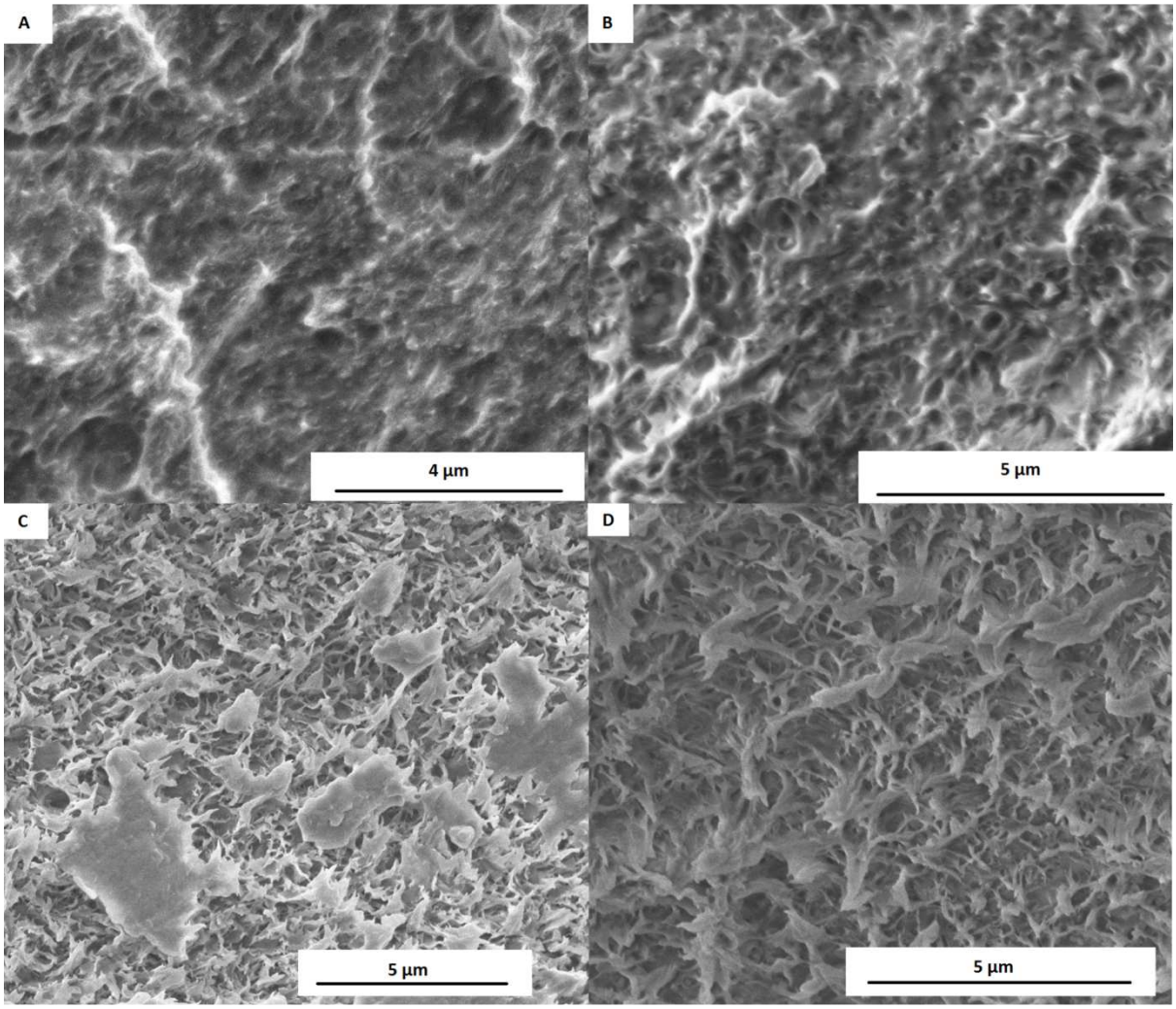

Figure 4.1 SEM of the cross-section of the fractured nanocomposites. A) PLA/CNF 5 wt%/C30B 1 wt%; B) PLA/CNC 5 wt%/C30B 1 wt%. C) PLA/CNF 1 wt%/C30B 5 wt%; D) PLA/CNC 1 wt%/C30B 5 wt%.

The cross-sectional views of the fractured surfaces at high nanocellulose (CNF and CNC) loading (Figure 4.1A and Figure 4.1B) show homogeneous samples without any large aggregates of CNF or CNC, thereby confirming the good dispersion of nanocellulose in the composites. Both composites with high nanoclay content (Figure 4.1C and Figure 4.1D) show a significantly different fractured interface compared to the nanofibres, where the platelet structure of the nanoclays is clearly visible. Additionally, the nanoclays are not as well dispersed as the nanocellulose, as can be seen from the

small aggregates of up to 5 µm in size for the CNF composite, whereas the CNC composite exhibits a more homogeneous fracture surface. Considering the high content of nanoclay in these samples, some aggregates would be expected on a fractured surface, as the fracture occurs at the weakest point of the film. The effective dispersion of the nanoclay at the nanoscale was investigated further by XRD and TEM, as shown in Figure 4.2.

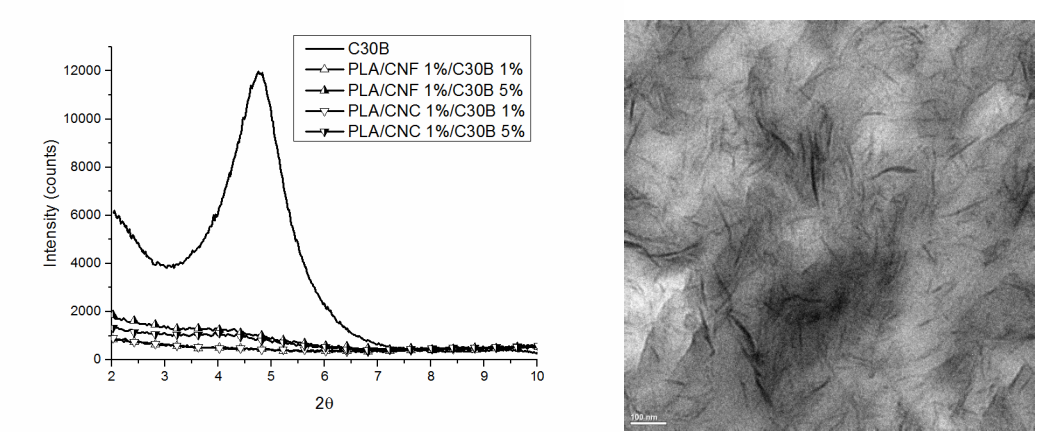

Figure 4.2 Left: XRD pattern of PLA/CNF/C30B and PLA/CNC/C30B composites (%wt) and neat C30B. Right: TEM of PLA/CNF 1 wt%/C30B 3 wt%.

As can be seen from the XRD in Figure 4.2 (left), the neat C30B (powder) exhibits a clear diffraction peak at around $2\theta = 4.75°$, which corresponds to the d-spacing of the platelets within the clay. This strong diffraction peak from aggregated nanoclay is not observed for the hybrid composites, illustrating that the nanoclay platelets were separated during processing and that the nanoclay in the composites, to a great extent, is fully exfoliated at low nanoclay loading. This could also result from dilution, but the samples with a high loading of nanoclay only show a very minor peak as an indication of the presence of small amounts of intercalated nanoclay. This was also seen from the TEM of a microtomed composite Figure 4.2 (right). Here, the nanoclay can be seen to be both intercalated (black lines) and exfoliated. In combination with the SEM micrographs from above, it shows that the nanoparticles are generally well dispersed with only a few small aggregates.

As mentioned above, an important parameter in barrier properties is the crystallinity of different materials, and so a degree of crystallinity was obtained for all the composites, with all of the samples evaluated by DSC, as shown in Figure 4.3.

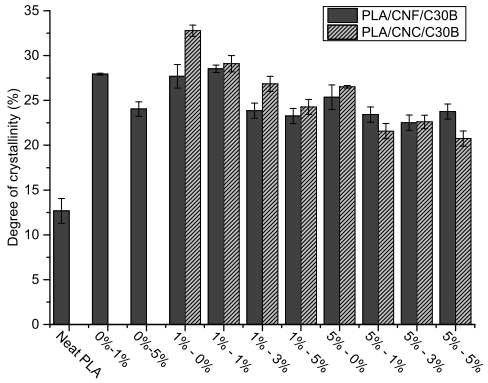

Figure 4.3 Degree of crystallinity of the hybrid nanocomposites.

It can be seen from Figure 4.3 that the addition of nanoclay or nanocellulose to the PLA results in a significant increase in crystallinity as expected. The crystallinity of the composites is seen to decrease with a higher loading of nanoparticle. However, the crystallinities are considered similar for all the hybrid composites with above 1 wt% nanocellulose and 1 wt% nanoclay. Moreover, no relevant changes in T_g or T_m were observed in any of the composites.

4.2 Evaluation of the performance of the composites as food packaging materials

Figure 4.4 illustrates the transparency of the nanocomposites. As can be seen, the addition of nanoparticles slightly decreases the transparency of the films; however, part of this decrease could be ascribed to the increased degree of crystallinity. When comparing hybrid composites it is notable that only those composites with 5 wt% clay show the UV blocking behaviour reported for PLA/C30B 1% composites, the reason for which is the slightly different dispersion of clay in both composites.

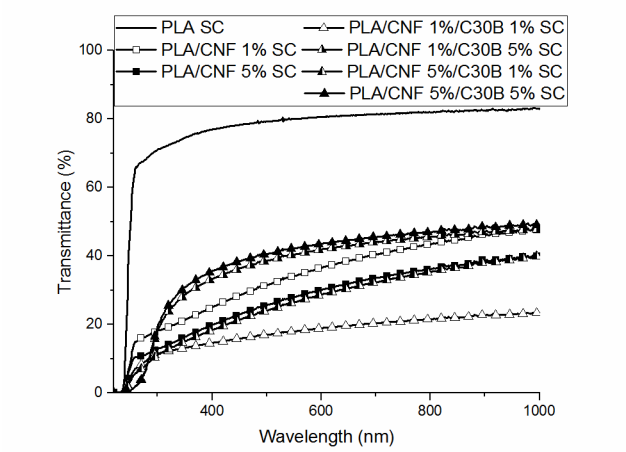

Figure 4.4 Optical transparency of neat PLA and composites.

The oxygen transmission rate (OTR) and water vapour transmission rate (WVTR) of the nanocomposites at 23°C and 50% RH (relative humidity) are shown in Figure 4.5. There it is clear that

there is a very significant decrease in the barrier properties of the nanocomposites compared to neat PLA. The OTR at 50% RH is representative of composites measured at both 0% and 50% RH (similar data was obtained for 0% RH). The OTRs for the hybrid nanocomposites were reduced by 74.8% at the lowest loading of 1wt% nanoclay and 1wt% nanocellulose. Increasing the content of nanocellulose at 1 wt% nanoclay decreased oxygen permeability by 80.3% at 5 wt% CNF/1 wt% C30B compared to PLA, while increasing nanoclay content to 5 wt% (1 wt% CNF, 5 wt% C30B) resulted in a decrease in OTR of 85.0%, with the highest loading (5 wt% C30B, 5 wt% CNF) ultimately reducing the overall OTR by 90.2% compared to PLA.

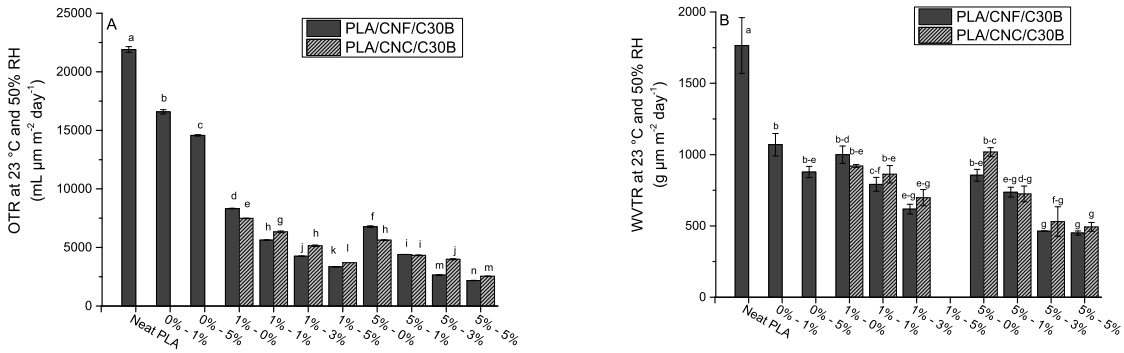

Figure 4.5 A) OTR and B) WVTR of the hybrid nanocomposites as a result of varied nanoclay and nanocellulose content (samples are shown as wt% nanoclay – wt% nanocellulose). The letters indicate significant differences (one-way ANOVA; $p<0.05$) between the composites.

Similarly, the WVTR was also reduced significantly, as shown in Figure 4.5B. Composites at high C30B and high CNF/CNC loading are very fragile, which unfortunately made it impossible to measure the WVTR for the 1 wt% C30B and 5 wt% nanocellulose composites. The WVTR decreased by 57-76% compared to PLA. It is evident that the addition of nanoclay produces a synergistic effect in combination with nanocellulose, whereby particular nanocomposites with 5 wt% of C30B and 5 wt% of CNF show a reduction of 90% in the OTR and 76% of the WVTR when compared to neat PLA, while already at a lower amount of nanoparticle, such as 1 wt% C30B and 1 wt% CNF, for instance, the hybrids show a significant reduction of 74% in OTR and 57% in WVTR. This makes hybrid nanocomposites very promising for food packaging applications.

However, addition of such large amount of nanoparticles, especially of nanoclay, has a significant impact on mechanical properties, as shown in Table 4.1.

Table 4.1 Mechanical properties of all hybrid composites, determined by tensile testing (%wt)[a]

		CNF/C30B						
		PLA	1%-1%	1%-3%	1%-5%	5%-1%	5%-3%	5%-5%
E	(GPa)	2.4 +/- 0.3	2.5 +/- 0.2	2.7 +/- 0.2	2.7 +/- 0.1	2.9 +/- 0.1	3.1 +/- 0.1	3.1 +/- 0.2
σ	(MPa)	55 +/- 2	53 +/- 2	43 +/- 1	18 +/- 5	51 +/- 3	27 +/- 2	16 +/- 3
ε	%	3.9 +/- 0.2	2.9 +/- 0.1	2.2 +/- 0.3	0.9 +/- 0.4	2.6 +/- 0.1	1.6 +/- 1.2	0.7 +/- 0.1
		CNC/C30B						
		PLA	1%-1%	1%-3%	1%-5%	5%-1%	5%-3%	5%-5%
E	(GPa)	2.4 +/- 0.3	2.2 +/- 0.3	2.3 +/- 0.1	2.2 +/- 0.2	2.6 +/- 0.3	2.7 +/- 0.2	3.0 +/- 0.1
σ	(MPa)	55 +/- 2	47 +/- 6	40 +/- 2	18 +/- 5	49 +/- 2	34 +/- 1	25 +/- 3
ε	%	3.9 +/- 0.2	3.1 +/- 0.2	2.4 +/- 0.2	1.2 +/- 0.3	3.0 +/- 0.5	1.6 +/- 0.3	1.1 +/- 0.2

a) E is the Young's modulus in GPa, ε strain at breaking point and σ stress at breaking in MPa.

As shown in Table 4.1, composites with high nanoclay content are highly brittle and show a significant reduction in elongation at breaking. This effect is directly correlated to nanoclay content in the composites and was also observed for the reference PLA/C30B nanocomposites as well, which were very difficult to handle. Adding nanocellulose (CNC or CNF) to the composites has the effect of reducing their brittleness and enabling the handling of thin films. Especially the low loading of clay was found to provide a good combination of mechanical and barrier properties.

Although the addition of nanoclay reduces mechanical properties at room temperature, there is a significant reinforcement effect at high temperatures, as shown by the dynamic mechanical analysis (DMA) in Figure 4.6.

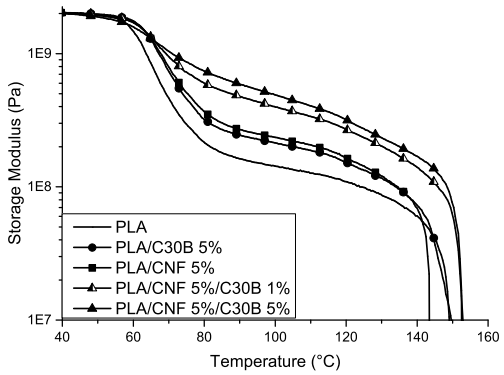

Figure 4.6 DMA of neat PLA and hybrid nanocomposites (%wt).

It is well known that large nanomaterial surface areas generally result in improved creep properties at high temperatures. The increased stability of hybrid composite films at higher temperatures is seen clearly for both the C30B and the CNF composites. Hybrid composites exhibit increased thermal stability even at low nanoclay loading, whereas increasing the content of nanoclay even further

appears to increase stability only moderately. This again illustrates that the two types of nanomaterials appear to result in a synergistic effect in terms of thermal stability and a reduction in creep at higher temperatures. This is expected to be a result of combining a fibrous and a platelet type of nanomaterial, where it is speculated that the nanocellulose creates a strong percolated network, whereas the platelet structure results in maintained integrity across larger areas of the film.

This added thermal stability can also be observed on the actual films after solvent casting from DMF at 80°C, as shown in Figure 4.7.

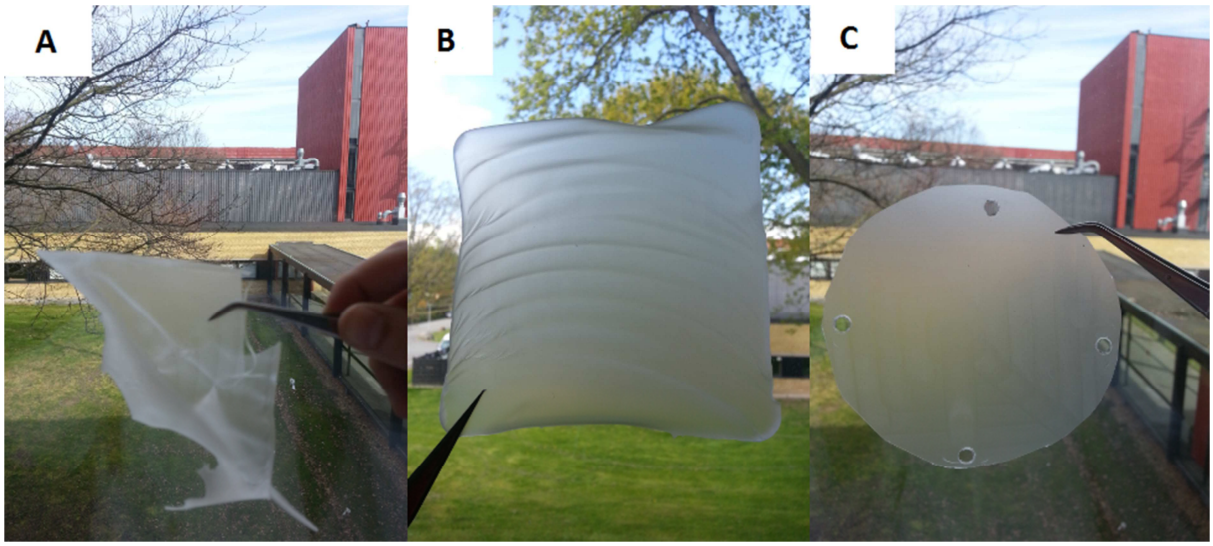

Figure 4.7 A) PLA, B) PLA/CNF 5% and C) PLA/CNF 1%/C30B 1% films after solvent casting from DMF at 80°C.

Here, it is clear that PLA cannot resist the drying process at higher temperatures. Conversely, the PLA/CNF 5 wt% nanocomposite does maintain film shape, although it is not completely flat. Finally, the hybrid PLA/CNF1%/C30B1% results in a completely flat film prepared in exactly the same conditions, proving the synergy and the reinforcing effect on nanocomposites.

4.3 Summary

In this chapter, it was established that the inclusion of different types of nanoparticles (both nanocelluloses and C30B) in a PLA matrix led to an increase in thermomechanical and barrier properties, an effect that was not observed when adding an increased amount of the same nanoparticle. Therefore, it can be concluded that CNF and C30B exhibit synergetic behaviour.

Hybrid composites showed up to a 90% decrease in OTR, a 76% decrease in WVTR and a great increase in thermomechanical properties. Furthermore, most parts of the hybrid composites studied herein showed similar transparency to composites with only one nanoparticle, meaning that

combining C30B and CNF does not have too dramatic an influence on transparency. Therefore, it can be concluded that hybrid composites are highly promising materials for food packaging applications.

5. Isothermal crystallisation behaviour of PLA and its composites, and a comparison with solvent casting-induced crystallinity

In the previous chapters, it was found that the addition of CNF and/or C30B to PLA led to superior material performance on some of the most critical requirements for films for food packaging applications, such as barrier and thermomechanical properties. However, one of the drawbacks of PLA, its slow crystallisation rate, was not discussed in previous chapters, and has been continued into this chapter to allow a discussion across the materials.

Indeed, some semi-crystalline polymer properties, such as mechanical or barrier properties (Picard et al. 2011; Gorrasi et al. 2013), benefit from a high degree of crystallinity (Perego et al. 1996; Garlotta 2001; Guinault et al. 2010); therefore, it is more likely that highly crystalline PLA will be closer to the required properties for food packaging than low crystalline PLA. Admittedly this makes the slow crystallisation rate of PLA a problem, but nanoparticles such as CNF or C30B (Suryanegara et al. 2009; Picard et al. 2011) are reported to be effective nucleating agents, and they can therefore enhance the crystallisation rate of PLA. For this reason, in the present chapter, an evaluation of the influence of CNF and/or C30B on the crystallisation of PLA is presented. In addition to the crystallisation kinetic, which is generally the most studied parameter, a deeper evaluation of other less studied aspects of crystallinity, such as spherulite size, geometry, dispersion and rigid amorphous (RAF) and mobile amorphous fractions (MAFs), will be undertaken. Furthermore, the composites were prepared by using solvent casting, which is a suitable lab-procedure, but might not be fully comparable with the crystallinity induced by industrially relevant procedure. For this reason

the crystallinity induced by the solvent casting procedure was compared with the crystallinity induced by isothermal crystallisation, which was considered comparable with the crystalline morphology induced by industrially relevant procedures.

The study was limited to composites with low nanoparticle concentrations, since in previous chapters it was found that further increases in nanoparticle concentration did not result in a greater increase in properties. Furthermore, as long as composites with CNF or CNC, exhibited similar properties, composites with CNC were excluded from further studies. Finally, the isothermal crystallization study will be performed at following temperatures: 140°C (above crystallization temperature), 120°C (approximately crystallization temperature) and 100°C (below crystallization temperature). Isothermal crystallization studies were also carried at 80°C but due to the low degree of crystallinity of all of the materials at this temperature, this data will be presented only where relevant.

5.1 Spherulite morphology and distribution by POM

Firstly, the spherulite morphology and distribution of the composites after solvent casting, in an amorphous state, and after full crystallisation at 100°C, 120°C and 140°C were evaluated by POM, and the results are summarised in Figure 5.1.

If comparing the composites on 1st row, solvent-cast composites, it can be noted that while PLA/CNF and PLA/CNF/C30B show micro-sized (around 40 μm) spherulites, albeit without covering the whole section, the spherulites present on PLA and PLA/C30B are not large enough to be observed on the POM (spherulites are below the micrometer scale). This effect is attributed to the fact that the composites were prepared using the best possible procedure for each material: PLA and PLA/C30B were solvent-casted using an apolar solvent (DCM) and evaporated at room temperature, while PLA/CNF and PLA/CNF/C30B were processed with dimethylformamide (DMF) and subsequently dried at 80°C (Appendix I).

When comparing the differences in crystalline morphology between the isothermally crystallised materials (rows 2 – 4) at different crystallisation temperatures, no clear differences are observed among the composites; however, they actually show a large difference when compared with PLA. The composites, at all crystallisation temperatures, show a larger amount of slightly smaller and better distributed spherulites than neat PLA. Furthermore, PLA also displays clearly differentiated crystalline morphology for different crystallisation temperatures. PLA crystallised at 100°C shows a non-homogeneous spherulite distribution, with small and big spherulites that are randomly

distributed within the matrix, while PLA crystallised at 120°C shows a larger spherulite size (around 65 µm) and, finally, when crystallised at 140°C the spherulites are well dispersed on the matrix and they cover the whole cross section.

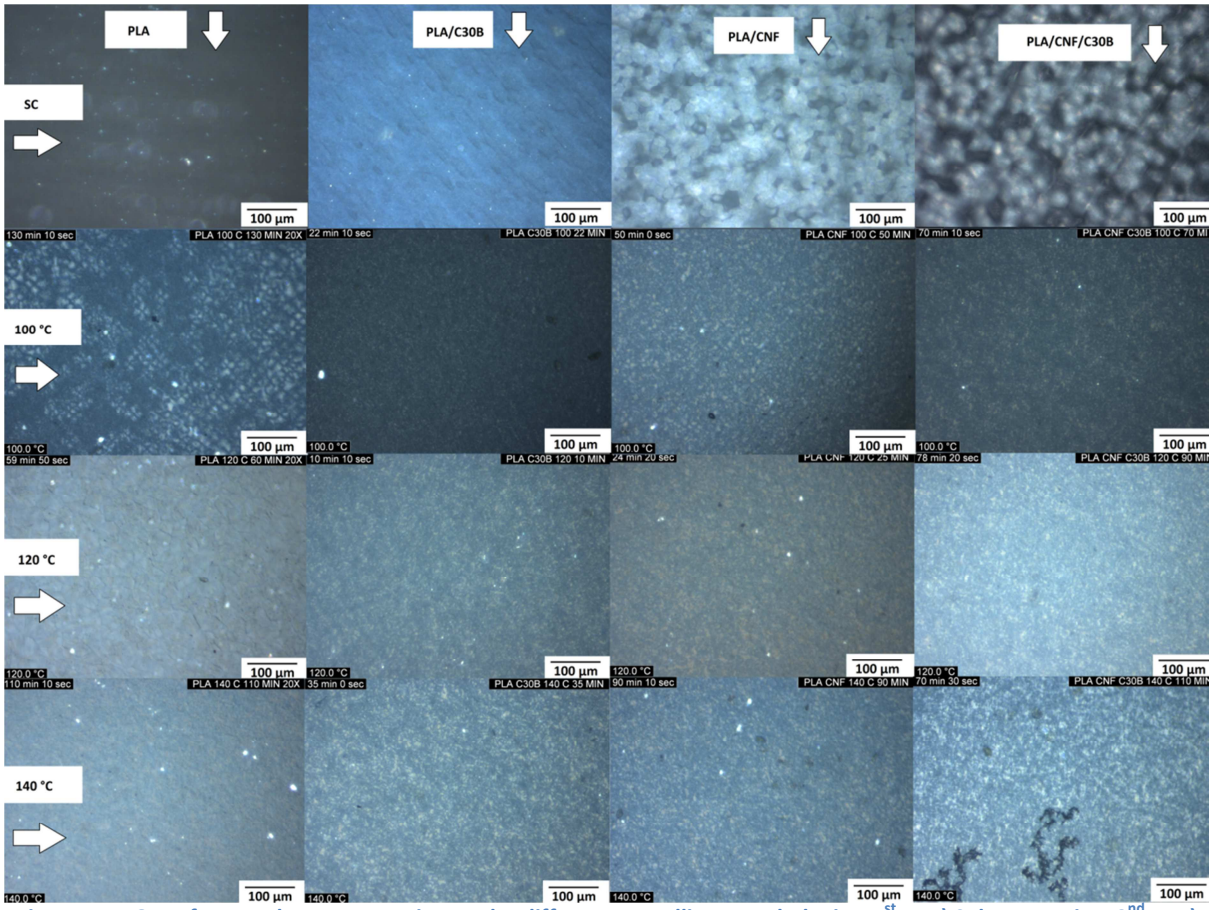

Figure 5.1 POM of PLA and nanocomposites under different crystalline morphologies. 1st row) Solvent casting, 2nd row) crystallised at 100°C, 3rd row) crystallised at 120°C) and 4th row) crystallised at 140°C.

Nevertheless, evaluating the crystalline morphology of fully crystallised composites is a challenging undertaking, as the high amount of spherulites makes it difficult to appreciate any differences between them. For this reason, in Figure 5.2, the POM of PLA and its nanocomposites at earlier stage of the isothermal crystallisation at 120°C can be found. Here, the microscopies highlight that while PLA has a larger spherulite size, while all of the composites have substantially smaller spherulite sizes that are much better distributed in the cross-section.

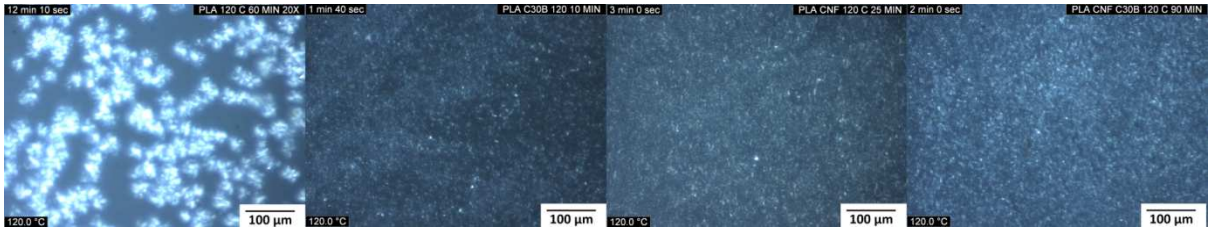

Figure 5.2 POM of PLA and its nanocomposites during crystallisation at 120°C.

It was determined that the solvent casting procedure at low temperatures led to different crystalline morphology than solvent casting at higher temperatures; furthermore, both procedures led to different crystalline morphology if compared with isothermal crystallisation. In general it was found that the processing temperature governed spherulite size. Finally, the nanocomposites showed a larger amount of smaller and better distributed spherulites when compared with neat PLA during the isothermal crystallisation procedure.

5.2 XRD studies

In order to elucidate which crystalline phase is generated at different crystallisation procedures, XRD patterns were collected. There are two thermally induced phases, α'(disordered) and α(ordered), and it has already been reported that lower processing temperatures tend to favour the creation of the disordered phase (Zhang et al. 2008). For this reason, in the present case XRD patterns were collected also at 80°C since this was likely to be a relevant temperature to observe the formation of the α' phase.

Figure 5.3 presents the XRD patterns of isothermally crystallised PLA and composites. In all cases it was found that while those samples which crystallised at 140°C, 120°C and 100°C had peaks at the same 2θ, the samples crystallised at 80°C showed a shift on the peaks to a lower 2θ. This shift to a lower 2θ has been reported previously in the literature and it was attributed to the α' phase (Zhang et al. 2008). Additionally, except for the composites crystallised at 80°C, a small peak at $2\theta = 23.4°$ was observed, which corresponds to reflection 213. The same peak has been ascribed to the α form (Zhang et al. 2008). Therefore it can be concluded that while the composites crystallised at 80°C showed only the α' phase, the rest showed the α phase. In addition, no variations on the position of the peak with increased time were observed, meaning that no recrystallisation processes were taking place.

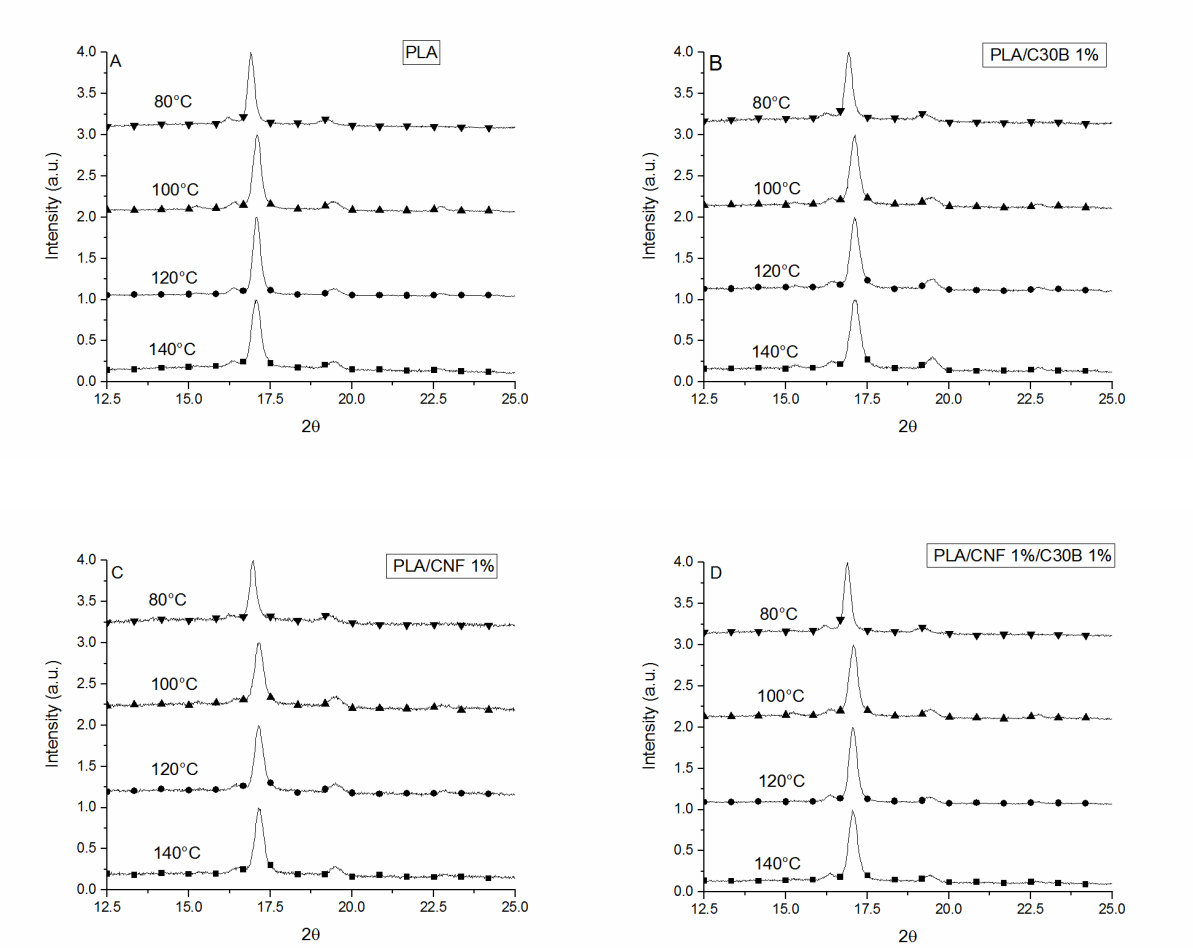

Figure 5.3 XRD patterns of PLA and nanocomposites crystallised at different temperatures. A) PLA, B) PLA/C30B 1%, C) PLA/CNF 1%, D) PLA/CNF 1%/C30B 1%.

Furthermore, in order to evaluate if the solvent casting procedure also induces the α´ phase, the XRD patterns of the solvent-cast composites, as well as the fully amorphous (they were obtained from hot pressing at 170°C followed by fast quenching) as well as fully crystallised composites (fully amorphous composites crystallised for 120 mins at 120°C) as a reference, are also shown in Figure 5.4. The XRD patterns of both figures are not fully comparable with the other samples, due to the fact that they were collected at different temperatures and with different detectors. The patterns in Figure 5.3 were collected during a crystallisation monitoring experiment and they had to be collected at 50°C due to cooling restrictions. On the other hand, the patterns in Figure 5.4 were collected at room temperature.

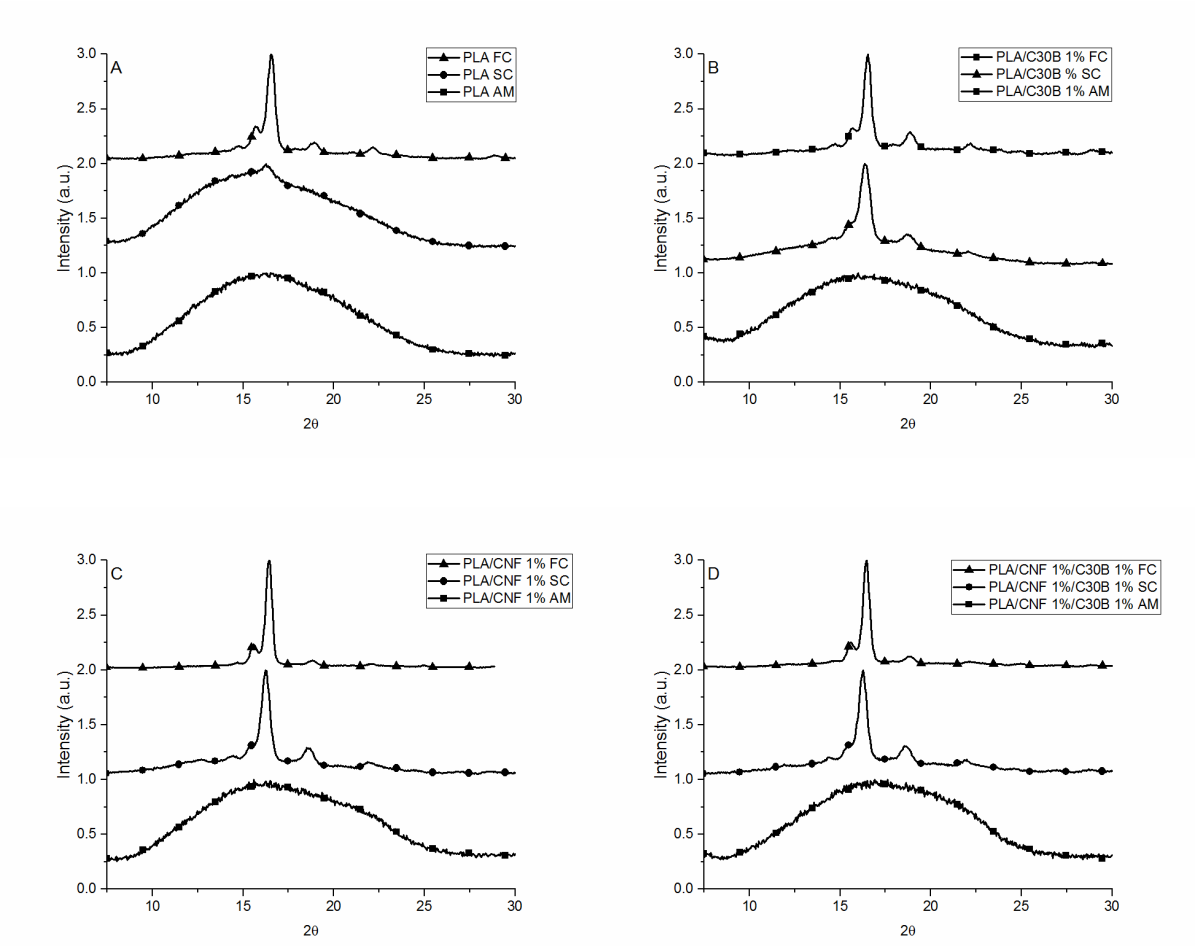

Figure 5.4 XRD patterns of solvent-cast, amorphous and isothermally treated (120 mins at 120°C) samples. A) PLA, B) PLA/C30B, C) PLA/CNF, D) PLA/CNF/C30B.

As highlighted above, there is also a shift in all of the peaks for the solvent cast samples when compared with the crystallised examples. In addition, any of the solvent casted samples show any significant peak at $2\theta = 23.4°$ therefore proving that solvent-cast materials exhibited the α' phase. No crystalline peak was found for quenched composites proving that they are completely amorphous.

5.3 Isothermal crystallisation behaviour by DSC

The isothermal crystallisation kinetic of PLA and its nanocomposites was monitored at 140°C, 120°C and 100°C, the results for which can be found in Figure 5.5. Nevertheless, it was found that the crystallisation of PLA at 140°C was not complete, therefore it was not evaluated.

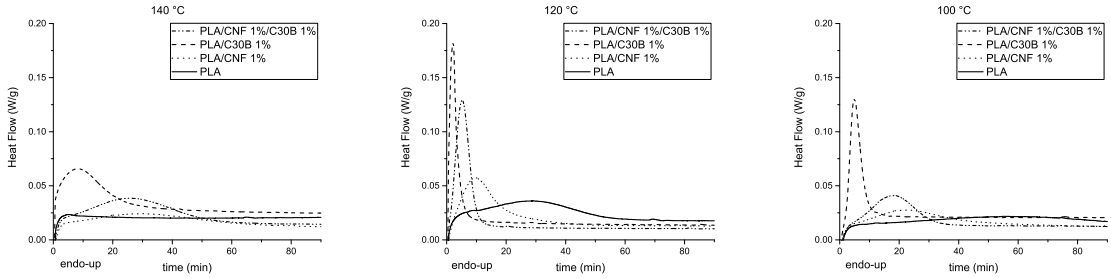

Figure 5.5 Heat flow-time diagram of the nanocomposites at different crystallisation temperatures.

In addition, for the sake of clarity a summary of the half crystallisation time is provided in Table 5.1.

Table 5.1 Comparison between the half-crystallisation times estimated by the Avrami kinetic model with the experimental data.

	PLA		PLA/C30B 1%	
T (°C)	t_{delay} [a]	$t_{1/2}(exp)$ [b]	t_{delay} [a]	$t_{1/2}(exp)$ [b]
140			0.5	11.5
120	2.4	26	0.4	2
100	4.9	11.5	1.8	3.7
	PLA/CNF 1%		PLA/CNF/C30B 1%	
T (°C)	t_{delay} [b]	$t_{1/2}(exp)$ [b]	t_{delay} [a]	$t_{1/2}(exp)$ [b]
140	2.7	30.8	2.2	25.2
120	1.8	10.3	0.8	4.8
100	2.9	24.5	3.4	15.2

a) time taken for the crystallisation process to start after reaching crystallisation temperature (min).
b) experimentally determined half-crystallisation time (min).

In Figure 5.5 and Table 5.1 it can be seen that nanocomposites crystallise faster than neat PLA in all of the studied conditions. Among all of the nanocomposites, the PLA/C30B showed better performance than CNF and CNF/C30B, especially at 140°C. The better performance of the C30B compared with the CNF could be explained by the fact that clay is more likely to have a higher specific area therefore increasing the number of nucleation sites. In addition, in general, it was found that the t_{delay}, the time taken for the crystallization to start after reaching crystallisation temperature, was more or less proportional to the half crystallization time. Finally, as was demonstrated on the XRD analysis, all of the presented crystallisation temperatures led to a PLA with a main α crystalline phase.

In order to retrieve more information regarding crystallisation kinetics, data from isothermal crystallisation within the range 10%-70% of relative crystallinity were fitted to the Avrami kinetic model (Lorenzo et al. 2007) (Eq 5.1).

$$\mathrm{Ln}\left(\text{-}\mathrm{Ln}\left(1\text{-}X_c\right)\right) = \mathrm{Ln}\ k + n^{*}\mathrm{Lnt} \quad \text{(Eq 5.1)}$$

where X_c is the relative degree of crystallinity, k is the overall kinetic constant, n is the Avrami index and t is the crystallisation time. Time 0 was considered the time at which crystallisation started to take place. All of the fits showed a R^2 higher than 0.985 and the values of n are summarized in Table 5.2.

Table 5.2 Summary of the values of "n" for neat PLA and composites crystallised at 140°C, 120°C and 100°C.

	Values of n			
T (°C)	PLA	PLA/C30B 1%	PLA/CNF 1%	PLA/CNF 1%/C30B 1%
140		1.52	1.94	2.12
120	1.97	1.73	1.91	2.43
100	2.27	2.36	1.99	2.49

The index n in the Avrami kinetic is caused by two factors (Eq 5.2) namely the growth directions of the spherulites (n_D), which is a value ranging from 1-3, depending of the growth directions of the spherulites, and by time-dependent crystallisation (n_N), which has a value between 0 for instantaneous nucleation and 1 for sporadic nucleation (Lorenzo et al. 2007).

$$n = n_D + n_N \quad \text{(Eq 5.2)}$$

In Table 5.2 it is revealed how, on the one hand, the PLA/C30B composite showed a strong tendency to decrease the value of n in line with increased crystallisation temperature. A similar trend has also been reported by other authors for PLA with 10% and 15% of C30B (Krikorian and Pochan 2004) and for composites with PLA and other organically modified clay at 1% and 3% of load (Li et al. 2009), although there are also other reports claiming a more moderate trend (Lee et al. 2008b), which can be attributed to different clay dispersion. Notwithstanding this point, the PLA/CNF composite had constant values regardless of crystallisation temperature, which is in agreement with some reports in the literature for low bacterial cellulose content in PLA (Ambrosio-Martín et al. 2015) and for non-modified nanocrystalline cellulose (Pei et al. 2010). Interestingly it was found that the hybrid composite PLA/CNF 1%/C30B 1% showed moderate variation in n values in line with temperature, which sit between nanocellulose and clay, thereby suggesting the simultaneous growth of both clay-

and nanocellulose-nucleated spherulites. The values of n for the neat PLA were not considered because, as can be seen in Figure 5.1, after full crystallisation at 120°C the PLA spherulites reached a diameter of approximately 65 µm, while PLA film showing a thickness of (75 µm). Consequently, a spherulite growing in PLA could be affected by the physical dimensions of the film.

5.4 Influence of crystallisation temperature and nanoparticles on thermal transitions

The effect of the crystallisation temperature and the presence of nanoparticles on thermal properties such as T_g and T_m was studied by DSC, and the results are shown in Table 5.3.

Table 5.3 Thermal properties (T_g and T_m) (°C) of the PLA and nanocomposites after full crystallisation at 140°C, 120°C and 100°C and in an amorphous state.

	PLA		PLA/C30B 1%		PLA/CNF 1%		PLA/CNF 1%/C30B 1%	
Crystallisation	T_g	T_m	T_g	T_m	T_g	T_m	T_g	T_m
140°C[a]	58.8	162.3	57.6	161.9	56.5	163.2	57.9	162.6
120°C[a]	61.7	154.9	58.8	154.4	60.0	155.3	59.6	154.4
100°C[a]	60.5	149.4	61.9	149.3	61.2	150.6	62.0	150.3
SC[b]	60.4	155.0	59.8	154.5	61.7	151.1	61.4	153.7
Amorphous[c]	55.5	-	56.2	-	54.9	-	55.2	-

a) Isothermal crystallisation at the corresponding crystallisation temperature.
b) Solvent casted composites: PLA and PLA/C30B at 23°C; PLA/CNF and PLA/CNF/C30B at 80°C.
c) The amorphous composites were obtained from a fast melt-quenching.

In general, the incorporation of CNF or C30B doesn´t have a significant impact on the thermal transitions of PLA, which is in agreement with some reports in the literature for solvent-casted PLA/C30B composites (Sanchez-Garcia and Lagaron 2010a) and solvent-casted PLA/CNF composites (Sanchez-Garcia and Lagaron 2010b) or PLA/CNC/montmorionite composites (Arjmandi et al. 2015a). However, the melting temperature of all of the materials is increased with increased crystallisation temperature (from 150°C for crystallisation at 100°C to 162°C for crystallisation at 140°C) while no clear influence of the nanoparticles can be observed in this thermal transition. Finally, it was found that the T_m of the solvent casted PLA/CNF and PLA/CNF/C30B was slightly below the ones from PLA and PLA/C30B, suggesting that the different crystalline morphology observed in Figure 5.1 could had a small impact, however, the variations among the materials are small, and close to the accuracy of DSC.

5.5 Crystallinity, and mobile amorphous and rigid amorphous fractions

In order to make a more accurate calculation of the degree of crystallinity it was retrieved from MDSC instead of normal DSC. The melting enthalpy of 100% α-crystalline PLA was considered to be

106 J g^{-1}, while the 100% α´-crystalline PLA was considered to be 25 J g^{-1} lower than the α (Righetti et al. 2015) (81 J g^{-1}). Furthermore, the mobile amorphous fraction (MAF) and rigid amorphous fractions of the composites were also estimated, the results for which are summarised in Table 5.4.

Table 5.4 Degree of crystallinity (DC), mobile amorphous fraction (MAF) and rigid amorphous fraction (RAF) of PLA and composites under different crystalline morphologies. The data for PLA at 140°C are not presented, due to incomplete crystallisation.

		PLA			PLA/C30B 1%	
Crystallisation	DC	MAF	RAF	DC	MAF	RAF
140°C[a]				36%	47%	16%
120°C[a]	36%	45%	19%	39%	42%	18%
100°C[a]	34%	48%	18%	36%	42%	21%
SC[b]	8%	89%	3%	32%	58%	9%
Amorphous	0%	100%	0%	0%	96%	3%
		PLA/CNF 1%			PLA/CNF/C30B 1%	
Crystallisation	DC	MAF	RAF	DC	MAF	RAF
140°C[a]	36%	47%	16%	37%	45%	16%
120°C[a]	39%	42%	18%	41%	40%	17%
100°C[a]	36%	41%	22%	37%	40%	21%
SC[b]	37%	45%	17%	37%	45%	16%
Amorphous	0%	96%	3%	0%	93%	5%

a) Isothermal crystallisation at the corresponding temperature.
b) Solvent casted composites: PLA and PLA/C30B at 23°C; PLA/CNF and PLA/CNF/C30B at 80°C.
c) The amorphous composites were obtained from a fast melt-quenching.

Table 5.4 shows how the results for the rigid amorphous region of neat PLA in range of the ones presented in the literature (Righetti and Tombari 2011; Saiter et al. 2016). It can be observed how solvent-cast composites at low temperatures (PLA/C30B) had a reduced RAF, when compared with composites processed at higher temperatures. This could be the result of small spherulites having better cohesion with amorphous domains and therefore inducing smaller RAFs than bigger spherulites. Furthermore, when comparing isothermally treated samples, all of the nanocomposites show a slightly reduced MAF, which is attributed to the presence of nanoparticles in the mobile amorphous fraction, although generally they show DC, MAF and RAF similar to neat PLA. However, for nanocomposites it seems that the amount of RAF decreases in line with an increase in crystallisation temperature. It was also observed that the hybrid PLA/CNF 1%/C30B 1% composite showed a slightly higher degree of crystallinity, when compared to the rest of the composites. This effect can be attributed to better packaging of the spherulites, due to a combination of both nanoparticles. Furthermore, the PLA had a really small degree of crystallinity after isothermal crystallisation at 140°C for 2 hours, due to incomplete crystallisation (Figure 5.5).

5.6 Unusual melting peak of composites with C30B

During isothermal crystallisation monitoring of PLA and composites by DSC, some differences on the shape of melting peak of PLA and composites crystallised at 100°C was found. The melting peak is shown in Figure 5.6.

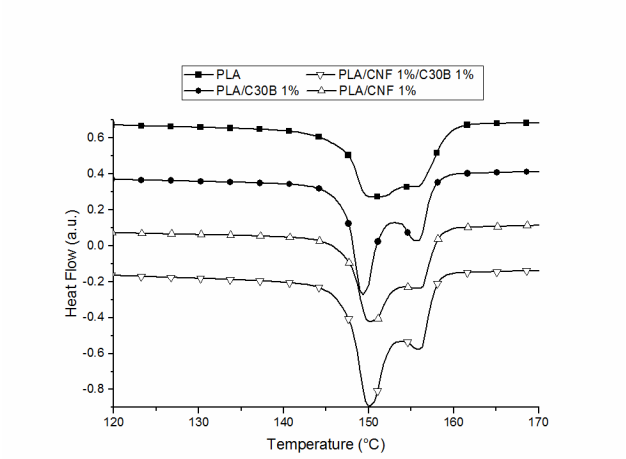

Figure 5.6 Heat flow vs time thermograms of the PLA and composites after 2 hours of isothermal crystallisation at 100°C.

In order to clarify the meaning of the peaks, the separated reversible and non-reversible heat flow retrieved from the MDSC was studied Figure 5.7.

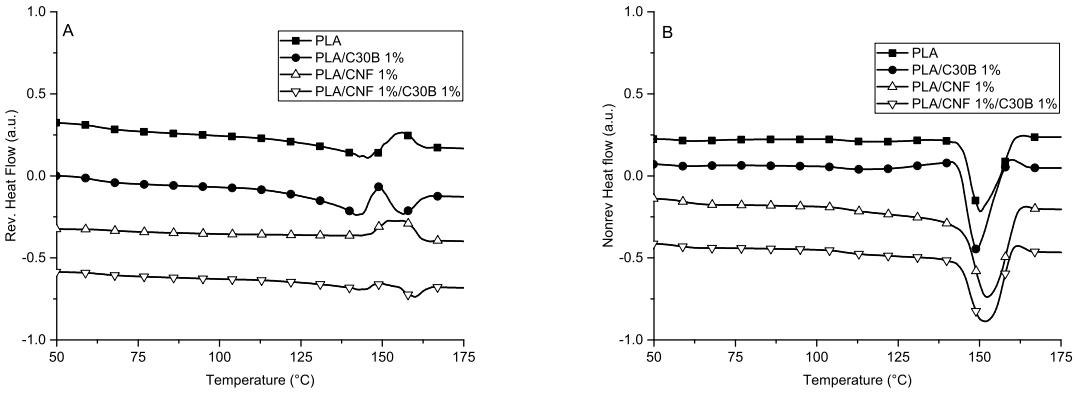

Figure 5.7 A) reversible heat flow B) non-reversible heat flow of PLA and nanocomposites during the heating cycle after quasisothermal crystallisation at 100 °C.

In Figure 5.7A, it is notable how the PLA/C30B has a small crystallisation peak around 150°C, which is attributed to the re-crystallisation of the α´ phase. This recrystallisation peak is not observed for CNF-based composites or for neat PLA, therefore it must be related to the clay. The clay was organically modified and had some long organic chains on its surface. These chains could disturb the formation of the ordered α phase, causing a small disorder in the crystalline structure aligned with the α´ phase. Furthermore, it can be seen how the PLA/CNF 1%/C30B 1% composite shows

crystallisation behaviour between PLA/CNF and PLA/C30B, which is in agreement with the observation made during the evaluation of the Avrami kinetic.

In any case, the area of the re-crystallization (the peak from reversible heating) is smaller than the area of the melting (the peak from the non-reversible heating) which suggests that the amount of created α' phase is small. This is in agreement with the observations from the monitoring of the crystallization by XRD, where it was concluded that the crystallization at 100°C was mainly leading to the formation of the α crystalline phase on PLA/C30B. Therefore it can be concluded that the amount of created α' crystalline phase is small.

5.7 Summary

It has been established that solvent casting induces completely different crystalline morphology, when compared with the isothermal crystallisation procedure. Although during chapter 3 it was established that all of the composites were showing a comparable degree of crystallinity it has been found that solvent casting procedure at low temperatures induces a large amount of small spherulites (below micro size) that cover the cross-section of the polymer but do not show a large RAF. On the other hand, high-temperature processing (either isothermal crystallisation or solvent casting) causes crystalline morphology consisting of large spherulites (above the micro scale), which in turn induces a larger RAF but does not cover the whole cross-section completely.

When comparing the isothermal crystallisation of PLA and composites, it is noteworthy that composite materials exhibit faster crystallisation, smaller spherulite size and better spherulite distribution than neat PLA, as well as a slightly decreased mobile amorphous fraction. When comparing crystalline morphology induced by C30B with that induced by CNF, it is evident that the first example induces a small α' phase when processed at 100°C; furthermore, it also has greater variations in crystalline growth direction aligned with temperature than CNF. Furthermore, both of them showed similar DC, MAF and RAF values. When combining both nanoparticles, it was found that both crystalline morphologies grew parallel to one another, and these composites showed intermediate crystallisation behaviour among PLA/CNF and PLA/C30B, albeit with a reduced mobile amorphous region and increased crystallinity. In any case, in general it can be concluded that all of the composites showed a similar crystalline morphology despite the above mentioned minor variations.

6. Effect of crystallinity on the optical and barrier properties of PLA-based nanocomposites

In the previous chapter it was found that different processing conditions led to different crystalline morphologies. The goal of this study is to evaluate how different crystalline morphologies affect different properties of PLA, which could ultimately allow for the tuning of processing conditions to modify properties according to the target application.

In the present chapter the effect of the different crystalline morphologies (solvent casting and isothermal crystallisation) PLA, PLA/C30B 1%, PLA/CNF 1% and PLA/CNF 1%/C30B 1% on optical transparency and water vapour transport (water sorption and water diffusion) is presented. Optical transparency is a key requirement on films for food packaging applications, and it is likely to be highly affected by crystallinity, since crystalline domains have higher density than amorphous domains and thus cause the scattering of light and subsequent decrease in transparency. Furthermore, the presence of nanoparticles can actually reduce transparency, and so their impact on this factor has to be evaluated.

Regarding mass transport properties, it has been found that the nanocomposites showed highly inflated barrier properties; however, apart from moderate barrier properties that should be decreased by 90% to reach the PET, PLA is known for having relatively high water sorption, which causes swelling problems. In general, mass transport through the polymer matrix is governed by sorption and diffusion, and it can be modelled according to the Sorption-diffusion model (Eq 6.1).

$$P=D*S \quad \text{(Eq 6.1)}$$

where P is permeability, D diffusivity and S is sorption. This means that any improvement (decrease) in water permeability could be due to a large decrease in diffusivity, a similar large decrease in water sorption or to a moderate decrease in both. This has a large influence on the optimal application for the material. Indeed, water sorption has been found to play a relevant role in PLA degradation during processing (Cairncross et al. 2007), and in addition it can also produce some anti-aesthetic swelling, which makes low water sorption necessary on food packaging. On the other hand, higher water sorption is related to enhanced biodegradability (Cairncross et al. 2006) and is used to evaluate the biocompatibility of a material on biomedical applications, where higher water sorption is a required characteristics of the materials.

In addition, as mentioned in the background, the PLA has to decrease its OTR by 85% and it´s WVTR by 92% while hybrid composites showed a decrease up to 90% on OTR and 76% on WVTR. This means that still the hybrid composites have to improve its water vapour barrier properties, therefore understanding how the nanoparticles and how the crystalline morphology affects the water vapour transport can help further optimisation of the materials.

In the present chapter the influence of crystalline morphology and presence nanoparticles on the water sorption and diffusion is going to be investigated by means of a QSM (Quartz spring Microbalance). The present work was partially done during an external stay at UNIBO under the supervision of Dr. Marco Giacinti.

6.1 A brief summary of crystalline morphology

For the sake of understanding, a brief summary of the crystalline morphology of PLA, PLA/C30B 1%, PLA/CNF 1% and PLA/CNF 1%/C30B 1% is presented in Table 6.1.

Table 6.1 Summary of the crystalline morphologies of different materials crystallised with different procedures.

	PLA	PLA/C30B 1%	PLA/CNF 1%	PLA/CNF 1%/C30B 1%
AM[a]	amorphous	amorphous	amorphous	amorphous
SC[b]	(8%), small spherulite size, α´	(32%), small spherulite size, α´	(37%), large spherulite size, not whole section coverage, α´	(37%), large spherulite size, not whole coverage, heterogeneous, α´
100°C[c]	(34%), large spherulite size, not whole section coverage, α	(36%), large spherulite size, whole coverage, good dispersion, α	(36%), large spherulite size, whole coverage, good dispersion, α	(37%), large spherulite size, whole coverage, good dispersion, α
120°C[c]	(36%), large spherulite size, α	(39%), large spherulite size, whole coverage, good dispersion, α	(39%), large spherulite size, whole coverage, good dispersion, α	(41%), large spherulite size, whole coverage, good dispersion, α
140°C[c]	Not fully crystallised	(36%), large spherulite size, whole coverage, good dispersion, α	(36%), large spherulite size, whole coverage, good dispersion, α	(37%), large spherulite size, whole coverage, good dispersion, α

a) (AM)Amorphous material obtained from fast quenching from the melting.
b) (SC)Solvent-casted: PLA and PLA/C30B at 23°C, PLA/CNF and PLA/CNF/C30B at 80°C.
c) (FC) Fully crystallized samples; amorphous samples crystallized for 2 h at 140°C, 120°C and 100°C.

6.2 Evaluation of the influence of crystalline morphology and nanoparticles on optical transparency

To simplify the discussion on the effect of crystallinity on the optical transparency of films, the subject will be divided into two parts. Firstly, the effect of the temperature of isothermal crystallisation on the optical transparency of the films was investigated (Figure 6.1), from where one temperature would be chosen for comparison with the other crystalline morphologies, i.e. the ones induced by solvent casting and amorphous composites.

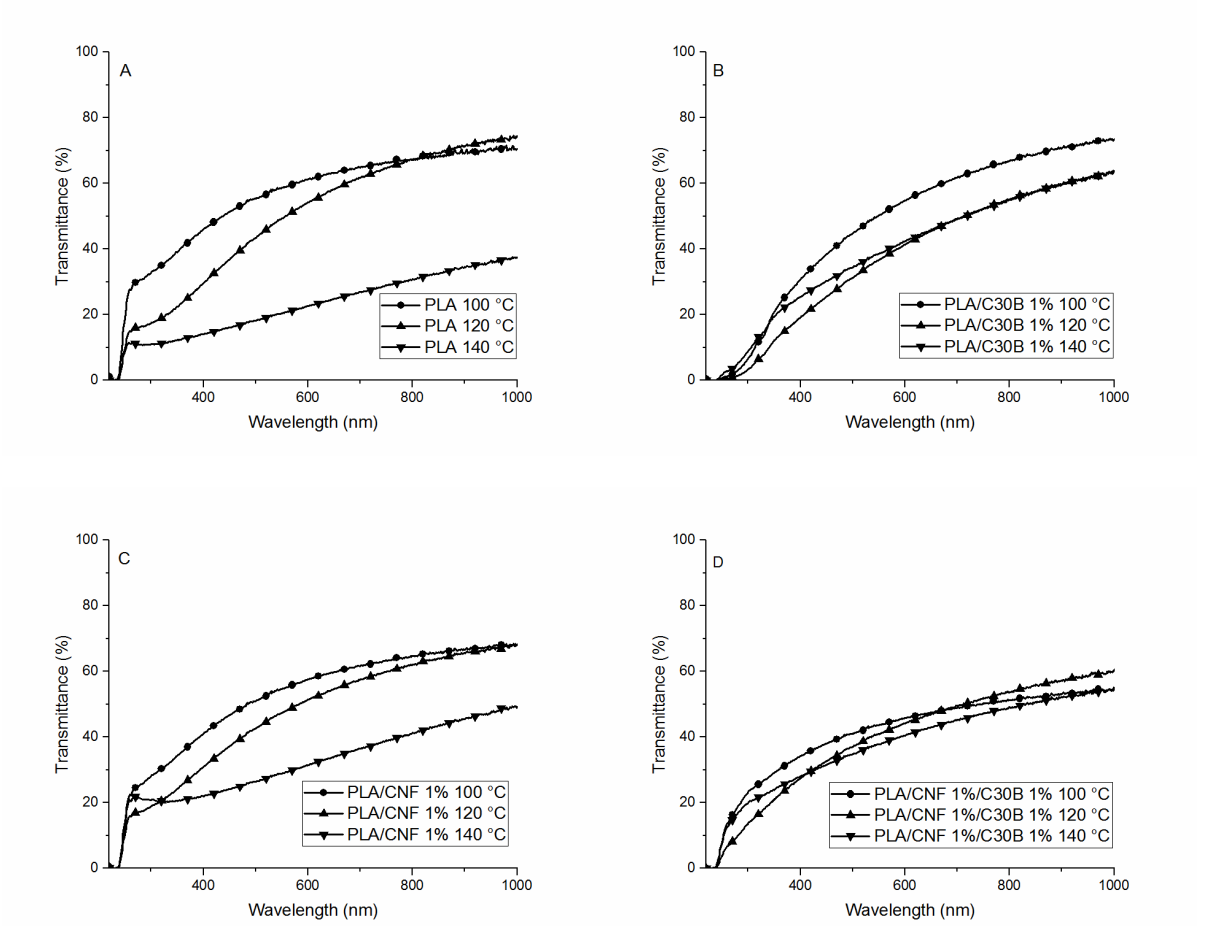

Figure 6.1 UV-VIS spectra of neat PLA and its nanocomposites after isothermal crystallisation at different temperatures.

Among all of the crystallisation temperatures, it can be seen how crystallisation at 100°C leads to more transparent materials, although the difference in materials crystallised at 120°C, in general, is small, and so composites crystallised at this temperature will be chosen for further characterisation. Surprisingly, crystallisation at 140°C affects dramatically the transparency of PLA and PLA/CNF composites while not having a dramatic influence on C30B-based composites. As long as in first place there is no noticeable change on crystalline morphology among PLA/CNF crystallized at 140°C and PLA/C30B and PLA/CNF/C30B crystallized at the same temperature and in second place the PLA showed an uncomplete crystallization (~23%) at this temperature, this effect is mostly attributed to a temperature induced internal deformation. As long as it is reported that exfoliated clay can anchor polymer chains (Saiter et al. 2016), this could avoid any shape degradation due to high temperature.

Thereafter the composites crystallized at 120°C were compared with the solvent casted and amorphous materials.

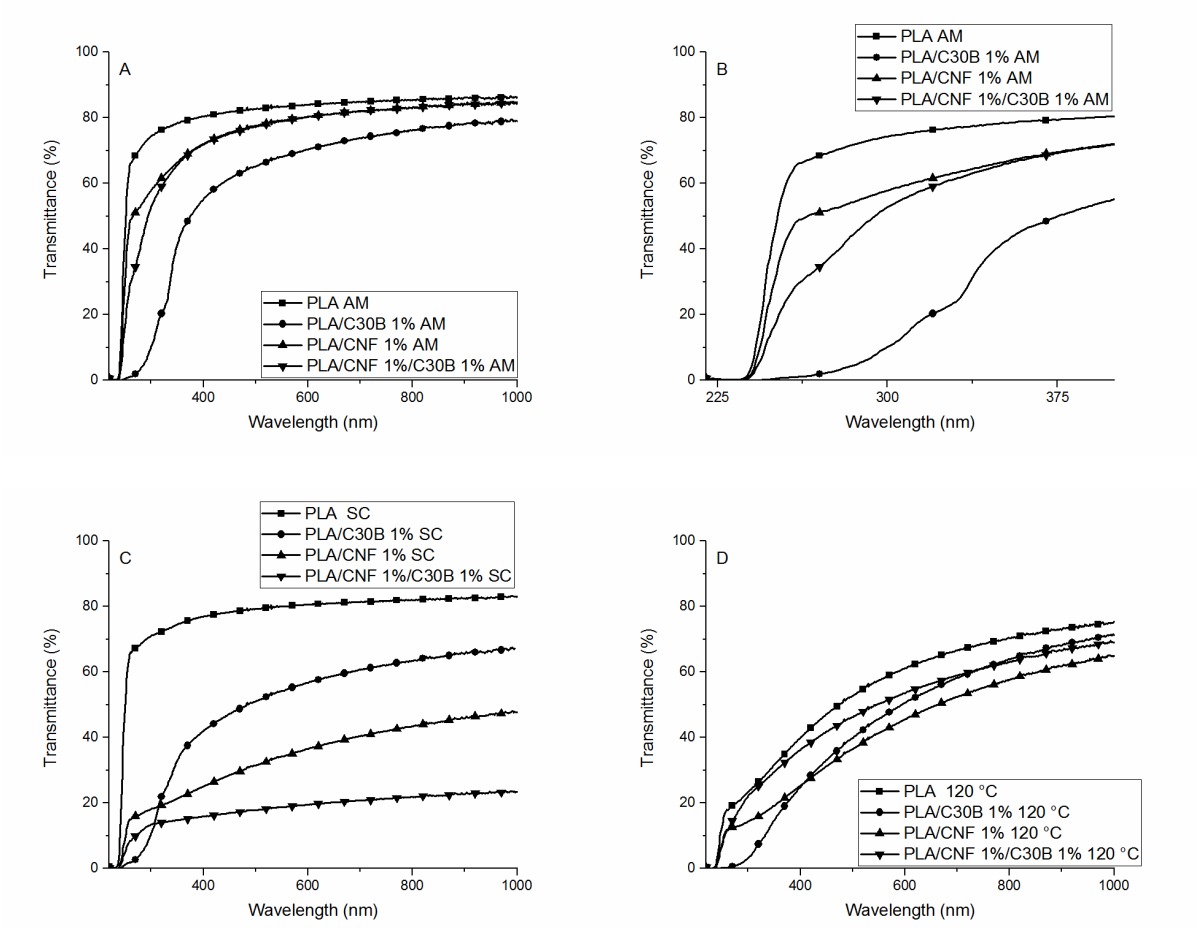

Figure 6.2 UV-VIS spectra of neat PLA and its nanocomposites, in A) amorphous state, B) amorphous state (zoom near UV region), C) solvent casting, D) full crystallisation.

When comparing amorphous (Figure 6.2A) and composite materials crystallised at 120°C (Figure 6.2D), it is evident how, for all of the cases, increased crystallinity leads to reduced transparency on the visible spectra. This is attributed to the fact that crystalline domains have higher density than amorphous domains, which will lead to light scattering. However, when comparing the crystallised composites (Figure 6.2D), is noted how the presence of nanoparticles does not significantly affect the transparency of the films, and a similar observation can be seen for amorphous composites (Figure 6.2A), although in this case the PLA/C30B shows a slightly decrease in transparency. However, when evaluating the transparency of the solvent-cast films, it can be seen how PLA/C30B solvent casted shows increased transparency when compared with the rest of the composites, regardless of whether or not they have a similar degree of crystallinity. This is attributed to the smaller spherulite size present on solvent casted PLA/C30B composites.

In addition, it can be seen in all of the cases how PLA/C30B shows UV-blocking behaviour but this is not observed on the PLA/CNF 1%/C30B 1%. Nevertheless, as illustrated in Figure 6.3, and as mentioned in previous chapter, hybrid composites do actually show UV-blocking behaviour, albeit at

a higher C30B load (5 wt%). This difference is attributed to the fact that the composites have been processed in different conditions.

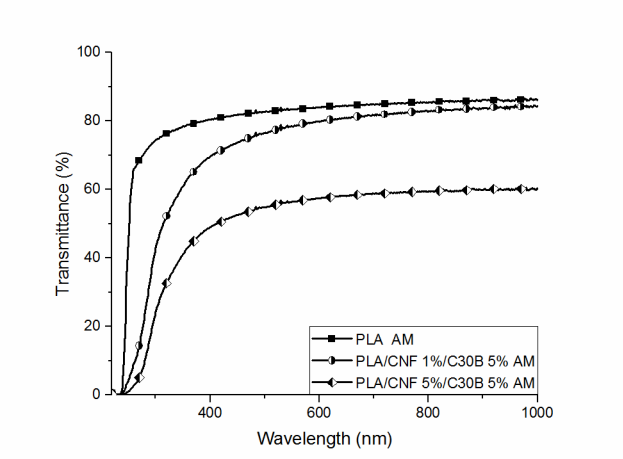

Figure 6.3 UV-Vis spectra of amorphous composites. A) PLA, B) PLA/CNF 1%/C30B 5% C) PLA/CNF 5%/C30B 5%.

Finally, it is noteworthy how, under full crystallisation, the hybrid composite with 1% CNF and 1% C30B shows good transparency, which is a required feature for films for food packaging applications.

6.3 Quartz Spring Microbalance (QSM)

In the present work water vapour sorption and water diffusivity through composites was evaluated by means of a QSM (Quartz Spring Microbalance) – an absorption-based experimental method for the study of mass transport properties in films and membranes (Figure 6.4). This technique does not provide permeability data directly, but it does allow the diffusivity and the solubility of a test vapour into a material to be characterised. If the latter then follows a simple solution diffusion permeation mechanism (Wijmans and Baker 1995), permeability can be obtained from this data and the effect of both parameters can be studied. In particular, the following equation can be considered to hold:

$$P=D*S \quad \text{(Eq 6.1)}$$

where P is permeability, D is diffusivity and S is the solubility coefficient, which is the slope of the equilibrium concentration versus the pressure curve.

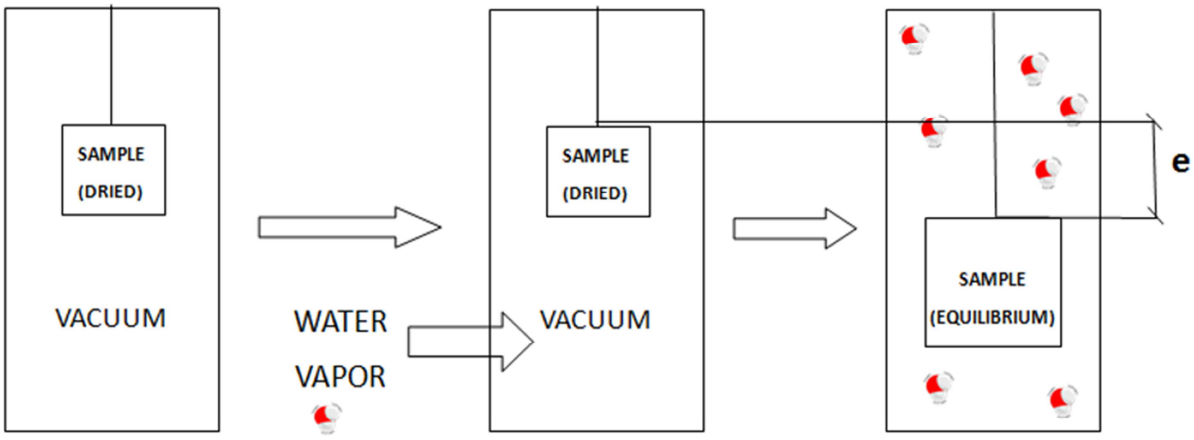

Figure 6.4 QSM Schema

The QSM used in the present work is based on the use of a non-rotating spring having a sensitivity of 1 mm/mg and a maximum load of 50 mg. The spring is mounted inside a water-jacketed glass column able to maintain temperature within ±0.5°C with respect to the experimental set point, which was 23°C in this case. Stainless steel tubes and valves allow connections between the different parts of the apparatus and to the vacuum system, constituted by a vacuum pump and a liquid nitrogen trap, which is used for sample degassing and the evacuation of the test vapour. The sample is observed through a CCD camera (Series 600 Smartimage sensors) manufactured by The DVT Corporation (Norcross, GA), and a strobe LED array illuminator, model IDRA-6, is placed behind the glass column to achieve optimal illumination and maximum image contrast. The QSM could be used to measure weight differences reliably in the order of 2 μg. A complete description of the experimental set up can be found in the literature (Piccinini et al. 2004).

Experiments were performed after complete dehydration of the film samples, obtained by keeping the balance under vacuum conditions until no weight change was observed. The vapour in the test solvent (water in this case) was then placed in contact with the specimen at the desired pressure, in order to start the experiments. As the water vapour started to penetrate into each sample, the mass of the latter increased and elongated the spring, the movements of which were recorded photographically. Once the sample arrived at equilibrium at the working water activity, the total amount of water absorbed could be calculated from elongation, and diffusivity could be obtained from the plot of mass increase versus time through the use of appropriate models (Crank 1975). Pressure inside the column could be increased further, and a new absorption step could be recorded at higher water activity. As long as the water sorption of PLA showed linear behaviour below ~75% water activity (Davis et al. 2012), at least three points were considered in this activity range, in order

to build the sorption isotherm and calculate the solubility coefficient, which is needed for permeability analysis, as explained above.

6.4 Influence of crystalline morphology and nanoparticles on water vapour diffusion

In Figure 6.5 the water diffusivity of the nanocomposites is shown.

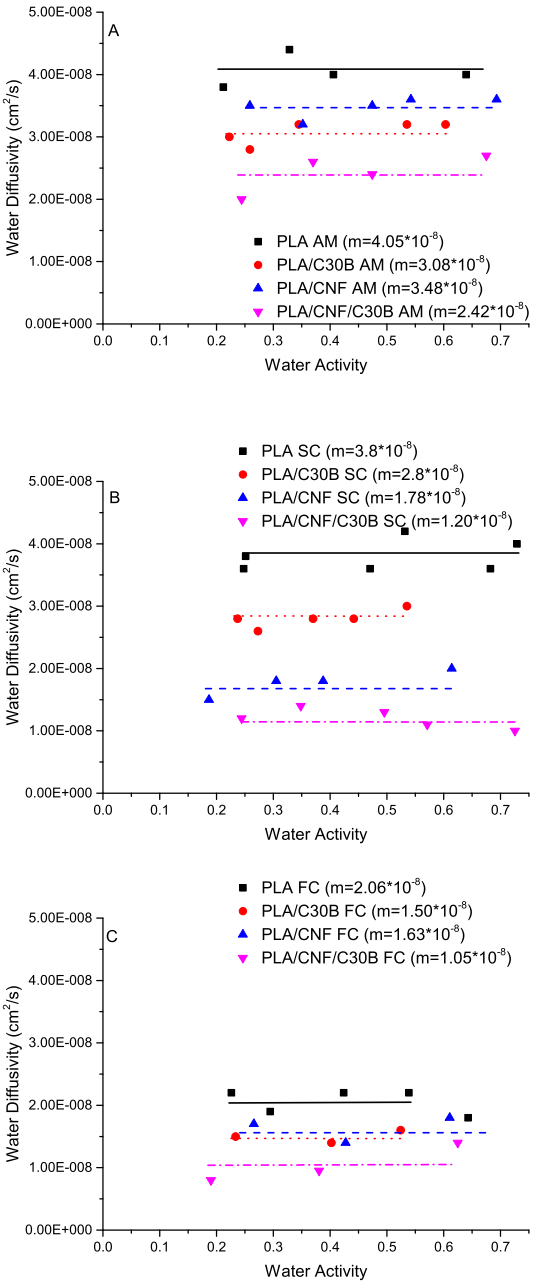

Figure 6.5 Diffusivity of PLA and its nanocomposites at different crystalline morphologies. (A) Fully amorphous (B) solvent casting and (C) isothermal crystallisation (2h at 120°C).

As long as no large variations in diffusivity with water activity (0-75%) are observed, which is in agreement with previous reports (Gorrasi et al. 2013; Davis et al. 2013), a constant value of diffusivity can be assumed for the different materials. The different diffusivity values ranged from 1.05 to 4.05*10^{-8} cm^2/s and are reported in the legend for Figure 6.5, for the sake of clarity.

Table 6.2 Decrease in diffusivity due to the addition of nanoparticles. Reference: PLA AM (amorphous) and PLA FC (fully crystallised) respectively.

	%Decrease		%Decrease
PLA AM	-	PLA FC	-
PLA/C30B 1% AM	24.0%	PLA/C30B 1% FC	27.2%
PLA/CNF 1% AM	14.1%	PLA/CNF 1% FC	20.7%
PLA/CNF 1%/C30B 1% AM	40.1%	PLA/CNF 1%/C30B 1% FC	49.0%

From Figure 6.5 it is evident how all of the materials show a large decrease in diffusivity with increased crystallinity, which is attributed to the fact that crystallinity is essentially impermeable and therefore increases the tortuous path. From Table 6.2 it can be seen that the decrease in diffusivity, due to the addition of nanoparticles, is more pronounced in fully crystallised composites when compared with amorphous composites. This means that any decrease in diffusivity, apart from being due to the presence of nanoparticles, is also due to modified crystallinity (better spherulite dispersion) when compared with neat PLA. When comparing CNF and C30B it is evident how CNF addition results in water diffusion reduction close to that conferred by C30B (21% vs 27%), after full crystallisation. These results confirm that nanocellulose is a promising bio-based and biodegradable reinforcing agent for enhancing the water vapour barrier properties of PLA. Furthermore, it is notable how, in any of the studied conditions, the hybrid composite shows a large decrease in diffusivity (49% on fully crystallised composites), making the combination of both nanoparticles an interesting approach for reducing diffusivity in composites.

It is interesting to note that solvent casted PLA/CNF (which shows micro-sized spherulites) shows greatly reduced water diffusivity when compared with solvent casted PLA/C30B (which exhibits sub-micron spherulites). Surprisingly, when evaluating composites at similar crystalline morphologies, in AM (amorphous) composites (Figure 6.5A) and FC (fully crystallised) composites (Figure 6.5C) the opposite behaviour is found. From this observation it can be concluded that spherulite size plays a critical role in the decrease in water diffusivity, larger the spherulite size, larger the decrease on diffusivity. This conclusion (decreased diffusivity with increased particle size) is in agreement with the observation made by (Gorrasi et al. 2008) for calcium sulphate anhydride particles.

6.5 Influence of crystalline morphology and nanoparticles on water vapour sorption

In Figure 6.6 the water sorption isotherm of the nanocomposites can be found.

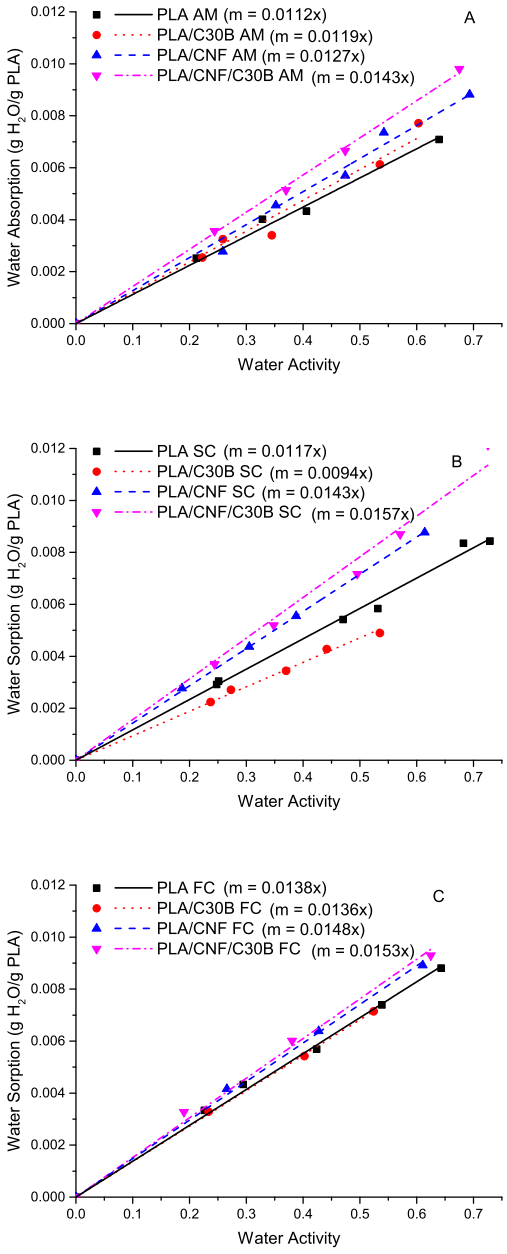

Figure 6.6 Water sorption of PLA and its nanocomposites at different crystalline morphologies. (A) amorphous (B) solvent casted and (C) isothermal crystallisation (2h at 120°C).

In Figure 6.6 it is evident how there is a linear behaviour of increased water sorption with increased water activity, which allows fitting the data to linear model from where the sorption coefficient can be easily calculated. It can be seen also how the incorporation of CNF in the polymer matrix leads also to increased water sorption, however no clear effect of the addition of C30B on the matrix can be observed. Surprisingly, it can also be noted how increased crystallinity from (amorphous to fully

crystallized samples) leads to increased water sorption. This is surprising since according to the classical definition of semicrystalline polymers, the crystallinity is essentially a non-permeable domain whereas the amorphous region is the one that can actually absorb water. Interestingly, it can be noted how solvent casted PLA/C30B (sub-micron spherulite size) shows a dramatically decreased water sorption coefficient when compared with any other material which is the behaviour that was expected from increased degree of crystallinity. However, peculiarly, the same material in the fully crystallised state (micro-sized spherulites) shows a large increase in water sorption, even though it has a similar degree of crystallinity. This suggests that crystalline morphology also has a significant influence on water sorption as well as water diffusion.

As mentioned above, according the traditional understanding of semicrystalline polymers, the crystalline domains can be considered as impermeable domains with negligible sorption capabilities, while the amorphous region can have sorption capacities. However, as mentioned in previous chapter, in semi-crystalline polymers such as PLA, there is an intermediate nanophase present at the interface between the crystals and the surrounding melt (Wunderlich 2003), known as the "rigid amorphous fraction" (RAF). In this case, a clear difference on the water sorption capabilities of both phases could explain this behaviour. Indeed, the RAF has been reported to have increased free volume (Lin et al. 2002) which lead to augmented sorption capabilities.

In order to evaluate how both fractions affects the water sorption the water sorption coefficient was plotted against MAF and RAF (Figure 6.7).

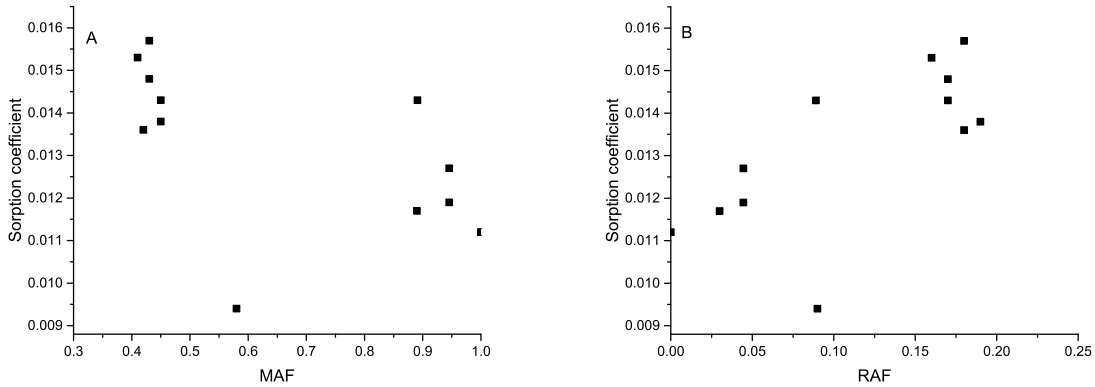

Figure 6.7 A) MAF vs water sorption coefficient B) RAF vs water sorption coefficient.

From Figure 6.7A it appears that there is a minor tendency toward decreased water sorption with increased MAF, which is actually counterintuitive, when comparing to the classical conception of semicrystalline polymers the MAF can absorb water, and so an increased MAF should lead to increased water sorption. However, this can be explained by the fact that decreased MAF is also

ascribed to increased RAF, and there is a stronger tendency of increased RAF with increased water activity. In addition it can be observed how a point is clearly out of trend in both plots. This point corresponds to solvent casted PLA/C30B (DC:32%, MAF:58%, RAF:9%) which in one hand is benefited from the large degree of crystallinity (meaning inferior number of permeable domains) but on the other hand doesn't show a large amount of rigid amorphous fraction.

The clear trend of increased water sorption with increased RAF is surprising since apart from the fact that the amount of RAF is relatively small (<20%) it is clear that RAF is not the only factor involved in determining water sorption (i.e. the MAF itself has to have some effect on water sorption, the degree of crystallinity will have some effect as a higher degree of crystallinity will mean a higher amount of impermeable domains, and other phenomena).

In order to evaluate the specific sorption of the RAF, the water sorption of the materials was modelled according to a three-phase model (Lin et al. 2002) (Eq 6.2). Briefly, the overall water sorption of the materials was divided as the sum of the water sorption of each of the three phases separately, expressed as:

$$S_{MAT}=DC*S_{DC}+MAF*S_{MAF}+RAF*S_{RAF} \quad (Eq\ 6.2)$$

where S_{MAT} is the sorption coefficient of the material; DC, MAF and RAF the amount of crystallinity, mobile amorphous and rigid amorphous fractions, respectively, and S_{DC}, S_{MAF} and S_{RAF} are the water vapour solubility coefficients of each fraction (0 for crystallinity, and 0.0112 for MAF, as calculated for 100% amorphous PLA (Figure 6.6)). The values of S_{RAF} are presented in Table 6.3.

Table 6.3 Specific water sorption coefficients of RAF for PLA and its nanocomposites under three different crystalline morphologies.

	S_{RAF}		
	AM	SC	FC
PLA		0.0577	0.0461
PLA/C30B 1%	0.0294	0.0323	0.0494
PLA/CNF 1%	0.0474	0.0545	0.0587
PLA/CNF 1%/C30B 1%	0.0485	0.0605	0.0643

From Table 6.3, it is evident how the specific sorption of the RAF varies with different materials and different crystalline morphologies, which can be attributed to the complexity of the RAF and to the presence of nanoparticles. In the same way that the degree of crystallinity was found not to be the only relevant parameter to evaluate the effect of crystallinity on water diffusion, other parameters such as the free volume of the RAF are important in respect to proper characterisation.

In any case, the rigid amorphous fraction of all of the materials showed a specific sorption coefficient in the same range (0.0501 +/- 0.011), which is substantially higher than the specific solubility coefficient of MAF (0.0112). This fact, apart from explaining the decreased water sorption with increased MAF, might also explain the different results found in the literature. When comparing the solubility coefficients of FC (fully crystallised) composites, it is evident how composites with CNF show substantially higher values than PLA and PLA/C30B. Unfortunately from the current data it couldn´t be determined if those variations were due to the sorption of the CNF itself or due to an increased free volume on the RAF created in regions close to the CNF.

Furthermore, it is evident how PLA/C30B 1% has lower S_{RAF} than the rest of the materials, especially in the AM and SC states. This is attributed to the long organic chains present in the C30B, which can partially fill the free volume present in the RAF close to the clay platelets. This effect is more pronounced when the amount of RAF induced by the clay platelets is greater than the RAF induced by other factors. In fact, in an AM state, when the RAF is considered to be only due to the presence of nanoparticles, the S_{RAF} presents the lower value (0.0294 g H_2O/g polymer), while in solvent casted and fully crystallised states (especially in the second one, since the full crystallisation showed higher RAF), where crystalline morphology also induces RAF, the S_{RAF} shows higher values (0.0323 and 0.0494 g H_2O/g polymer). This means that the crystallinity induces a RAF with an increased water sorption if compared with the RAF induced by the nanoparticles.

In conclusion, the results confirm that the RAF fraction has increased water sorption when compared with the MAF.

6.6 Influence of crystalline morphology and nanoparticles on the WVTR

From the data on water vapour diffusion, and water vapour sorption, the water vapour transmission rate (WVTR) at 23°C and 50% water activity could be estimated by means of Eq 6.1, the results for which are presented in Figure 6.8. For the sake of comparison, the decrease in the WVTR, due to full crystallisation, is also presented in the figure.

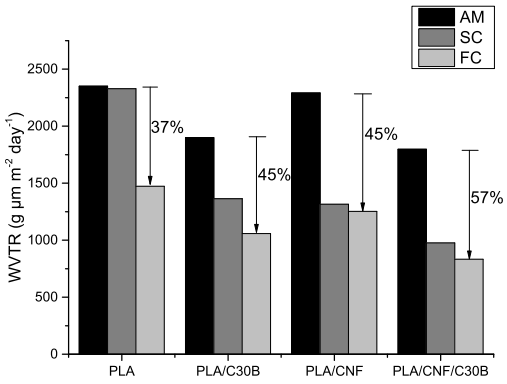

Figure 6.8 Water vapour transmission rate of PLA and its nanocomposites at different crystalline morphologies. (AM) Fully amorphous (SC) solvent casting and (FC) isothermal crystallisation. The arrows indicate the decrease in the WVTR due to full crystallisation of the same material (from amorphous to fully crystalized samples).

From Figure 6.8 it can be observed that there is a large decrease in the WVTR when moving away from the amorphous composites to fully crystallised ones. Full crystallisation was found to have a contradictory effect on the two variables that affect permeability (Eq 6.1), namely diffusivity and solubility. On the one hand, full crystallisation led to a strong decrease in water diffusion (Figure 6.5), but conversely it also led to a slight increase in water sorption (Figure 6.6). It can be noted that the WVTR decreases significantly after full crystallisation, meaning that the decrease in diffusivity has a greater impact than the increase in water sorption in PLA composites. A similar observation was done for oxygen and helium permeability (Guinault et al. 2012).

When evaluating the effect of the full crystallisation of PLA and composites (Figure 6.8), it is evident how the decrease in the WVTR, due to crystallisation, is greater for nanocomposites (45% for PLA/C30B and PLA/CNF and 57% for PLA/CNF/C30B) than for neat PLA (37%), meaning that the improvement in barrier properties is not only related to the presence of nanoparticles, but also to its ability to modify crystalline morphology.

Finally, the PLA/CNF 1%/C30B 1% nanocomposite, either in an amorphous or a fully crystallised state, showed a significant decrease in terms of WVTR. In fact the fully crystallized hybrid composite showed a 44% decrease on the WVTR when compared with the fully crystallized PLA proving that the combination of clay and nanocellulose is a powerful method for enhancing the barrier properties of nanocomposites. It could be claimed that this improvement is the result of increased amounts of nanoparticles (the hybrid PLA/CNF 1%/C30B 1% composite has double the amount of nanoparticles than PLA/C30B 1% and PLA/CNF 1%); however, in previous chapters it was concluded that increased nanoparticle content only resulted in a moderate improvement in barrier properties.

6.7 Summary

In this work it has been found that crystallinity has a great influence on the optical transparency and barrier properties of nanocomposites. As expected, increased crystallinity led to enhanced barrier properties, which is interesting for food packaging films, but also to reduced transparency, which is a drawback for this application. It was found that the sub-micron sized spherulites (induced by solvent casting at low temperature) had a lesser impact on both properties than the micro-sized spherulites induced at high-temperature processing. Furthermore, the impact of crystallinity on transparency was found to be greater than the impact of the nanoparticles.

When evaluating the effect of crystallinity on the barrier properties of PLA, it was found that apart from the degree of crystallinity there are other relevant parameters, such as spherulite size, which had a critical influence on water diffusivity and the so-called rigid amorphous fraction (RAF), which had 4.1-5.1-fold higher water sorption than the mobile amorphous fraction (MAF).

Furthermore, it was demonstrated that CNF reduced water diffusivity to a similar extent to C30B, proving that CNF is a good reinforcing agent for improving the barrier properties of PLA. Nanoparticles, in general, and cellulose nanofibres in particular actually benefit from their nucleating agent behaviour, which modifies the crystalline morphology of PLA. Finally, the fully crystallised composite, even with such low amounts as 1% of CNF and 1% of C30B, led to a 44% decrease in WVTR when compared with fully crystallised PLA, making this material promising for food packaging applications.

7. Hybrid PLA/surface modified cellulose nanofibres/clay composites for controlled release applications

In the previous chapter it was found that hybrid composites exhibited reduced water diffusivity when compared with neat PLA, and as a result they could therefore represent an interesting material for controlled release applications. Reduced diffusivity will increase the tortuous path that the released molecule has to follow in order to leave the polymer, and hence decrease the release. For this reason, in the present work I investigated whether this can be applied in a controlled release scenario.

In the present case carvacrol was chosen as a release agent, due to its antimicrobial activity (Nostro and Papalia 2012), its bio-based and biodegradable origins and its potential as a plasticiser (Nostro et al. 2012) and in addition, the CNF was surface-modified for two reasons: firstly to enhance the CNF dispersion on the matrix. As mentioned in larger detail in Appendix 1, the use of DMF to prepare CNF based composites was justified because the most commonly used solvent (DCM) led to a large CNF aggregates, therefore a strategy to enhance the CNF dispersion in the matrix was required within the matrix. Secondly, because the surface modification of CNF can add an extra function to the composite. Additionally, the hybrid composites showed a high brittleness that the addition of a plasticiser could solve.

There are many molecules that can make the CNF hydrophobic; hence, in order to facilitate the dispersion of CNF within the matrix, I have therefore used in this work a hydrophobic molecule that

might provide an extra function to the composite. In the present case it was chosen to graft hydrocinnamic acid, since it was found to decrease substantially the aroma barrier on PLA and hence could decrease the release of carvacrol even further. In fact, clay nanocomposites have been used on controlled release applications (San Román et al. 2013; Ramos et al. 2014) and the surface modified CNF has been used on PLA to reduce the diffusivity of tertbutylhydroquinone by approximately a factor of two (Almasi et al. 2014).

The present work was partially done during an external stay at Grenoble INP Pagora under the supervision of Dr. Julien Bras. A manuscript is under preparation for submission to a journal.

7.1 Characterization of the surface modification of CNF

Surface modification was done by using SOLREACT (Espino-Pérez et al. 2014), as detailed in Chapter 9. Briefly, a CNF suspension in water was mixed with HA (hydrocinnamic acid) and kept under vacuum conditions and at a high temperature (130°C) until the water evaporated completely. Thereafter, the hydrocinnamic acid started to react with the CNF through an esterification reaction, and the resulting water was removed by the high temperatures and by the vacuum. The processing temperature was 130°C, which is above the boiling point of the water thus allowing the evaporation of water and the melting point of hydrocinnamic acid, while it is below the boiling point of hydrocinnamic acid and the degradation of CNF.

In Figure 7.1A the complete FTIR spectra of the neat CNF and gCNF can be observed.

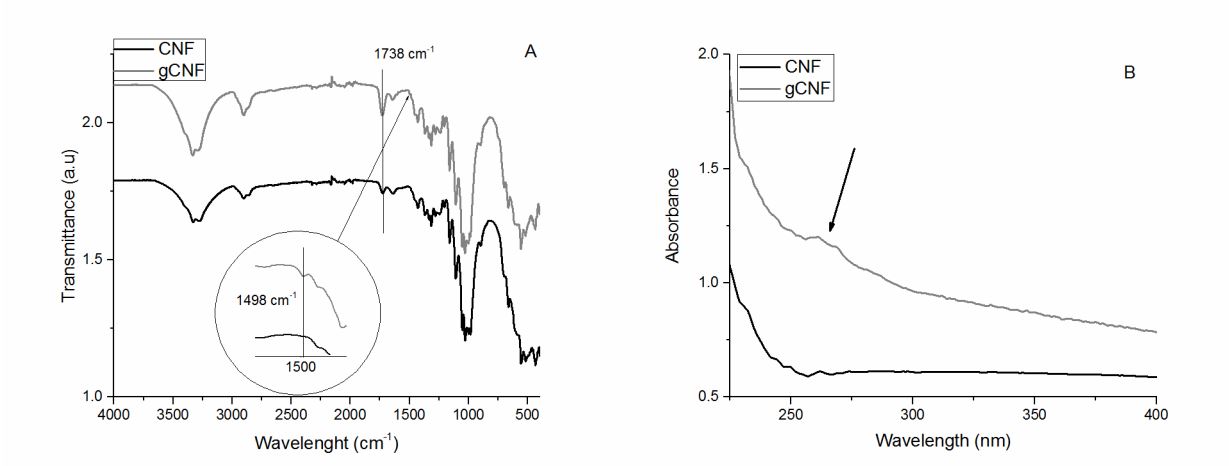

Figure 7.1 A) FTIR spectra of neat CNF and gCNF, b) UV-Vis spectroscopy of CNF and gCNF films.

Here, it is evident how the peak at 1738 cm^{-1}, which corresponds to C=O vibrations from the ester functions of the carboxylic acids, grows significantly from cellulose nanofibres (CNF) into surface-modified cellulose nanofibres (gCNF), proving that grafting did indeed take place. A small peak at

1738 cm^{-1} can be seen for the non-grafted CNF, due to the presence of acetyl groups, which is characteristic of this specific CNF extraction method. Furthermore, no peaks at 1700 cm^{-1} related to carboxylic acid reagent were found, thereby proving that there were no remaining unreacted carboxylic groups (Espino-Pérez et al. 2014). Finally, there is a very small peak present at 1498 cm^{-1}, which is attributed to the aromatic C=C in plane symmetrical stretching (Mandal and Chakrabarty 2011) which is present on the hydrocinnamic acid (Espino-Pérez et al. 2014). Furthermore, as seen in Figure 7.1B, the gCNF film shows slight absorbance around 270 nm, which is absent on neat CNF film. This peak is attributed to the absorbance of the aromatic rings of hydrocinnamic acid, proving the presence of hydrocinnamic acid despite several cycles of cleaning.

Moreover, in Figure 7.2, a suspension of grafted and non-grafted CNF in water after 16 hours can be observed.

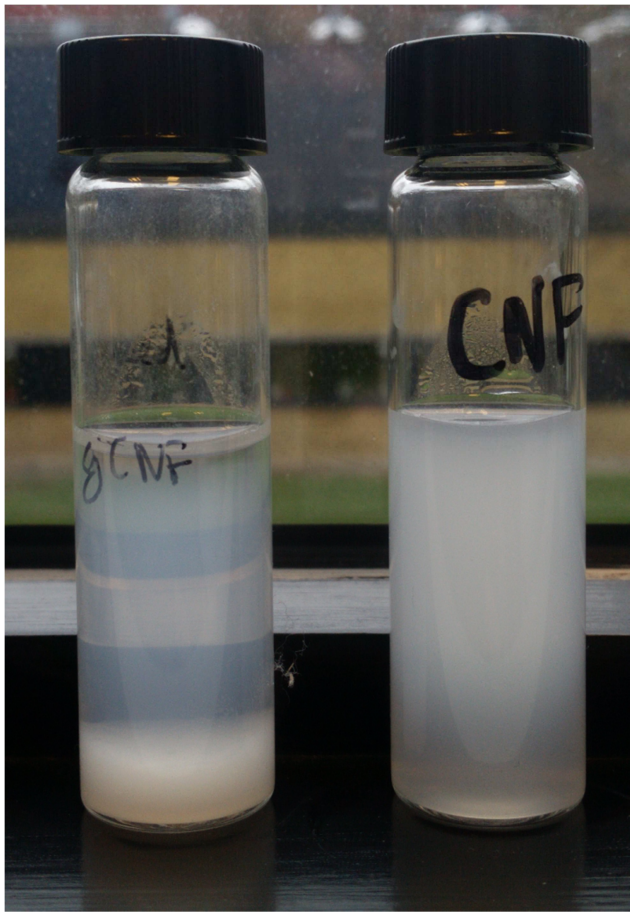

Figure 7.2 Stability of suspensions of gCNF (left) and CNF (right) at 0.4 wt% nanomaterial in water after 16 hours.

As can be noted, the grafted CNF shows completely different behaviour to the non-grafted CNF. In the case of the water suspension it can be seen clearly how, due to the hydrophobicity of the gCNF, the suspension is not stable in water, proving the surface modification of the CNF.

Finally, the gCNF (79° +/- 5°) based film showed a superior advancing contact angle when compared with the neat CNF (49° +/- 3°) based film which is attributed to the hydrophobicity of the grafted chain. All of those results confirm that the grafting has taken place in a considerable extent although still a small amount of non-surface modified CNF might still be present.

7.2 Effect of surface modification on material structure

In Figure 7.3 the TGA of the CNF and gCNF can be seen. It is evident how, between 50-150°C, the mass loss of the neat CNF is higher than the gCNF, which is attributed to the fact that the gCNF is more hydrophobic and hence more likely to absorb less water. Furthermore, there is a decrease in the onset temperature for the gCNF, compared with the non-grafted CNF. The faster degradation of the gCNF is ascribed to the fact that the thermal stability decreases with increased chain length of the esters (Tosh 2011).

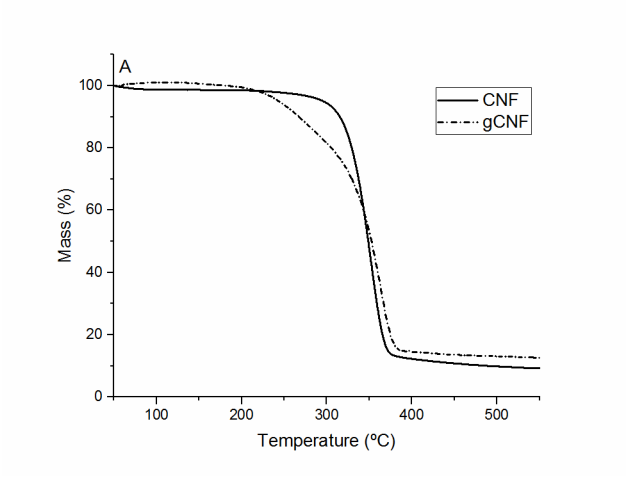

Figure 7.3 TGA of CNF and gCNF.

Furthermore, in Figure 7.4, the XRD pattern of the grafted and non-grafted CNF is shown. The XRD spectra shows the expected peaks from a cellulose material with peaks at $2\theta=15.3^{o}$ and $2\theta=22.8^{o}$. The crystallinity index of the extracted fibres was calculated using the Buschle-Diller and Zeronian equation (Eq 2.1).

$$I_C = 1 - \frac{I_1}{I_2} \text{ (Eq 2.1)}$$

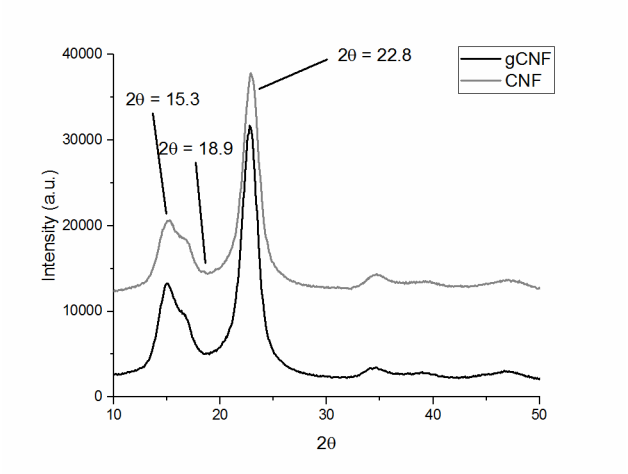

Figure 7.4 XRD patterns of the CNF and gCNF.

Where I_1 is the peak at 2θ=18.8° (amorphous peak) and I_2 is the peak at 2θ=22.8° (crystalline peak), I_c, the crystalline index, was determined to be 84%. All samples have a crystalline organisation, as shown by the presence of the peaks at (15.8°) and (22.8°). From the peak at 22.8° of the XRD pattern the degrees of crystallinity of the neat CNF and gCNF was calculated and determined to the same (84%) meaning that the grafting procedure did not affect the structure of the CNF. This is attributed to the strong pre-treatments of the CNF.

7.3 Evaluation of the dispersion of composites

The composites were prepared by solvent casting procedure using DCM as a solvent as detailed in experimental procedures (chapter 9). Briefly, suspensions of CNF and gCNF in DCM were prepared by solvent exchange (several cycles of centrifugation and re-dispersion) to DCM. In the case of C30B the suspension was prepared by ultrasonication of 2.5 g of C30B in 250 mL of DCM. Thereafter these suspensions were mixed with the desired amount of PLA and carvacrol and the suspension was rinsed to 100 mL with additional DCM. After that the films were casted in a Teflon mold and the DCM was evaporated overnight at room temperature in a climatic chamber to be thereafter dried for 300 min at 50°C in an oven. Using this protocol 5 composites were prepared: neat PLA, PLA +6wt% carvacrol (CR), PLA/CNF 3% + 6wt% carvacrol, PLA/gCNF 3t% + 6wt% carvacrol and PLA/gCNF 3%/C30B 5% + 6wt% carvacrol.

In Figure 7.5 (picture of the films) and Figure 7.6 (SEM) the dispersion of both PLA/CNF 3% and PLA/gCNF 3% films is studied.

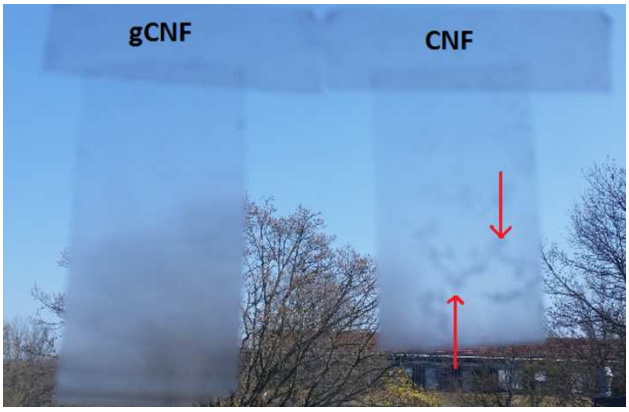

Figure 7.5 A) Pictures of PLA/gCNF 3% + 6% CR and PLA/CNF 3% + 6% CR film (wt%).

In Figure 7.5 it can be seen clearly that while the non-modified CNF shows clear aggregates, the gCNF does not show them. This is in agreement with previous experiences where it was found that the DCM (dichloromethane) was leading to large CNF aggregates when used to prepare PLA/CNF composites. For this reason, CNF and CNC based composites had to be prepared using DMF (dimethylformamide) which was considered the best possible solvent (Appendix 1). Nevertheless, for the scope of this work it was decided to use DCM as solvent because this would be an effective way to prove how the surface modification can enhance the dispersion of the gCNF as reported in the literature(Dufresne 2010).

In addition, in a representative SEM of both composites is presented. As illustrated, the non-grafted CNF-based composite showed clear aggregates that can be observed without any magnification. However, the gCNF did not show any aggregates, neither on the picture nor on the SEM, and so it can be concluded that the gCNF composite is well-dispersed.

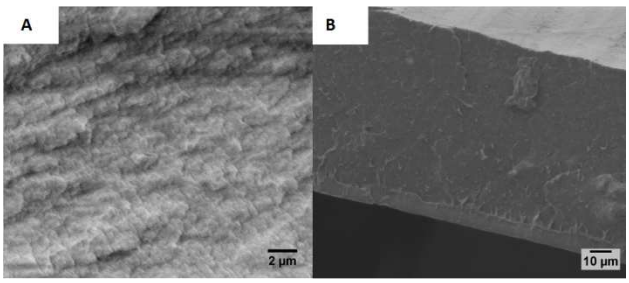

Figure 7.6 A) Scanning Electron Micrograph of PLA/gCNF 3% + 6wt% CR composite B) Scanning Electron Micrograph of PLA/CNF 3% + 6wt% CR composite.

In Figure 7.7 the scanning electron micrographs of the cross-section of the PLA/gCNF 3%/C30B 5%+CR, as well as the XRD patterns of C30B and the hybrid composites, are presented.

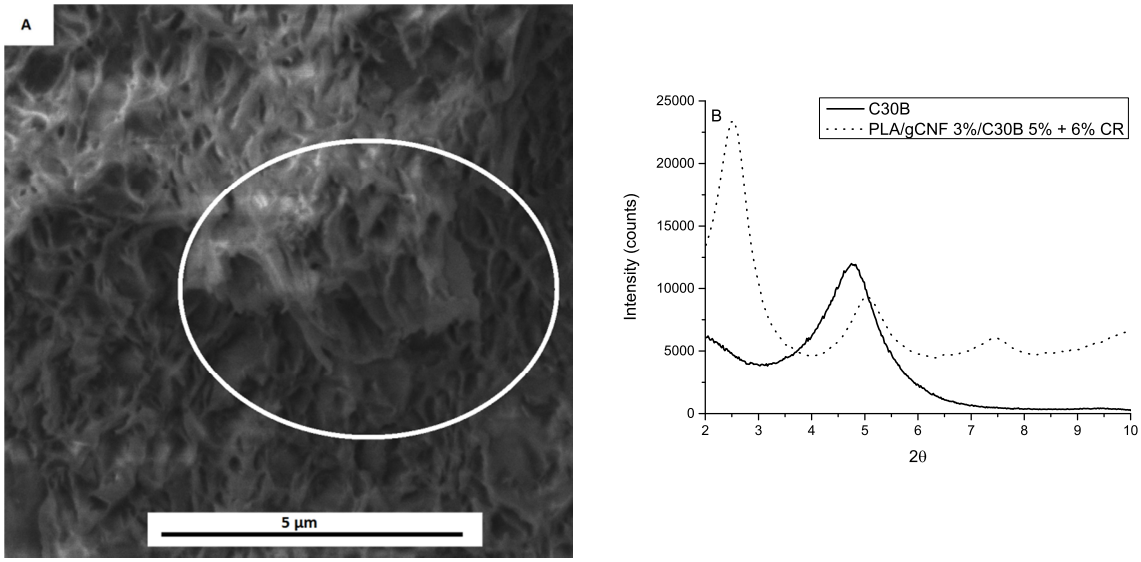

Figure 7.7 A) Scanning electron micrograph of PLA/gCNF 3%/C30B 5% + 6 wt% CR composite B) XRD pattern of the same composite (neat C30B as reference)

Although from the SEM no very large aggregates were found, a few clay platelets were observed. The clay dispersion was further investigated by XRD. As is evident from the XRD pattern of the hybrid PLA/gCNF 3%/C30B 5%, the peak of the neat C30B ($2\theta = 4.8°$) is present on composites at ($2\theta = 2.5°$ and $2\theta = 5.2°$), although the first peak is much stronger than the second one. This means that there is an increase in the d-spacing of the clay that can only be explained as being the result of incorporating polymer chains within the clay galleries (McLauchlin and Thomas 2009). Hence, it can be concluded that the clay is mainly intercalated. The reason for the different clay dispersion of those hybrid composites when compared with the clay composites presented in chapters 3 and 4, is that this work was done at the facilities of Grenoble INP-Pagora hence by using a different ultrasonicator.

7.4 Effect of carvacrol addition on the performance of PLA and composites as food packaging materials

In Figure 7.8 the UV-Vis spectrometry results for composites are presented. Here, it is evident that the addition of CNF or gCNF to the PLA matrix did not have a significant influence on the optical properties of the composite, though the PLA/gCNF 3%/C30B 5% + 6wt% CR composite shows a significant decrease in transmittance, which is attributed to incomplete dispersed clay. Furthermore, it can be seen clearly that the composite with clay shows UV-blocking capabilities (Figure 7.8). The absence of transmittance between 260 and 280 nm is the result of the presence of carvacrol, which absorbs UV light in this range.

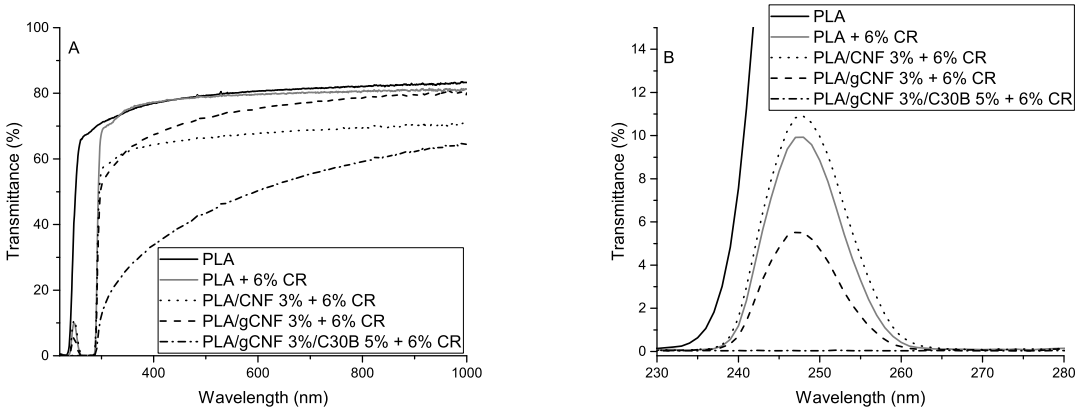

Figure 7.8 UV-VIS transmittance of neat PLA and composites. A) Whole range (220 nm-1000 nm) B) zoom-in of the range 220-280 nm.

The mechanical properties were investigated by DSC and tensile stress tensing as showed in Figure 7.9. The results retrieved from the second heating cycle of DSC showed that the T_g of the carvacrol-loaded materials were ranging 39-33°C, which is significantly below the T_g of PLA and composites without carvacrol under any crystalline morphology, thus confirming the plasticisation.

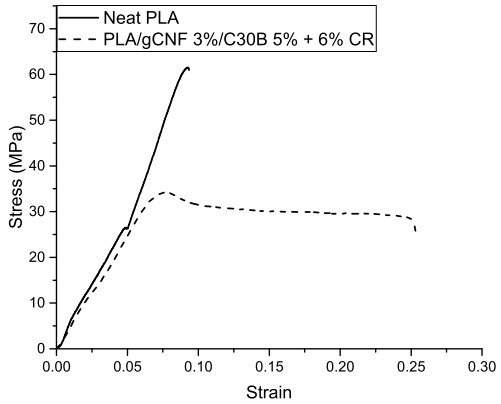

Figure 7.9 Strain-stress diagram of neat PLA and carvacrol-loaded materials.

Testing the mechanical properties of composites was found to be challenging because of their tendency of breaking in the holding point. Only valid results could be retrieved from neat PLA and the hybrid composite. In any case it is clearly shown in Figure 7.9 how the carvacrol loaded hybrid composite shows an increased elongation at break. This is because, as reported, the essential oils have a plasticising effect in polymers (Ramos et al. 2014) and PLA/CNC composites (Salmieri et al. 2014). Finally, the TGA showed no mass loss near boiling point of DCM, it was concluded that no significant amount of DCM was present on the samples.

As barrier properties are important in food packaging, the effect of adding carvacrol to the WVTR on composites was investigated, and the results can be found in Figure 7.10.

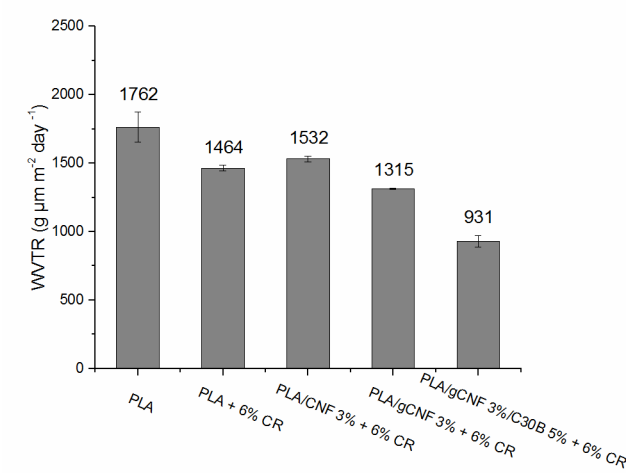

Figure 7.10 WVTR (measured at 23°C and 50% RH) of the neat PLA and carvacrol loaded composites (wt%).

When comparing PLA and PLA/+ 6% CR it is evident how the addition of carvacrol slightly decreases the WVTR of PLA. It was also observed how the addition of CNF actually slightly increases the WVTR, probably due to the formation of aggregates. On the contrary the addition of the better dispersed gCNF slightly decreases the WVTR, probably due to the enhanced dispersion of CNF. Finally, the PLA/gCNF 3%/C30B 5% + 6wt% CR show a 49% reduction in the WVTR when compared with neat PLA, thereby suggesting that this hybrid material is very suitable as a barrier material.

7.5 Impact of the presence of nanoparticles on the controlled release of carvacrol

Finally, the controlled release of carvacrol to a fatty food simulant (MeOH 95%) of composites was evaluated by the use of UV-Vis spectroscopy. Briefly, approximately 40 mg of film was placed in a vial with 20 mL of MeOH 95 V/V% and periodically one aliquot (300 µL) was taken for UV-Vis spectroscopy. The results for which are shown in Figure 7.11.

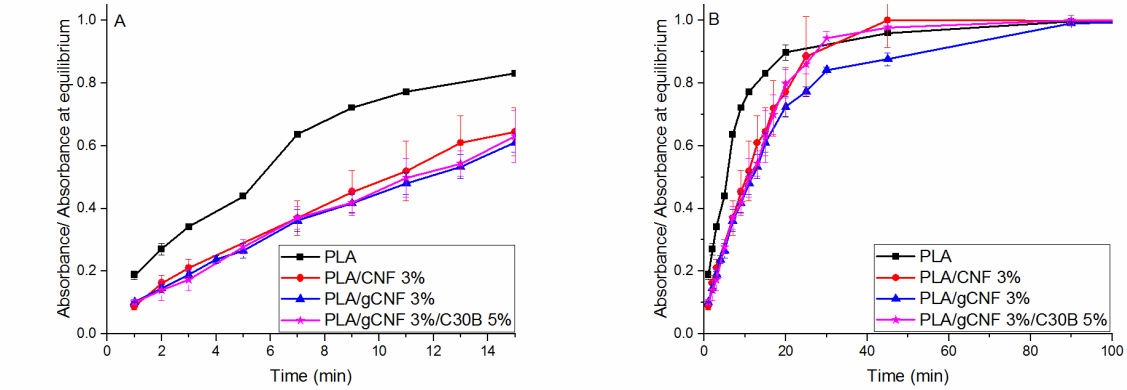

Figure 7.11 Controlled release behaviour of PLA and nanocomposites a) Zoom-in first 15 minutes of experiment. B) whole range.

There it can be seen how there is a clear decrease in the release kinetic, due to the addition of nanoparticles. From Figure 7.11A it can be seen how all of the composites show a reduced release rate if compared with neat PLA. In fact, after 9 minutes of experiment, PLA has released approximately the 72% of the carvacrol, while the rest of the composites released a substantially lower amount; (PLA/CNF a 45%, and both PLA/gCNF 3%/C30B 5% and PLA/gCNF a 41%). Finally, it is noteworthy to highlight that at larger experiment times (40-80 min) the PLA/gCNF 3% composite showed a reduced release when compared with the rest of the materials.

The moderate performance of the PLA/gCNF 3%/C30B 5% can attributed to the poor clay dispersion leading to a low amount of clay platelets within the matrix, as well as to the reduced amount of PLA (higher the nanoparticle content, lower the amount of amorphous region hence reduced carvacrol absorption capacity of the material). On top of that, in the intercalated morphology, carvacrol molecules could be inside clay galleries, where a faster mass transport is likely to happen.

Finally, all of the materials showed a milky appearance, in contrast with the high transparency prior to the immersion on MeOH, after the testing, suggesting that the carvacrol release under those conditions is due to swelling which is known to be a controlled release mechanism (Mastromatteo et al. 2010).

7.6 Summary

Acetylated CNF was successfully surface modified with hydrocinnamic acid by using SOLREACT. The effect of the carvacrol addition and surface modification of CNF on the performance of hybrid CNF/C30B composites as food packaging material was evaluated. It was found that the surface modification of the CNF greatly enhanced the dispersion of nanocellulose within the matrix and that the incorporation of carvacrol successfully plasticised the hybrid CNF/C30B composite. The hybrid PLA/gCNF 3%/C30B 5% showed a largely reduced carvacrol release rate when compared with neat PLA, an increased elongation at break and a large decrease in the WVTR, and UV-blocking behaviour, thereby showing that hybrid composites have a high potential for controlled release applications.

8. Conclusion and future work

8.1 Conclusion

In this work it was proven that alkali-acetylation treatments can be used to extract CNF. This procedure leads to a high yield of acetylated CNF with low amounts of micro-sized fibres, by using a potentially upscalable procedure. Regardless of other potential applications, these CNF examples demonstrated the high potential of being able to reinforce PLA films on food packaging; PLA/CNF composites had a large increase in thermomechanical and barrier properties, when compared with PLA or other potential alternative nanoparticles such as nanoclay. Furthermore, PLA reinforced with both CNF and C30B improved greatly in terms of barrier and thermomechanical properties, which made hybrid composites a real alternative to traditionally used packaging materials.

Moreover, an evaluation of the influence of CNF and C30B on isothermal crystallisation behaviour was carried out. Apart from minor differences, which are mainly represented by the faster nucleation provided by C30B, it was found that both CNF and C30B induced similar crystalline morphologies which were clearly different from the neat PLA example. The presence of nanoparticles, which are nucleating agents, caused more regular crystallinity and better spherulite distribution, which was found to have a certain influence decreasing water vapour barrier properties. While the full crystallization at 120°C of fully amorphous samples decreased the WVTR of PLA by 33%, it decreased by 45% the WVTR of PLA/CNF and PLA/C30B composites and by 57% the WVTR of PLA/CNF/C30B composite.

The effect of crystallinity and the presence of nanoparticles on the properties of PLA were compared, and it was ascertained that crystalline morphology has a higher impact on optical

transparency than the moderate presence of nanoparticles, except for the UV clocking capabilities of C30B. The impact of crystalline morphology in terms of WVTR was found to be highly dependent on processing temperature. While high temperature processing induced a larger spherulite size, highly efficient to decrease water diffusion, it was also inducing a larger RAF fraction which showed 4.1- 5.1 times higher water sorption than MAF. In the other hand, low temperature processing was leading to smaller spherulite size, less effective in decreasing water sorption, but which reduced the amount of induced RAF therefore, reducing the water sorption. Moreover, it was found that CNF and C30B showed similar efficacies reducing water diffusion, although, the CNF composites showed larger water sorption. Finally, it was determined that even the addition of quantities as low as 1% of CNF and 1% of C30B significantly decreased the WVTR (a 44% decrease when comparing fully crystallised PLA and fully crystallised PLA/CNF 1%/C30B 1%) due to a large decrease in water diffusion.

Due to this strong decrease in water diffusion, caused by both crystallinity and the presence of both nanoparticles, it was considered that hybrid materials could have potential for controlled release applications, and therefore carvacrol-loaded composites were prepared. In order to enhance the dispersion of CNF within the matrix during the solvent casting procedure, as well as to decrease the release speed, hydrocinnamic acid was grafted onto the surface of the nanocellulose.

In general, it was concluded that the combination of CNF and C30B successfully improved critical weaknesses of PLA, such as low thermomechanical resistance, slow crystallisation kinetics and moderated barrier properties, without affecting dramatically optical transparency. Furthermore, it was found that RAF showed a largely increased water sorption, which is another of the drawbacks of PLA. Finally, the addition of carvacrol was found to plasticise PLA successfully, which was another weakness of PLA. Therefore, it has to be concluded that hybrid composites are a promising material for food packaging applications.

8.2 Future work

8.2.1 CNF production

In the second chapter, it was discovered that a combination of alkali-acetylation pre-treatments leads to the production of CNF. Since the chemicals used in this process are not likely to be expensive and are already used in the pulp and paper industry, and that the necessary mechanical stirring is not likely to consume a significant amount of energy, this is a procedure that is likely to be industrially relevant, and optimisation works should be carried out which could increase the amounts processed and reduce treatment times, especially for mechanical methods.

8.2.2 Composite preparation

In the present work, it was found that the combination of nanocellulose and clay within the matrix led to a PLA-based nanocomposite with increased properties, when compared with neat PLA. Furthermore, the effect of crystalline morphology on the final properties was evaluated. However, the composites were prepared by using the solvent casting approach, which is unlikely to be an industrially-relevant procedure, and so these particular composites should be prepared by employing a procedure such as melt compounding.

In addition, the lack of surface charge of the CNF used on this study, suggests their suitability for electrospinning. Actually the electrospinning has been proposed as a method for pre-incorporating CNF in a polymer matrix. This concentrate could be thereafter incorporated to a larger amount of polymer in an extruder (Martínez-Sanz et al. 2012).

9. Experimental work

9.1 Determining the DC, RAF and MAF by MDSC

The DC, MAF and RAF were calculated by MDSC using a modulation of ± 0.50°C every 30 seconds on all of the heating cycles.

The degree of crystallinity (DC) was determined by means of (Eq 9.1).

$$DC = \frac{\Delta H_{nonrev} - \Delta H_{rev}}{\Delta H_0} \quad \text{(Eq 9.1)}$$

where DC is the degree of crystallinity of the composite, ΔH_{nonrev} is non-reversible enthalpy and ΔH_{rev} is reversible enthalpy. A melting enthalpy ΔH_0 of 106 J g^{-1} for 100% crystalline α–poly (L-lactide) was used as reported (Zuza et al. 2008), while enthalpy 25 J g^{-1} lower (81 J g^{-1}) was considered for the α´phase, as suggested in the literature (Righetti et al. 2015).

The amount of mobile amorphous fraction (MAF) and rigid amorphous fraction (RAF) on the composites was facilitated by adapting an existing protocol for PLA (Zuza et al. 2008). First, heat capacity variations of PLA and composites in an amorphous state were determined from at least four specimens. Thereafter, MAF was determined by means of (Eq 9.2).

$$MAF = \frac{\Delta Cp}{\Delta Cp'} \frac{\Delta Cp_{PLA}}{\Delta Cp_{MAT}} \text{(Eq 9.2)}$$

where ΔCp is the specific heat change of the tested specimen at its T_g, while ΔCp´ is the specific heat change of the same specimen in a completely amorphous state. ΔCp_{PLA} is the heat capacity variation

of amorphous PLA and finally, ΔCp_{MAT} is the heat capacity variation of tested material in an amorphous state.

RAF was calculated by means of Eq 9.3:

$$\% \text{ RAF} = 100 - \%\text{MAF} - \%\text{DC} - X_n \quad \text{(Eq 9.3)}$$

Where RAF is the rigid amorphous fraction, MAF, the mobile amorphous fraction, DC the degree of crystallinity and X_n nanoparticle content.

9.2 Surface modification of cellulose nanofibres

The CNF samples were grafted with hydrocinnamic acid, using SOLREACT (Espino-Pérez et al. 2014). A 150 mL solution of CNF at 1% w/V was adjusted to pH 4.3 by adding HCl 0.01 N and the mixed with 26g of hydrocinnamic acid (approximately in a 1:10 molar ratio). This mixture was collected in a two-necked 250 mL flask, in which a thermometer was placed in one of the necks, to control the temperature inside the flask, while the other neck was connected to a cooler. The cooler was connected to a three-neck round bottom flask which was connected to a vacuum pump (Figure 9.1).

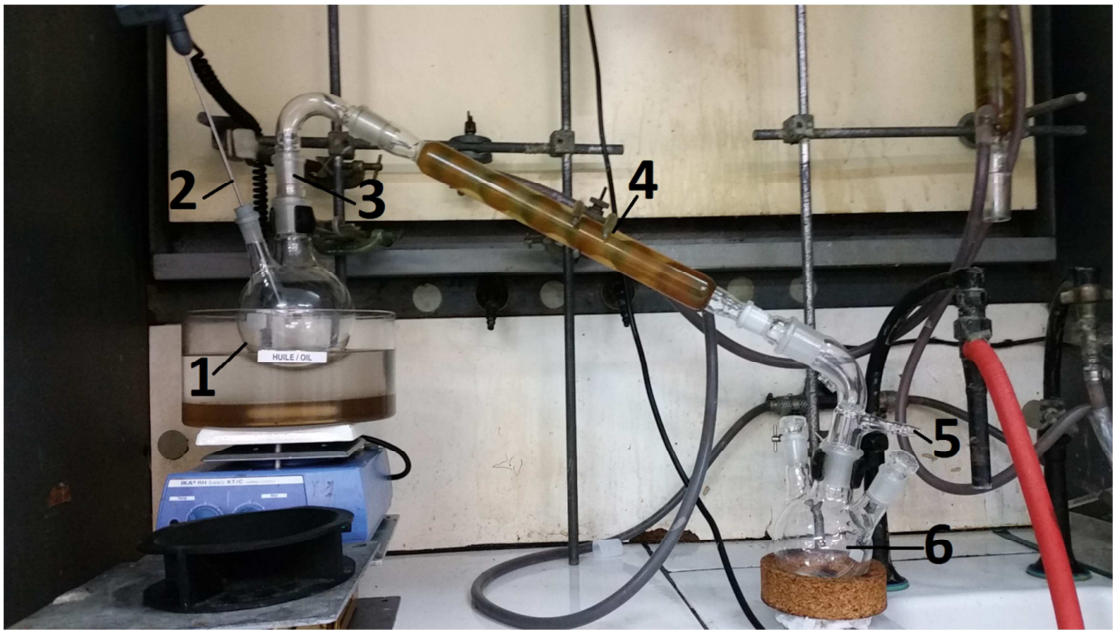

Figure 9.1 Experimental set-up. 1) Reactor, 2) Thermometer, 3) Connection with the cooler, 4) Cooler, 5) Input of the vacuum pump and 6) Water collector.

The system was set to 130°C for a reaction time of 16 hours. The product was recovered by washing the reactor with ethanol, and then it was centrifuged for 10 minutes at 10000 rpm and re-suspended in ethanol. This procedure was repeated three times, in order to remove all of the non-reacted hydrocinnamic acid from the mixture. Finally, the grafted CNF was centrifuged and the solvent exchanged to DCM three times.

The non-grafted CNF was solvent exchanged from water to ethanol three times, and thereafter it was solvent exchanged to DCM three times under the same conditions as gCNF.

9.3 Preparation of carvacrol-loaded composites

A) PLA

A total of 3.3 g PLA was dissolved in 100 mL DCM with magnetic stirring at room temperature for 4 hours. Thereafter, the solution was cast in a 12x12 cm Teflon mould (50 mL/each mould) and the DCM was evaporated at room temperature for 17 hours. Finally, the films were dried for 300 mins at 50°C.

B) PLA + 6wt% carvacrol

A total of 3.3 g PLA was dissolved in 100 mL DCM with magnetic stirring at room temperature for 4 hours. Thereafter, 0.2 mL carvacrol of carvacrol ere added and the solution was cast in a 12x12 cm Teflon mould (50 mL/each mould) and the DCM was evaporated at room temperature for 17 hours. Finally, the films were dried for 300 mins at 50°C.

C) PLA/CNF 3% and PLA/gCNF 3% + 6wt% carvacrol

The non-grafted and grafted CNF solutions were solvent exchanged to DCM three times.

To prepare the PLA/CNF 3% + carvacrol solution, 3.3 g of PLA were added to a solution of 30 mL of CNF (0.33 wt%), 0.2 mL carvacrol and 70 mL DCM.

To prepare the PLA/gCNF 3% + carvacrol solution, 3.3 g of PLA were added to a solution of 36 mL gCNF (0.27 wt%), 0.2 mL carvacrol and 64 mL DCM.

Both mixtures were kept under strong magnetic stirring for 4 hours, and they were thereafter cast in two 12x12 cm Teflon moulds (50 mL/each mould). Finally, the DCM was selectively evaporated from the mixture at room temperature for 17 hours, followed by a drying time of 300 mins at 50°C.

D) PLA/gCNF 3%/C30B 5% + 6wt% carvacrol

First, 2.5g of C30B were pre-dispersed on 250 mL of DCM by magnetic stirring for 72 hours. Second, the mixture was submitted to HIUS (Branson Sonifier 250) for 3 hours with the following conditions: 60% output power and a 50% cycle for 3 hours. Third, the solution was rinsed again to 250 mL.

The PLA/gCNF/3% C30B 5% + carvacrol (6%) solution was prepared by adding 3.3 g of PLA to a 36 mL solution CNF (at 0.27 wt%), 0.2 mL carvacrol, 18 mL C30B solution and 46 mL DCM.

The mixture was kept under strong magnetic stirring for 4 hours to be cast thereafter in two Teflon moulds of 12x12 cm (50 mL/mold) covered by a filter paper, and the DCM was selectively evaporated at room temperature for 17 hours. Finally, the samples were dried for 300 mins at 50°C.

References

Abdul Khalil HPS, Davoudpour Y, Islam MN, et al (2014) Production and modification of nanofibrillated cellulose using various mechanical processes: a review. Carbohydr Polym 99:649–65. doi: 10.1016/j.carbpol.2013.08.069

Abdulkhani A, Hosseinzadeh J, Ashori A, et al (2014) Preparation and characterization of modified cellulose nanofibers reinforced polylactic acid nanocomposite. Polym Test 35:73–79. doi: 10.1016/j.polymertesting.2014.03.002

Abushammala H, Krossing I, Laborie M-P (2015) Ionic liquid-mediated technology to produce cellulose nanocrystals directly from wood. Carbohydr Polym 134:609–616. doi: 10.1016/j.carbpol.2015.07.079

Alexandre B, Langevin D, Médéric P, et al (2009) Water barrier properties of polyamide 12/montmorillonite nanocomposite membranes: Structure and volume fraction effects. J Memb Sci 328:186–204. doi: 10.1016/j.memsci.2008.12.004

Almasi H, Ghanbarzadeh B, Dehghannya J, et al (2014) Development of a novel controlled-release nanocomposite based on poly(lactic acid) to increase the oxidative stability of soybean oil. Food Addit Contam Part A 31:1586–1597. doi: 10.1080/19440049.2014.935962

Ambrosio-Martín J, Lopez-Rubio A, Fabra MJ, et al (2015) Assessment of ball milling methodology to develop polylactide-bacterial cellulose nanocrystals nanocomposites. J Appl Polym Sci 132: 41605. doi: 10.1002/app.41605

Arjmandi R, Hassan A, Haafiz MKM, et al (2015a) Effect of hydrolysed cellulose nanowhiskers on properties of montmorillonite/polylactic acid nanocomposites. Int J Biol Macromol 81:91–99. doi: 10.1016/j.ijbiomac.2015.11.028

Arjmandi R, Hassan A, Mohamad Haafiz MK, Zakaria Z (2015b) Partial replacement effect of montmorillonite with cellulose nanowhiskers on polylactic acid nanocomposites. Int J Biol Macromol 81:91–99. doi: 10.1016/j.ijbiomac.2015.07.062

Aulin C, Gällstedt M, Lindström T (2010) Oxygen and oil barrier properties of microfibrillated cellulose films and coatings. Cellulose 17:559–574. doi: 10.1007/s10570-009-9393-y

Aulin C, Salazar-Alvarez G, Lindström T (2012) High strength, flexible and transparent nanofibrillated cellulose–nanoclay biohybrid films with tunable oxygen and water vapor permeability. Nanoscale 4:6622–6628. doi: 10.1039/c2nr31726e

Azizi Samir MAS, Alloin F, Dufresne A (2005) Review of recent research into cellulosic whiskers, their properties and their application in nanocomposite field. Biomacromolecules 6:612–26. doi: 10.1021/bm0493685

Belbekhouche S, Bras J, Siqueira G, et al (2011) Water sorption behavior and gas barrier properties of cellulose whiskers and microfibrils films. Carbohydr Polym 83:1740–1748. doi: 10.1016/j.carbpol.2010.10.036

Bismarck A, Aranberri-Askargorta I, Springer J, et al (2001) Surface characterization of natural fibers; surface properties and the water up-take behavior of modified sisal and coir fibers. Green Chem 3:100–107. doi: 10.1039/b100365h

Bogoeva-Gaceva G, Avella M, Malinconico M, et al (2007) Natural fiber eco-composites. Polym Compos 28:98–107. doi: 10.1002/pc.20270

Bouwmeester H, Hollman PCH, Peters RJB (2015) Potential Health Impact of Environmentally Released Micro- and Nanoplastics in the Human Food Production Chain: Experiences from Nanotoxicology. Environ Sci Technol 49:8932–8947. doi: 10.1021/acs.est.5b01090

Cairncross RA, Becker JG, Ramaswamy S, O'connor R (2006) Moisture Sorption, Transport, and Hydrolytic Degradation in Polylactide. Appl Biochem Biotechnol 131:774–785. doi: 10.1385/ABAB:131:1:774

Cairncross RA, Ramaswamy S, O'Connor R (2007) Moisture Sorption and Transport in Polylactide. Int

Polym Process 22:33–37. doi: 10.3139/217.0985

Chang J, An YU, Sur GS (2003) Poly(lactic acid) nanocomposites with various organoclays. I. Thermomechanical properties, morphology, and gas permeability. J Polym Sci Part B Polym Phys 41:94–103. doi: 10.1002/polb.10349

Chen G, Kim H, Park BH, Yoon J (2005) Controlled Functionalization of Multiwalled Carbon Nanotubes with Various Molecular-Weight Poly(l-lactic acid). J Phys Chem B 109:22237–22243. doi: 10.1021/jp054768n

Cherian BM, Leão AL, de Souza SF, et al (2010) Isolation of nanocellulose from pineapple leaf fibres by steam explosion. Carbohydr Polym 81:720–725. doi: 10.1016/j.carbpol.2010.03.046

Chinh NT, Trang NTT, Thanh DTM, et al (2014) Thermal property, morphology, and hydrolysis ability of poly(lactic acid)/chitosan nanocomposites using polyethylene oxide. J Appl Polym Sci 132:41690. doi: 10.1002/app.41690

Cocca M, Lorenzo ML Di, Malinconico M, Frezza V (2011) Influence of crystal polymorphism on mechanical and barrier properties of poly(l-lactic acid). Eur Polym J 47:1073–1080. doi: 10.1016/j.eurpolymj.2011.02.009

Colomines G, Ducruet V, Courgneau Ć, et al (2010) Barrier properties of poly(lactic acid) and its morphological changes induced by aroma compound sorption. Polym Int 59:818–826. doi: 10.1002/pi.2793

Corrêa MCS, Branciforti MC, Pollet E, et al (2011) Elaboration and Characterization of Nano-Biocomposites Based on Plasticized Poly(Hydroxybutyrate-Co-Hydroxyvalerate) with Organo-Modified Montmorillonite. J Polym Environ 20:283–290. doi: 10.1007/s10924-011-0379-0

Courgneau C, Domenek S, Guinault A, et al (2011) Analysis of the Structure-Properties Relationships of Different Multiphase Systems Based on Plasticized Poly(Lactic Acid). J Polym Environ 19:362–371. doi: 10.1007/s10924-011-0285-5

Courgneau C, Domenek S, Lebossé R, et al (2012) Effect of crystallization on barrier properties of formulated polylactide. Polym Int 61:180–189. doi: 10.1002/pi.3167

Crank J (1975) The mathematics of diffusion, 2nd edition.Oxford University Press.

Davis EM, Minelli M, Baschetti MG, et al (2012) Nonequilibrium sorption of water in polylactide.

Macromolecules 45:7486–7494. doi: 10.1021/ma301484u

Davis EM, Minelli M, Giacinti Baschetti M, Elabd YA (2013) Non-Fickian Diffusion of Water in Polylactide. Ind Eng Chem Res 52:8664–8673. doi: 10.1021/ie302342m

de Morais Teixeira E, Corrêa AC, Manzoli A, et al (2010) Cellulose nanofibers from white and naturally colored cotton fibers. Cellulose 17:595–606. doi: 10.1007/s10570-010-9403-0

Deepa B, Abraham E, Cherian BM, et al (2011) Structure, morphology and thermal characteristics of banana nano fibers obtained by steam explosion. Bioresour Technol 102:1988–1997. doi: 10.1016/j.biortech.2010.09.030

Del Nobile MA, Conte A, Buonocore GG, et al (2009) Active packaging by extrusion processing of recyclable and biodegradable polymers. J Food Eng 93:1–6. doi: 10.1016/j.jfoodeng.2008.12.022

Dennison DB, Kirk JR (1978) Oxygen effect on the degradation of ascorbic acid in a dehydrated food system. J Food Sci 43:609–618. doi: 10.1111/j.1365-2621.1978.tb02365.x

Drieskens M, Peeters R, Mullens J, et al (2009) Structure versus properties relationship of poly(lactic acid). I. Effect of crystallinity on barrier properties. J Polym Sci Part B Polym Phys 47:2247–2258. doi: 10.1002/polb.21822

Duan Z, Thomas NL, Huang W (2013) Water vapour permeability of poly(lactic acid) nanocomposites. J Memb Sci 445:112–118. doi: 10.1016/j.memsci.2013.06.008

Dufresne A (2010) Processing of Polymer Nanocomposites Reinforced with Polysaccharide Nanocrystals. Molecules 15:4111–4128. doi: 10.3390/molecules15064111

Eichhorn S, Dufresne A (2010) Review: current international research into cellulose nanofibres and nanocomposites. J Mater Sci 45:1–33. doi: 10.1007/s10853-009-3874-0

Espino-Pérez E, Bras J, Ducruet V, et al (2013) Influence of chemical surface modification of cellulose nanowhiskers on thermal, mechanical, and barrier properties of poly(lactide) based bionanocomposites. Eur Polym J 49:3144–3154. doi: 10.1016/j.eurpolymj.2013.07.017

Espino-Pérez E, Domenek S, Belgacem N, et al (2014) Green Process for Chemical Functionalization of Nanocellulose with Carboxylic Acids. Biomacromolecules 15:4551–4560. doi: 10.1021/bm5013458

Fornes TD, Hunter DL, Paul DR (2004) Nylon-6 Nanocomposites from Alkylammonium-Modified Clay: The Role of Alkyl Tails on Exfoliation. Macromolecules 37:1793–1798. doi: 10.1021/ma0305481

Fortunati E, Armentano I, Zhou Q (2012a) Multifunctional bionanocomposite films of poly (lactic acid), cellulose nanocrystals and silver nanoparticles. Carbohydr Polym 87:1596–1605. doi: 10.1016/j.carbpol.2011.09.066

Fortunati E, Peltzer M, Armentano I (2012b) Effects of modified cellulose nanocrystals on the barrier and migration properties of PLA nano-biocomposites. Carbohydr Polym 90:948–56. doi: 10.1016/j.carbpol.2012.06.025

Fundador NG V., Iwata T (2013) Enhanced crystallization of poly(d-lactide) by xylan esters. Polym Degrad Stab 98:2482–2487. doi: 10.1016/j.polymdegradstab.2013.06.013

Garlotta D (2001) A Literature Review of Poly(Lactic Acid). J Polym Environ 9:63–84. doi: 10.1023/A:1020200822435

Gorrasi G, Anastasio R, Bassi L, Pantani R (2013) Barrier properties of PLA to water vapour: Effect of temperature and morphology. Macromol Res 21:1110–1117. doi: 10.1007/s13233-013-1144-0

Gorrasi G, Vittoria V, Murariu M, et al (2008) Effect of filler content and size on transport properties of water vapor in PLA/calcium sulfate composites. Biomacromolecules 9:984–990. doi: 10.1021/bm700568n

Guinault A, Sollogoub C, Domenek S, et al (2010) Influence of crystallinity on gas barrier and mechanical properties of pla food packaging films. Int J Mater Form 3:603–606. doi: 10.1007/s12289-010-0842-9

Guinault A, Sollogoub C, Ducruet V, Domenek S (2012) Impact of crystallinity of poly(lactide) on helium and oxygen barrier properties. Eur Polym J 48:779–788. doi: 10.1016/j.eurpolymj.2012.01.014

Habibi Y, Lucia LA, Rojas OJ (2010) Cellulose Nanocrystals: Chemistry, Self-Assembly, and Applications. Chem Rev 110:3479–3500. doi: 10.1021/cr900339w

Halden RU (2010) Plastics and Health Risks. Annu Rev Public Health 31:179–194. doi: 10.1146/annurev.publhealth.012809.103714

Henriksson M, Henriksson G, Berglund LA, Lindström T (2007) An environmentally friendly method

for enzyme-assisted preparation of microfibrillated cellulose (MFC) nanofibers. Eur Polym J 43:3434–3441. doi: 10.1016/j.eurpolymj.2007.05.038

Hoffmann M (1998) Inorganic-Organic Polymers with Barrier Properties for Water Vapor, Oxygen and Flavors. J Sol-Gel Sci Technol 2:141–146. doi: 10.1023/A:1008628029870

Hong J, Kim DS (2013) Preparation and physical properties of polylactide/cellulose nanowhisker/nanoclay composites. Polym Compos 34:293–298. doi: 10.1002/pc.22413

Isogai A, Saito T, Fukuzumi H (2011) TEMPO-oxidized cellulose nanofibers. Nanoscale 3:71–85. doi: 10.1039/c0nr00583e

Jandas PJ, Mohanty S, Nayak SK (2013) Thermal properties and cold crystallization kinetics of surface-treated banana fiber (BF)-reinforced poly(lactic acid) (PLA) nanocomposites. J Therm Anal Calorim 114:1265–1278. doi: 10.1007/s10973-013-3102-7

Johansson F, Leufvén A (1994) Influence of sorbed vegetable oil and relative humidity on the oxygen transmission rate through various polymer packaging films. Packag Technol Sci 7:275–281. doi: 10.1002/pts.2770070604

Jonoobi M, Harun J, Mathew AP, Oksman K (2010) Mechanical properties of cellulose nanofiber (CNF) reinforced polylactic acid (PLA) prepared by twin screw extrusion. Compos Sci Technol 70:1742–1747. doi: 10.1016/j.compscitech.2010.07.005

Jonoobi M, Mathew AP, Abdi MM, et al (2012a) A Comparison of Modified and Unmodified Cellulose Nanofiber Reinforced Polylactic Acid (PLA) Prepared by Twin Screw Extrusion. J Polym Environ 20:991–997. doi: 10.1007/s10924-012-0503-9

Jonoobi M, Mathew AP, Oksman K (2012b) Producing low-cost cellulose nanofiber from sludge as new source of raw materials. Ind Crops Prod 40:232–238. doi: 10.1016/j.indcrop.2012.03.018

Kasuga T, Maeda H, Kato K, et al (2003) Preparation of poly(lactic acid) composites containing calcium carbonate (vaterite). Biomaterials 24:3247–3253. doi: 10.1016/S0142-9612(03)00190-X

Khalil HA, Bhat AH, Yusra AI (2012) Green composites from sustainable cellulose nanofibrils: a review. Carbohydr Polym 87:963–979. doi: 10.1016/j.carbpol.2011.08.078

Koo D, Du A, Palmese GR, Cairncross RA (2012) Moisture management of polylactides: The effect of heat treatment. Polymer 53:1115–1123. doi: 10.1016/j.polymer.2012.01.024

Kose R, Kondo T (2013) Size effects of cellulose nanofibers for enhancing the crystallization of poly(lactic acid). J Appl Polym Sci 128:1200–1205. doi: 10.1002/app.38308

Kowalczyk M, Piorkowska E, Kulpinski P, Pracella M (2011) Mechanical and thermal properties of PLA composites with cellulose nanofibers and standard size fibers. Compos Part A Appl Sci Manuf 42:1509–1514. doi: 10.1016/j.compositesa.2011.07.003

Krikorian V, Pochan DJ (2004) Unusual Crystallization Behavior of Organoclay Reinforced Poly(l-lactic acid) Nanocomposites. Macromolecules 37:6480–6491. doi: 10.1021/ma049283w

Lee J-W, Son S-M, Hong S-I (2008a) Characterization of protein-coated polypropylene films as a novel composite structure for active food packaging application. J Food Eng 86:484–493. doi: 10.1016/j.jfoodeng.2007.10.025

Lee S-H, Wang S, Teramoto Y (2008b) Isothermal crystallization behavior of hybrid biocomposite consisting of regenerated cellulose fiber, clay, and poly(lactic acid). J Appl Polym Sci 108:870–875. doi: 10.1002/app.26853

Leszczyńska A, Njuguna J, Pielichowski K, Banerjee JR (2007) Polymer/montmorillonite nanocomposites with improved thermal properties. Part I. Factors influencing thermal stability and mechanisms of thermal stability improvement. Thermochim Acta 453:75–96. doi: 10.1016/j.tca.2006.11.002

Li X, Yin J, Yu Z, et al (2009) Isothermal crystallization behavior of poly(L-lactic acid)/organo-montmorillonite nanocomposites. Polym Compos 30:1338–1344. doi: 10.1002/pc.20721

Lin J, Shenogin S, Nazarenko S (2002) Oxygen solubility and specific volume of rigid amorphous fraction in semicrystalline poly(ethylene terephthalate). Polymer 43:4733–4743. doi: 10.1016/S0032-3861(02)00278-1

Lin TT, Liu XY, He C (2010) A DFT study on poly(lactic acid) polymorphs. Polymer 51:2779–2785. doi: 10.1016/j.polymer.2010.03.062

Liu A, Walther A, Ikkala O, et al (2011) Clay nanopaper with tough cellulose nanofiber matrix for fire retardancy and gas barrier functions. Biomacromolecules 12:633–641. doi: 10.1021/bm101296z

Lorenzo AT, Arnal ML, Albuerne J, Müller AJ (2007) DSC isothermal polymer crystallization kinetics measurements and the use of the Avrami equation to fit the data: Guidelines to avoid common

problems. Polym Test 26:222–231. doi: 10.1016/j.polymertesting.2006.10.005

Mandal A, Chakrabarty D (2011) Isolation of nanocellulose from waste sugarcane bagasse (SCB) and its characterization. Carbohydr Polym 86:1291–1299. doi: 10.1016/j.carbpol.2011.06.030

Martínez-Sanz M, Lopez-Rubio A, Lagaron JM (2012) Optimization of the dispersion of unmodified bacterial cellulose nanowhiskers into polylactide via melt compounding to significantly enhance barrier and mechanical properties. Biomacromolecules 13:3887–3899. doi: 10.1021/bm301430j

Mastromatteo M, Mastromatteo M, Conte A, Del Nobile MA (2010) Advances in controlled release devices for food packaging applications. Trends Food Sci Technol 21:591–598. doi: 10.1016/j.tifs.2010.07.010

McLauchlin AR, Thomas NL (2009) Preparation and thermal characterisation of poly(lactic acid) nanocomposites prepared from organoclays based on an amphoteric surfactant. Polym Degrad Stab 94:868–872. doi: 10.1016/j.polymdegradstab.2009.01.012

Minelli M, Baschetti MG, Doghieri F, et al (2010) Investigation of mass transport properties of microfibrillated cellulose (MFC) films. J Memb Sci 358:67–75. doi: 10.1016/j.memsci.2010.04.030

Mohanty AK, Misra M, Drzal LT (2002) Sustainable Bio-Composites from renewable resources: Opportunities and challenges in the green materials world. J Polym Environ 10:19–26. doi: 10.1023/A:1021013921916

Mohapatra AK, Mohanty S, Nayak SK (2012) Poly(lactic acid) and layered silicate nanocomposites prepared by melt mixing: Thermomechanical and morphological properties. Polym Compos 33:2095–2104. doi: 10.1002/pc.22316

Mondragon G, Fernandes S, Retegi A, et al (2014) A common strategy to extracting cellulose nanoentities from different plants. Ind Crops Prod 55:140–148. doi: 10.1016/j.indcrop.2014.02.014

Moore TT, Mahajan R, Vu DQ, Koros WJ (2004) Hybrid Membrane Materials Comprising Organic Polymers with Rigid Dispersed Phases. AIChE J 50:311–321. doi: 10.1002/aic.10029

Morán JI, Alvarez VA, Cyras VP, Vázquez A (2007) Extraction of cellulose and preparation of nanocellulose from sisal fibers. Cellulose 15:149–159. doi: 10.1007/s10570-007-9145-9

Mwaikambo LY, Ansell MP (1999) The effect of chemical treatment on the properties of hemp, sisal, jute and kapok for composite reinforcement. Die Angew Makromol Chemie 272:108–116. doi: 10.1002/(SICI)1522-9505(19991201)272:1<108::AID-APMC108>3.0.CO;2-9

Najafi N, Heuzey MC, Carreau PJ (2012) Polylactide (PLA)-clay nanocomposites prepared by melt compounding in the presence of a chain extender. Compos Sci Technol 72:608–615. doi: 10.1016/j.compscitech.2012.01.005

Nampoothiri KM, Nair N, John R (2010) An overview of the recent developments in polylactide (PLA) research. Bioresour Technol 101:8493–501. doi: 10.1016/j.biortech.2010.05.092

Nostro A, Papalia T (2012) Antimicrobial Activity of Carvacrol: Current Progress and Future Prospectives. Recent Pat Antiinfect Drug Discov 7:28–35. doi: 10.2174/157489112799829684

Nostro A, Scaffaro R, D'Arrigo M, et al (2012) Study on carvacrol and cinnamaldehyde polymeric films: mechanical properties, release kinetics and antibacterial and antibiofilm activities. Appl Microbiol Biotechnol 96:1029–1038. doi: 10.1007/s00253-012-4091-3

Novo LP, Bras J, García A, et al (2015) Subcritical Water: A Method for Green Production of Cellulose Nanocrystals. ACS Sustain Chem Eng 3:2839–2846. doi: 10.1021/acssuschemeng.5b00762

Park S, Baker JO, Himmel ME, et al (2010) Cellulose crystallinity index: measurement techniques and their impact on interpreting cellulase performance. Biotechnol Biofuels 3:10. doi: 10.1186/1754-6834-3-10

Pei A, Zhou Q, Berglund LA (2010) Functionalized cellulose nanocrystals as biobased nucleation agents in poly(l-lactide) (PLLA) – Crystallization and mechanical property effects. Compos Sci Technol 70:815–821. doi: 10.1016/j.compscitech.2010.01.018

Perego G, Cella GD, Bastioli C (1996) Effect of molecular weight and crystallinity on poly(lactic acid) mechanical properties. J Appl Polym Sci 59:37–43. doi: 10.1002/(SICI)1097-4628(19960103)59:1<37::AID-APP6>3.0.CO;2-N

Picard E, Espuche E, Fulchiron R (2011) Effect of an organo-modified montmorillonite on PLA crystallization and gas barrier properties. Appl Clay Sci 53:58–65. doi: 10.1016/j.clay.2011.04.023

Piccinini E, Giacinti Baschetti M, Sarti G. (2004) Use of an automated spring balance for the simultaneous measurement of sorption and swelling in polymeric films. J Memb Sci 234:95–

100. doi: 10.1016/j.memsci.2003.12.024

Qing Y, Sabo R, Zhu JY, et al (2013) A comparative study of cellulose nanofibrils disintegrated via multiple processing approaches. Carbohydr Polym 97:226–34. doi: 10.1016/j.carbpol.2013.04.086

Ramos M, Jiménez A, Peltzer M, Garrigós MC (2014) Development of novel nano-biocomposite antioxidant films based on poly (lactic acid) and thymol for active packaging. Food Chem 162:149–155. doi: 10.1016/j.foodchem.2014.04.026

Rasal RM, Janorkar A, Hirt DE (2010) Poly(lactic acid) modifications. Prog Polym Sci 35:338–356. doi: 10.1016/j.progpolymsci.2009.12.003

Rhim JW, Hong SI, Ha CS (2009) Tensile, water vapor barrier and antimicrobial properties of PLA/nanoclay composite films. LWT - Food Sci Technol 42:612–617. doi: 10.1016/j.lwt.2008.02.015

Righetti MC, Gazzano M, Di Lorenzo ML, Androsch R (2015) Enthalpy of melting of α′- and α-crystals of poly(l-lactic acid). Eur Polym J 70:215–220. doi: 10.1016/j.eurpolymj.2015.07.024

Righetti MC, Tombari E (2011) Crystalline, mobile amorphous and rigid amorphous fractions in poly(L-lactic acid) by TMDSC. Thermochim Acta 522:118–127. doi: 10.1016/j.tca.2010.12.024

Robertson (2006) Food Packaging: Principles and Practice, 2nd edition. CRC Press

Rochman CM, Browne MA, Halpern BS, et al (2013) Policy: Classify plastic waste as hazardous. Nature 494:169–71. doi: 10.1038/494169a

Rodionova G, Lenes M, Eriksen Ø, Gregersen Ø (2010) Surface chemical modification of microfibrillated cellulose: improvement of barrier properties for packaging applications. Cellulose 18:127–134. doi: 10.1007/s10570-010-9474-y

Saiter A, Delpouve N, Dargent E, et al (2016) Probing the chain segment mobility at the interface of semi-crystalline polylactide/clay nanocomposites. Eur Polym J 78:274–289. doi: 10.1016/j.eurpolymj.2016.03.040

Saito T, Isogai A (2004) TEMPO-mediated oxidation of native cellulose. The effect of oxidation conditions on chemical and crystal structures of the water-insoluble fractions. Biomacromolecules 5:1983–1989. doi: 10.1021/bm0497769

Salmieri S, Islam F, Khan RA, et al (2014) Antimicrobial nanocomposite films made of poly(lactic acid)–cellulose nanocrystals (PLA–CNC) in food applications—part B: effect of oregano essential oil release on the inactivation of Listeria monocytogenes in mixed vegetables. Cellulose 21:4271–4285. doi: 10.1007/s10570-014-0406-0

San Román MS, Holgado MJ, Salinas B, Rives V (2013) Drug release from layered double hydroxides and from their polylactic acid (PLA) nanocomposites. Appl Clay Sci 71:1–7. doi: 10.1016/j.clay.2012.10.014

Sanchez-Garcia MD, Lagaron JM (2010a) Novel clay-based nanobiocomposites of biopolyesters with synergistic barrier to UV light, gas, and vapour. J Appl Polym Sci 118:188–199. doi: 10.1002/app.31986

Sanchez-Garcia MD, Lagaron JM (2010b) On the use of plant cellulose nanowhiskers to enhance the barrier properties of polylactic acid. Cellulose 17:987–1004. doi: 10.1007/s10570-010-9430-x

Sengupta R, Chakraborty S, Bandyopadhyay S, et al (2007) A short review on rubber/clay nanocomposites with emphasis on mechanical properties. Polym Eng Sci 47:1956–1974. doi: 10.1002/pen.20921

Sheth M, Kumar RA, Dave V, et al (1997) Biodegradable polymer blends of poly(lactic acid) and poly(ethylene glycol). J Appl Polym Sci 66:1495–1505. doi: 10.1002/(SICI)1097-4628(19971121)66:8<1495::AID-APP10>3.0.CO;2-3

Siparsky GL, Voorhees KJ, Dorgan JR, Schilling K (1997) Water transport in polylactic acid (PLA), PLA/polycaprolactone copolymers, and PLA/polyethylene glycol blends. J Environ Polym Degrad 5:125–136. doi: 10.1007/BF02763656

Siqueira G, Bras J, Dufresne A (2009) Cellulose whiskers versus microfibrils: influence of the nature of the nanoparticle and its surface functionalization on the thermal and mechanical properties of nanocomposites. Biomacromolecules 10:425–32. doi: 10.1021/bm801193d

Siqueira G, Bras J, Dufresne A (2010a) New process of chemical grafting of cellulose nanoparticles with a long chain isocyanate. Langmuir 26:402–11. doi: 10.1021/la9028595

Siqueira G, Bras J, Dufresne A (2010b) Luffa cylindrica as a lignocellulosic source of fiber, microfibrillated cellulose, and cellulose nanocrystals. BioResources 5:727–740.

Siracusa V, Rocculi P, Romani S, Rosa MD (2008) Biodegradable polymers for food packaging: a

review. Trends Food Sci Technol 19:634–643. doi: 10.1016/j.tifs.2008.07.003

Siró I, Plackett D, Hedenqvist M, et al (2011) Highly transparent films from carboxymethylated microfibrillated cellulose: The effect of multiple homogenization steps on key properties. J Appl Polym Sci 119:2652–2660. doi: 10.1002/app.32831

Sorrentino A, Gorrasi G, Vittoria V (2007) Potential perspectives of bio-nanocomposites for food packaging applications. Trends Food Sci Technol 18:84–95. doi: 10.1016/j.tifs.2006.09.004

Spoljaric S, Salminen A, Dang Luong N, et al (2013) Nanofibrillated cellulose, poly(vinyl alcohol), montmorillonite clay hybrid nanocomposites with superior barrier and thermomechanical properties. Polym Compos 35:1117–1131. doi: 10.1002/pc.22759

Subramanian MR, Talluri S, Christopher LP (2015) Production of lactic acid using a new homofermentative Enterococcus faecalis isolate. Microb Biotechnol 8:221–9. doi: 10.1111/1751-7915.12133

Suryanegara L, Nakagaito AN, Yano H (2009) The effect of crystallization of PLA on the thermal and mechanical properties of microfibrillated cellulose-reinforced PLA composites. Compos Sci Technol 69:1187–1192. doi: 10.1016/j.compscitech.2009.02.022

Suyatma NE, Copinet A, Tighzert L, Coma V (2004) Mechanical and Barrier Properties of Biodegradable Films Made from Chitosan and Poly (Lactic Acid) Blends. J Polym Environ 12:1–6. doi: 10.1023/B:JOOE.0000003121.12800.4e

Tejado A, Alam MN, Antal M, et al (2012) Energy requirements for the disintegration of cellulose fibers into cellulose nanofibers. Cellulose 19:831–842. doi: 10.1007/s10570-012-9694-4

Tingaut P, Zimmermann T, Lopez-Suevos F (2010) Synthesis and Characterization of Bionanocomposites with Tunable Properties from Poly(lactic acid) and Acetylated Microfibrillated Cellulose. Biomacromolecules 11:454–464. doi: 10.1021/bm901186u

Tosh B (2011) Thermal analysis of cellulose esters prepared from different molecular weight fractions of high α-cellulose pulp. Indian J Chem Technol 18:451–457.

Tsuji H, Okino R, Daimon H, Fujie K (2006) Water vapor permeability of poly(lactide)s: Effects of molecular characteristics and crystallinity. J Appl Polym Sci 99:2245–2252. doi: 10.1002/app.22698

Wang S, Cheng Q (2009) A novel process to isolate fibrils from cellulose fibers by high-intensity ultrasonication, Part 1: Process optimization. J Appl Polym Sci 113:1270–1275. doi: 10.1002/app.30072

Wijmans JG, Baker RW (1995) The solution-diffusion model: A review. J Memb Sci 107:1–21. doi: 10.1016/0376-7388(95)00102-I

Wu C-N, Saito T, Yang Q, et al (2014) Increase in the Water Contact Angle of Composite Film Surfaces Caused by the Assembly of Hydrophilic Nanocellulose Fibrils and Nanoclay Platelets. ACS Appl Mater Interfaces 6:12707–12712. doi: 10.1021/am502701e

Wunderlich B (2003) Reversible crystallization and the rigid-amorphous phase in semicrystalline macromolecules. Prog Polym Sci 28:383–450. doi: 10.1016/S0079-6700(02)00085-0

Yuniarto K, Welt BA, Purwanto A, et al (2014) Effect of Plasticizer on Oxygen Permeability of Cast Polylactic acid (PLA) Films Determined using Dynamic Accumulation Method. Journal of Applied Packaging Research 6:51-57.

Zaharia A, Sarbu A, Radu A-L, et al (2015) Preparation and characterization of polyacrylamide-modified kaolinite containing poly [acrylic acid-co-methylene bisacrylamide] nanocomposite hydrogels. Appl Clay Sci 103:46–54. doi: 10.1016/j.clay.2014.11.009

Zaidi L, Bruzaud S, Bourmaud A, et al (2009) Relationship between structure and rheological, mechanical and thermal properties of polylactide/Cloisite 30B nanocomposites. J Appl Polym Sci 116:1357–1365. doi: 10.1002/app.31655

Żenkiewicz M, Richert J (2008) Permeability of polylactide nanocomposite films for water vapour, oxygen and carbon dioxide. Polym Test 27:835–840. doi: 10.1016/j.polymertesting.2008.06.005

Zhang J, Tashiro K, Tsuji H, Domb AJ (2008) Disorder-to-Order Phase Transition and Multiple Melting Behavior of Poly(l-lactide) Investigated by Simultaneous Measurements of WAXD and DSC. Macromolecules 41:1352–1357. doi: 10.1021/ma0706071

Zuza E, Ugartemendia JM, Lopez A, et al (2008) Glass transition behavior and dynamic fragility in polylactides containing mobile and rigid amorphous fractions. Polymer 49:4427–4432. doi: 10.1016/j.polymer.2008.08.012

APPENDICES

APPENDIX 1: Optimisation of nanocomposite preparation, processing and testing.

Appendix 1. Optimization of nanocomposite preparation, processing and testing.

In the present annex, the optimization of certain experimental procedures is going to be presented.

A. Optimization of the solvent casting procedures

As explained in the "Objectives" chapter 1, the work on composites with single nanoparticle and hybrid composites was focused on barrier properties; hence a very good film quality is required. For this reason the solvent casting approach was considered the best possible choice for composite preparation. However, even if the solvent casting is a promising procedure to achieve great quality films, still an optimized protocol is required to have reliable results.

In general the solvent casting procedure consists of these steps:

1) Pre-dispersion of the polymer and the nanoparticles in a solvent.
2) Mix both solutions in the required quantity to have the desired nanoparticle concentration on the polymer matrix. Another dispersion step might be required.
3) Cast the mixture in a Teflon mold.
4) Slow drying procedure, where the most part of the solvent is removed.
5) Harsh drying where the residual solvent is removed.

As long as the goal of this study was to compare the potential of both nanoparticles as reinforcing agent of PLA, an optimized protocol for each composite combination had to be developed. This

involved two main research: 1) finding a good procedure and instrumentation to obtain a good film physical quality (uniform thickness, absence of bubbles and/or contamination) and 2) finding an optimized protocol to have a good dispersion of nanoparticles within the matrix.

B. Instrumentation, equipment and general protocol

During the first attempts of making solvent casting films it was found that most part of the films were not showing uniform thickness. This was probably due to the fact that the surface where the Teflon molds were placed was not completely perpendicular to the gravity. Furthermore, the evaporation of certain solvents was simply too fast to achieve a good film quality and sometimes the films could be contaminated by dust. As long as those defects could affect the properties of the film an optimized protocol was made and specific instrumentation was developed with the help of DTU´s workshop to assure a good film quality (Figure Appendix 1.1).

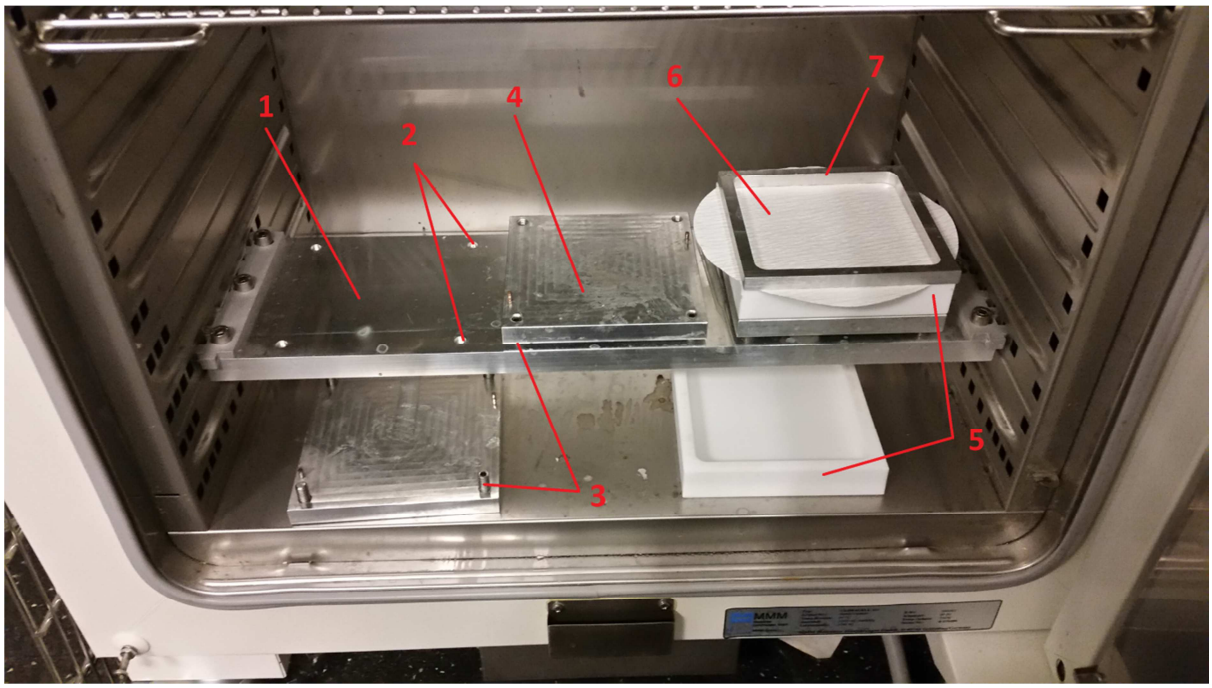

Figure Appendix 1.1 Optimized instrumentation for solvent casting procedure.

A shelve (1) was coupled inside a climatic chamber and an oven. The shelve had some holes (2) for mountry of positioning screws (3). These screws could be adjusted at different heights; hence, it was possible to align the mold holder (4) to make sure that it was not unbalanced or misaligned. Square-shaped Teflon molds (5) were especially developed, with a high bottom thickness since this was a requirement to have a flat mold. The samples were covered with lab paper (6) (5-13 µm), to avoid contamination and disturbances from the air flow. Finally, an iron crown (7) made sure that the filter paper was remaining in position during the whole drying procedure.

C. Dispersion optimization: PLA and PLA/C30B composites

There are many papers on preparing PLA/C30B composites by solvent casting using DCM as solvent, and in this case it was found that a good dispersion of the composites could be achieved using this solvent in the case of clay composites. In order to optimise the clay dispersion protocol, two PLA/C30B 5% composites were prepared by using two different dispersion protocols (one "mild" and one "harsh") and the oxygen barrier properties of both composites were compared to evaluate which of the clay dispersion protocol had the best performance .

Both protocols were based on a similar approach:

1) Preparing a suspension of a 1% w/V solution in C30B on DCM by strong magnetic stirring for 3 days.
2) Pre-dispersing the C30B suspension in DCM by a combination of high intensity ultrasonication at 200 W and rotatory disk homogenization at 20.000 rpm.
3) Mixing this suspension with a solution of PLA in DCM.
4) A second dispersion protocol (high intensity sonication and homogenization).
5) A soft ultrasonication in ultrasound bath to remove the remaining bubbles.

The only difference between the two protocols was the ultrasonication and homogenization time in steps 2 and 4.

a) Ultrasonication and homogenization time on the 2^{nd} step, 1 hour each step, and 30 minutes on the 4^{th} step.
b) 3 hour of ultrasonication and 90 min of homogenization time on the 2^{nd} step, and 1 hour and 30 min respectively on the 4^{th} step.

It was found that the B) protocol was leading to slightly better barrier properties so this protocol was chosen.

D. Improving the CNF extraction and individualization

In order to improve the fibrillation of the CNF from the acetylated pulp, a glass bottle was modified (Figure Appendix 1.2) and some glass spikes were introduced within it. The goal of this design was to disturb the flow induced by magnetic stirring, which was mainly "moving" the suspension, to increase collisions of the acetylated fibers hence increasing the efficiency of the procedure.

Figure Appendix 1.2 Optimized device for magnetic stirring of CNF suspension.

E. PLA/CNF and PLA/CNC composites: Solvent and drying time-temperature scanning

Unfortunately, for the nanocellulose, it was found that probably due to the low surface charge of the CNF it was difficult to find a proper solvent to prepare well dispersed nanocomposites using solvents as DCM/THF (Figure Appendix 1.3) for that reason several solvents such as Acetone/DCM, anisole, THF/DCM, DMF, DMAc and NMP were evaluated as solvents. The solvents were tested on 6 areas: Good dispersion (of the CNF in a solvent suspension), solubility of PLA in that solvent, stability of the suspension, vapour pressure (higher vapour pressure easier the removal of the solvent), film formation and CNF dispersion on the film (if the solvent had good film forming ability and if it was no clear CNF aggregates on it). The table with all results could be found in Table Appendix 1.1.

Table Appendix 1.1 Effects of different solvents on CNF and PLA/CNF composites. (0= very bad, reason to eliminate the solvent, 1 = very bad, 2 = bad, 3 = fine, 4 = good)

	SOLVENTS FOR CNF							
	WATER	DCM/ACETONE	DCM	THF/DCM	ANISOLE	DMF	DMAc	NMP
GOOD DISPERSION	4	1	0	4	4	4	4	4
PLA SOLUBLE IN IT	0	3	4	3	3	3	3	3
ESTABLE SUSPENSION	4	1	1	3	3	4	4	4
LOW VAPOR PRESSURE	3	4	3	3	2	2	1	0
GOOD FILM FORMATION		0	0	0	4	4	2	
GOOD FILM DISPERSION		0	0	0	4	4	3	

It was found that the Acetone/DCM and THF/DCM were leading to poorly dispersed composites and that the high boiling point of NMP made the evaporation of the solvent a challenge. It was also found that DMF, anisole and in a lesser extent DMAc, were suitable solvents, but for a very narrow margin the DMF was used as a solvent.

Figure Appendix 1.3 Film prepared using DCM/THF as solvent

As long as the DCM has a boiling point of 39.6°C, the solvent evaporation was found not to be a challenge for PLA/C30B composite. Furthermore, the fact that the composites were solvent casted within a climatic chamber (closed environment) helped slowing down the evaporation of the solvent hence achieving a very good film quality and a high degree of crystallinity.

But, for composites with CNF, where DMF was used as a solvent, the situation was different. The DMF has a boiling point of 153°C, which requires higher drying temperature. At that temperature the film could be deformed. A screening on different time-temperature conditions was performed in order to choose the best conditions. It was found that the drying at 50°C and 60°C was not good enough to make high quality films (Figure Appendix 1.4A and B), 70°C was leading to good film quality (Figure Appendix 1.4C) but still was slightly opaque, so a drying at 80°C and 15 h was preferred (Figure Appendix 1.5).

Figure Appendix 1.4 Evaluation of different drying Time-Temperature conditions (A) 24 h at 50°C + 24 h at 60°C; (B) 16 h at 60 °C; (C) 16 h at 70°C for PLA/CNF 3% composite.

Figure Appendix 1.5 PLA/CNF 3% film after drying for 15h at 80 °C.

Furthermore, as long as it was considered that 80°C could be nearby from the crystallization temperature, the drying time was considered to be critical, since even small extra drying time could increase the degree of crystallinity of films, hence affecting the properties. For that reason a timer was connected to the oven (Figure Appendix 1.6), to make sure that the drying procedure was taking exactly 15 hours.

Figure Appendix 1.6 Timer for controlling the drying conditions of the films.

In all of the cases the composites were dried in a second stance at 50°C under vacuum (3 mmHg) for 24 hours to remove the remaining solvent.

Finally, the trials to produce a film of PLA using this protocol failed; probably due to the low thermostability of PLA the quality of the achieved film was found not satisfactory enough to have good results (Figure Appendix 1.7).

Figure Appendix 1.7 PLA film using DMF as solvent casting.

Furthermore, several trials to hot-press the PLA and composite films led to films with some defects, therefore, the properties that required a large amount of material for testing (i.e. mechanical

testing, barrier properties) could not be studied with the most part of the facilities available at DPC, however, other properties such as optical properties could be tested, and access to other facilities was granted within the framework of an external stay at UNIBO (University of Bologna).

Figure Appendix 1.8 Hot pressed PLA film. On red are marked the defect of the film.

In general it was found that hot pressing the composites for 5 minutes at 170°C, followed by a fast cooling, was leading to amorphous nanocomposites (AM) with a relatively small amount of defects. After that, the quenched nanocomposites were placed into an oven at 120°C for 2 hours in order to obtain fully crystallized nanocomposites (FC).

F. Permeability measurements

Apart from achieving a good film quality, optimizing the measuring conditions is key to achieve reliable results. This was very critical especially for WVTR measures, where the mass increase due to water absorption in silica gel had to be monitored every hour. This was an issue, since it was estimated that a PLA film of approximately 100 µm thickness, though the area of the aluminium cups available on the lab, could exhibit a mass increase around 2 mg/h, while the cup itself weighted around 170 g. For that reason, with the help of the workshop, the thickness of the cups was reduced as much as possible, hence reducing the weigth of the cups to approximately 50 g (Figure Appendix 1.9).

Figure Appendix 1.9 Aluminium cups used to measure the WVTR, (left) before the thickness reduction operation (right) after the mass reduction operation.

Finally, during the OTR measure optimization procedure, it was found that PLA and composites were exhibiting an OTR ranging 40 – 300 mL m^{-2} day^{-1} which was a value very close to the calibration of the instrument (70 mL m^{-2} day^{-1}). For that reason, the measures were done at the same conditions as the ones used to calibrate the instrument. Furthermore, to ensure that the device was properly calibrated, the OTR of a reference film was measured before and after analysing a set of samples.

APPENDIX 2: Chemically extracted nanocellulose from sisal fibres by employing a simple and industrially relevant process.

Trifol, J., Sillard, C., Plackett, D., Bras, J., Szabo, P., Daugaard, A. E., Chemically extracted nanocellulose from sisal fibres by employing a simple and industrially relevant process. *Cellulose* (under review).

Chemically extracted nanocellulose from sisal fibres by a simple and industrially relevant process

J. Trifol[a], C. Sillard[b], D. Plackett[c], P. Szabo[a] , J. Bras[b], A. E. Daugaard[a]

[a] *Danish Polymer Centre, Department of Chemical and Biochemical Engineering, Technical University of Denmark, Søltofts Plads, Building 229, DK – 2800 Kgs. Lyngby, Denmark*

[b] *LGP2/Grenoble INP-Pagora/CNRS, 461 rue de la papeterie, Domaine universitaire, C10065, 38402 Saint Martin d'Hères Cedex, France*

[c] *Faculty of Pharmaceutical Sciences, University of British Columbia, 2405 Wesbrook Mall, Vancouver, BC V6T 1Z3, Canada*

Keywords:

Sisal fibres; Cellulose nanofibres (CNFs); Cellulose films; acetylation, nanofibers

Abstract:

A novel type of acetylated cellulose nanofibre (CNF) was extracted successfully from sisal fibres using chemical methods. Initially, a strong alkali treatment was used to swell the fibres, followed by a bleaching step to remove the residual lignin and finally an acetylation step to reduce the impact of the intermolecular hydrogen bonds in the nanocellulose. The result of this sequence of up-scalable chemical treatments was a pulp consisting mainly of micro-sized fibres, which allowed simpler handling through filtration and purification steps and permitted the isolation of an intermediate product with a high solid content. An aqueous dispersion of CNF could be obtained directly from this intermediate pulp by simple magnetic stirring. As a proof of concept, the dispersion was used directly for preparing a highly transparent CNF film. This illustrates clearly that the prepared nanofibres are very high in purity and that the process provides a substantial yield of CNF. Finally, CNF films with alkali extracts were also prepared, resulting in more flat films with an increased mass yield.

1. INTRODUCTION

Cellulose is the most abundant bio-derived polymer in the world, with a yearly production of about 10^{11} tons (Azizi Samir et al. 2005). This production originates mainly from plants, but there are other sources of cellulose such as bacteria, tunicates and algae(Moon et al. 2011). Cellulose has the empirical formula ($C_6H_{10}O_5$) and is a linear homopolysaccharide with hundreds to thousands of glucose units connected through 1-4-β-glucosidic bonds. Cellulose is semicrystalline and therefore contains both amorphous and crystalline domains of various types depending on the source of cellulose. Due to the recently increased focus on sustainability, lignocellulosic materials in general, and cellulose in particular, have been investigated widely in search of novel application fields such as biofuels(Baker and Keisler 2011), polymer reinforcement(Saheb and Jog 1999) and biomedical applications(Czaja et al. 2007) (Lin and Dufresne 2014). A turning point in this development occurred when Herrick et al.(Herrick et al. 1983) successfully isolated microfibrilated cellulose using mechanical methods to break up the hierarchical structure of cellulose. The cellulosic fibres can be considered bundles of nanosized

cellulosic fibres (CNFs) comprising of cellulosic fibrils with a high aspect ratio, having diameters on the nanoscale and lengths on the microscale. CNFs have been shown to have very interesting properties, such as a specific Young's modulus that is 3.4 times higher than that of steel(Eichhorn et al. 2010). Research into applications of the nanosized cellulosic materials has increasingly caught the interest of the scientific community(Lavoine et al. 2012), and the subject has been widely studied for applications such as hydrogels(Chang and Zhang 2011), aerogels(Fischer et al. 2006), barrier coatings(Minelli et al. 2010) and polymer reinforcement(Siró and Plackett 2010). Films containing such nanofibres are reported to have very good mechanical properties(Siró and Plackett 2010), high transparency(Siró et al. 2011), good oxygen barrier properties at low relative humidity as well as medium water vapour barrier properties(Lavoine et al. 2012) due to the high water uptake of the nanofibres(Minelli et al. 2010).

In order to bring CNF applications to market, an industrially relevant method that can extract and break up the strong association between fibres to prepare them for use in composites is required. Usually, the procedures for obtaining CNFs are based on applying high shear forces to extracted fibres e.g. by grinding, micro fluidisation, homogenisation or other similar techniques. These methods usually require large quantities of energy and are performed in high dilution or using processes that are not directly up-scalable or cost-effective. Therefore extensive research has been invested in finding methods for pre-treatment, such as enzymatic treatments or using (2,2,6,6-tetramethylpiperidin-1-yl)oxyl (TEMPO) for oxidation of the cellulose to decrease the required amount of energy to weaken hydrogen bonds between fibres(Qing et al. 2013),(Abdul Khalil et al. 2014). Here a novel method to obtain a high yield of partially acetylated CNF, by employing a simple chemical treatment followed by a low energy dispersion step, is presented. The intermediary pulp achieved after the chemical treatments is easy to filter and dry, which makes it highly suitable for transportation.

2. EXPERIMENTAL

2.1 Materials and methods

Cellulose nanofibres were extracted from sisal, which was kindly supplied by Expor Sisal S.L., while sodium hydroxide, nitric acid (ACS reagent, 70%) and acetic acid (99%-100%) were purchased from Sigma Aldrich and sodium chlorite (25 wt% in water) was obtained from Merck. All of the reagents were used as received.

Thermogravimetric analysis (TGA) was performed on a thermal TGA Q500 (TA) instrument from 25-600°C with a heating rate of 10 K/min under nitrogen flow. Fourier transform infrared spectroscopy (FT-IR) was obtained by triplicate on a Thermo-Fisher is50 FT-IR spectrometer equipped with a universal attenuated total reflection (ATR) sampling accessory with a diamond crystal at a resolution of 4 cm^{-1} in the range of 500-4000 cm^{-1}.

The rheological data was obtained with a TA Instruments AR2000 controlled stress rotational rheometer using a cone-and-plate geometry. The aluminium cone had a diameter of 60 mm and a 1° cone angle. Viscosity measurements were obtained in steady shear at 25°C.

Scanning electron microscopy (SEM) of the sisal and processed fibres was carried out using a Hitachi T3030 with a 5 kV field. The CNF was characterised by SEM on an FEI Quanta 200 ESEM FEG. X-ray diffraction was performed using a Panalytical X'Pert Pro MPD-Ray diffractometer with an Ni-filtered Cu Kα radiation (λ=1.54 Å) source, a voltage of 45 kV, a current of 40 mA and scans from 5° to 60°. Transmission electron

micrographs were obtained using a Hitachi HT770 microscope operating at 100 kV. A drop of an aqueous CNF suspension (0.2 % CNF) was deposited on a 200 mesh carbon/formvar copper grid (TED PELLA, USA) and imaged without the addition of staining agents or other chemicals.

CNF surface charge was measured conductiometrically. Briefly, 7.5 g of an aqueous dispersion of 1wt% of CNF was diluted with 100 mL of distilled water and 15 mL of hydrochloric acid (0.01 M). This mixture was kept under magnetic stirring until no change in conductivity was observed. The solution was titrated with a solution of sodium hydroxide (0.025 M), while the conductivity was measured every 0.5 mL.

Optical properties were measured in triplicates using a UV-Vis spectrometer (Polar Star Omega) in the range of 200 nm – 1000 nm and a Gardener Haze-Gard Plus to analyse the transmittance, haze and clarity of the specimens. Transmittance is the percentage of light transmitted through the sample, haze the amount of transmitted light that is scattered more than 2.5° and clarity the amount of transmitted light that is scattered less than 2.5°.

The surface properties of CNF films were estimated by advancing contact angle (CA) measurements on a Dataphysics Contact Angle System OCA20. Specimens of 2 x 1 cm were placed on a glass slide and a drop of water (6 µL) was deposited on the specimen surface. Thereafter, the needle was placed into the drop and the advancing CA was determined as the constant value obtained with a flow of 0.5 µL/s. The CA was determined as an average of at least five measurements.

Water absorption analysis was performed in duplicates based on the mass increase of samples (100-300 mg) conditioned in a climatic chamber overnight at 23ºC with a relative humidity of 10%, 25%, 50% and 75%, respectively.

The water vapour transmission rate (WVTR) of the films was measured in triplicate according to the norm NF H 00-030 at 23 °C and 25%, 50%, 75% and 90% RH. Silica gel was used as desiccating agent and the cups had a specific exchange surface of S =28.27 cm^2. The mass increase of the cups due to the water absorption of silica gel was plotted against the time and the slope was calculated. The WVTR was calculated as shown below, where n is the slope, l is the thickness of the film and S the specific exchange surface.

$$WVTR = \frac{n * l}{S}$$

The mechanical properties were measured by duplicate in a DMA RSA3 (TA Instruments, USA) working in tensile mode. The samples were preconditioned at 23 °C and 50% RH for 24 hours prior to the measurement, which was carried at a speed of 1 mm/min with a distance between the fixtures of 10 mm.

2.2 Procedures

2.2.1 Extraction and isolation of the acetylated CNF pulp (SMBA)

Sisal fibres (50 g) were cut and rinsed with an aqueous solution of sodium hydroxide (1.5 L, 2 wt%) at 23°C for 16 hours. The rinsed fibres were isolated by filtration and washed with distilled water until constant pH of the washing water was achieved. The alkali treatment (mercerisation) was repeated three times (1.5 hours at boiling temperature) with a stronger alkali solution (1.5 L, 10 wt%) followed by filtration, after which the pulp (SM) was suspended in distilled water (1.25 L), and the temperature was increased to 70°C. Once this temperature

was reached, acetic acid (8 mL) followed by sodium chlorite ($NaClO_2$, 40 mL) was added once every hour for 7 hours. Finally, the bleached pulp was isolated by filtration and washed with distilled water until a constant pH was reached (SMB). Thereafter, this pulp was suspended in a mixture of nitric acid (150 mL) and acetic acid (900 mL), and the mixture was stirred at boiling temperature for 90 minutes. The mixture was cooled by dilution with cold distilled water (ratio 1:5) and the acetylated pulp was isolated by filtration. The product was rinsed with distilled water until a constant pH level was achieved and the acetylated pulp (SMBA) was used without further purification.

2.2.2 Extraction of lignin and hemicellulose for compounding (residue solution)

Sisal fibres (35 g) were mixed with an aqueous solution of sodium hydroxide (300 mL, 10 wt%), and the mixture was refluxed for 2 hours. The fibres were filtered off and the filtrate was cooled and dialysed in a regenerated cellulose membrane (Cellu Sep T3, MWCO 12,000-14,000) against distilled water until pH was constant. The dialysed residue containing cellulose, lignin and hemicellulose was used without further purification.

2.2.3 Preparation of CNF films

An aqueous dispersion of CNF in water (1 wt%) was prepared by dilution of the SMBA pulp with distilled water followed by magnetic stirring for five days in an Erlenmeyer flask. The dispersion was centrifuged at 5000 rpm for 10 minutes, and the supernatant (0.8 wt%) was transferred to a Teflon mould. A transparent CNF film was formed by concentration of the solution in a climatic chamber for one week at 19°C and 65% relative humidity (RH), resulting in a transparent film with a thickness of 20-30 µm.

2.2.4 Preparation of the CNF/residue films

CNF/residue films were prepared from the aqueous CNF dispersion prepared as described above for the CNF films. Additionally, the supernatant was mixed with the residue solution (extracted cellulose, lignin and hemicellulose from the mercerisation) to obtain a mixture with 70 wt% CNF and 30 wt% residue. The mixture was cast in a Teflon mould and dried in a climatic chamber for one week at 19°C and 65% RH, resulting in the formation of a transparent CNF/residue film with a thickness of 20-30 µm.

3. RESULTS AND DISCUSSION

3.1 From raw materials to nanomaterials

The developed method employs simple and industrially relevant processes for the conversion of sisal fibres into CNF. Each of the steps is described in detail in the experimental section, as shown in Figure 1.

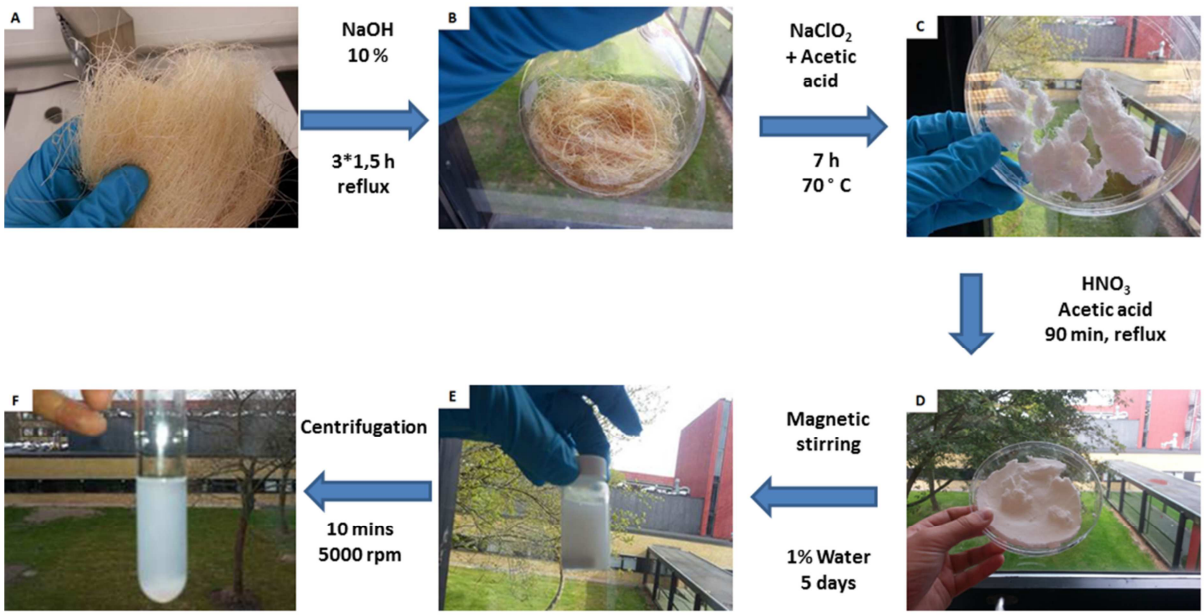

Figure 1. Overview of the CNF extraction protocol. A) Sisal fibres (S); B) Sisal fibres after alkali treatments (SM); C) Sisal fibres after mercerisation and bleaching (SMB); D) Sisal fibres after mercerisation, bleaching and acetylation (SMBA); E) SMBA after dispersion in water (CNF) and F) Stable CNF dispersion after centrifugation.

All of the steps directly change the structure of the fibres. An initial alkali treatment was used to remove oil residues and impurities from the fibres. Three subsequent stronger alkali treatments of sisal (S), to acquire mercerised fibres (SM, B in Figure 1), was used to swell the fibres and to extract lignin and hemicellulose from the fibres. The repeated mercerisation minimized adsorption of these impurities on the surface of the fibres compared to one longer mercerization step. After alkali treatment the fibres were light-brown in colour, which is attributed to deposition of the extracted lignin on the surface of the fibres. The deposited lignin was removed in the following bleaching step (SMB, C in Figure 1), and finally the influence of hydrogen bonds between the fibres was reduced through acetylation of the fibres (SMBA, D in Figure 1). This extraction protocol is based on two separate modifications of the fibres. Firstly, the alkali treatment swells the fibres, breaks the strong association, due to hydrogen bonds, between the cellulose chains and opens up the structure to additional chemical treatments(Mwaikambo and Ansell 1999). Secondly, in the swollen state, the OH groups from the cellulose nanofibers are grafted with acetate groups, which thereby permanently reduces the energy required to break the strong association between cellulose nanofibers in subsequent processing steps.

The result of this sequence of chemical treatments was a pulp consisting mainly of modified micro-sized fibres, which could easily be reduced to a low water content by filtration or decantation, and therefore would be easy to transport or store as a precursor for later preparation of CNF dispersions. An aqueous dispersion of CNF with high nanofiber purity could be obtained directly from this intermediate by magnetic stirring (product E in Figure 1), and any agglomerates could at this stage be removed by centrifugation or simple filtration.

The yield of cellulosic material after each step of the extraction protocol is shown in Figure 2.

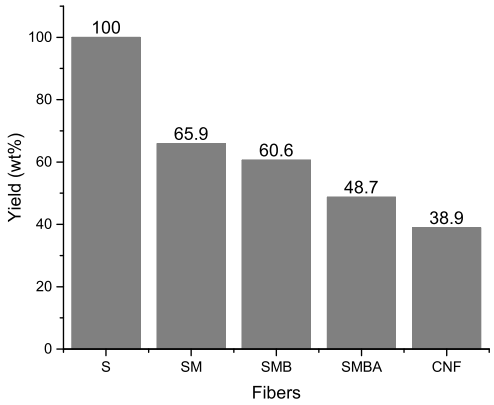

Figure 2. Mass yield of the treated fibres after drying of a sample of the respective suspensions (dry basis).

The amount of extracted cellulose fibres depends strongly on the type of fibres used for the process. Sisal fibres are generally reported to consist of about 60-70 wt% cellulose, 10-15 wt% hemicellulose and 8-12 wt% lignin(Bismarck et al. 2001; Mondragon et al. 2014). After all of the chemical treatments and purification steps, 39 wt% of the original sisal fibres has been converted into a CNF dispersion, which corresponds to an extraction of approximately 60 wt% of the total amount of cellulose from the sisal fibres. This compares to other extraction protocols, where e.g. 65 wt% of cellulose nanofibers have been extracted from cotton(de Morais Teixeira et al. 2010) or 50-60 wt% were extracted from softwood(Tejado et al. 2012).

3.2 Characterization of the pulp

The isolated material was characterised by SEM after each step, in order to illustrate the effects of each of the treatments, as shown in Figure 3.

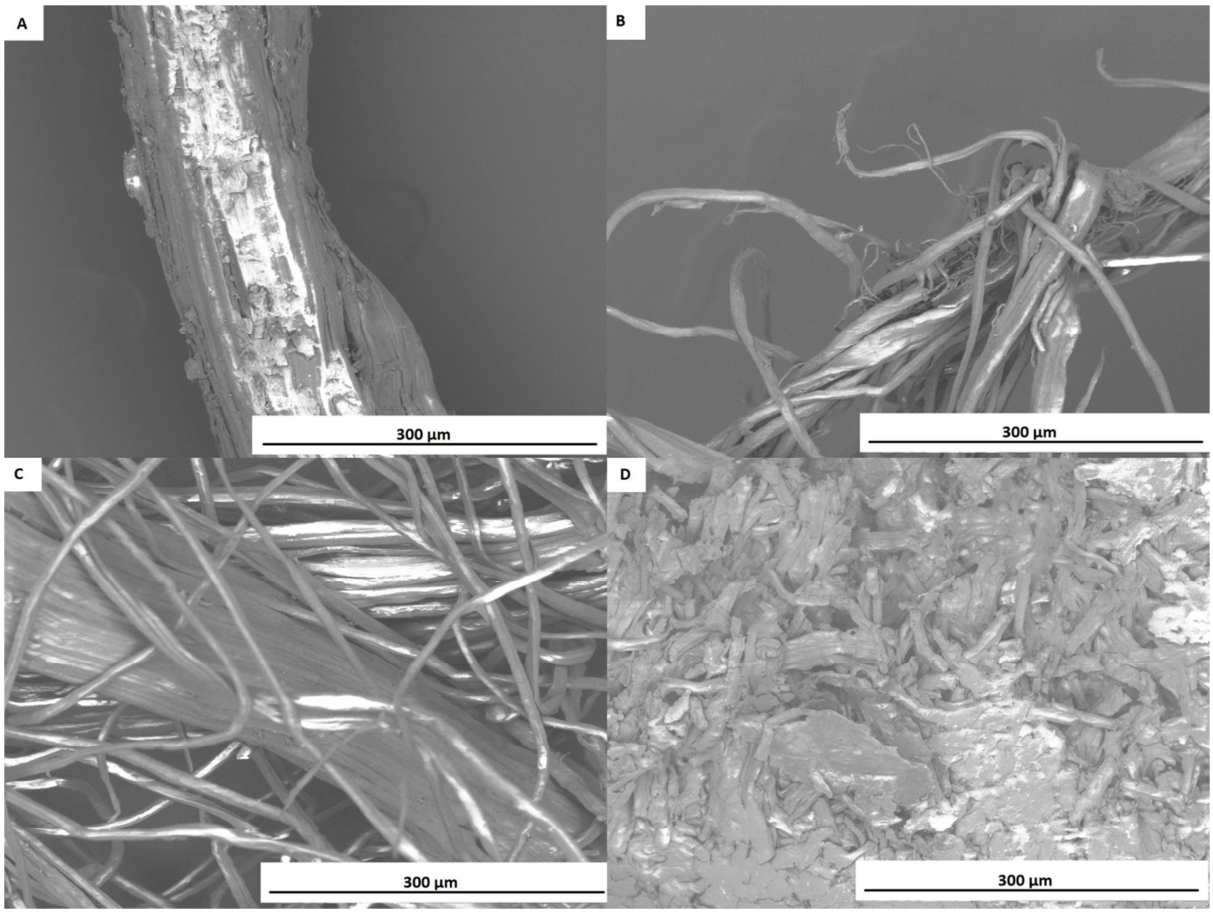

Figure 3. SEM pictures of the fibres at the various stages of the process showing the transgression from large fibre bundles to the fully treated acetylated fibres in the final pulp.

The micrographs in Figure 3 show how each step in the process affects the fibres. The strong alkali treatment swells the fibres and results in the formation of free individual fibres (SM). In the bleaching step even more individual fibres are produced (SMB) due to the removal of the remaining lignin, which reduces the cohesion between the fibrils. Finally, it can be seen how the acetylation step destroys the structure of the macroscopic fibres (SMBA), thereby resulting in the formation of a more uniform mass consisting of much smaller fibres. The results of the extraction protocol in terms of chemical and thermal properties can be seen in Figure 4.

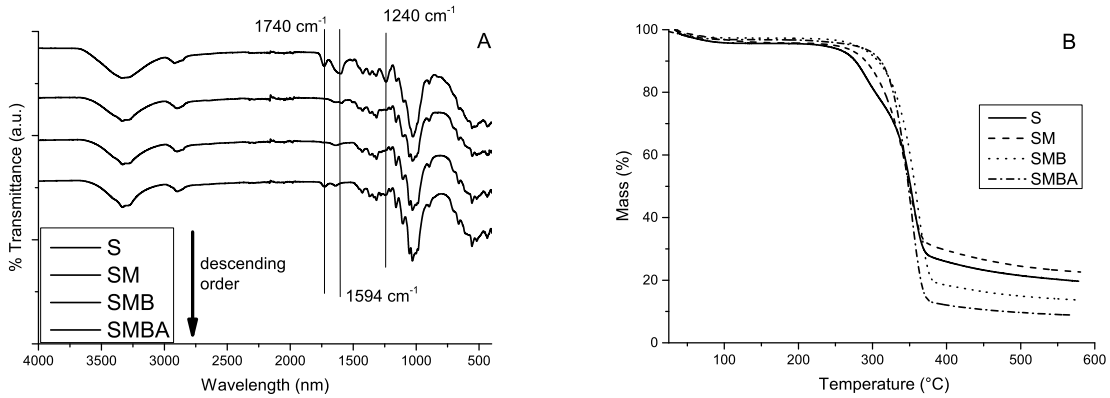

Figure 4. Analysis of the extracted CNF at each step in the process by FT-IR (A) and by TGA (B).

In Figure 4a the chemical changes to the fibres are illustrated by changes in the IR spectra. Here the removal of hemicellulose during the first alkali treatment from S to SM can be seen through disappearance of the peaks at 1740 cm^{-1} (which are related to acetyl and ester groups, characteristic of hemicellulose) and at 1240 cm^{-1} (C-O stretching vibration of the hemicellulose). In addition to this, the disappearance of the peak at 1594 cm^{-1} (related to the C-C in the plane symmetrical stretching of aromatic rings, characteristic of lignin) from SM to SMB shows that lignin has been removed from the fibre. This is corroborated by the fact that the fibres are completely white after bleaching. The removal of the hemicellulose is confirmed by TGA in Figure 4b. Hemicellulose usually degrades between 200-400°C, which results in an increase in the onset of thermal degradation after both the alkali treatment and the bleaching step compared to the pure sisal fibres.

Finally, acetylation of the pulp in the last step of the process is confirmed by reappearance of the peak at 1740 cm^{-1}, attributed to new acetate groups. The intensity of the carbonyl stretch indicates that only a partial acetylation has taken place. The extracted residues were also analysed (SI-Figure 1). It was found that the alkali treatments removed not only lignin and hemicellulose, but also significant amounts of cellulose. The surface charge of the extracted CNF was investigated employing conductimetry, which showed that the isolated CNF had no significant surface charge.

3.2 Characterization of the CNF

Introduction of acetate groups on the surface of the fibres, however, is not enough to fully separate the nanofibres. This acetylation results in reduced cohesion between the nanofibres, but a very small amount of energy is still required in order to separate the fibres. To illustrate this process, an aqueous solution of SMBA (1 wt%) was simply stirred for five days on a magnetic stirrer. Samples of this solution were analysed by optical microscopy after different stirring times as shown in

Figure 5.

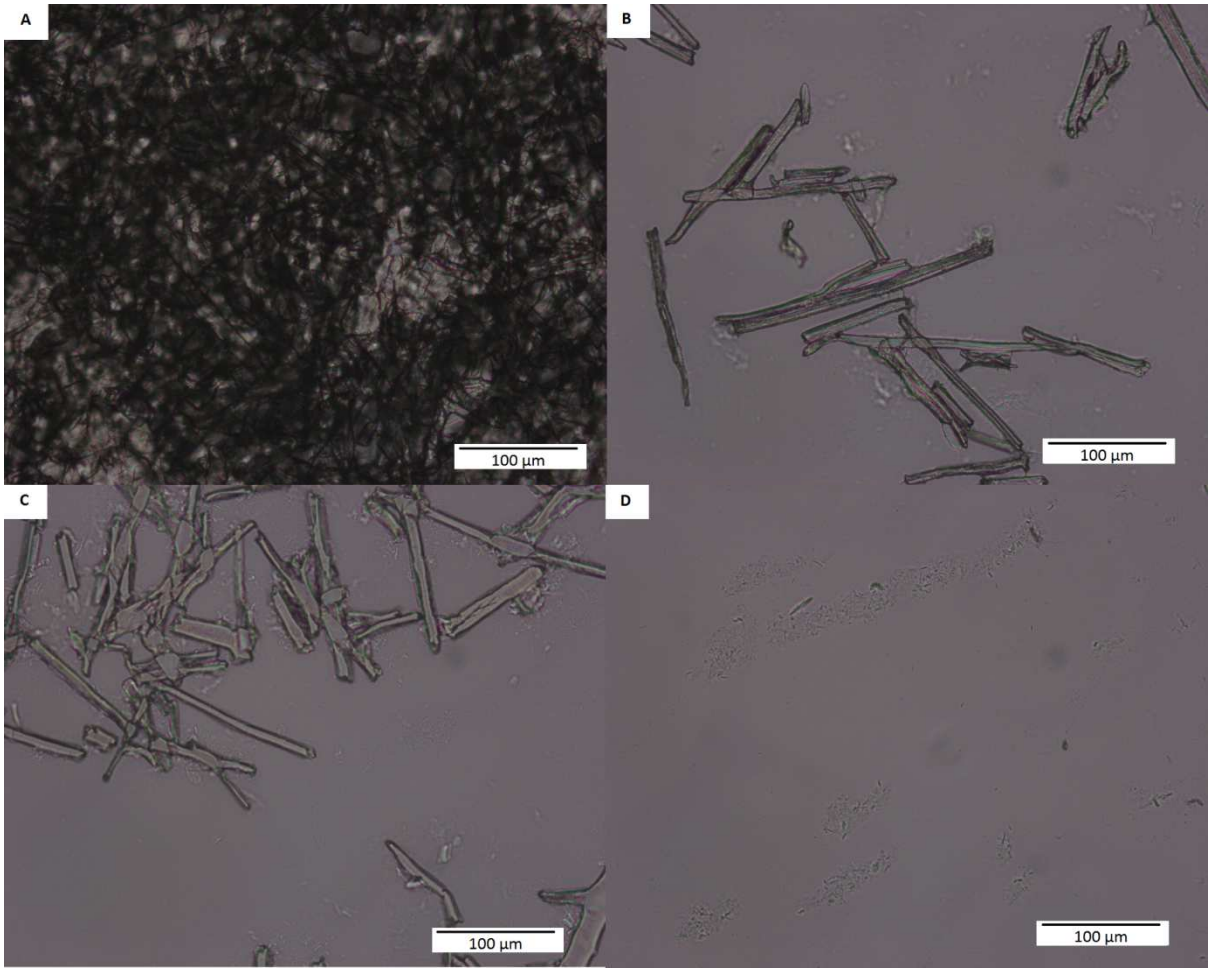

Figure 5. Optical micrographs of a 1wt% mixture of the acetylated pulp (SMBA) after magnetic stirring in water for 0 min (A), 15 min (B), 1 hour (C) and 48 hours (D).

Here it can be seen how a very simple process like magnetic stirring breaks up the aggregates and ultimately results in the preparation of a stable aqueous dispersion of the nanofibres after 48 hours. After two days of magnetic stirring, it is no longer possible to see large fibres in the optical microscope, thus suggesting that the majority of the fibres are on a nanoscale.

In order to corroborate the effect of the magnetic stirring the viscosity of a 4 wt% SMBA in water mixture was measured after 2 hours and 20 hours of magnetic stirring. Furthermore, the viscosity of both solutions was compared to the viscosity of commercially available CNF as shown in Figure 6.

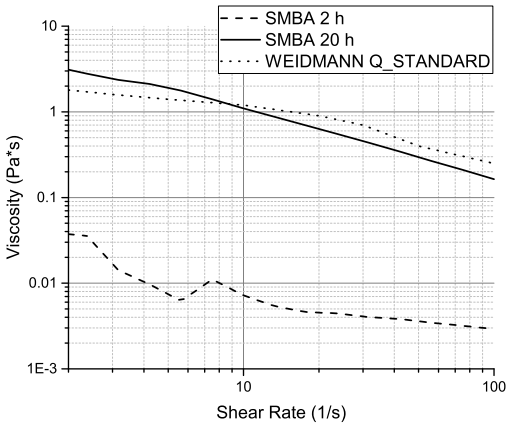

Figure 6. Viscosity of 4 wt% SMBA in water after magnetic stirring during 2 hours and 20 hours compared to a commercial CNF (Weidmann Q standard).

The viscosity is dramatically increased between 2 and 20 hours of magnetic stirring, proving that it successfully disperses the CNF. Furthermore, it was observed that after 20 hours the viscosity became so high that magnetic stirring was no longer powerful enough to efficiently stir the suspension. The viscosity of the resulting dispersion after 20 hours was similar to a commercially available CNF produced by Weidmann (Q standard).

In order to evaluate the dimensions of the prepared nanofibres, a drop of a 0.6 wt% CNF dispersion was casted on an aluminium film, resulting in the formation of a thin film with a film thickness of around 100 nm. The prepared film was sputtered and investigated by SEM, which showed a uniform distribution of nanofibers on the surface (SI-Figure 2). The size of the cellulose nanofibers were additionally investigated using transmission electron microscopy (TEM) as shown in Figure 7.

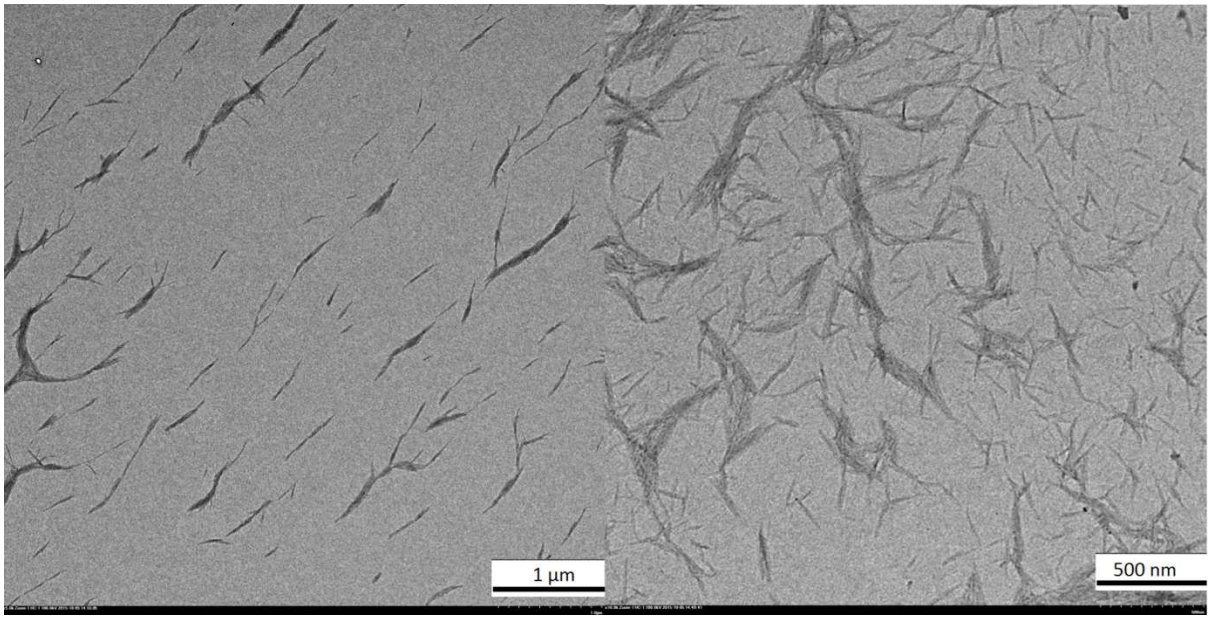

Figure 7. Analysis of the structure of the isolated CNF by TEM at different magnifications.

From both SEM and TEM it is clear that no large fibres are present in the film casted from the dispersion. The fibres are estimated to have a diameter of 27 +/- 13 nm and a length of 658 +/- 290 nm. This aspect ratio is

lower than when the CNF is prepared by using, for example, TEMPO-mediated oxidation and mechanical methods such as homogenisation, ultrasound or grinding(Moon et al. 2011), which is attributed to harsh conditions during the extraction process, expected to result in chain scission of the cellulose backbones and shorter fibres.

The crystallinity of the nanofibers was investigated by X-ray diffraction (XRD), as shown in Figure 8.

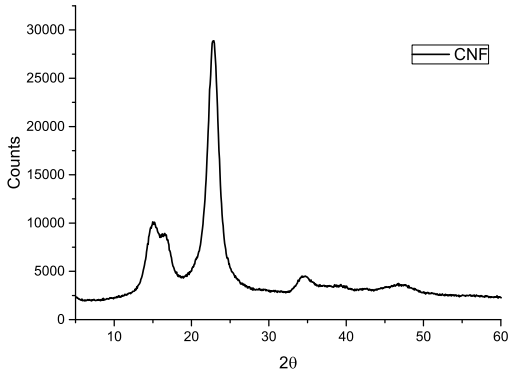

Figure 8. XRD analysis of the purified CNF.

The XRD spectrum shows the expected peaks from a cellulose material with peaks at 2θ=15.13 and 2θ=22.88°. The degree of crystallinity of the extracted fibres was calculated based on the peak at 22.88 °, and it was determined to be 84.2%. This is comparable to the degree of crystallinity reported by Lavoine et al. (Lavoine et al. 2012), where similar crystallinities were observed for sisal-based CNF (90%), *Luffa cylindrical fibres* (90%) as well as for Tempo oxidized CNF (TOCN) (90%).

3.3 CNF film properties

To illustrate the purity of the CNF dispersion it was used to prepare larger CNF based films by solution casting of either the pure CNF dispersion or of a combination of the CNF dispersion and the extracted residues. The prepared films have a high clarity and a good transparency as shown in Figure 9.

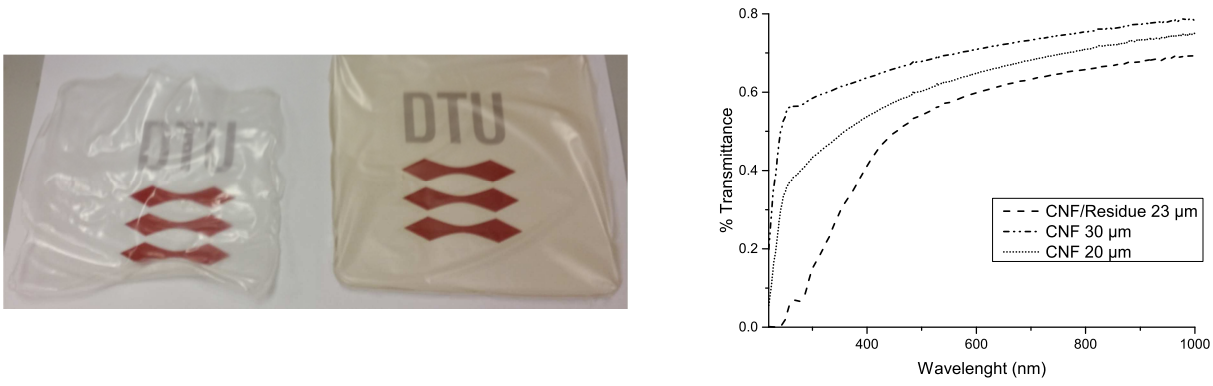

Figure 9. Left: Optical image of the prepared film (pure CNF on the left and CNF with residue solution on the right); Right: Transmittance of the CNF films determined by UV-vis spectroscopy.

The film prepared from the pure CNF is fully transparent, and with a high clarity (69,8% clarity, 26,76% haze) whereas the film with the added residues (extracted cellulose, lignin and hemicellulose from the mercerisation step) resulted in a light-brown but more uniform film with a slightly reduced clarity (44,6% clarity, 36,2% haze) (see Table 1, supporting information). While a high haze makes the films useful for solar cell applications, a film with a high clarity is interesting for other applications such as food packaging.

The CNF/Residue film additionally has a decreasesd UV transmittance, due to the presence of lignin that acts as a UV absorber and as antioxidant. Ultimately, these materials are intended for use as packaging materials and for this application a reduced UV transmittance as well as the antioxidative properties of the lignin looks extremely promising with respect to preservation of packaged food. The residues were also incorporated into the film, in order to investigate if they could potentially decrease the water sorption of the films as well as to investigate any effects on film forming. The cross-sectional view of the films by SEM can be seen in Figure 10.

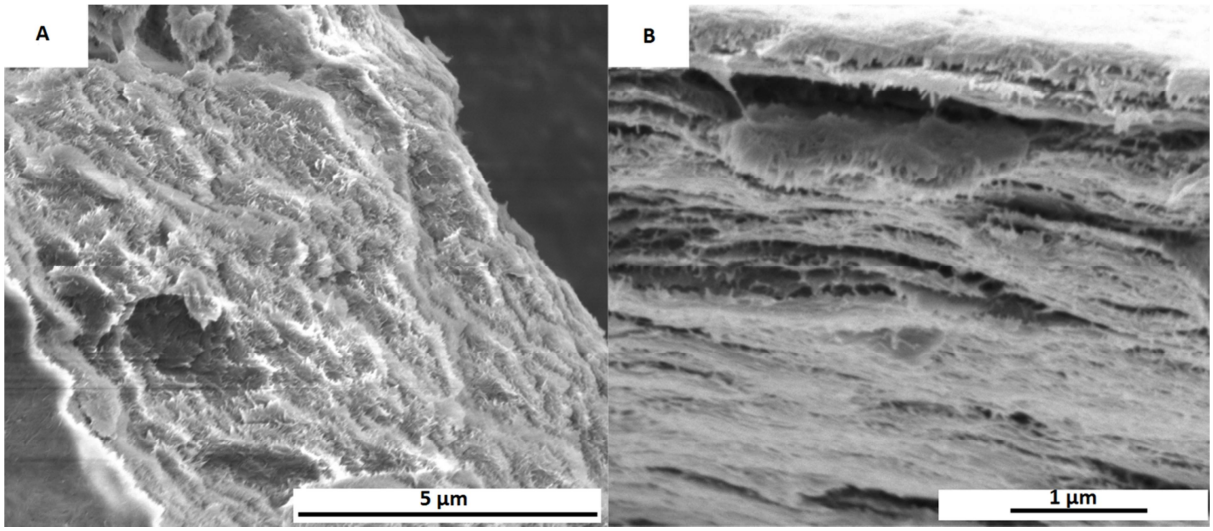

Figure 10. SEM analysis of a fractured cross section of a) Neat CNF film and B) CNF/Residue film.

The SEM micrographs show that there are no large agglomerates on the fractured interphase from the films, illustrating the high purity of the CNF dispersions (SEMs of the surface view of the films can be seen in the supporting information in SI-Figure 3 and 4). The micrographs also show a clear differences in the layered structures of the two films, where the CNF/Residue film is clearly much more compact compared to the pristine CNF film, which appears to have a more open structure. This feature of the CNF/Residue film is attributed to the lignin in the residue, which is expected to result in a reduced swelling of the CNF during the drying stage due to the hydrophobicity of lignin.

The mechanical properties of the films were investigated (SI-Table2), showing that in particular the pure CNF film had lower tensile strength and comparable elongation at break compared to other nanocellulose films(Henriksson et al. 2008; Siró et al. 2011). The pure CNF films were very brittle and had an uneven surface, which made the mechanical analysis very difficult. In contrary to this, the CNF/Residue films were more uniform and easier to handle, which resulted in a significant increase in tensile strength and elongation. CNF films, apart from their brittleness, have been reported to have good properties at low relative humidity, but their barrier properties dramatically decreases with increasing relative humidity(Aulin et al. 2010; Minelli et al. 2010). For this reason, any process that could decrease water sorption would be very useful for new applications

of CNF films. The CNF nanomaterials prepared here are partially acetylated, which could potentially affect water sorption. In an effort to elucidate this, the advancing water contact angles of the prepared films were determined. Both films have comparable water contact angles of 48.8° +/- 2.7 for the CNF film and 52.4° +/- 1.1 for the CNF/Res film, which is similar to other non-functionalised nanocelluloses (41.2° (Rodionova et al. 2010), 50-60°(Siqueira et al. 2010), 50°(Wu et al. 2014)). Apparently the acetylation does not significantly increase the hydrophobicity of the thin films. The actual water sorption of the films can be seen in the supporting information (SI-Figure 5). The observed water sorption, approximately 2,6% at 23°C and 50% rel. humidity for both types of films, was slightly decreased compared to other nanocellulose films, where CNF and nanocrystalline cellulose have been shown to have water sorption of 6.5% at 25°C and 50% rel. humidity (Belbekhouche et al. 2011), or 4% at 35°C and 50% rel. humidity for enzymatically pre-treated CNF(Minelli et al. 2010).

4. CONCLUSIONS

In this study a method is presented whereby a high yield of acetylated CNF can be prepared by employing a chemical treatment protocol. This method of extracting cellulose nanofibres has several advantages. The raw pulp produced after the chemical treatments is produced in a high yield of 48% and can be easily filtered and purified. The isolated SMBA pulp does not form hydrogels, and can be reduced to a water content of 50%, resulting in a potential reduction in transportation costs of the pulp. The chemicals used in the process are very common and not particularly expensive. Moreover, it is possible through well-established processes in the paper industry to reclaim these chemicals. The process directly affords acetylated fibres, which results in an easy dispersion method by low energy methods such as magnetic stirring. The prepared dispersions were seen to contain a high purity of nanofibers, with no large aggregates present, as illustrated by both SEM and TEM as well as through preparation of highly transparent CNF films. In an attempt to improve the film forming properties of the CNF films the alkali residue was reintroduced into the CNF films, which lead not only to an overall higher mass yield, but also to flatter films, which illustrated the potential of the residue as a novel cementing agent for the CNF films. The inclusion of the alkali residue in the material was found to improve UV blocking capabilities, which could be very interesting in terms of applications in food packaging.

ACKNOWLEDGEMENTS

The author would like to acknowledge the FP7 - People - 2011, ITN Marie Curie International Training Network (ITN), COST Action FP1003 and COST Action FP1105 for financial support. Lars Schulte is acknowledged for his assistance with the microscopy analyses, Richard Andersson for carrying out the transmission electron microscopy and Sebastien Raynaud for assisting with measuring the optical properties of the composites with the Hazemeter. This paper is in memoriam of Professor Iñaki Mondragon Egaña, whose dedication is a great source of inspiration for the first author.

5. REFERENCES

Abdul Khalil HPS, Davoudpour Y, Islam MN, Mustapha A, Sudesh K, Dungani R, Jawaid M (2014) Production and modification of nanofibrillated cellulose using various mechanical processes: a review. Carbohydr Polym 99:649–65. doi: 10.1016/j.carbpol.2013.08.069

Aulin C, Gällstedt M, Lindström T (2010) Oxygen and oil barrier properties of microfibrillated cellulose films

317 and coatings. Cellulose 17:559–574. doi: 10.1007/s10570-009-9393-y

318 Azizi Samir MAS, Alloin F, Dufresne A (2005) Review of recent research into cellulosic whiskers, their
319 properties and their application in nanocomposite field. Biomacromolecules 6:612–26. doi:
320 10.1021/bm0493685

321 Baker E, Keisler JM (2011) Cellulosic biofuels: Expert views on prospects for advancement. Energy 36:595–
322 605. doi: 10.1016/j.energy.2010.09.058

323 Belbekhouche S, Bras J, Siqueira G, Chappey C, Lebrun L, Khelifi B, Marais S, Dufresne A (2011) Water
324 sorption behavior and gas barrier properties of cellulose whiskers and microfibrils films. Carbohydr
325 Polym 83:1740–1748. doi: 10.1016/j.carbpol.2010.10.036

326 Bismarck A, Aranberri-Askargorta I, Springer J, Mohanty AK, Misra M, Hinrichsen G, Czapla S (2001) Surface
327 characterization of natural fibers; surface properties and the water up-take behavior of modified sisal and
328 coir fibers. Green Chem 3:100–107. doi: 10.1039/b100365h

329 Chang C, Zhang L (2011) Cellulose-based hydrogels: Present status and application prospects. Carbohydr
330 Polym 84:40–53. doi: 10.1016/j.carbpol.2010.12.023

331 Czaja WK, Young DJ, Kawecki M, Brown RM (2007) The future prospects of microbial cellulose in biomedical
332 applications. Biomacromolecules 8:1–12. doi: 10.1021/bm060620d

333 de Morais Teixeira E, Corrêa AC, Manzoli A, de Lima Leite F, de Oliveira CR, Mattoso LHC (2010) Cellulose
334 nanofibers from white and naturally colored cotton fibers. Cellulose 17:595–606. doi: 10.1007/s10570-
335 010-9403-0

336 Eichhorn SJ, Dufresne A, Aranguren M, Marcovich NE, Capadona JR, Rowan SJ, Weder C, Thielemans W,
337 Roman M, Renneckar S, Gindl W, Veigel S, Keckes J, Yano H, Abe K, Nogi M, Nakagaito AN,
338 Mangalam A, Simonsen J, Benight AS, Bismarck A, Berglund LA, Peijs T (2010) Review: current
339 international research into cellulose nanofibres and nanocomposites. J Mater Sci 45:1–33. doi:
340 10.1007/s10853-009-3874-0

341 Fischer F, Rigacci A, Pirard R, Berthon-Fabry S, Achard P (2006) Cellulose-based aerogels. Polymer 47:7636–
342 7645. doi: 10.1016/j.polymer.2006.09.004

343 Henriksson M, Berglund LA, Isaksson P, Lindström T, Nishino T (2008) Cellulose nanopaper structures of high
344 toughness. Biomacromolecules 9:1579–1585. doi: 10.1021/bm800038n

345 Herrick FW, Casebier RL, Hamilton KJ, Sandberg KR (1983) Microfibrillated Cellulose: Morphology and
346 Accessibility. J Appl Polym Sci Appl Polym Symp 37:797–813.

347 Lavoine N, Desloges I, Dufresne A, Bras J (2012) Microfibrillated cellulose - its barrier properties and
348 applications in cellulosic materials: a review. Carbohydr Polym 90:735–64. doi:
349 10.1016/j.carbpol.2012.05.026

350 Lin N, Dufresne A (2014) Nanocellulose in biomedicine: Current status and future prospect. Eur Polym J
351 59:302–325. doi: 10.1016/j.eurpolymj.2014.07.025

352 Minelli M, Baschetti MG, Doghieri F, Ankerfors M, Lindström T, Siró I, Plackett D (2010) Investigation of
353 mass transport properties of microfibrillated cellulose (MFC) films. J Memb Sci 358:67–75. doi:
354 10.1016/j.memsci.2010.04.030

355 Mondragon G, Fernandes S, Retegi a., Peña C, Algar I, Eceiza a., Arbelaiz a. (2014) A common strategy to
356 extracting cellulose nanoentities from different plants. Ind Crops Prod 55:140–148. doi:
357 10.1016/j.indcrop.2014.02.014

358 Moon RJ, Martini A, Nairn J, Simonsen J, Youngblood J (2011) Cellulose nanomaterials review: structure,
359 properties and nanocomposites. Chem Soc Rev 40:3941–94. doi: 10.1039/c0cs00108b

360 Mwaikambo LY, Ansell MP (1999) The effect of chemical treatment on the properties of hemp, sisal, jute and
361 kapok for composite reinforcement. Die Angew Makromol Chemie 272:108–116. doi:
362 10.1002/(SICI)1522-9505(19991201)272:1<108::AID-APMC108>3.0.CO;2-9

363 Qing Y, Sabo R, Zhu JY, Agarwal U, Cai Z, Wu Y (2013) A comparative study of cellulose nanofibrils
364 disintegrated via multiple processing approaches. Carbohydr Polym 97:226–34. doi:
365 10.1016/j.carbpol.2013.04.086

366 Rodionova G, Lenes M, Eriksen Ø, Gregersen Ø (2010) Surface chemical modification of microfibrillated
367 cellulose: improvement of barrier properties for packaging applications. Cellulose 18:127–134. doi:
368 10.1007/s10570-010-9474-y

369 Saheb DN, Jog JP (1999) Natural fiber polymer composites: A review. Adv Polym Technol 18:351–363. doi:
370 10.1002/(SICI)1098-2329(199924)18:4<351::AID-ADV6>3.0.CO;2-X

371 Siqueira G, Bras J, Dufresne A (2010) New process of chemical grafting of cellulose nanoparticles with a long
372 chain isocyanate. Langmuir 26:402–11. doi: 10.1021/la9028595

373 Siró I, Plackett D (2010) Microfibrillated cellulose and new nanocomposite materials: a review. Cellulose
374 17:459–494. doi: 10.1007/s10570-010-9405-y

375 Siró I, Plackett D, Hedenqvist M, Ankerfors M, Lindström T (2011) Highly transparent films from
376 carboxymethylated microfibrillated cellulose: The effect of multiple homogenization steps on key
377 properties. J Appl Polym Sci 119:2652–2660. doi: 10.1002/app.32831

378 Tejado A, Alam MN, Antal M, Yang H, van de Ven TGM (2012) Energy requirements for the disintegration of
379 cellulose fibers into cellulose nanofibers. Cellulose 19:831–842. doi: 10.1007/s10570-012-9694-4

380 Wu C-N, Saito T, Yang Q, Fukuzumi H, Isogai A (2014) Increase in the water contact angle of composite film
381 surfaces caused by the assembly of hydrophilic nanocellulose fibrils and nanoclay platelets. ACS Appl
382 Mater Interfaces 6:12707–12. doi: 10.1021/am502701e

383

APPENDIX 3: A comparison of partially acetylated nanocellulose, nanocrystalline cellulose and nanoclay as fillers for high-performance polylactide nanocomposites.

Trifol J., Plackett D., Sillard C., Hassager O., Daugaard A.E., Bras J., Szabo P. A comparison of partially acetylated nanocellulose, nanocrystalline cellulose and nanoclay as fillers for high-performance polylactide nanocomposites. *J Appl Polym Sci* 2016; **133**:1–13. doi:10.1002/app.43257.

Journal of Applied Polymer Science

A comparison of partially acetylated nanocellulose, nanocrystalline cellulose, and nanoclay as fillers for high-performance polylactide nanocomposites

Jon Trifol,[1] David Plackett,[2] Cecile Sillard,[3] Ole Hassager,[1] Anders Egede Daugaard,[1] Julien Bras,[3] Peter Szabo[1]

[1]Department of Chemical and Biochemical Engineering, Danish Polymer Centre, Søltofts Plads, Building 229, DK - 2800 Kgs, Lyngby, Denmark

[2]Faculty of Pharmaceutical Sciences, University of British Columbia, 2405 Wesbrook Mall, Vancouver, BC, V6T 1Z3, Canada

[3]Université Grenoble Alpes, LGP2, F-38000 Grenoble, France CNRS, LGP2, F-38000 Grenoble, France

Correspondence to: P. Szabo (E-mail: ps@kt.dtu.dk)

ABSTRACT: Partially acetylated cellulose nanofibers (CNF) were chemically extracted from sisal fibers and the performance of those CNF as nanofillers for polylactide (PLA) for food packaging applications was evaluated. Three PLA nanocomposites; PLA/CNF (cellulose nanofibers), PLA/CNC (nanocrystalline cellulose), and PLA/C30B (Cloisite™ 30B, an organically modified montmorillonite clay) were prepared and their properties were evaluated. It was found that CNF reinforced composites showed a larger decrease on oxygen transmission rate (OTR) than the clay-based composites; (PLA/CNF 1% nanocomposite showed a 63% of reduction at 23°C and 50% RH while PLA/C30B 1% showed a 26% decrease) and similar behavior on terms of water vapor barrier properties with 46 and 43%, respectively of decrease on water vapor transmission rate at 23°C and 50% RH (relative humidity). In terms of mechanical and thermomechanical properties, CNF-based nanocomposites showed better performance than clay-based composites without affecting significantly the optical transparency. © 2015 Wiley Periodicals, Inc. J. Appl. Polym. Sci. **2016**, *133*, 43257.

KEYWORDS: barrier properties; cellulose nanofibers (CNF); microfibrillated cellulose; nanoclays; polylactic acid

Received 26 August 2015; accepted 19 November 2015

DOI: 10.1002/app.43257

INTRODUCTION

The use of petrochemical products for packaging applications represents a serious global environmental challenge, not only from the point of view of the availability of the raw material but also due to disposal of the products. For that reason in recent years, especially in the packaging industry, a considerate effort has been made in order to develop both biobased and biodegradable materials to substitute the materials that are being used currently (e.g., PE and PET). The use of biobased and biodegradable polymers such as polylactide (PLA) is finding an increasing number of applications which has led to perspectives of high growing in production and market.[1,2] Traditionally, PLA has been deemed to have inferior material performance compared to the most widely used synthetic polymers for which it might substitute. In particular, poor thermomechanical properties, brittleness, slow crystallization, medium oxygen, and water vapor barrier properties have been some of the major technical obstacles in expanding applications for PLA.[3]

To improve the properties of PLA, several different strategies have been adopted. These strategies include modifying PLA (e.g., block copolymers),[4] blending with other polymers such as PEG, use of reinforcing agents such as natural fibers,[5] nanoclays,[6] nanocellulose,[7] chitosan,[8] xylans,[9] and calcium carbonate[10] among others. Cellulose nanofibers (CNF) or cellulose nanocrystals (CNC), which can be obtained from lignocellulosic materials or from bacteria or algae,[11,12] have received the attention of numerous researchers not only for their biodegradability, bio-based origin, and availability but also due to their good reinforcing properties[13] which makes it a promising nanofiller for PLA. There are already several reports on PLA/CNF nanocomposites,[14–16] with various results reported. The reason for such variations might be the large number of parameters involved in the reinforcing effect, such as the quality of the

Additional Supporting Information may be found in the online version of this article.

reinforcing agent (aspect ratio/yield), the dispersion of the filler in the matrix, and the presence of aggregates amongst others.

The mechanical properties of PLA/nanocellulose composites have been widely studied, and while in one hand there are reports claiming a great reduction in the tensile strength and Young modulus 47%,[17] in the other hand there are other works reporting a slight improvement of the mechanical properties,[18] but, generally, the reinforcing of CNF is more pronounced at temperatures above the T_g, when the mechanical resistance of the polymer dramatically decreases. In food packaging applications, good thermomechanical stability is required not only for special applications such as microwave heated food, but also for processes such as thermoforming.

Apart from the thermomechanical properties, the barrier properties are critical for some food packaging applications. For example, oxygen can enhance microbiological activity and oxidize the food; water vapor ingress can lead to deterioration of dry products and aroma barrier properties may also be required. Although a frequent reference material for barrier properties is PET, implying that the OTR of PLA should be decreased by 90%, there is a huge range of food packaging applications (i.e., MAP (modified atmosphere packaging), poultry product packaging, vegetable packaging, and so on), where any kind of improvement in barrier properties of PLA could make this material useful, even if the improvement in barrier properties does not reach the same level as PET.

In theory, nanofillers such as C30B increase the so-called tortuous path through a polymer film, meaning that gas or water molecules passing through the films have to follow a longer path, so, diffusivity and hence permeability are thereby reduced. The studies on the effect of CNF on the barrier properties of PLA show also a large variation. From a decrease of 90% in the oxygen permeability at 75% RH on PLA/CNC 2% films[17] to moderate improvements (9–43%)[16] and finally there are reports of a reduction on both oxygen and water barrier properties.[19] Finally, nanocellulose has been reported to have a nucleating agent behavior[18,20] of PLA.

A key point to obtain enhanced properties of PLA/CNF nanocomposites is to achieve a very good dispersion of nanofillers in the polymer matrix. The dispersion of hydrophilic nanocellulose within a hydrophobic still remains a challenge, and some strategies such as the use of surfactants[21] or grafting hydrophobic chains onto nanocellulose surface[22] are usually required in order to achieve good dispersion. In previous publications a method to produce high yield partially acetylated-CNF by means of chemical methods was developed.[23] Because of the high yield and the partially grafted nature of those nanofillers they may be promising additives to enhance the performance of PLA for food packaging applications.

The aim of this work is to compare the performance of those CNF not only with the neat PLA, but also with CNC and clay. From the diverse amount of clay, such as montmorillonite,[24] kaolin,[25] the C30B, a commercially available organically modified clay, was selected, since it has been widely used to reinforce PLA, increasing the tensile modulus by 13% and impact strength by 27% at 3% load,[26] 63% the tensile modulus at 5% load,[27] and by decreasing the water vapor permeability by 40% at 5% load.[28]

EXPERIMENTAL

Materials and Methods

L-polylactide (Ingeo 2003D) was kindly supplied by Natureworks (Minnesota, MN). Nanocellulose was extracted from sisal which was kindly supplied by Expor Sisal S.L. The chosen nanoclay was the commercially available Cloisite 30B which is reported to have a cationic exchange capacity (CEC) of 90[29] and a tetraalkyl ammonium salt as a surfactant modifier. NaOH, sulfuric acid (95–97%), nitric acid (ACS reagent, 70%), acetic acid (99–100%), *N*,*N*-dimethyl formamide (98%, ACS reagent) and dichloromethane (99, 8% chromasolv) were purchased from Sigma–Aldrich and sodium chlorite (25% w/w aqueous solution) from Merck. All of the reagents were used as received.

The thickness of cast PLA films (12 × 12 cm^2) was determined using a digital micrometer with a tolerance of ±1% at nine points (eight points on the edges and one in the middle). Films were examined microscopically to check for bubbles or other contamination and discarded if not deemed suitable for use.

The dispersion of the nanofiller in the matrix was studied by X-ray diffraction (XRD) using a Philips X'Pert Pro diffraction system containing a Cu tube ($\lambda = 1.542$ Å) operating at 40 kV and 40 mA. TEM (FEI Tecnai T20 G2) and SEM (FEI Helios EBS3, FEI Inspect) operating at 200 and 5 kV, respectively were also employed.

Thermal properties such as glass transition (T_g), melting temperature (T_m), and degree of crystallinity (X_c) of PLA and the nanocomposites were determined by DSC (TA DSC Q1000) with heating and cooling rates of 10°C min^{-1} in a range of 0–200°C in a heat/cool/heat cycle. A melting enthalpy (ΔH_0) of 93 J g^{-1} for 100% crystalline L-polylactide) was used as reported by Ref. 30. To determine X_c for the first and second heating cycles eq. (1) was used.

$$Xc = \frac{1}{1 - M_{NF}} \frac{\Delta H_m - \Delta H_C}{\Delta H_0} \quad (1)$$

Where X_c is the degree of crystallinity of the composite, M_{NF} the content of nanofiller, ΔH_m is the melting enthalpy (the area of the peak which minimum is at T_m) and ΔH_C is the crystallization enthalpy.

The isothermal crystallization studies were conducted using the following cycle: heating at 10°C min^{-1} to 200°C, hold at 200°C for 2 min and cooled down to 0°C at 20°C min^{-1}. Subsequently, each sample was heated at 20°C until 120°C and then held at that temperature for 2 h. Finally, the samples were cooled to 0°C at 10°C min^{-1} and heated until 200°C at 10°C min^{-1}.

The spherulite size and shape of the nanocomposites due to the solvent casting approach was compared with the crystallinity induced by isothermal crystallization. The neat PLA and the nanocomposites were placed between two microscope crystal slides and introduced in a heating device connected to an

optical microscope with polarized light. The samples were heated until 200°C for 2 min and thereafter were cooled to room temperature using a tissue impregnated with ethanol. Finally the samples were introduced in the heating chamber at 100°C and the crystallization process was recorded by a camera.

The optical properties were measured at least at three different points on each cast film using a UV–vis spectrometer (Polar Star Omega) in the range of 200–1000 nm.

The oxygen transmission rate (OTR) was measured in triplicate sample sets using a Lyssy OPT-5000 Oxygen permeability tester. Experiments were performed at 23°C at 0% or 50% RH. Results were expressed in units of mL μm m^{-2} day^{-1}.

The water vapor transmission rate (WVTR) of the films was measured in triplicate sample sets according to the norm NF H 00-030[22] at 23°C and 50% RH using silica gel as desiccating agent with a specific exchange surface (S) 28.27 cm^2. The mass increase of the cups, due to the water absorption of silica gel was plotted against time having slope n. The WVTR was calculated with eq. (2) in which l is the thickness of the film.

$$\mathrm{WVTR} = \frac{n * l}{S} \tag{2}$$

The mechanical properties of sample films were measured in an Instron Universal Testing Machine Model 4507 (Instron Engineering Corporation, Canton, MA) equipped with pneumatic jaws of type I BA using dumbbell-shaped samples. The properties were measured at a strain rate of 2.5 mm min^{-1}. This testing was carried out using five 5 × 1 cm^2 samples from each film type after thickness measurement at four locations. The samples were preconditioned at 23°C and 50% RH.

The thermomechanical properties of test films were measured in duplicate samples using a DMA RSA3 (TA Instruments, USA) equipment working in tensile mode. The measurements were performed at a constant frequency of 1 Hz and strain amplitude of 0.05% with a distance between jaws of 10 mm. The samples were heated at 10°C min^{-1} from room temperature to 110°C, were held at this temperature for 20 min and then cooled to 25°C at 10°C min^{-1}. In a final step, the samples were heated to 180°C at 10°C min^{-1}. The analysis of each sample was carried twice to check the reproducibility of the measurements.

Preparation of CNF and CNC

CNF Preparation. Our method for isolation of the cellulose nanofibers (CNF) has been already discussed.[23] The method consists of a sequence of chemical treatments to sisal fibers:

A. *Washing*: 50 g of sisal fibers (S) of around 200 μm of diameter, were cut to ~2 cm of length, and washed with 1.5 L of a solution of 2% NaOH at room temperature overnight in a 2-L round bottom flask. After that the fibers were filtered and washed, adding distilled water until no further change was observed in the pH of the aqueous suspension
B. *Mercerization (SM)*: After that the washed fibers were collected and treated with 1.5 L of a solution of NaOH at 10% in a 2-L round bottom flask and were held for 1.5 h at boiling temperature. This procedure was repeated two more times and the fibers were washed.
C. *Bleaching (SMB)*: The mercerized pulp (SM) collected in 1.25 L of distilled water in a 2-L round bottom flask and the temperature was raised to 70°C. Once this temperature was achieved, 10 mL of acetic acid and 50 mL of $NaClO_2$ were added once per hour for the next 7 h. Finally, the bleached pulp was filtered and cleaned until no change in the pH was observed.
D. *Acetylation (SMBA)*: The bleached pulp (SMB) was collected in a 2-L round bottom flask with 150 mL of nitric acid and 900 mL of acetic acid. This solution was kept at boiling temperature and magnetic stirring for 90 min and after that, the reaction medium was cooled by diluting with cold water (ratio 1:5).

This pulp was submitted either for a dispersion-centrifugation procedure to achieve CNF or to acid hydrolysis to achieve CNW.

1. *CNF isolation*: To extract and individualize CNF, the SMBA was washed with DMF and solvent exchanged into DMF three times with no intermediate redispersion to be finally diluted with DMF until achieve a solution of 1% of CNF on DMF. This mixture was kept under vigorous magnetic stirring for 3 days and then was centrifuged (~2500 rpm for 10 min) to separate the individualized nanofibers from the remaining aggregates. The supernatant was collected and the precipitate—remaining aggregates—was discarded.
2. *CNC isolation*: CNC were obtained by acid hydrolysis of SMBA. Nearly 20 g SMBA pulp was treated with 400 mL of 32% sulfuric acid at 45 °C for 2 h under magnetic stirring. The suspension was then diluted five-fold with water and dialyzed until no change in pH was observed. Finally, the product was solvent exchanged into DCM and thereafter to DMF. The CNC in DMF was held for 24 h under strong magnetic stirring and was then centrifuged to separate the aggregates (~1500 rpm for 10 min). The supernatant containing CNC was used to make the nanocomposites.

Preparation of Nanocomposites

Neat PLA film and three types of nanocomposites: (a) PLA/C30B; (b) PLA/CNF, and (c) PLA/CNC were prepared by solvent casting. Briefly, separately, PLA and nanofillers were dissolved/predispersed in a solvent, and thereafter the two solutions were mixed, casted in a Teflon mold and dried.

Neat PLA Film. For the neat PLA, 10 g of PLA were dissolved in 200 mL of DCM (dichloromethane) using magnetic stirring, overnight. After that, 100 mL of the DCM solution were poured in a 250 mL Erlenmeyer and the solution was raised until 250 mL by adding extra DCM. Thereafter, the suspension was degassed by ultrasonication for 5 min and 240 mL of that solution was poured slowly into three Teflon molds (80 mL/each mold). The three molds were covered by a 5- to 13-μm filter paper and they were kept in a Climacell climatic chamber (MMM Group) at 23°C for 16 h. Subsequently, the resulting PLA/C30B films were dried at 50°C under vacuum for a minimum of 24 h.

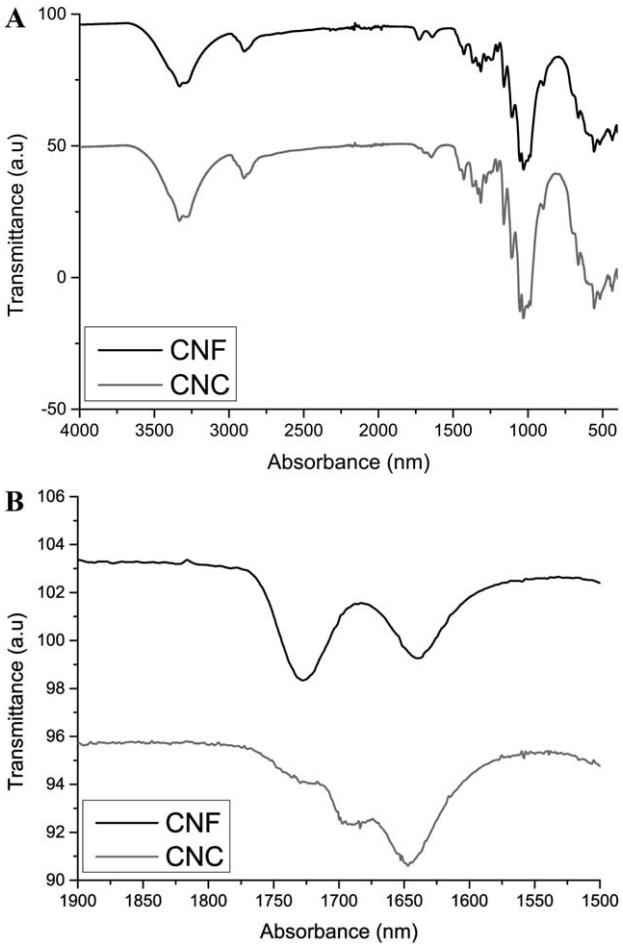

Figure 1. FT-IR of the CNC and CNF. Left: 4000–400 cm^{-1}; Right: Zoom 1900–1500 cm^{-1}.

PLA/C30B Nanocomposites. To prepare the C30B nanocomposites, first, the C30B was predispersed on DCM in the following way: 3.0 g of C30B were mixed with 300 mL of DCM and this mixture was magnetically stirred for 24 h. Thereafter, nanoclay suspension in a DCM solution was ultrasonicated for 3 h at 200W and homogenized for 90 min, which was found to be the optimal procedure for the clay dispersion, with an Ultraturrax homogenizer (Jonke & Kunnel IKA Ultraturrax T25) at 20,500 rpm.

Thereafter, the previously prepared PLA solution and the predispersed nanoclay suspension were mixed to obtain the desired concentration of C30B in PLA. After that, they were kept for 10 min under strong magnetic stirring, and finally, the volume was then increased to 250 mL with DCM. This solution was thereafter ultrasonicated for 90 min, homogenized for 30 min and the necessary DCM was added to increase the volume again to 250 mL. Finally, the suspension was degassed by ultrasonication for 5 min and 240 mL of the solution was poured slowly into three Teflon molds (80 mL/each mold). The three molds were covered by a 5–13 μm filter paper and they were kept in a Climacell climatic chamber (MMM Group) at 23°C for 16 h. Subsequently, the resulting PLA/C30B films were dried at 50°C under vacuum for a minimum of 24 h.

PLA/CNF and PLA/CNC Nanocomposites. To elaborate nanocellulose-based composites, several solvents (water, acetone, dichloromethane (DCM), tetrahydrofuran (THF), dimethylformamide (DMF), dimethylacetamide (DMAc), and *N*-methyl-2-pyrrolidone (NMP)) were evaluated for PLA/nanocellulose film preparation, and after evaluating different aspects, it was found that DMF was the most suitable solvent for nanocellulose-based composites.

Nearly 3.3 g of PLA were dissolved in 66 mL of DMF by mixing and keeping them for 2 h at 70°C under vigorous stirring. After 2 h, the nanocellulose suspension on DMF, obtained in CNF/CNC isolation procedure, was added and the solution was increased to 100 mL with additional DMF. The PLA/nanocellulose mixtures were thereafter kept under vigorous stirring and ultrasonicated at 200 W for 10 min. Finally the solution was casted into two Teflon molds covered by a 5- to 13-μm filter paper (50 mL/each mold). In each case, remaining solvent was removed from cast films by drying at 80°C for 15 h followed by drying under vacuum at 50°C for 24 h.

Thermal Treatments. To achieve quenched nanocomposites, the films were hot pressed for 5 min at 170°C followed by a fast cooling in order to achieve essentially amorphous nanocomposites (AM). After that, to achieve fully crystallized nanocomposites, the quenched nanocomposites were placed into an oven at 120°C for 2 h in order to obtain fully crystallized nanocomposites (FC).

RESULTS AND DISCUSSION

The nanofillers were characterized by FT-IR and XRD as can be seen in Figures 1 and [2].

As can be clearly seen in Figure 1, there is a difference between the CNC and CNF FT-IR spectra at 1740 cm^{-1}. The CNF shows absorbance on the peak at 1740 cm^{-1}, corresponding to the carbonyl groups grafted onto the nanocellulose during the acetylation procedure that have been removed during the acid hydrolysis.

As can be seen in Figure 2, the crystallinity of the CNC and CNF are very similar, this is due to the fact that the acetylation

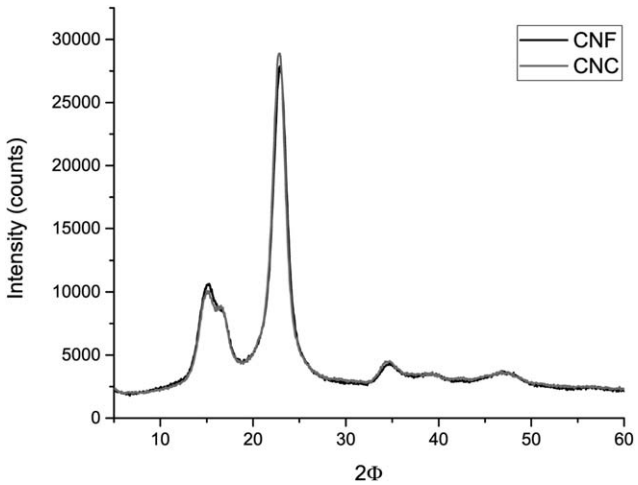

Figure 2. XRD patterns of CNF and CNC.

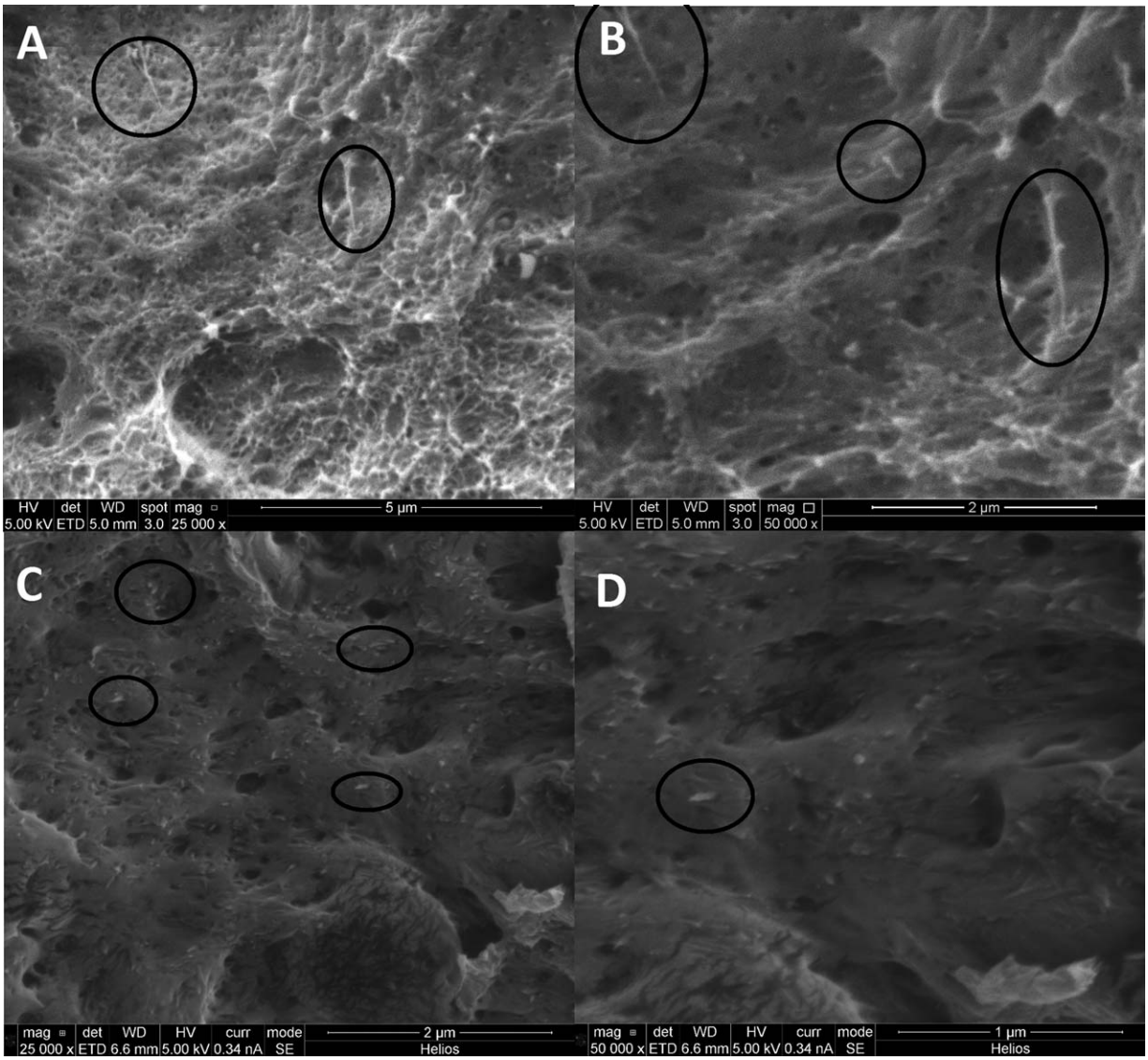

Figure 3. Cross section of PLA/CNF nanocomposites (up) and PLA/CNC nanocomposites (down).

is already a strong treatment that it has already degraded the amorphous domains of the cellulose. Actually, due to those aggressive treatments, it was decided to perform the acid hydrolysis of the CNC at milder conditions to avoid a too high degradation of the cellulose.

Nanocomposite Preparation

For the film making process a critical point was the choice of solvents. The C30B-based nanocomposites were made using DCM as solvent; the reason is that C30B is a hydrophobic clay so it has more affinity with hydrophobic solvents, and there are many reports on using DCM to disperse the C30B in the literature.

For nanocellulose-based nanocomposites it was found that it was not possible to achieve a good dispersion of CNF using DCM, so another solvent was required in order to make a fair comparison between clay and nanocellulose (good dispersion vs. good dispersion). After comparing different solvents (DCM, acetone/DCM, THF, DMF, DMAc, and NMP) it was found that the DMF (dimethylformamide) was the most suitable solvent although the DMAc was showing well dispersed composites too.

Nanocomposite Dispersion Study

In Figure 3 the SEM images of PLA/CNF and PLA/CNC nanocomposites are shown, where no large aggregates within the matrix can be observed for any of the nanocellulose entities. Furthermore, in Figure 3, some individualized CNF and CNC can be observed, proving that we have successfully dispersed the CNF within the matrix. In general, not very clear differences could be observed between CNF and CNC although the CNF is partially acetylated. The authors attribute this effect to the fact that the DMF is a very good solvent for the nanocellulose, (both nanofillers showed a stable dispersion at 1% on DMF), so, the compatibilizing effect of the acetate groups is negligible in this case.

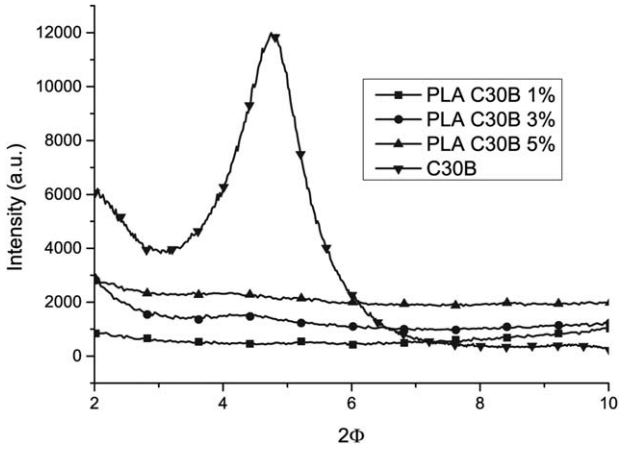

Figure 4. XRD pattern of PLA C30B based nanocomposites.

From the XRD pattern (Figure 4) it can be observed that the peak of neat C30B at ($2\phi = 4.8$), which correspond to the *d*-spacing of the clay, almost disappears in the nanocomposites, especially at 1% load. The absence of a peak means that there is not a constant distance between clay platelets, suggesting that there aren't large aggregates of clay, hence suggesting that there is a good dispersion of clay within the matrix. Moreover, from the TEM images (some representative images could be found on Figure 5) it can be seen that the clay is well dispersed with no evidence of large aggregates.

Crystallinity

Polymer crystallinity is reported to play an important role in determining mechanical and barrier properties.[31,32] Thus, describing the degree of crystallinity of the nanocomposites is critical in terms of extracting conclusions about nanocomposite properties.

All of the nanocomposites showed higher degrees of crystallinity than neat PLA and no significant changes were observed in T_g or T_m. None of the films showed crystallization peaks during the cooling and the heating/cooling/heating procedure. In Figure 6, the degree of crystallinity of the composites is shown and as can be seen that all of the nanocomposites—except

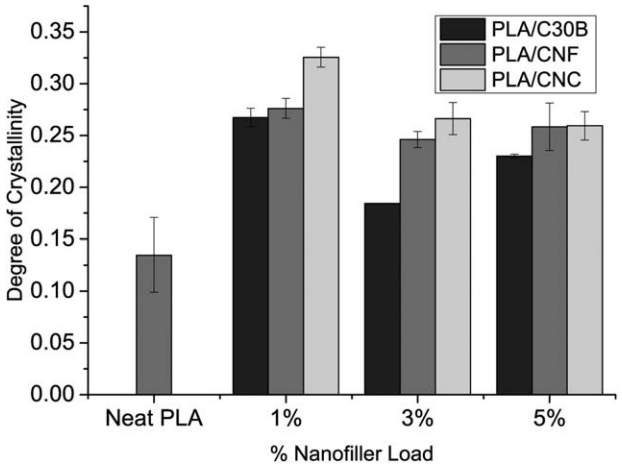

Figure 6. Degree of crystallinity of the nanocomposites (from the 1st heating cycle).

PLA/C30B 3%—have a similar degree of crystallinity, making the nanocomposites at those loads very suitable for comparison.

As previously explained, the slow crystallization time of PLA is a drawback for the industrial application of this polymer, so the addition of fillers that could enhance the crystallization rate would be an important improvement. The nanoclay, the cellulose nanofibers, and nanocrystals[18,33] have been reported to be nucleating agents for PLA thus influencing the crystallization kinetics. To compare the nucleating agent behaviour, the isothermal crystallization process of PLA and the nanocomposites at 1% load at 120°C was studied. The nanocomposites at 1% load were chosen since they had the best dispersion and therefore should be less influenced by the presence of aggregates.

As can be seen in Figure 7, all of the nanocomposites show an endothermic peak shifted to shorter crystallization time. In the case of CNF and CNC, it seems that they show similar crystallization behavior, and slower crystallization kinetics than when using the C30B as an additive. Finally, all of the nanocomposites and the neat PLA reached approximately the same degree

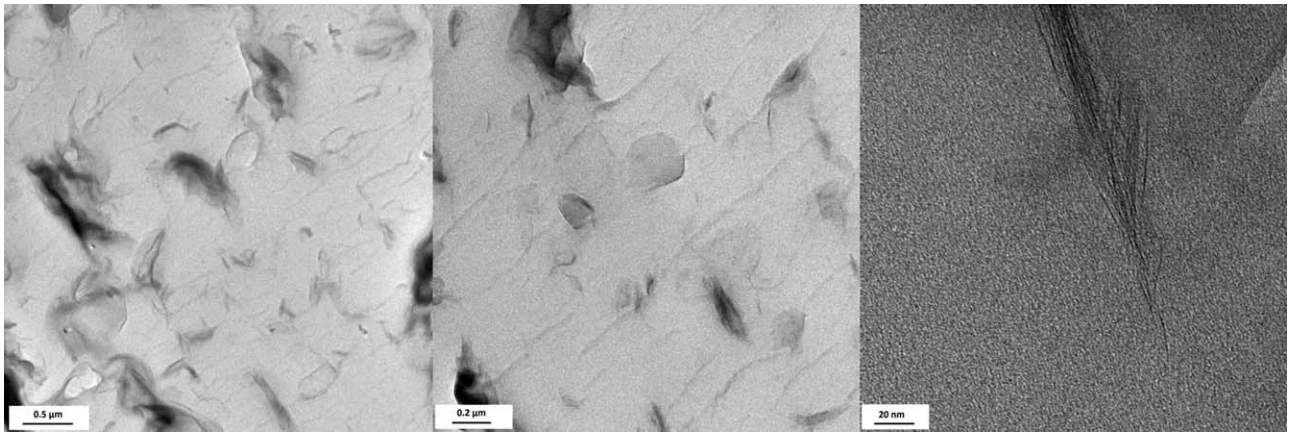

Figure 5. TEM of PLA/C30B 5% Nanocomposite.

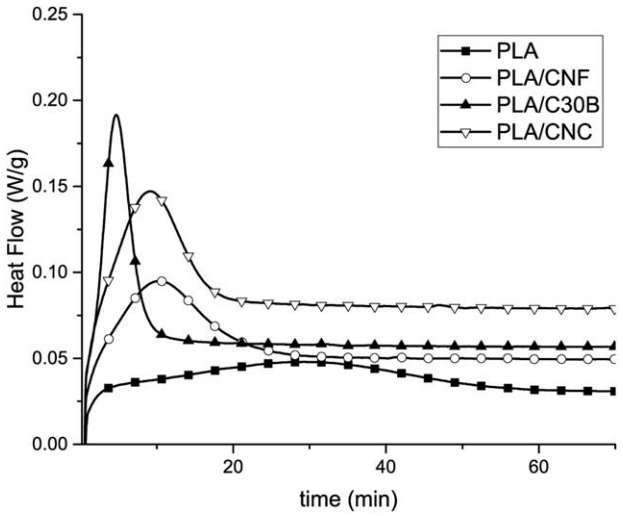

Figure 7. Isothermal crystallization of the nanocomposites at 120°C.

of crystallinity after the isothermal crystallization process (between 35 and 38%).

The results for the clay as nucleating agent is due to the clay platelets—if well dispersed—having much better aspect ratio than nanocellulose-based entities. While the nanocelluose obtained with this method is around 20 nm diameter and 550 nm length, the platelets montmorionite are around 400 nm × 300 nm and few nanometers of thickness if well dispersed, so providing more nucleating sites thus leading to faster crystallization.

The crystallinity is a very complex phenomenon and although it has been classically studied by DSC, this technique does not give all the relevant information. For that reason, polarized optical microscopy (POM) was applied to obtain more information about the spherulite size and distribution.

Briefly, it was found that while PLA and PLA/C30B composites showed a crystalline morphology where was difficult to distinguish the spherulites, the PLA/CNF and PLA/CNC showed a crystalline morphology where the spherulites could be clearly distinguished. Furthermore, the polarized optical micrographs of the samples after isothermal crystallization procedure at 100°C can be found on the Supporting Information. A further study underway to elucidate the influence of the crystalline morphology on the mass transport properties of the film is going to be subject of incoming publications.

Optical Properties

The optical properties of the nanocomposites have not been as widely studied although they are relevant in the case of the food packaging applications. For many applications the industry requires transparent and colorless films. An opaque film will not allow the customer to see the food, making it less likely that the consumer will buy it and a yellow film can give food an artificial color.

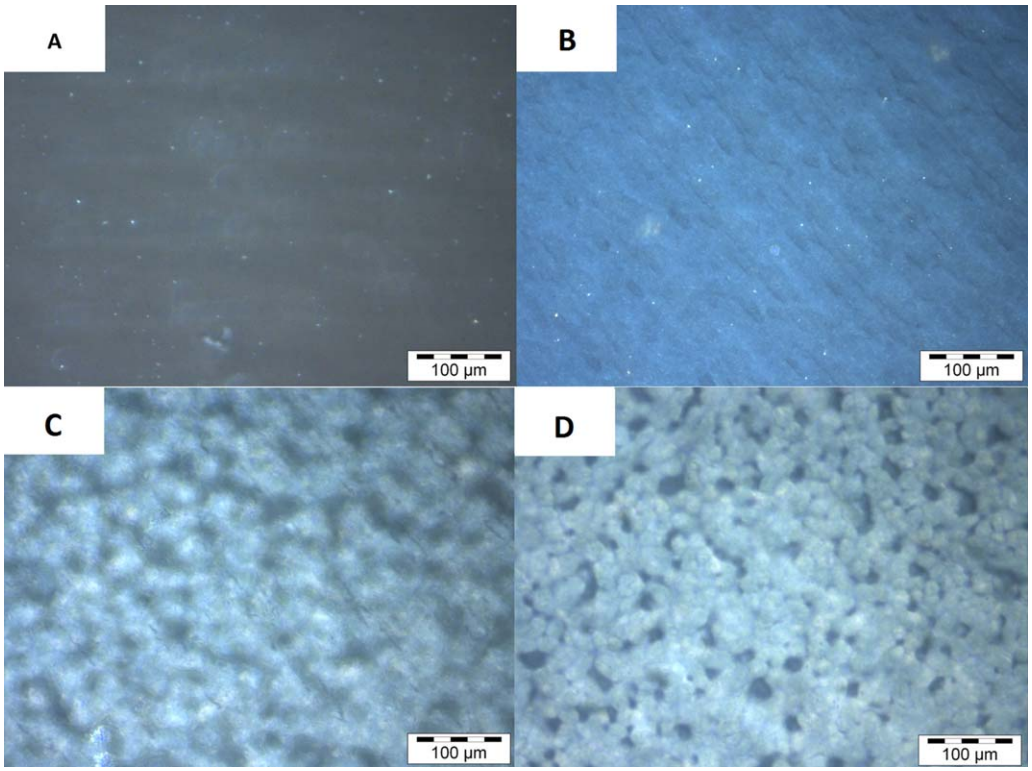

Figure 8. POM of the (A) PLA, (B) PLA/C30B 1%, (C) PLA/CNF 1%, and (D) PLA/CNC 1% films after solvent casting. [Color figure can be viewed in the online issue, which is available at wileyonlinelibrary.com.]

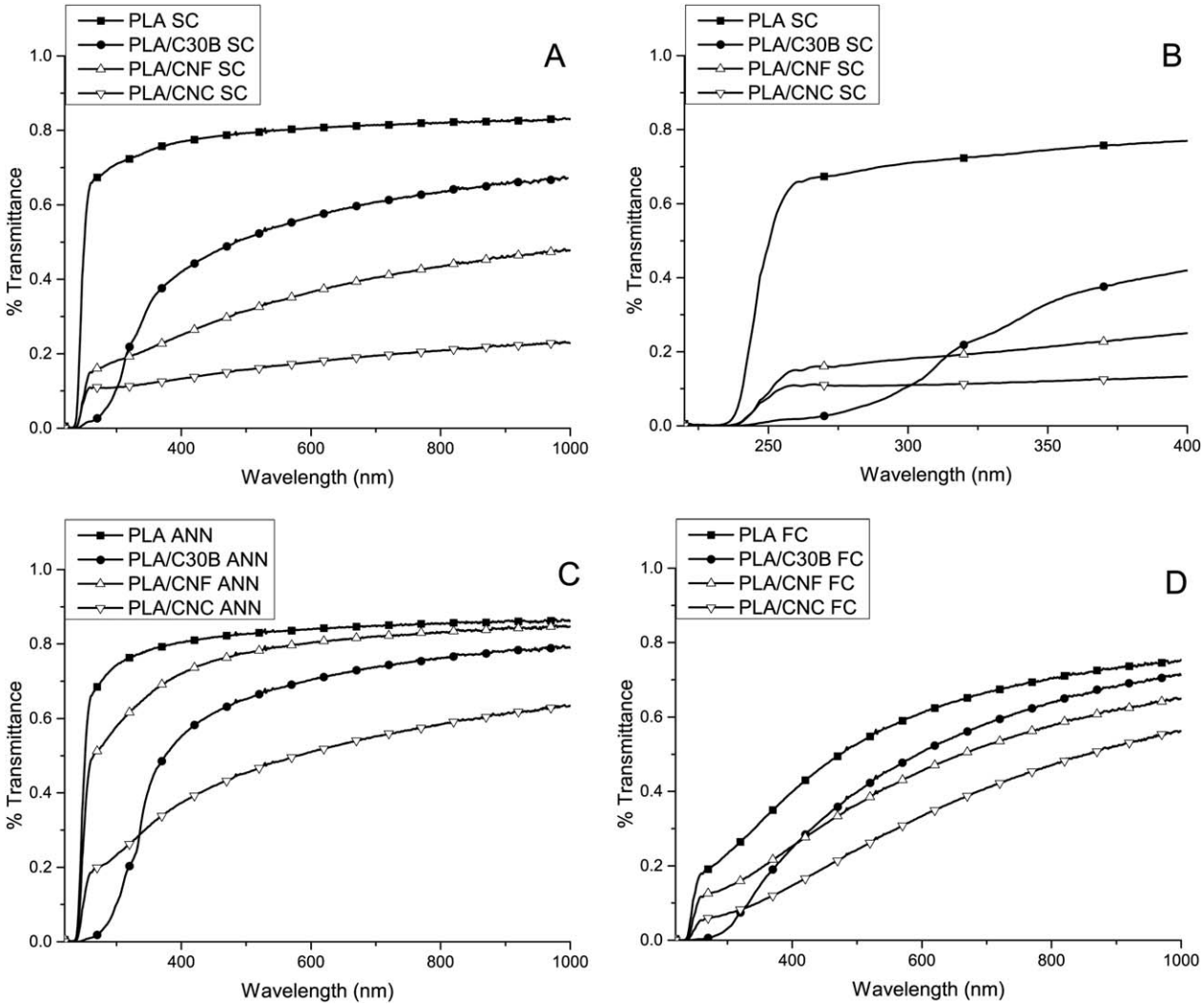

Figure 9. Transmittance of the nanocomposites at 1% filler after solvent casting (A) and (B), after annealing (C) and after isothermal crystallization (D).

As shown in Figure 8 the composites prepared by solvent casting (SC) showed a different crystalline morphology. To eliminate the differences the films prepared by solvent casting were hot pressed for 5 min at 170°C followed by a fast cooling in order to achieve essentially amorphous nanocomposites (AM). After that the annealed nanocomposites were placed into an oven at 120°C for 2 h in order to obtain fully crystallized nanocomposites (FC).

The UV–vis spectroscopy of the samples can be found in Figure 9. All of the samples showed a standard deviation below 10% on absorbance.

From the data it can be seen that the nanocomposites made by solvent casting show reduced transparency compared to the neat PLA film [Figure 9(A,B)]. However, after annealing and isothermal crystallization processes [Figure 9(C,D)] the difference is smaller; probably due to the fact that while after solvent casting procedure (SC) there is a large difference between PLA and nanocomposites in terms of degree of crystallinity (Figure 6); this difference is negligible for annealed (AM) or fully crystallized composites (FC). So, it can be concluded that the addition of small amounts of C30B or CNF doesn't affect significantly the optical properties of the films.

From Figure 9(B) it can be seen how C30B shows a UV blocking capability, which can be desirable in some food packaging applications.[34]

Finally, there is a big difference between annealed [Figure 9(C)] and fully crystallized composites [Figure 9(D)] being the annealed composites more transparent than the fully crystallized ones. This is due to differences in refractive indexes between crystalline and amorphous domains. This difference can be mainly seen on the range of 220–500 nm. The fact that PLA/CNF SC and PLA/CNC SC composites (big spherulite size) show a similar behavior than the fully crystallized composites (big spherulite too), while PLA SC and PLA/C30B SC (small spherulites) show a similar behavior to the quenched composites (no spherulites), suggest that spherulite size has a slight influence on the optical properties of the nanocomposites.

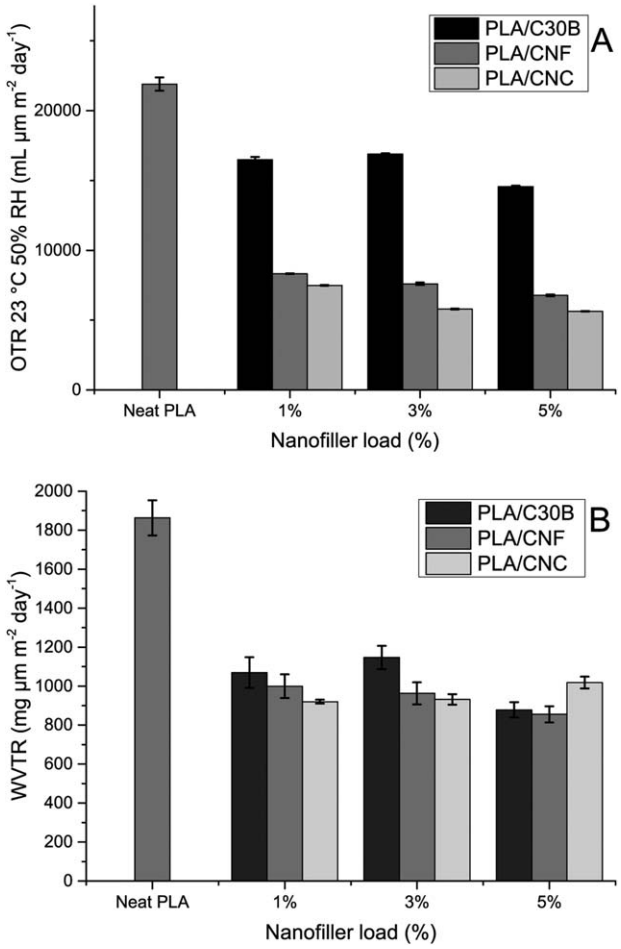

Figure 10. OTR and WVTR of PLA and nanocomposites at 23°C and 50% or RH.

Barrier Properties

Generally the permeability results for PLA and PLA/C30B-based nanocomposites were comparable to those found in the literature either for WVTR[35] or for OTR.[30,34] For PLA/CNF-based nanocomposites there are, to the knowledge of the authors, no other publication using those particular partially acetylated CNF describing barrier properties, but, in the case of CNC, as explained in the introduction, various values for oxygen and water barrier properties can be found in the literature.

In Figure 10, the OTR and WVTR of the neat PLA and its nanocomposites at 23°C and 50% RH can be seen. The results of the OTR at 23 and 0% RH can be found in the Supporting Information.

As can be clearly observed in Figure 10(A) all of the nanocomposites showed better barrier properties than the neat PLA, which could be attributed partially to the fact that the composites showed higher degree of crystallinity than the neat PLA. Surprisingly, nanocellulose-based composites showed lower oxygen transmission rate than nanoclay-based composites. Figure 10(B) also show a great reduction in the WVTR of composites, but, in this case it can be seen that all three nanofillers showed similar behavior, meaning that nanoclay has better performance reducing the WVTR than OTR while CNF has better performance reducing the OTR rather than WVTR. This is probably due to the fact that the clay is likely more hydrophobic than nanocellulose. Finally, In general it can be seen that the addition of nanofillers to PLA matrix is a very promising way to enhance the barrier properties.

The reason of the improvement on the barrier properties could be partially due to the increased crystallinity of the nanocomposites due to the nucleating agent behavior, while the difference between CNF and C30B could be partially due to the different crystalline morphology. A further study underway to elucidate the influence of the nanofillers and crystalline morphology on the mass transport properties of the composites is going to be subject of incoming publications.

Mechanical Properties

The mechanical properties are critical for food packaging applications, since the packaging has to protect the food from damage during the whole supply chain. Although the Young modulus and stress at break of PLA are adequate for food packaging the neat PLA is still too brittle for some food packaging applications, although a range of novel formulations of PLA are now available. Mechanical tests were performed for PLA and its nanocomposites to check the effect of each of the nanofillers on the mechanical properties. The results can be seen in Supporting Information Table I-SI and the values for PLA were in the range of other reports.[15,36] In this work we have found that although the addition of nanofiller did not affect dramatically the mechanical properties of the nanocomposites; PLA/CNF composites showed a slightly better performance than the other nanofillers. The PLA/CNF 1% nanocomposite showed around a 10% of improvement in terms of elongation and stress at break while a 5% loss on Young modulus. Although the mechanical properties, despite the brittleness, of PLA, the low thermomechanical stability keeps the thermoforming of PLA a challenge for the industry. Moreover, there are some food applications that require higher thermal stability of PLA such as disposable glasses for hot drinks. The thermomechanical resistance was investigated by DMA as shown in Figure 11.

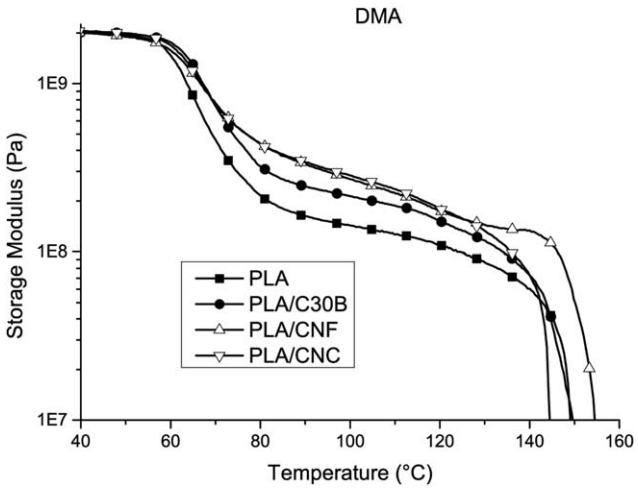

Figure 11. DMA of the nanocomposites.

As can be seen in Figure 11, there is a clear improvement in the thermomechanical properties of PLA and the nanocomposites when surpassing the T_g of PLA. After this point, the mechanical properties of the neat PLA decreases very rapidly whereas the nanocomposites offer greater resistance; this being more pronounced for CNF reinforced composites than for C30B reinforced ones. We ascribed this to the fact that nanocellulose can make stronger percolated networks while the reinforcement of the clay—due to stress transfer mechanism—is not as effective. There is little difference between the effect of CNF and CNC probably due to the fact that CNF is expected to be better dispersed; CNC can form stronger percolated networks due to stronger hydrogen bonding interaction between fillers. Finally, to the understanding of the authors the differences in crystallinity can be neglected in this case since all of the samples were preheated for 20 min at 110°C.

CONCLUSIONS

The performance of a partially acetylated novel CNF as filler for PLA for food packaging applications was compared with the neat PLA and other nanofillers such as clay (C30B) and nanocrystalline cellulose (CNC). It was found that the addition of only a 1% of CNF lead to significant improvements on the performance of PLA for food packaging (a 64% of decrease on oxygen transmission rate, a 46% of decrease on water vapor transmission rate and significant improvement in thermomechanical properties and crystallization kinetic, without a significant influence on the transparency of the films), although part of this improvement could be due to the increased crystallinity present in the nanofillers due to the nucleating agent affect. Comparing CNF with C30B as reinforcing agent, it can be seen how nanocellulose, apart from being biodegradable while clay it is not, has a much better performance than the clay as oxygen barrier, a slightly better performance in thermomechanical and water barrier properties, making this nanofiller a promising candidate for food packaging applications.

ACKNOWLEDGMENTS

The author is thankful to the FP7 - People - 2011, ITN Marie Curie International Training Network (ITN) for the financial support and to COST Action FP1003. The authors wanted to acknowledge Lars Schulte for making the electron microscopies, and Francis Clegg and Christopher Breen for the XRD analysis. This article is on memoriam of Professor Iñaki Mondragon Egaña whose dedication for the science is inspiration for us. LGP2 is part of the LabEx Tec 21 (Investissements d'Avenir - grant agreement n°ANR-11-LABX-0030) and of the Énergies du Futur and PolyNat Carnot Institutes (Investissements d'Avenir - grant agreements n°ANR-11-CARN-007-01 and ANR-11-CARN-030-01).

REFERENCES

1. Available at: http://www.foodproductiondaily.com/Packaging/PLA-bioplastics-production-could-hit-1m-tonnes-by-2020-nova-Institut (Accessed August 2015).
2. Available at: http://www.marketsandmarkets.com/Market-Reports/polylacticacid-387.html (Accessed August 2015).
3. Madhavan Nampoothiri, K.; Nair, N. R.; John, R. P. *Bioresour. Technol.* **2010**, *101*, 8493.
4. Rasal, R. M.; Janorkar, A. V.; Hirt, D. E. *Prog. Polym. Sci.* **2010**, *35*, 338.
5. Bogoeva-Gaceva, G.; Avella, M.; Malinconico, M.; Buzarovska, A.; Grozdanov, A.; Gentile, G.; Errico, M. E. *Polym. Compos.* **2007**, *28*, 98.
6. Najafi, N.; Heuzey, M. C.; Carreau, P. J. *Polym. Eng. Sci.* **2013**, *53*, 1053.
7. Abdul Khalil, H. P. S.; Bhat, A. H.; Ireana Yusra, A. F. *Carbohydr. Polym.* **2012**, *87*, 963.
8. Chinh, N. T.; Trang, N. T. T.; Thanh, D. T. M.; Hang, T. T. X.; Giang, N. V.; Quan, P. M.; Dung, N. T.; Hoang, T. *J. Appl. Polym. Sci.* **2015**, *132*, 41690.
9. Fundador, N. G. V.; Iwata, T. *Polym. Degrad. Stab.* **2013**, *98*, 2482.
10. Kasuga, T.; Maeda, H.; Kato, K.; Nogami, M.; Hata, K.; Ueda, M. *Biomaterials* **2003**, *24*, 3247.
11. Le Bras, D.; Stromme, M.; Mihranyan, A. *J. Phys. Chem. B* **2015**, *119*, 5911.
12. Mihranyan, A.; Edsman, K.; Strømme, M. *Food Hydrocolloids* **2007**, *21*, 267.
13. Eichhorn, S. J.; Dufresne, A.; Aranguren, M.; Marcovich, N. E.; Capadona, J. R.; Rowan, S. J.; Weder, C.; Thielemans, W.; Roman, M.; Renneckar, S.; Gindl, W.; Veigel, S.; Keckes, J.; Yano, H.; Abe, K.; Nogi, M.; Nakagaito, A. N.; Mangalam, A.; Simonsen, J.; Benight, A. S.; Bismarck, A.; Berglund, L. A.; Peijs, T. *J. Mater. Sci.* **2009**, *45*, 1.
14. Siqueira, G.; Bras, J.; Dufresne, A. *Biomacromolecules* **2009**, *10*, 425.
15. Kowalczyk, M.; Piorkowska, E.; Kulpinski, P.; Pracella, M. *Compos. A Appl. Sci. Manufact.* **2011**, *42*, 1509.
16. Fortunati, E.; Peltzer, M.; Armentano, I.; Torre, L.; Jimenez, A.; Kenny, J. M. *Carbohydr. Polym.* **2012**, *90*, 948.
17. Sanchez-Garcia, M. D.; Lagaron, J. M. *Cellulose* **2010**, *17*, 987.
18. Pei, A.; Zhou, Q.; Berglund, L. A. *Compos. Sci. Technol.* **2010**, *70*, 815.
19. Espino-Pérez, E.; Bras, J.; Ducruet, V.; Guinault, A.; Dufresne, A.; Domenek, S. *Eur. Polym. J.* **2013**, *49*, 3144.
20. Kose, R.; Kondo, T. *J. Appl. Polym. Sci.* **2013**, *128*, 1200.
21. Fortunati, E.; Armentano, I.; Zhou, Q.; Iannoni, A.; Saino, E.; Visai, L.; Berglund, L. A.; Kenny, J. M. *Carbohydr. Polym.* **2012**, *87*, 1596.
22. Siqueira, G.; Bras, J.; Dufresne, A. *Langmuir* **2010**, *26*, 402.
23. Trifol, J.; Plackett, D.; Sillard, C.; Bras, J.; Hassager, O.; Daugaard, A.; Szabo, P. TAPPI Nano, Vancouver, **2014**.
24. Leszczyńska, A.; Njuguna, J.; Pielichowski, K.; Banerjee, J. R. *Thermochim. Acta* **2007**, *453*, 75.
25. Zaharia, A.; Sarbu, A.; Radu, A. L.; Jankova, K.; Daugaard, A.; Hvilsted, S.; Perrin, F. X.; Teodorescu, M.;

Munteanu, C.; Fruth-Oprisan, V. *Appl. Clay Sci.* **2015**, *103*, 46.

26. Mohapatra, A. K.; Mohanty, S.; Nayak, S. K. *J. Thermoplast. Compos. Mater.* **2013**, *27*, 699.
27. Zaidi, L.; Bruzaud, S. P.; Bourmaud, A.; Médéric, P.; Kaci, M.; Grohens, Y. *J. Appl. Polym. Sci.* **2009**.
28. Duan, Z.; Thomas, N. L.; Huang, W. *J. Membr. Sci.* **2013**, *445*, 112.
29. Oh, S. B.; Kim, Y. J.; Kim, J. H. *J. Appl. Polym. Sci.* **2006**, *99*, 869.
30. Najafi, N.; Heuzey, M. C.; Carreau, P. J. *Compos. Sci. Technol.* **2012**, *72*, 608.
31. Suryanegara, L.; Nakagaito, A. N.; Yano, H. *Compos. Sci. Technol.* **2009**, *69*, 1187.
32. Picard, E.; Espuche, E.; Fulchiron, R. *Appl. Clay Sci.* **2011**, *53*, 58.
33. Frone, A. N.; Berlioz, S.; Chailan, J. F.; Panaitescu, D. M. *Carbohydr. Polym.* **2013**, *91*, 377.
34. Sanchez-Garcia, M. D.; Lagaron, J. M. *J. Appl. Polym. Sci.* **2010**, *118*, 188.
35. Żenkiewicz, M.; Richert, J. *Polym. Test.* **2008**, *27*, 835.
36. Courgneau, C.; Domenek, S.; Guinault, A.; Avérous, L.; Ducruet, V. *J. Polym. Environ.* **2011**, *19*, 362.

APPENDIX 4: Hybrid poly (lactic acid)/nanocellulose/nanoclay composites with synergistically enhanced barrier properties and improved thermomechanical resistance.

Trifol, J., Plackett, D., Sillard, C., Szabo, P., Bras, J., Daugaard, A.E., Hybrid poly (lactic acid)/nanocellulose/nanoclay composites with synergistically enhanced barrier properties and improved thermomechanical resistance. *Polymer International 2016.* doi:10.1002/pi.5154

Hybrid poly(lactic acid)/nanocellulose/nanoclay composites with synergistically enhanced barrier properties and improved thermomechanical resistance

Jon Trifol[a], David Plackett[b], Cecile Sillard[c], Peter Szabo[a], Julien Bras[c], Anders E. Daugaard[a]

[a] *Danish Polymer Centre, Department of Chemical and Biochemical Engineering, Technical University of Denmark, Søltofts Plads, Building 229, DK – 2800, Kgs. Lyngby, Denmark*

[b] *Faculty of Pharmaceutical Sciences, University of British Columbia, 2405 Wesbrook Mall, Vancouver, BC V6T 1Z3, Canada*

[c] *LGP2/Grenoble INP-Pagora/CNRS, 461 rue de la papeterie, Domaine universitaire, C10065, 38402 Saint Martin d'Hères Cedex, France*

Keywords:

Cellulose nanofibres (CNF), nanoclay, polylactic acid (PLA), nanocomposites, barrier properties, thermomechanical properties

Abstract:

Poly(lactic acid) (PLA)-based hybrid nanocomposites (PLA, nanoclay and nanocellulose) were prepared by reinforcing neat PLA with commercially available nanoclay (Cloisite C30B) and nanocellulose, in the form of either partially acetylated cellulose nanofibres (CNF) or nanocrystalline cellulose (CNC). Composites with 1 or 5 wt% of nanocellulose, in combination with 1, 3 and 5 wt% of nanoclay, were prepared, and their barrier properties were investigated. It was found that the combination of clay and nanocellulose clearly results in synergistic behaviour in terms of the oxygen transmission rate (OTR) through a reduction of up to 90% in OTR and a further reduction in the water vapour transmission rate (WVTR) of up to 76%. In addition, the nanocomposite films showed improved thermomechanical resistance and improved crystallisation kinetics while maintaining high film transparency. This makes hybrid PLA/CNF/C30B nanocomposites a very promising material for food packaging applications.

This article has been accepted for publication and undergone full peer review but has not been through the copyediting, typesetting, pagination and proofreading process, which may lead to differences between this version and the Version of Record. Please cite this article as doi: 10.1002/pi.5154

Introduction

There is a constant interest in finding bio-based materials for food packaging, in order to substitute currently used petrochemical-based polymers such as polyethylene (PE), polypropylene (PP) and poly(ethylene terephthalate) (PET). However, biopolymers are generally considered to have poorer performance than classical petroleum-based polymers. In the specific case of PLA, its brittleness, slow crystallisation rate, poor thermostability and only moderate oxygen and water vapour barrier properties have prevented its use as a packaging material[1]. Accordingly, many different strategies have been investigated to enhance the performance of PLA, including its chemical or physical modification[2], blending[3], the use of reinforcing agents such as natural fibres[4], other kinds of natural fillers[5] or nanomaterials[6,7]. Among these options, nanocellulose, in the form of either cellulose nanofibres or nanocrystalline cellulose, has been particularly widely used, both as a single reinforcing agent [8] or as a multilayer structure[9], not only due to good reinforcing properties[10], but also due to their inherent biodegradability, bio-based origins and availability.

In our previous work acetylated cellulose nanofibres (CNFs) were prepared through a combination of alkali and acetylation treatments, while nanocrystalline cellulose (CNC) was prepared by acid hydrolysis[11]. The prepared nanocelluloses were compared with commercially available nanoclay (cloisite-C30B) as fillers for PLA-based nanocomposites for food packaging applications. The CNF based composites had significantly improved thermal stability and decreased oxygen transmission rate (OTR) as well as reduced water vapour transmission rate (WVTR) (up to a 64% decrease in OTR at 23°C and 50% RH and up to a 46% of decrease in WVTR). However, these changes are not sufficient when compared with the properties of PET, which is considered the industrial standard in terms of permeability. Indeed, barrier properties are critical for food packaging applications, since oxygen and water can augment microbiological activity, which in turn will boost food degradation.

PET has an OTR of approximately 3000 – 4200 mL µm m^{-2} day^{-1} at 25°C and different relative humidities[12] and WVTR values of around 420 g µm m^{-2} day^{-1} at 23°C and 85% RH[13], while PLA shows an OTR ranging from 11000 – 36000 mL µm m^{-2} day^{-1} at 23°C[14,15] and a WVTR of 5250 g µm m^{-2} day^{-1} at 23°C and 90% RH[16]. In order for PLA to become an industrial alternative to PET, an even more significant reduction is therefore required.

For the specific case of PLA, the effect of crystallinity on water barrier properties in general, and on water sorption in particular, is still not fully understood, and so many different results can be found in the literature. Some reports, for instance, claim that water absorption decreases in line with increased crystallinity[17], while others report the opposite behaviour[18]. Finally, some papers report different behaviours in water sorption and water diffusion measurements, depending on test conditions[19]. In any case, despite crystallinity effects, it has been proven that improvements in the barrier properties of nanocomposites is related, at least partially, to the nanomaterial[20]. This is known to play an important role in mass transport phenomena by increasing the tortuous path, and thus decreasing diffusivity.

Although PLA nanocellulose composites have exhibited better performance compared to PLA/nanoclay in terms of enhanced barrier and thermomechanical properties, a combination of both nanocellulose and nanoclay within the polymer matrix would be an interesting combination that might enhance the performance of the material even further. Such a combination of nanoclay and nanocellulose fibres was investigated in preparation of thin nanoclay/nanocellulose films. In one case, addition of 20 wt% of vermiculite to a CNF matrix led to a decrease in OTR of 86% at 50% RH and 94% at 80% RH[21], while incorporation of 50 wt% of MNT to a CNF matrix resulted in a five-fold reduction in OTR at 95% RH[22].

The combination of nanoclay and nanocellulose has also been investigated in polymer composites, where poly(vinyl alcohol)/nanocellulose-based composites showed increased thermomechanical properties, reduced strain at break and a decreased oxygen transmission rate above 30% RH (although they also showed increased water absorption) in line with increased clay content[23]. The

replacement of 1 wt% of nanoclay with 1 wt% of CNC in a PLA/montmorillonite composite containing 5 wt% nanoclay led to an eight-fold increase of strain at break for the composites (from 10.6% to 78.8%)[24]. In a similar fashion the addition of CNC to the composite led to enhanced water absorption and different water diffusion, depending on the amount of CNC added[25]. Finally, the combination of CNC and nanoclay led to improved thermomechanical properties for PLA-grafted maleic acid composites[26].

The present work aimed at determining possible synergistic effects as a result of combining nanocellulose and nanoclay in PLA nanocomposites, by focusing on properties that will have to be improved in order for PLA to become an industrially relevant alternative polymer for food packaging.

Experimental

Materials

Polylactic acid (Ingeo 2003D) was supplied by Natureworks (Minnesota, USA). Cellulose nanoreinforcements were extracted from sisal (Agave Sisalana, which was kindly supplied by Expor Sisal S.L) according to a previously described procedure[11]. The nanoclay was Cloisite 30B (C30B), which is commercially available and well described in the literature[27–29]. NaOH, sulfuric acid (95%-97%), nitric acid (ACS reagent, 70%), acetic acid (99%-100%), N, N – dimethyl formamide (98%, ACS reagent) and dichloromethane (99.8% chromasolv) were purchased from Sigma Aldrich, while sodium chlorite (25% w/w on water) was supplied by Merck. All of the reagents were used as received.

Preparation of CNF and CNC

The acetylated cellulose nanofibre (CNF) and nanocrystalline cellulose (CNC) extraction and isolation procedures have been described elsewhere[11], a summary of which can be found in the supporting information. Briefly, this method is based on grafting acetate groups onto the surface of the swollen cellulose nanofibres, in order to inhibit hydrogen bonding, thus allowing for the easy extraction and individualisation of the fibres. The protocol consists of a sequence of chemical treatments (alkali

treatments, bleaching and acetylation) of the sisal fibres followed by preparing for the dispersion of nanofibres (either CNF or CNC) in DMF via magnetic stirring.

Nanocomposite preparation

A neat PLA film and two types of hybrid composites with 1 or 5 wt% of nanocellulose in combination with 1, 3 and 5 wt% of nanoclay (PLA/CNF/C30B and PLA/CNC/C30B) were prepared by mixing three premixes followed by film formation by solvent casting in Teflon moulds. A specially prepared rack ensured the high reproducibility of film thicknesses and uniform films. PLA/C30B, PLA/CNF and PLA/CNC composites were used as reference materials, prepared as described elsewhere[11], and a summary of the preparation procedure is included in the supporting information.

A) Neat PLA reference film

PLA (5 g) was dissolved in dichloromethane (250 mL) by magnetic stirring overnight at room temperature. The mixture was degassed in an ultrasonic bath for 5 minutes, and the PLA solution was then poured slowly into three Teflon moulds, 80 mL in each mould. The three moulds were covered by a 5-13 μm filter paper, kept in a Climacell climatic chamber (MMM Group) at 23°C for 16 hours and thereafter dried at 50°C in a vacuum for at least 24 hours. The prepared PLA films were 75 μm ± 2.3 μm in thickness.

B) PLA/CNF/C30B and PLA/CNC/C30B composite films

The hybrid composites were prepared by mixing a standard solution of PLA (A), a standard dispersion of nanocellulose (for both CNF and CNC) (B) and a standard dispersion of nanoclay (C). Both nanocellulose dispersions in DMF (B) were obtained directly as a result of the preparation procedure as a 0.8 w/v% dispersion. Nanoclay dispersion (C) was achieved by stirring Cloisite C30B (2 g) in DMF (200 mL) for 24 hours, followed by ultrasonication at 200 W for 30 minutes, to obtain a stable dispersion that could be used for preparing the hybrid composites. The PLA standard solution (A) was freshly prepared prior to use by magnetically stirring PLA (3.3 g) in DMF (65 mL) vigorously at 70°C for 2 hours. Dispersions with a specific nanocellulose and nanoclay content were then prepared by mixing premixes A, B and C, all of which were diluted to 105 mL with additional DMF. The

dispersions were stirred vigorously and ultrasonicated at 200 W for 10 minutes and finally cast into a Teflon mould (12 cm x 12 cm). The solvent was then removed by drying at 80°C for 15 hours, which was followed by additional drying *in vacuo* at 50°C for at least 24 hours. Film thicknesses were measured at least nine different points with a digital micrometer (with an absolute error of 1 µm). It was found that all of the composites showed similar thicknesses and that each film had a small standard deviation. These differences in thicknesses between the different films can be attributed to the inherent uncertainty of the solvent casting procedure rather than to the effect of the nanofillers. The hybrid composites PLA/CNF/C30B showed a thickness ranging from 81 to 93 µm with a standard deviation below 3.1 µm, while the PLA/CNC/C30B composites were prepared with a thickness ranging from 86 to 95 µm with a standard deviation below 4.5 µm.

Characterisation methods

The dispersion of nanofillers within the polymer matrix was studied by X-Ray diffraction (XRD) (Philips X'Pert Pro diffraction system utilising a Cu-tube (λ = 1.542 Å), operating at 40 kV and 40 mA, and scanning electron microscopy (SEM) (FEI Quanta 200 ESEM FEG) and transmission electron microscopy (FEI Tecnai T20 G2). The thermal properties (glass transition temperature (T_g), melting temperature (T_m) and degree of crystallinity (X_c)) of neat PLA and the nanocomposites were determined by differential scanning calorimetry (DSC) (TA DSC Q1000), using a heating rate of 10°C/min across a range of 0 – 200°C in a heating/cooling/heating cycle. The melting enthalpy of 100% crystalline poly(L-lactide) was considered to be 93 J g^{-1}, as reported previously[30]. To determine X_c, the following expression was used for both the first and the second heating cycle:

$$Xc = \frac{\Delta H_m - \Delta H_C}{\Delta H_0}$$

where X_c is the degree of crystallinity of the composite, ΔH_m is melting enthalpy, ΔH_c is crystallisation enthalpy and 93 J g^{-1} was considered as the melting enthalpy of 100% crystalline PLA. Isothermal crystallisation studies were performed by heating samples from RT to 200°C at 10°C/min, where they were stabilised for 2 minutes and thereafter cooled down to 0°C at 20°C/min. Next, the

samples were heated at 20°C/min until they reached 120°C and were then kept for 2 hours at that temperature. Finally, the samples were cooled to 0°C at 10°C/min and heated until they reached 200°C at 10°C/min. Optical properties were measured at at least three different points using a UV-Vis spectrometer (Polar Star Omega) in the range of 200 nm – 1000 nm. The oxygen transmission rate (OTR) was measured in triplicate, using a Lyssy OPT-5000 oxygen permeability tester. OTR measurements were performed at 23°C at 0% and 50% of RH, and the results were expressed in mL µm m^{-2} day^{-1}. The water vapour transmission rate (WVTR) of the films was measured in triplicate according to the norm NF H 00-030 at 23°C and 50% RH. Silica gel was used as a desiccating agent, and the cups had a specific exchange surface of S =28.27 cm^2. The mass increase in the cups, due to the water absorption of silica gel, was plotted against time, and the slope was calculated. The WVTR was calculated as shown below, where n is the change in mass per time, l the thickness of the film and S is the area of the investigated surface.

$$WVTR = \frac{n * l}{S}$$

One-way ANOVA analysis for calculation of the statistical significance of the OTR and WVTR data was done in Minitab 17, with statistical significance established at $p<0.05$. Mechanical properties were measured using an Instron Universal Testing Machine Model 4507 (Instron Engineering Corporation, Canton, USA) equipped with pneumatic fixtures of type I BA dumbbell-shaped samples at 2.5 mm min^{-1}. Five specimens 5x1 cm in size were taken from each film. Thermomechanical properties were measured in duplicate, using DMA RSA3 (TA Instruments, USA) equipment working in tensile mode. All of the measurements were performed at a constant frequency (of 1 Hz) and a strain amplitude of 0.05%. The distance between the fixtures was 10 mm. The samples were heated at 10°C /min from room temperature until reaching 110°C, and they were kept for 20 minutes at this temperature. Thereafter, the samples were cooled down to 25°C at 10°C/min and then heated to 180°C at 10°C/min. The analysis was repeated to check for the reproducibility of the measurements.

Results and discussion

The dispersion of nanocellulose and nanoclay in the composites was evaluated by SEM of the cross-sectional views of fractured films as shown in Figure 1.

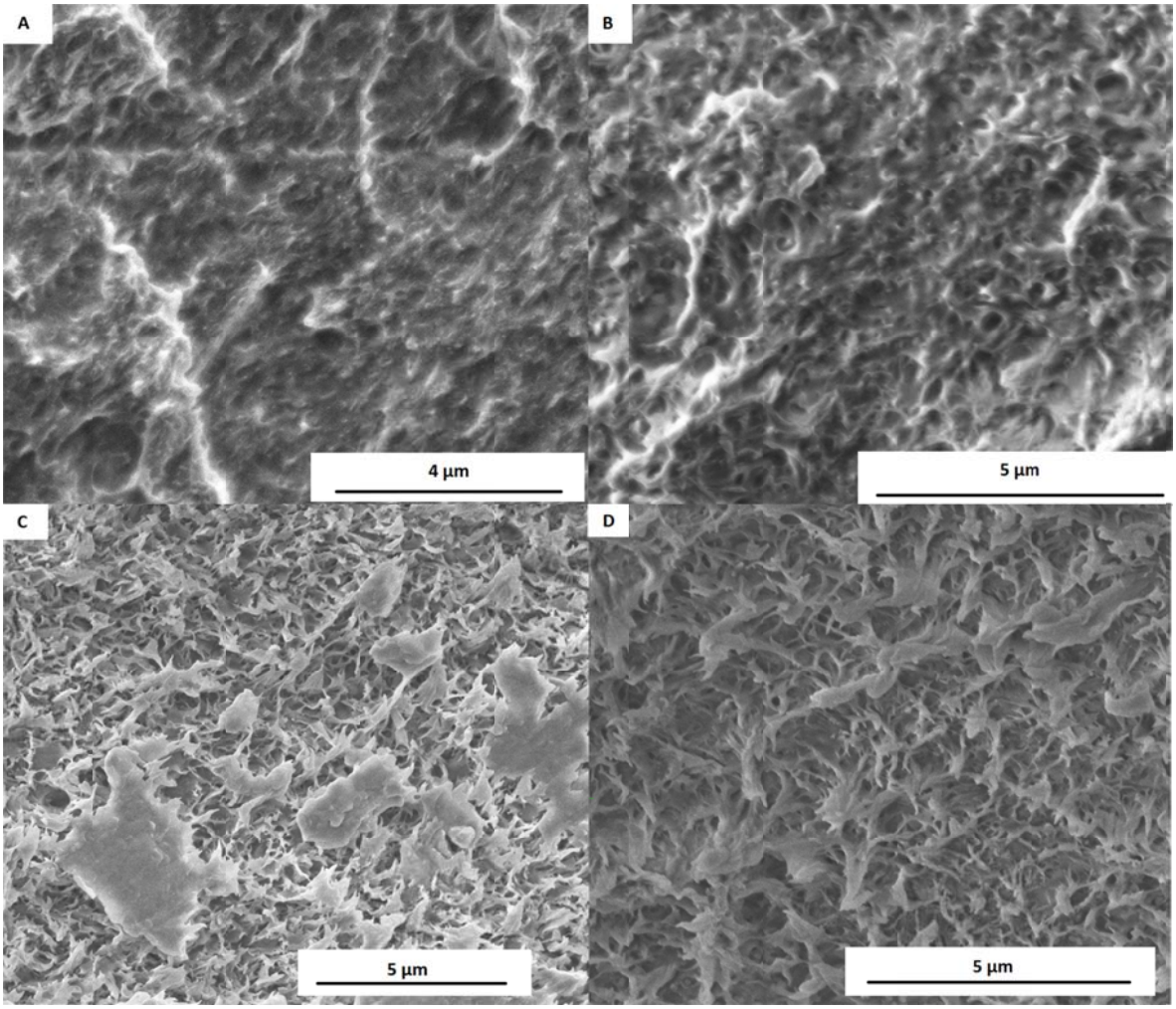

Figure 1. SEM of the cross-section of the fractured nanocomposites. A) PLA/CNF 5 wt%/C30B 1 wt%; B) PLA/CNC 5 wt%/C30B 1 wt%. C) PLA/CNF 1 wt%/C30B 5 wt%; D) PLA/CNC 1 wt%/C30B 5 wt%.

Composites with the highest nanocellulose and the lowest C30B content (5 wt% nanocellulose-1 wt% C30B) were chosen to evaluate the dispersion of nanocellulose, while composites with lowest nanocellulose and highest C30B content (1 wt% nanocellulose-5 wt% C30B) were chosen to evaluate the clay dispersion (SEMs of the cross-sectional views of the composites with 1wt% nanocellulose and 1 wt% C30B can be seen in the supporting information, SI-Figure 1 and SI-Figure 2). The cross-sectional views of the fractured surfaces at high loading of nanocellulose (Figure 1A and 1B) shows homogeneous samples without any large aggregates of nanocellulose, confirming a good dispersion of nanocellulose in the composites. Both composites with a high content of nanoclay (Figure 1C and 1D) show a significantly different fractured interface compared to the composites with a high nanocellulose loading, where the platelet structure of the nanoclays is clearly visible. The nanoclays are not as well dispersed as the nanocellulose, as can be seen from the small aggregates of up to 5 µm in size for the CNF composite, whereas the CNC composite show a more homogeneous fracture surface. Considering the high content of nanoclay in these samples some aggregates would be expected on a fractured surface, as the fracture occurs at the weakest point of the film.

The effective dispersion of the nanoclay at the nanoscale was investigated further by XRD and TEM, as shown in Figure 2.

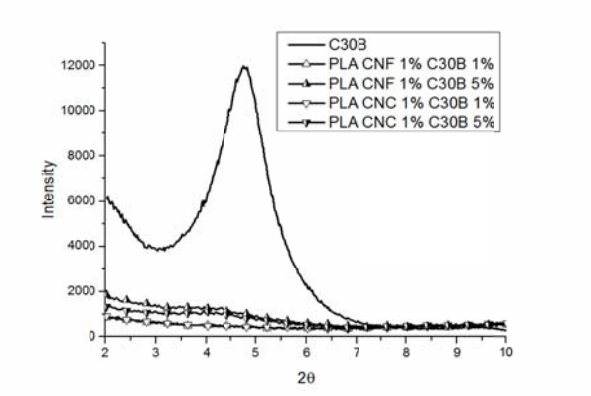

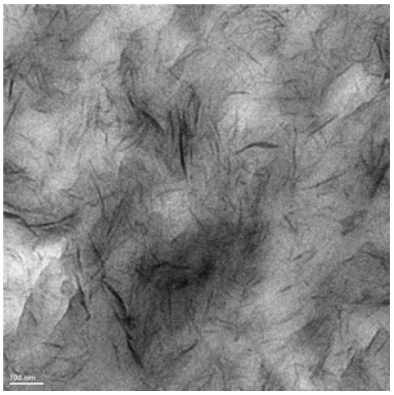

Figure 2. Left: XRD pattern of PLA/CNF/C30B and PLA/CNC/C30B nanocomposites (%wt) and neat C30B. Right: TEM of PLA/CNF 1 wt%/C30B 3 wt%.

As can be seen from the XRD in Figure 2 (left), the neat C30B (powder) exhibits a clear diffraction peak at around 2θ ~ 4.5 - 5°, which corresponds to the d-spacing of the platelets within the clay. This strong diffraction peak from aggregated nanoclay is not observed for the hybrid composites, illustrating that the nanoclay platelets were separated during processing and that the nanoclay in the composites is highly exfoliated at low nanoclay loading. This could also result from dilution, however, the samples at high loading of nanoclay only show a very minor peak as an indication of the presence of small amounts of intercalated nanoclay. This was also seen from TEM of a microtomed composite (Figure 2, right). Here the nanoclay can be seen to be both intercalated (black lines) and exfoliated. In combination with the SEM micrographs from above it shows that the nanofillers are generally well dispersed with few small aggregates. In the current study the target application was food packaging materials, where barrier properties can be of great importance. As mentioned above, an important parameter in barrier properties is the crystallinity of different materials, and therefore all of the samples were evaluated by DSC, as shown in Figure 3.

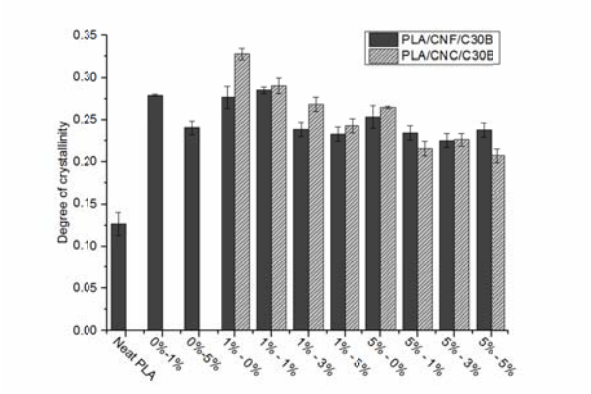

Figure 3. Degree of crystallinity of the hybrid nanocomposites.

It can be seen from Figure 3 that the addition of nanoclay or nanocellulose to the PLA results in a significant increase in crystallinity as expected. The crystallinity of the composites is seen to decrease with a higher loading of nanofiller. However, the crystallinities are considered similar for all

the hybrid composites with above 1wt% nanocellulose and 1 wt% nanoclay. Moreover, no relevant changes in T_g or T_m were observed in any of the composites.

PLA is known to exhibit slow crystallisation behaviour, which is a drawback for certain industrially relevant applications. Hence, the influence of nanofillers as nucleating agents in hybrid nanocomposites on the crystallisation kinetic was investigated. In Figure 4A, plots of heat flow versus time during isothermal crystallisation at 120°C of PLA, PLA/CNF 1%, PLA/C30B 1% and PLA/CNF1% /C30B 1% are shown, while Figure 4B shows the same for PLA, PLA/CNC 1%, PLA/C30B 1% and PLA/CNC 1%/C30B 1%.

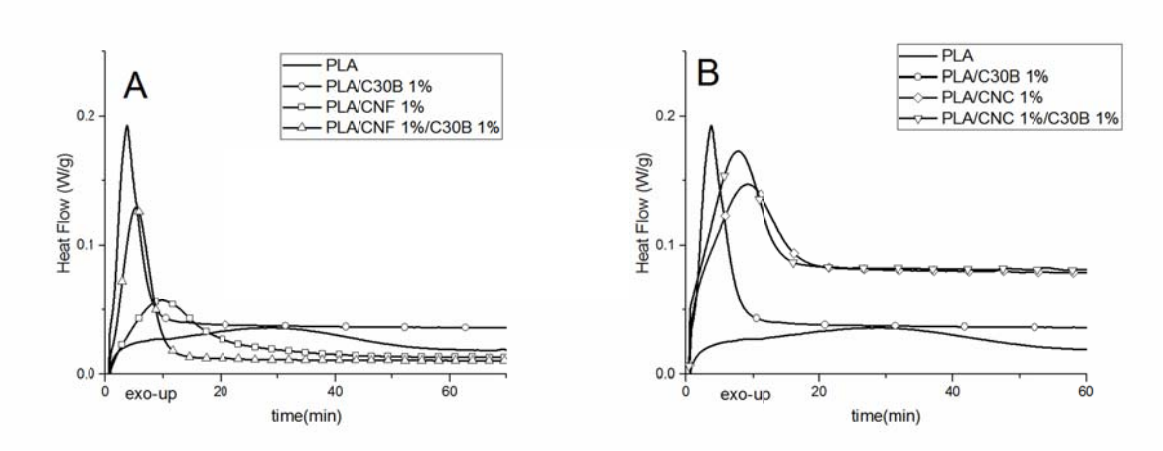

Figure 4. Heat flow versus time for the neat PLA, PLA/C30B 1%, PLA/CNF 1% and PLA/CNF 1%/C30B 1% (A) and PLA, PLA/C30B 1%, PLA/CNC 1% and PLA/CNC 1%/C30B 1% (B), showing the impact on crystallisation kinetics as a result of nanocellulose and nanoclay content (%wt).

It is clearly evident that the exothermic peak – the crystallisation peak – has shifted towards shorter crystallisation times for all of the nanocomposites, indicating that all of the nanofillers have clear nucleating agent behaviour. Nanoclay-based composites (PLA/C30B) have very fast crystallisation times compared to neat PLA, while PLA/CNF or PLA/CNC shows crystallisation behaviour between that and the neat PLA. The CNF hybrid (PLA/CNF/C30B) was found to exhibit intermediate crystallisation behaviour very similar to that of PLA/C30B, while the CNC hybrid (PLA/CNC/C30B)

showed a crystallisation behaviour similar to the CNC/PLA composite. Interestingly, hybrid nanocomposite, even with a low loading such as 1 wt% of CNF and 1 wt% of C30B, shows a significant decrease in half crystallisation time, which is an important parameter when considering the commercial production of PLA-based packaging materials.

The oxygen transmission rate (OTR) and water vapour transmission rate (WVTR) of the nanocomposites at 23°C and 50% RH are shown in Figure 5.

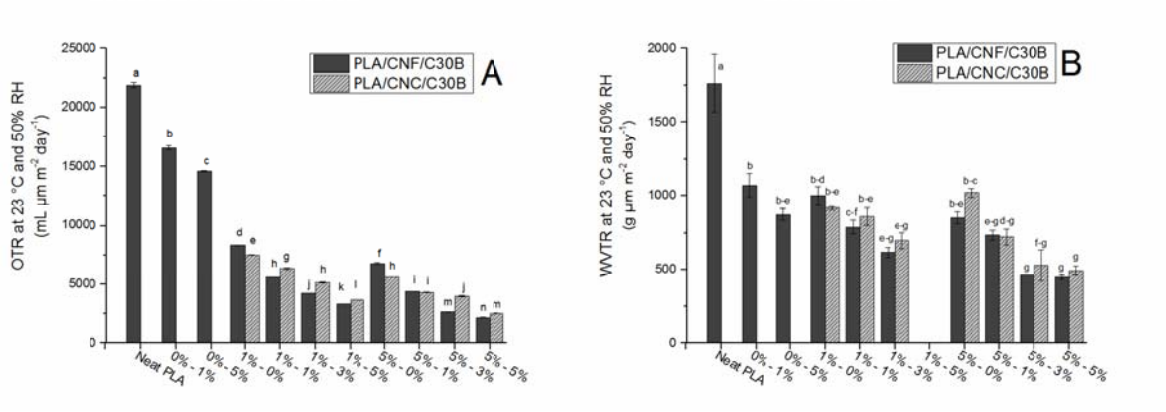

Figure 5. A) OTR and B) WVTR of the hybrid nanocomposites as a result of varied nanoclay and nanocellulose content (samples are shown as wt% nanoclay – wt% nanocellulose). The letters indicate significant difference (one-way ANOVA; $p<0.05$) between the composites.

In Figure 5 it is clear that there is a very significant decrease in the permeability of the nanocomposites compared to neat PLA. The OTR at 50% RH is representative of composites measured at both 0% and 50% RH (similar data for 0% RH can be found in the supporting information). All of the hybrid composites show a statistically different OTR, which was reduced by 74.8% at the lowest loading of 1 wt% nanoclay and 1 wt% nanocellulose. Increasing the content of nanocellulose at 1 wt% nanoclay decreased oxygen permeability by 80.3% at 5 wt% CNF/ 1 wt% C30B compared to PLA, while increasing the nanoclay content to 5 wt% (1 wt% CNF, 5 wt% C30B) resulted in a decrease in OTR of 85.0%, with the highest loading (5 wt% C30B, 5 wt% CNF) ultimately reducing the overall OTR by 90.2% compared to PLA.

Similarly, the WVTR of the composites was also reduced significantly compared to PLA, as shown in Figure 5B. Composites at high C30B and low CNF/CNC loading are very fragile, which unfortunately

made it impossible to measure the WVTR for the 1 wt% C30B and 5 wt% nanocellulose composites. The WVTR was decreased by 57-76% compared to PLA, however, there is not a statistical difference in the WVTR between the different hybrid composites. It is evident that the addition of nanoclay produces a synergistic effect in combination with the nanocellulose, whereby particular nanocomposites with 5 wt% of C30B and 5 wt% of CNF show a reduction of 90% in the OTR and 76% of the WVTR when compared to neat PLA, while already at lower amount of fillers such as 1 wt% C30B and 1 wt% CNF, for instance, the hybrids show a significant reduction of 74% in OTR and 57% in WVTR. This makes hybrid nanocomposites very promising for food packaging applications.

However, such large nanofiller additions, especially of nanoclay, have a significant impact on mechanical properties, as shown in Table 1.

As shown in Table 1, composites with high nanoclay content are highly brittle and show a significant reduction in elongation at break. This effect is directly correlated to nanoclay content in the composites and was also observed for the reference PLA/C30B nanocomposites as well, which were very difficult to handle. Adding nanocellulose to the composites has the effect of reducing their brittleness and enabling the handling of thin films. Especially the low loading of clay was found to provide a good combination of mechanical and barrier properties.

Although the addition of nanoclay reduces mechanical properties at room temperature, there is a significant reinforcement effect at high temperatures, as shown by the dynamic mechanical analysis (DMA) shown in Figure 6.

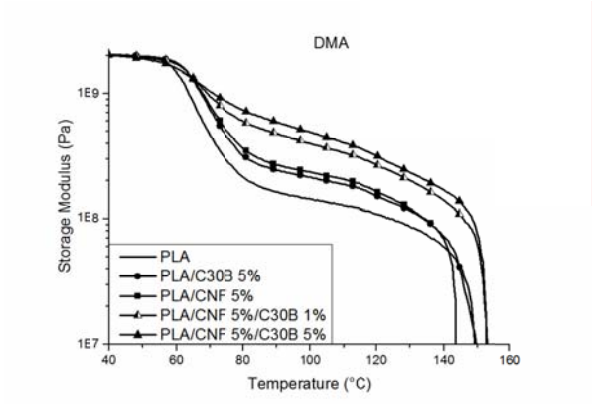

Figure 6. DMA of neat PLA and hybrid nanocomposites (%wt).

It is well known that large surface areas of nanomaterials generally result in improved creep properties at high temperatures. The increased stability of hybrid composite films at higher temperatures is seen clearly for both the C30B and the CNF composites. Hybrid composites exhibit increased thermal stability even at low nanoclay loading, whereas increasing the content of nanoclay even further appears to increase stability only moderately. This again illustrates that the two types of nanomaterials appear to result in a synergistic effect in terms of thermal stability and a reduction in creep at higher temperature. This is expected to be a result of combining a fibrous and a platelet type of nanomaterial, where it is speculated that the nanocellulose creates a strong percolated network, whereas the platelet structure results in maintained integrity across larger areas of the film.

This added thermal stability can also be observed on the actual films after solvent casting from DMF at 80^{o}C, as shown in Figure 7.

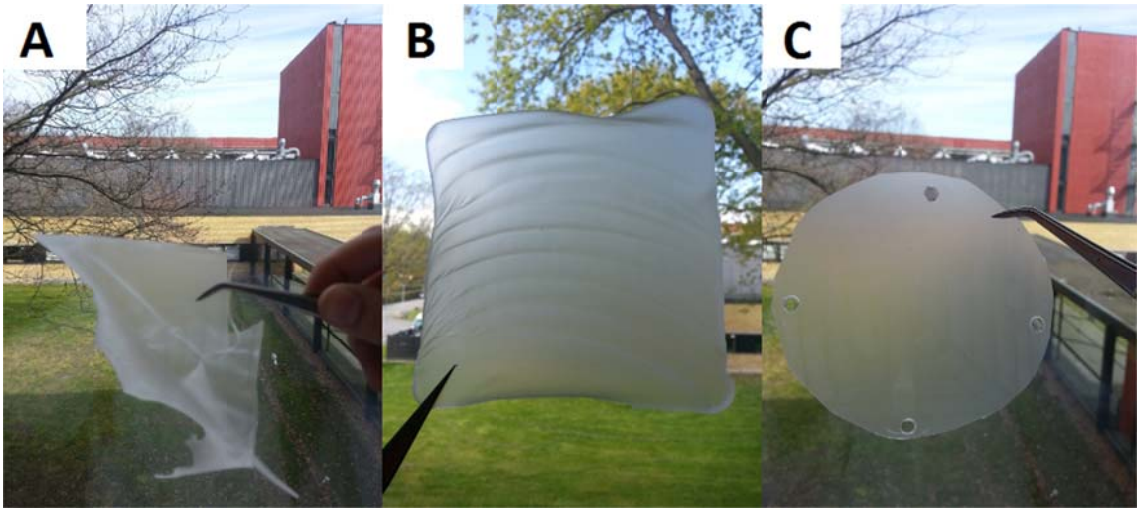

Figure 7. A) PLA, B) PLA/CNF 5% and C) PLA/CNF/C30B 1%-1% films after solvent casting from DMF at 80°C.

Here, it is clear that PLA cannot resist the drying process at higher temperatures. Conversely, the PLA/CNF 5 wt% nanocomposite can maintain film shape, although it is not completely flat. Finally,

the hybrid PLA/CNF1%/C30B1% results in a completely flat film prepared in the exact same conditions, proving the synergy and the reinforcing effect on the nanocomposites.

The transparency of the films can be controlled to some extent by choosing thermal conditions during the crystallisation process. It is well known that solvent casting results in the formation of different crystalline morphologies compared to what would be expected from an industrially relevant processing method such as melt compounding. Low temperature processing, below 100°C, as used in the solvent casting procedure, induces mainly α´ crystalline morphology, while processing at a higher temperature usually leads to an α polymorph[31]. Furthermore, a more significantly amorphous rigid region is also ascribed to lower processing temperatures[32]. The influence of processing conditions on the transmittance of the films was evaluated by UV-vis spectroscopy, as shown in Figure 8.

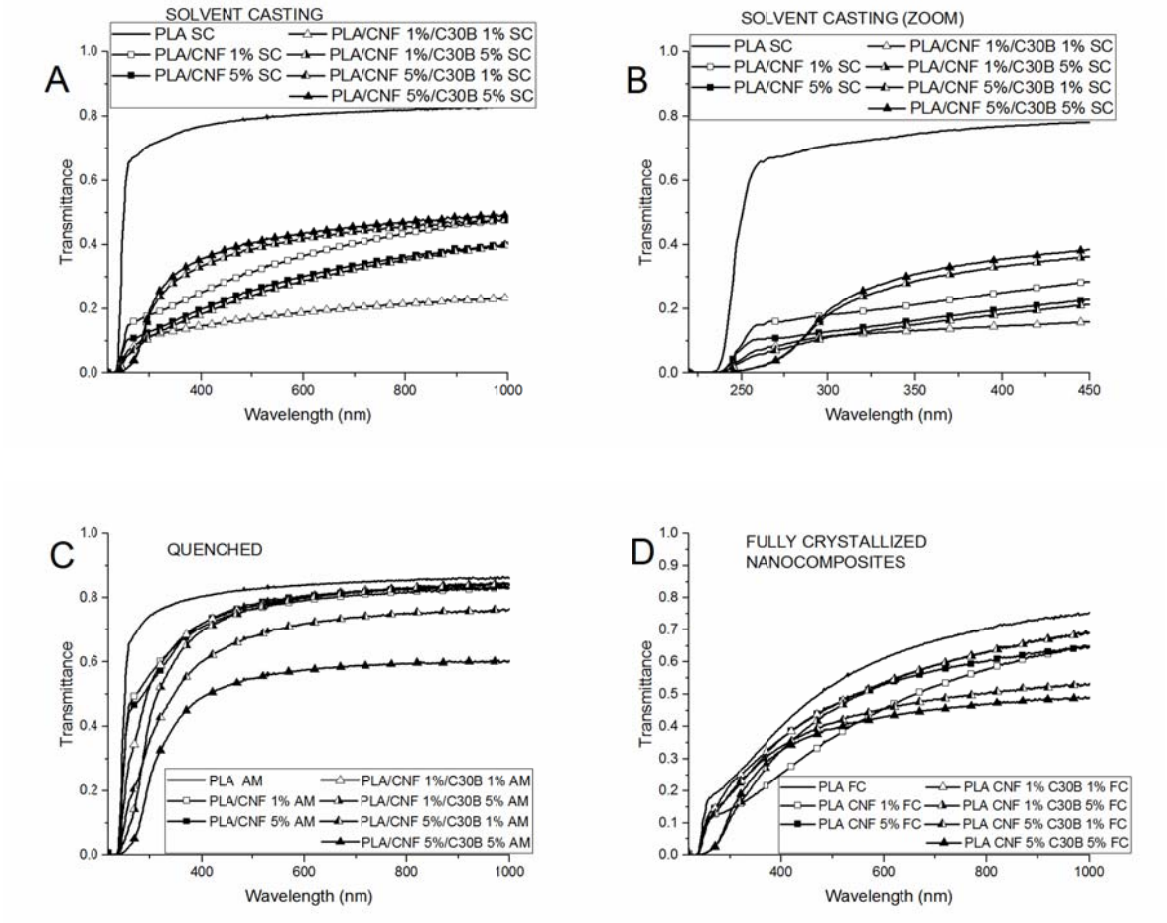

Figure 8. UV-Vis transmittance of the nanocomposites at different crystalline morphologies. A and B showing solvent-cast composites, while C shows the quenched samples having the lowest degree of crystallinity and D the fully crystallised composites.

A quenching procedure, employed to achieve amorphous composites, followed by an isothermal crystallisation procedure at 120°C was performed and evaluated by UV-vis spectroscopy. There was a large difference between the composites prepared by solvent casting and the thermally treated examples. However, in general, it can be seen that most of the nanocomposites have a transmittance similar to the neat PLA when they have similar crystalline morphology. The only exception is nanocomposites with 5 wt% of CNF and 5 wt% of C30B, which showed reduced transparency. Finally, it can be observed that the nanocomposites with 5 wt% of C30B showed significantly reduced transparency in the UV range, which is a desired property for food packaging applications. The thermally treated samples, however, were found to have small defects in the films, thereby preventing further testing for permeability. A deeper evaluation of the effect of crystallinity, amorphous regions and the amount and type of nanofiller on the water vapour barrier properties of the composites with a Quartz Spring Microbalance is currently being investigated.

Conclusion

Novel hybrid composites showing synergistic behaviour, following the combination of PLA, nanocellulose and nanoclay, were prepared. The hybrid materials showed improved properties in terms of crystallisation kinetics, maintained optical transmission as well as improved thermal and mechanical stability. It was established that the hybrid composites have significantly improved barrier properties, where the hybrid containing 5 wt% of C30B and 5 wt% of CNF showed the highest decrease in OTR of 90% and a decrease of 76% in the WVTR. Furthermore, the addition of even small quantities of nanoclay, such as 1 wt% of C30B and 1 wt% of CNF, for example, was seen to lead to a significant decrease of 74% in the OTR and 57% in the WVTR, whilst also maintaining good thermal stability, optical properties and sufficiently good mechanical stability. Hybrid composites were identified as a very promising approach for improving PLA barrier properties and enabling the use of

PLA for food packaging applications. Before such composites can be applied for food packaging it is of course essential to investigate the effects of having nanomaterials in close contact with foods and identify any adverse effects of disposing of such materials.

Acknowledgements

The author is thankful to the FP7 - People - 2011, ITN Marie Curie International Training Network (ITN) for their financial support and to COST Action FP1003 for funding an STSM, to Lars Schulte for the support on the SEM and to Francis Clegg and Christopher Breen for the XRD. LGP2 is part of the LabEx Tec 21 (Investissements d'Avenir - grant agreement n°ANR-11-LABX-0030) and of the Énergies du Futur and PolyNat Carnot Institutes (Investissements d'Avenir - grant agreements n°ANR-11-CARN-007-01 and ANR-11-CARN-030-01).

References

1. Nampoothiri KM, Nair N, John R. An overview of the recent developments in polylactide (PLA) research. *Bioresour Technol* **101:**8493–501 (2010).
2. Rasal RM, Janorkar AV, Hirt DE. Poly(lactic acid) modifications. *Prog Polym Sci* **35**:338–356 (2010).
3. Sengupta R, Chakraborty S, Bandyopadhyay S, et al. A Short Review on Rubber/Clay Nanocomposites With Emphasis on Mechanical Properties. *Engineering* **47**:21–25 (2007).
4. Bogoeva-Gaceva G, Avella M, Malinconico M, et al. Natural fiber eco-composites. *Polym Compos* **28**:98–107 (2007).
5. Li L, Ding S, Zhou C. Preparation and degradation of PLA/Chitosan composite materials. *J Appl Polym Sci* **91**:274–277 (2004).
6. Najafi N, Heuzey MC, Carreau PJ. Polylactide (PLA)-clay nanocomposites prepared by melt compounding in the presence of a chain extender. *Compos Sci Technol* **72**:608–615 (2012).
7. Chen G, Kim H, Park BH, et al. Controlled Functionalization of Multiwalled Carbon Nanotubes with Various Molecular-Weight Poly(L-lactic acid). *J Chem Phys B* **109**:22237–22243 (2005).

8. Iwatake A, Nogi M, Yano H. Cellulose nanofiber-reinforced polylactic acid. *Compos Sci Technol* **68**:2103–2106 (2008).

9. Aulin C, Karabulut E, Tran A, et al. Transparent nanocellulosic multilayer thin films on polylactic acid with tunable gas barrier properties. *ACS Appl Mater Interfaces* **5**:7352–7359 (2013).

10. Eichhorn S, Dufresne A. Review: current international research into cellulose nanofibres and nanocomposites. *J Mater Sci* **45**:1–33 (2010).

11. Trifol J, Plackett D, Sillard C, et al. A comparison of partially acetylated nanocellulose, nanocrystalline cellulose, and nanoclay as fillers for high-performance polylactide nanocomposites. *J Appl Polym Sci* **133**:1–11 (2016).

12. Johansson F, Leufvén A. Influence of sorbed vegetable oil and relative humidity on the oxygen transmission rate through various polymer packaging films. *Packag Technol Sci* **7**:275–281 (1994).

13. Hoffmann M. Inorganic-Organic Polymers with Barrier Properties for Water Vapor, Oxygen and Flavors. *J Sol-Gel Sci Technol* **2**:141–146 (1998).

14. Chang J, An YU, Sur GS. Poly(lactic acid) nanocomposites with various organoclays. I. Thermomechanical properties, morphology, and gas permeability. *J Polym Sci Part B Polym Phys* **41**:94–103 (2003).

15. Yuniarto K, Welt BA, Purwanto A, et al. Effect of Plasticizer on Oxygen Permeability of Cast Polylactic acid (PLA) Films Determined using Dynamic Accumulation Method. *J Appl Packag Res* **6:**51-56 (2014).

16. Tsuji H, Okino R, Daimon H, et al. Water vapor permeability of poly(lactide)s: Effects of molecular characteristics and crystallinity. *J Appl Polym Sci* **99**:2245–2252 (2006).

17. Cairncross RA, Becker JG, Ramaswamy S, et al. Moisture Sorption, Transport, and Hydrolytic

Degradation in Polylactide. *Appl Biochem Biotechnol* **131**:774–785 (2006).

18. Koo D, Du A, Palmese GR, et al. Moisture management of polylactides: The effect of heat treatment. *Polymer* **53**:1115–1123 (2012).

19. Siparsky GL, Voorhees KJ, Dorgan JR, et al. Water transport in polylactic acid (PLA), PLA/polycaprolactone copolymers, and PLA/polyethylene glycol blends. *J Environ Polym Degrad* **5**:125–136 (1997).

20. Picard E, Espuche E, Fulchiron R. Effect of an organo-modified montmorillonite on PLA crystallization and gas barrier properties. *Appl Clay Sci* **53**:58–65 (2011).

21. Aulin C, Salazar-Alvarez G, Lindström T. High strength, flexible and transparent nanofibrillated cellulose-nanoclay biohybrid films with tunable oxygen and water vapor permeability. *Nanoscale* **4**:6622– 6628 (2012).

22. Liu A, Walther A, Ikkala O, et al. Clay nanopaper with tough cellulose nanofiber matrix for fire retardancy and gas barrier functions. *Biomacromolecules* **12**:633–41 (2011).

23. Spoljaric S, Salminen A, Dang Luong N, et al. Nanofibrillated cellulose, poly(vinyl alcohol), montmorillonite clay hybrid nanocomposites with superior barrier and thermomechanical properties. *Polym Compos* **35**:1117–1131 (2013).

24. Arjmandi R, Hassan A, Mohamad Haafiz MK, et al. Partial replacement effect of montmorillonite with cellulose nanowhiskers on polylactic acid nanocomposites. *Int J Biol Macromol* **81**:91–99 (2015).

25. Arjmandi R, Hassan A, Haafiz MKM, et al. Effect of hydrolysed cellulose nanowhiskers on properties of montmorillonite/polylactic acid nanocomposites. *Int J Biol Macromol* **82**:998–1010 (2016).

26. Hong J, Kim DS. Preparation and physical properties of polylactide/cellulose nanowhisker/nanoclay composites. *Polym Compos* **34**:293–298 (2013).

27. Mohapatra AK, Mohanty S, Nayak SK. Poly(lactic acid) and layered silicate nanocomposites prepared by melt mixing: Thermomechanical and morphological properties. *Polym Compos* **33**:2095–2104 (2012).

28. Katiyar V, Gerds N, Koch CB, et al. Melt processing of poly(L-lactic acid) in the presence of organomodified anionic or cationic clays. *J Appl Polym Sci* **122**:112–125 (2011).

29. Rhim JW, Hong SI, Ha CS. Tensile, water vapor barrier and antimicrobial properties of PLA/nanoclay composite films. *LWT - Food Sci Technol* **42**:612–617 (2009).

30. Sinha Ray S, Okamoto M. Biodegradable polylactide and its nanocomposites: Opening a new dimension for plastics and composites. *Macromol Rapid Commun* **24**:815–840 (2003).

31. Zhang J, Tashiro K, Tsuji H, et al. Disorder-to-order phase transition and multiple melting behavior of poly (l-lactide) investigated by simultaneous measurements of WAXD and DSC. *Macromolecules **41***:1352–1357 (2008).

32. Righetti MC, Tombari E. Crystalline, mobile amorphous and rigid amorphous fractions in poly(L-lactic acid) by TMDSC. *Thermochim Acta* **522**:118–127 (2011).

Table 1 Mechanical properties of all hybrid composites, determined by tensile testing[a].

			CNF/C30B					
		PLA	1%-1%	1%-3%	1%-5%	5%-1%	5%-3%	5%-5%
E	(GPa)	2.4 +/- 0.3	2.5 +/- 0.2	2.7 +/- 0.2	2.7 +/- 0.1	2.9 +/- 0.1	3.1 +/- 0.1	3.1 +/- 0.2
σ	(MPa)	55 +/- 2	53 +/- 2	43 +/- 1	18 +/- 5	51 +/- 3	27 +/- 2	16 +/- 3
ε	%	3.9 +/- 0.2	2.9 +/- 0.1	2.2 +/- 0.3	0.9 +/- 0.4	2.6 +/- 0.1	1.6 +/- 1.2	0.7 +/- 0.1
			CNC/C30B					
		PLA	1%-1%	1%-3%	1%-5%	5%-1%	5%-3%	5%-5%

E	(GPa)	2.4 +/- 0.3	2.2 +/- 0.3	2.3 +/- 0.1	2.2 +/- 0.2	2.6 +/- 0.3	2.7 +/- 0.2	3.0 +/- 0.1
σ	(MPa)	55 +/- 2	47 +/- 6	40 +/- 2	18 +/- 5	49 +/- 2	34 +/- 1	25 +/- 3
ε	%	3.9 +/- 0.2	3.1 +/- 0.2	2.4 +/- 0.2	1.2 +/- 0.3	3.0 +/- 0.5	1.6 +/- 0.3	1.1 +/- 0.2

a) E is the Young's modulus in GPa, ε strain at breaking point and σ stress at breaking in MPa.

APPENDIX 5: Author statements.

Technical University of Denmark

Joint author statement

If a thesis contains articles (i.e. published journal and conference articles, unpublished manuscripts, chapters etc.) made in collaboration with other researchers, a joint-author statement verifying the PhD student's contribution to each article should be made by all authors. However, if an article has more than three authors the statement may be signed by a representative sample, cf. article 12, section 4 and 5 of the Ministerial Order No. 1039 27 August 2013 about the PhD degree. We refer to the Vancouver protocol's definition of authorship.

A representative sample of authors is comprised of

- Corresponding author and/or principal/first author (defined by the PhD student), and if there are more authors:
- 1-2 authors (preferably international/non-supervisor authors)

Titel of the article	A comparison of chemically extracted, partially acetylated nanocellulose, nanocrystalline cellulose and nanoclay as fillers for high-performance polylactide nanocomposites
Author(s)	J. Trifol, D. Plackett, C. Sillard, O. Hassager, A. E. Daugaard, J. Bras, P. Szabo
Journal/conference * if applicable	
Name of PhD student	Jon Trifol
Date of Birth	11-10-1983

Description of the PhD student's contribution to the abovementioned article

The PhD student has made all of the experimental work and the most part of the analisys by himself. Furthermore, the Phd student has written the first draft of the article and has incorporated the suggestions of the rest of the coauthors.

Signature of the PhD student

Date

Signatures of co-authors

As a co-author I state that the description given above to the best of my knowledge corresponds to the process and I have no further comments.

Date (DD/MM/YY)	Name	Signature
25/8/2015	PETER SZABO	P. Szabo
27/8-2015	OLE HASSAGER	
28/8 -2015	Anders Daugaard	
28/8 /2015	Julien BRAS	

Technical University of Denmark

Joint author statement

If a thesis contains articles (i.e. published journal and conference articles, unpublished manuscripts, chapters etc.) made in collaboration with other researchers, a joint-author statement verifying the PhD student's contribution to each article should be made by all authors. However, if an article has more than three authors the statement may be signed by a representative sample, cf. article 12, section 4 and 5 of the Ministerial Order No. 1039 27 August 2013 about the PhD degree. We refer to the Vancouver protocol's definition of authorship.

A representative sample of authors is comprised of

- Corresponding author and/or principal/first author (defined by the PhD student), and if there are more authors:
- 1-2 authors (preferably international/non-supervisor authors)

Titel of the article	Hybrid poly(lactic acid)/nanocellulose/nanoclay composites with synergistically enhanced barrier properties and improved thermomechanical resistance
Author(s)	J. Trifol, D. Plackett, C. Sillard, O. Hassager, J. Bras, P. Szabo, A. E. Daugaard
Journal/conference * if applicable	
Name of PhD student	Jon Trifol
Date of Birth	11-10-1983

Description of the PhD student's contribution to the abovementioned article

The PhD student has made all of the experimental work and the most part of the analisys by himself. Furthermore, the Phd student has written the first draft of the article and has incorporated the suggestions of the rest of the coauthors.

Signature of the PhD student

Date

Signatures of co-authors

As a co-author I state that the description given above to the best of my knowledge corresponds to the process and I have no further comments.

Date (DD/MM/YY)	Name	Signature
25/8/2015	PETER SZABO	P. Szabo.
27/8-2015	OLE HASSAGER	
28/8 -2015	Anders Daugaard	
28/8/2015	Julien BRAS	

Technical University of Denmark

Joint author statement

If a thesis contains articles (i.e. published journal and conference articles, unpublished manuscripts, chapters etc.) made in collaboration with other researchers, a joint-author statement verifying the PhD student's contribution to each article should be made by all authors. However, if an article has more than three authors the statement may be signed by a representative sample, cf. article 12, section 4 and 5 of the Ministerial Order No. 1039 27 August 2013 about the PhD degree. We refer to the Vancouver protocol's definition of authorship.

A representative sample of authors is comprised of

- Corresponding author and/or principal/first author (defined by the PhD student), and if there are more authors:
- 1-2 authors (preferably international/non-supervisor authors)

Titel of the article	*Chemically extracted nanocellulose from sisal fibres by employing a simple and industrially relevant process*
Author(s)	J. Trifol[a], C. Sillard[b], D. Plackett[c], O. Hassager[a], J. Bras[b], P. Szabo[a], A. E. Daugaard[a]
Journal/conference * if applicable	
Name of PhD student	Jon Trifol
Date of Birth	11-10-1983

Description of the PhD student's contribution to the abovementioned article

The PhD student has made all of the experimental work and the most part of the analisys by himself. Furthermore the PhD student has written the first draft of the publication.

Signature of the PhD student

Date

Signatures of co-authors

As a co-author I state that the description given above to the best of my knowledge corresponds to the process and I have no further comments.

Date (DD/MM/YY)	Name	Signature
25/8/2015	PETER SZABO	P. Szabo.
27/08/2015	OLE HASSAGER	
28/8/2015	Anders Daugaard	
28/8/2015	Julien BRAS	

Technical University of Denmark

Joint author statement

If a thesis contains articles (i.e. published journal and conference articles, unpublished manuscripts, chapters etc.) made in collaboration with other researchers, a joint-author statement verifying the PhD student's contribution to each article should be made by all authors. However, if an article has more than three authors the statement may be signed by a representative sample, cf. article 12, section 4 and 5 of the Ministerial Order No. 1039 27 August 2013 about the PhD degree. We refer to the Vancouver protocol's definition of authorship.

A representative sample of authors is comprised of

- Corresponding author and/or principal/first author (defined by the PhD student), and if there are more authors:
- 1-2 authors (preferably international/non-supervisor authors)

Titel of the article	Hybrid poly(lactic acid)/nanocellulose/nanoclay composites with synergistically enhanced barrier properties and improved thermomechanical resistance
Author(s)	J. Trifol, D. Plackett, C. Sillard, O. Hassager, J. Bras, P. Szabo, A. E. Daugaard
Journal/conference * if applicable	
Name of PhD student	Jon Trifol
Date of Birth	11-10-1983

Description of the PhD student's contribution to the abovementioned article

The PhD student has made all of the experimental work and the most part of the analisys by himself. Furthermore, the Phd student has written the first draft of the article and has incorporated the suggestions of the rest of the coauthors.

Signature of the PhD student ..... Date .....

Signatures of co-authors

As a co-author I state that the description given above to the best of my knowledge corresponds to the process and I have no further comments.

Date (DD/MM/YY)	Name	Signature
25/8/2015	PETER SZABO	P. Szabo.
27/8-2015	OLE HASSAGER	
28/8-2015	Anders Daugaard	
7/11-2015	Cécile Sillard	

Technical University of Denmark

Joint author statement

If a thesis contains articles (i.e. published journal and conference articles, unpublished manuscripts, chapters etc.) made in collaboration with other researchers, a joint-author statement verifying the PhD student's contribution to each article should be made by all authors. However, if an article has more than three authors the statement may be signed by a representative sample, cf. article 12, section 4 and 5 of the Ministerial Order No. 1039 27 August 2013 about the PhD degree. We refer to the Vancouver protocol's definition of authorship.

A representative sample of authors is comprised of

- Corresponding author and/or principal/first author (defined by the PhD student), and if there are more authors:
- 1-2 authors (preferably international/non-supervisor authors)

Titel of the article: *Chemically extracted nanocellulose from sisal fibres by employing a simple and industrially relevant process*

Author(s): J. Trifol[a], C. Sillard[b], D. Plackett[c], O. Hassager[a], J. Bras[b], P. Szabo[a], A. E. Daugaard[a]

Journal/conference
* if applicable

Name of PhD student: Jon Trifol

Date of Birth: 11-10-1983

Description of the PhD student's contribution to the abovementioned article

The PhD student has made all of the experimental work and the most part of the analisys by himself. Furthermore the PhD student has written the first draft of the publication.

Signature of the PhD student

Date

Signatures of co-authors

As a co-author I state that the description given above to the best of my knowledge corresponds to the process and I have no further comments.

Date (DD/MM/YY)	Name	Signature
25/8/2015	PETER SZABO	P. Szabo.
27/08/2015	OLE HASSAGER	
28/8/2015	Anders Daugaard	
27/8/2015	Cecile Sillard	

Technical University of Denmark

Joint author statement

If a thesis contains articles (i.e. published journal and conference articles, unpublished manuscripts, chapters etc.) made in collaboration with other researchers, a joint-author statement verifying the PhD student's contribution to each article should be made by all authors. However, if an article has more than three authors the statement may be signed by a representative sample, cf. article 12, section 4 and 5 of the Ministerial Order No. 1039 27 August 2013 about the PhD degree. We refer to the Vancouver protocol's definition of authorship.

A representative sample of authors is comprised of

- Corresponding author and/or principal/first author (defined by the PhD student), and if there are more authors:
- 1-2 authors (preferably international/non-supervisor authors)

Titel of the article	A comparison of chemically extracted, partially acetylated nanocellulose, nanocrystalline cellulose and nanoclay as fillers for high-performance polylactide nanocomposites
Author(s)	J. Trifol, D. Plackett, C. Sillard, O. Hassager, A. E. Daugaard, J. Bras, P. Szabo
Journal/conference * if applicable	
Name of PhD student	Jon Trifol
Date of Birth	11-10-1983

Description of the PhD student's contribution to the abovementioned article

The PhD student has made all of the experimental work and the most part of the analisys by himself. Furthermore, the Phd student has written the first draft of the article and has incorporated the suggestions of the rest of the coauthors.

Signature of the PhD student ..... Date .....

Signatures of co-authors

As a co-author I state that the description given above to the best of my knowledge corresponds to the process and I have no further comments.

Date (DD/MM/YY)	Name	Signature
25/8/2015	PETER SZABO	P. Szabo
27/8-2015	OLE HASSAGER	
28/8-2015	Anders Daugaard	
2 8/9-2015	Cecile Sillere	

Joint author statement

If a thesis contains articles (i.e. published journal and conference articles, unpublished manuscripts, chapters etc.) made in collaboration with other researchers, a joint-author statement verifying the PhD student's contribution to each article should be made by all authors. However, if an article has more than three authors the statement may be signed by a representative sample, cf. article 12, section 4 and 5 of the Ministerial Order No. 1039 27 August 2013 about the PhD degree. We refer to the Vancouver protocol's definition of authorship.

A representative sample of authors is comprised of

- Corresponding author and/or principal/first author (defined by the PhD student), and if there are more authors:
- 1-2 authors (preferably international/non-supervisor authors)

Titel of the article	Hybrid poly(lactic acid)/nanocellulose/nanoclay composites with synergistically enhanced barrier properties and improved thermomechanical resistance
Author(s)	J. Trifol, D. Plackett, C. Sillard, O. Hassager, J. Bras, P. Szabo, A. E. Daugaard
Journal/conference * if applicable	
Name of PhD student	Jon Trifol
Date of Birth	11-10-1983

Description of the PhD student's contribution to the abovementioned article

The PhD student has made all of the experimental work and the most part of the analisys by himself. Furthermore, the Phd student has written the first draft of the article and has incorporated the suggestions of the rest of the coauthors.

Signature of the PhD student _____ Date _____

Signatures of co-authors

As a co-author I state that the description given above to the best of my knowledge corresponds to the process and I have no further comments.

Date (DD/MM/YY)	Name	Signature
25/8/2015	PETER SZABO	P.Szab.
27/8-2015	OLE HASSAGER	
28/8 -2015	Anders Daugaard	
28/8/2015	David Plackett	D Plackett

Technical University of Denmark

Joint author statement

If a thesis contains articles (i.e. published journal and conference articles, unpublished manuscripts, chapters etc.) made in collaboration with other researchers, a joint-author statement verifying the PhD student's contribution to each article should be made by all authors. However, if an article has more than three authors the statement may be signed by a representative sample, cf. article 12, section 4 and 5 of the Ministerial Order No. 1039 27 August 2013 about the PhD degree. We refer to the Vancouver protocol's definition of authorship.

A representative sample of authors is comprised of

- Corresponding author and/or principal/first author (defined by the PhD student), and if there are more authors:
- 1-2 authors (preferably international/non-supervisor authors)

Titel of the article	*Chemically extracted nanocellulose from sisal fibres by employing a simple and industrially relevant process*
Author(s)	J. Trifol[a], C. Sillard[b], D. Plackett[c], O. Hassager[a], J. Bras[b], P. Szabo[a], A. E. Daugaard[a]
Journal/conference * if applicable	
Name of PhD student	Jon Trifol
Date of Birth	11-10-1983

Description of the PhD student's contribution to the abovementioned article

The PhD student has made all of the experimental work and the most part of the analisys by himself. Furthermore the PhD student has written the first draft of the publication.

Signature of the PhD student

Date

Signatures of co-authors

As a co-author I state that the description given above to the best of my knowledge corresponds to the process and I have no further comments.

Date (DD/MM/YY)	Name	Signature
25/8/2015	PETER SZABO	P. Szabo.
27/08/2015	OLE HASSAGER	
28/8/2015	Anders Daugaard	
28/8/2015	David Plackett	

Joint author statement

If a thesis contains articles (i.e. published journal and conference articles, unpublished manuscripts, chapters etc.) made in collaboration with other researchers, a joint-author statement verifying the PhD student's contribution to each article should be made by all authors. However, if an article has more than three authors the statement may be signed by a representative sample, cf. article 12, section 4 and 5 of the Ministerial Order No. 1039 27 August 2013 about the PhD degree. We refer to the Vancouver protocol's definition of authorship.

A representative sample of authors is comprised of

- Corresponding author and/or principal/first author (defined by the PhD student), and if there are more authors:
- 1-2 authors (preferably international/non-supervisor authors)

Titel of the article	A comparison of chemically extracted, partially acetylated nanocellulose, nanocrystalline cellulose and nanoclay as fillers for high-performance polylactide nanocomposites
Author(s)	J. Trifol, D. Plackett, C. Sillard, O. Hassager, A. E. Daugaard, J. Bras, P. Szabo
Journal/conference * if applicable	
Name of PhD student	Jon Trifol
Date of Birth	11-10-1983

Description of the PhD student's contribution to the abovementioned article

The PhD student has made all of the experimental work and the most part of the analisys by himself. Furthermore, the Phd student has written the first draft of the article and has incorporated the suggestions of the rest of the coauthors.

Signature
of the PhD student _____ Date _____

Signatures of co-authors

As a co-author I state that the description given above to the best of my knowledge corresponds to the process and I have no further comments.

Date (DD/MM/YY)	Name	Signature
25/8/2015	PETER SZABO	P. Szabo
27/8-2015	OLE HASSAGER	
28/8-2015	Anders Daugaard	
28/8/2015	David Plackett	D Plackett